Development of Control Methodologies for Energy Storage Systems in Electricity Distribution Networks

Shohana Rahman Deeba
M.Sc. in Electrical and Electronic Engineering
B.Sc. in Electrical and Electronic Engineering

A thesis submitted for the degree of Doctor of Philosophy at
The University of Queensland in 2017
School of Information Technology and Electrical Engineering

Abstract

Prompted by technical issues that have arisen due to the widespread deployment of distributed intermittent renewable generators, rapidly rising peak demand and reductions in battery price, the use of Battery-Based Energy Storage Systems (BESS) in power networks is on the rise. While BESS has the potential to deliver technical benefits, the best possible sizing, location and usage govern the financial viability. Prevailing models of determining BESS size, location and charging patterns have treated them as independent problems and lack explicit dependence on factors such as load growth rate, PV penetration level, network size and structure. Furthermore, the existing literature does not provide any guidelines on possible interaction between network operators and retailers to employ batteries for a distribution network operator's benefit.

To bridge the existing research gaps, a generic approach to select appropriate sizing and siting of BESS for supporting both distribution utilities and customers is developed in this thesis. A method is established to model network upgrade deferral as a function of load growth rate, renewable generation penetration and peak shave fraction. This model is then used for the formulation of an optimisation problem which benefits from multi-period power flow analysis to co-optimise the size, location and dispatch scheduling of BESS for a pre-specified number of units to be deployed in a given distribution network. The proposed approach is implemented on a segment of the Australian medium voltage distribution network under multiple practical and potential future scenarios. Moreover, the developed methodology is utilised to obtain appropriate sizing and siting while controlling a BESS in the rest of the thesis.

BESS are widely considered as a potential solution to counter the voltage regulation challenges arising due to solar Photovoltaic (PV) generation in low voltage distribution networks. Although the present approaches of using BESS are promising, the resulting voltage regulation performance and the prolongation of the lifetime of usually costly BESS units are heavily reliant on the underlying control algorithms. The existing BESS control approaches require frequent micro-cycles for voltage regulation and hence, put additional stress on BESS cycle-life. Furthermore, the vast majority of voltage regulation and storage management techniques in the literature lack the essential steps of experimental validation of their proposed approaches under realistic conditions.

In this thesis, a new control method is proposed and practically validated to ensure smooth BESS operation amenable for prolonged BESS life without compromising the voltage regulation performance. The approach is based on the finite short-term forecast of PV generation to obtain forecast voltage trajectories. The forecast PV generation in conjunction with calculated feasible BESS charge-discharge trajectories is utilised to regulate voltage response over a finite time horizon that substantially reduces the charge-discharge cycling of BESS.

As the uptake of BESS for photovoltaic applications rises, their aggregated use for network voltage regulation is considered as an impending option. Therefore, a generic approach to coordinate distributed BESS of customers with a view to system voltage regulation through the help of a demand response aggregator is developed. The proposed control algorithms are practically validated by using a Hardware-in-the-Loop (HIL) setup comprising of a Real Time Digital Simulator (RTDS) and a dSPACE controller board.

Declaration by author

This thesis is composed of my original work, and contains no material previously published or written by another person except where due reference has been made in the text. I have clearly stated the contribution by others to jointly-authored works that I have included in my thesis.

I have clearly stated the contribution of others to my thesis as a whole, including statistical assistance, survey design, data analysis, significant technical procedures, professional editorial advice, and any other original research work used or reported in my thesis. The content of my thesis is the result of work I have carried out since the commencement of my research higher degree candidature and does not include a substantial part of work that has been submitted to qualify for the award of any other degree or diploma in any university or other tertiary institution. I have clearly stated which parts of my thesis, if any, have been submitted to qualify for another award.

I acknowledge that an electronic copy of my thesis must be lodged with the University Library and, subject to the policy and procedures of The University of Queensland, the thesis be made available for research and study in accordance with the Copyright Act 1968 unless a period of embargo has been approved by the Dean of the Graduate School.

I acknowledge that copyright of all material contained in my thesis resides with the copyright holder(s) of that material. Where appropriate I have obtained copyright permission from the copyright holder to reproduce material in this thesis.

<u>Publications during candidature</u>

Peer-reviewed Journal Paper:

(1) **S R Deeba**, R. Sharma, T. K. Saha, D. Chakraborty and A. Thomas, "Evaluation of Technical and Financial Benefits of Battery-Based Energy Storage Systems in Distribution Networks", *IET Renewable Power Generation*, vol. 10, no. 8, pp. 1149-1160, September 2016.

Peer-reviewed Conference Papers:

(1) **S. R. Deeba**, "A Battery Management Approach to Improve Steady State Voltage Performance of an LV Distribution Feeder", *Australasian Universities Power Engineering Conference*, 25-28 September, 2016, Brisbane, Australia.

(2) **S. R. Deeba**, R. Sharma, T. K. Saha and A. Thomas, "Investigation of Voltage Performance of an LV Distribution Network for Improving Rooftop Photovoltaic Uptake in Australia", *IEEE Power and Energy Society General Meeting*, 17-21 July, 2016, Boston, MA, USA.

(3) **S. R. Deeba**, R. Sharma, T. K. Saha and D. Chakraborty, "A Tool to Estimate Maximum Arbitrage from Battery Energy Storage by Maintaining Voltage Limits in an LV Network", *IEEE PES Asia-Pacific Power and Energy Engineering Conference*, 15-18 November, 2015, Brisbane, Australia.

(4) **S. R. Deeba**, R. Sharma and T. K. Saha, "Coordinated Control of Multi-Functional Battery Energy Storage System in an Unbalanced Network," *Australasian Universities Power Engineering Conference*, 28 September - 1 October, 2014, Perth, Australia.

(5) T. Aziz, **S. R. Deeba** and N. Masood, "Investigation of Post-Fault Voltage Recovery Performance with Battery-Based Energy Storage Systems in a Microgrid", *Australasian Universities Power Engineering Conference*, 25-28 September, 2016, Brisbane, Australia.

Publications included in this thesis

(1) **S R Deeba**, R. Sharma, T. K. Saha, D. Chakraborty and A. Thomas, "Evaluation of Technical and Financial Benefits of Battery-Based Energy Storage Systems in Distribution Networks", *IET Renewable Power Generation*, vol. 10, no. 8, pp. 1149-1160, September 2016.

This paper is partially incorporated in Chapter 2 and significantly in Chapter 3.

Contributor	Statement of contribution
S R Deeba (Candidate)	Simulation and modelling (95%) Result interpretation and discussion (75%) Paper writing (75%)
R. Sharma	Result interpretation and discussion (15%) Paper writing and review (10%)
T. K. Saha	Result interpretation and discussion (5%) Paper writing and review (5%)
D. Chakraborty	Simulation and modelling (5%) Paper writing and review (5%)
A. Thomas	Result interpretation and discussion (5%) Paper writing and review (5%)

(2) **S. R. Deeba**, "A Battery Management Approach to Improve Steady State Voltage Performance of an LV Distribution Feeder", *Australasian Universities Power Engineering Conference*, 25-28 September, 2016, Brisbane, Australia.

This paper is partially incorporated in Chapter 2 and significantly in Chapter 4.

Contributor	Statement of contribution
S R Deeba (Candidate)	Simulation and modelling (100%) Result interpretation and discussion (100%) Paper writing (100%)

(3) **S. R. Deeba**, R. Sharma, T. K. Saha and A. Thomas, "Investigation of Voltage Performance of an LV Distribution Network for Improving Rooftop Photovoltaic Uptake in Australia", *IEEE Power and Energy Society General Meeting*, 17-21 July, 2016, Boston, MA, USA.

This paper is partially incorporated in Chapter 2 and significantly in Chapter 4.

Contributor	Statement of contribution
S R Deeba (Candidate)	Simulation and modelling (100%) Result interpretation and discussion (70%) Paper writing (70%)
R. Sharma	Result interpretation and discussion (15%) Paper writing and review (15%)
T. K. Saha	Result interpretation and discussion (10%) Paper writing and review (10%)
A. Thomas	Result interpretation and discussion (5%) Paper writing and review (5%)

(4) **S. R. Deeba**, R. Sharma, T. K. Saha and D. Chakraborty, "A Tool to Estimate Maximum Arbitrage from Battery Energy Storage by Maintaining Voltage Limits in an LV Network", *IEEE PES Asia-Pacific Power and Energy Engineering Conference*, 15-18 November, 2015, Brisbane, Australia.

This paper is partially incorporated in Chapter 2 and significantly in Chapter 4.

Contributor	Statement of contribution
S R Deeba (Candidate)	Simulation and modelling (100%) Result interpretation and discussion (75%) Paper writing (75%)
R. Sharma	Result interpretation and discussion (10%) Paper writing and review (10%)
T. K. Saha	Result interpretation and discussion (10%) Paper writing and review (10%)
D. Chakraborty	Result interpretation and discussion (5%) Paper writing and review (5%)

(5) **S. R. Deeba**, R. Sharma and T. K. Saha, “Coordinated Control of Multi-Functional Battery Energy Storage System in an Unbalanced Network," *Australasian Universities Power Engineering Conference*, 28 September - 1 October, 2014, Perth, Australia.

This paper is partially incorporated in Chapter 2 and significantly in Chapter 4.

Contributor	Statement of contribution
S R Deeba (Candidate)	Simulation and modelling (100%) Result interpretation and discussion (75%) Paper writing (75%)
R. Sharma	Result interpretation and discussion (15%) Paper writing and review (15%)
T. K. Saha	Result interpretation and discussion (10%) Paper writing and review (10%)

Contributions by others to the thesis

“No contributions by others.”

Statement of parts of the thesis submitted to qualify for the award of another degree

“None”.

Acknowledgements

I would like to express my sincere gratitude to my advisors Professor Tapan Kumar Saha and Dr Rahul Sharma for their constant support, guidance and umpteen discussions during the journey of accomplishment of this dissertation. They kept a perfect balance between supervision and encouragement for independence. My learnings from them will always influence me for the rest of my life. Thank you very much Professor Saha and Dr Sharma!

I sincerely acknowledge the financial support from Professor Tapan Saha and The University of Queensland through the UQ International Student Scholarship. I would like to thank my advisors, School of ITEE and IEEE Queensland Section for sponsoring me to attend a number of top-ranked conferences around the world. I would also like to thank the Australian Federal Government's Department of Education and industry partners for their useful support through a Research Infrastructure Project.

I would like to express thanks to the following personnel for providing necessary data, valuable information, fruitful discussions and helpful comments: Dr Andrew Thomas from the Energy Queensland, Dr Debraj Chakraborty from IIT Mumbai, Dr Prabir Barooah from the University of Florida. Special thanks to Dr Nadali Mahmoudi from the University of Queensland and Dr Md Jan E Alam from the Pacific Northwest National Laboratory, U.S. I appreciate their suggestions and help on several research works during their stay in the University of Queensland.

I would sincerely like to thank all my colleagues and staff members from the Power and Energy Systems Research Group of The University of Queensland for their support and encouragement. Thanks to Ms Maureen Shields and Ms Mandeep Waraich for their assistance and generosity. I am also thankful to Mr Steve Wright from the school of ITEE for his help in a hardware laboratory.

Last, but definitely not the least, I am grateful to my parents and family members for motivation of choosing a research career, for their love, affection and constant advice to achieve excellence in academic pursuits. I would like to express special thanks to my husband Dr Nahid Al Masood for his encouragement, cooperation and cheering me up throughout this journey. Thank you very much Nahid for always being there for me!

Keywords

battery energy storage systems, battery storage control, battery cycle life, demand response, network upgrade deferral, reverse power flow, solar PV, high PV penetration, voltage rise, voltage regulation.

Australian and New Zealand Standard Research Classifications (ANZSRC)

ANZSRC code: 090607, Power and Energy Systems Engineering (excl. Renewable Power), 70%

ANZSRC code: 090608, Renewable Power and Energy Systems Engineering (excl. Solar Cells), 30%

Fields of Research (FoR) Classification

FoR code: 0906, Electrical and Electronic Engineering, 100%

Table of Contents

List of Figures

List of Tables

List of Abbreviations

PV	Photovoltaic
BESS	Battery-Based Energy Storage System
DNO	Distribution Network Operator
DRA	Demand Response Aggregator
DOD	Depth-of-Discharge
SoC	State of Charge
RTDS	Real Time Digital Simulator
HIL	Hardware-in-the-Loop
VR	Voltage Regulation
SVR	Step Voltage Regulator
OLTC	On-Load Tap Changing Transformer
GE	General Electric
NREL	National Renewable Energy Laboratory
kVA	Kilo Volt-Ampere
IEEE	Institute of Electrical and Electronics Engineers
ANSI	American National Standards Institute
AS	Australian Standard
NZS	New Zealand Standard
ARENA	Australian Renewable Energy Agency
OPF	Optimal Power Flow
NEM	National Electricity Market
PCC	Point of Common Coupling
RTF	Real-Time Forecast-Based
VAR	Volt-Ampere Reactive
kWh	Kilo Watt Hour
TOU	Time of Use
GAMS	Generic Algebraic Modelling System
USD	US Dollar
LV	Low Voltage
DAB	Daily Arbitrage Benefits
ICU	Inverter Control Unit
ECU	External Control Unit

kV	Kilo Volt
kW	Kilo Watt
MW	Mega Watt
EMTP	Electromagnetic Transient Programming
DC	Direct Current
AC	Alternating Current
VSC	Voltage Source Converter
PLL	Phase Locked Loop
GTAI/O	Gigabit Transceiver Input/output
ADC	Analog to Digital
DAC	Digital to Analog
p.u.	Per Unit

Chapter 1 Introduction

1.1 Background

During the past decades, electricity power systems have faced radical revolution with the worldwide uptake of renewable energy technologies. Solar Photovoltaics (PV), a commonly used renewable resource, have a high proliferation in power distribution systems. Like many other countries, the uptake of solar PV in Australia has been rapidly growing over the last few years. The growth is due to Australia's recent climate change abatement policy to reduce carbon emissions 26-28% by 2030 [1]. At present, the installed capacity of solar PV in Australia has reached 5.6 GW as shown in Figure 1.1 [2].

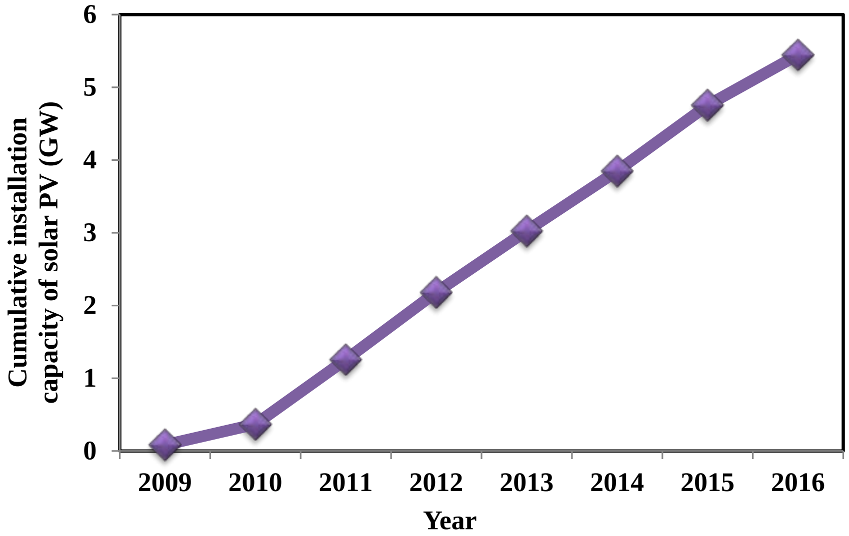

Figure 1.1 Cumulative installation capacity of solar PV for the last 8 years [2]

Distributed solar PV has been proven as advantageous in many ways especially for carbon emission reduction and lessening customers' electricity expense. Furthermore, solar PV users are subsidised through a 'feed-in-tariff' scheme that was launched in 2008 [3]. Unlike conventional synchronous generators, PV power is intermittent and variable with limited controllability. Traditionally, the power flow is unidirectional from a distribution substation to loads; however, large integration of PV has changed the usual paradigm. When PV output exceeds local demand, the excess PV power is injected into the upstream network and the power flow direction turns out to be from loads towards the substation. The existing voltage control devices are not designed to tackle such reverse and variable power flow. Therefore, growth in PV installations can be accompanied by some technical challenges such as voltage rise, fluctuations and malfunction of the existing voltage regulation equipment [4]. To mitigate such challenges, the existing and future PV installations must be properly managed to facilitate continued growth of renewable energy resources in distribution systems.

Distribution systems are designed to perform under peak demand that generally tends to increase every year. Usually, peak demand occurs in the evening and hence, solar PV is unable to reduce the system peak. Traditionally, peaking power plants have been employed to serve peak demand. In modern power systems, demand side management is seen as a potential solution to reduce peak consumption instead of adding more peaking plants [5]. Reducing a certain amount of demand at peak time is known as peak shaving, which is useful to reduce or defer a network augmentation. Figure 1.2 shows a distribution feeder's load curves from 2009 to 2013 [6]. With the proliferation of PV over time, the lower peak of a load curve goes down. At the same time, the upper peak of the load curve goes up due to ever growing peak demand.

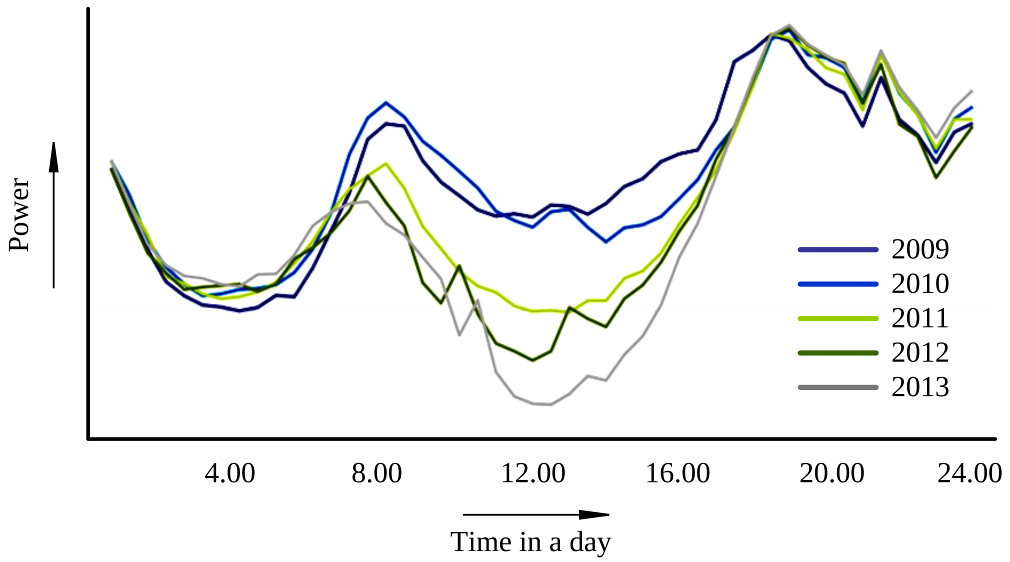

Figure 1.2 Load curves of a distribution feeder in Australia [6]

Battery-Based Energy Storage Systems (BESS) can be utilised to properly manage network loading during peak and off-peak demand situations. BESS is an emerging technology, which can act as a load while charging and as a generation source while discharging [7]. Currently, the available BESS technologies include lead-acid, zinc-metal/air, nickel-metal oxide, sodium-sulphur, lithium-ion and flow batteries [7]. The projected cost of BESS technologies is presented in Figure 1.3, which indicates lithium-ion BESS cost is expected to significantly reduce by 2020 [8].

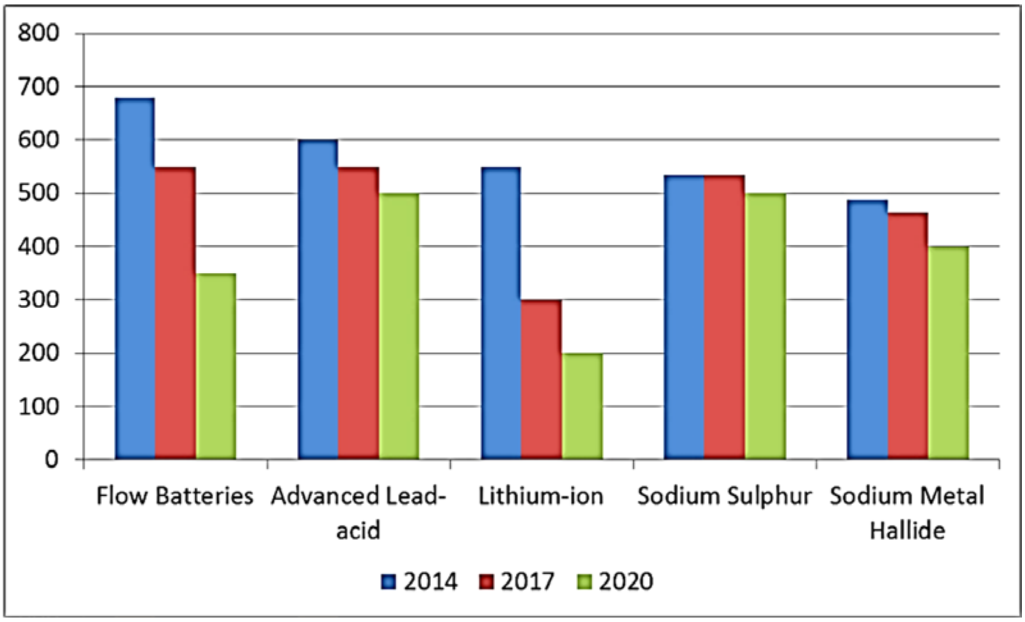

Figure 1.3 Projected costs of different battery technologies [8]

It is evident from different studies that with the advancement of technology and declining costs, BESS is a potential option to ensure satisfactory and resilient operation of power systems. However, proper utilisation of BESS in multiple applications, such as system peak reduction and voltage regulation, is heavily dependent on their underlying control algorithms. Furthermore, analysing the technical and financial benefits of BESS is also crucial. Therefore, appropriate control algorithms and financial viability of BESS for the two applications are thoroughly investigated in this thesis.

1.2 Motivation

Distribution networks require regular reinforcements to meet ever growing peak demand. Usually, network reinforcement requires a significant investment, which is often passed on to the consumer in the form of network charges [9]. It is now well known that this investment can be deferred by peak shaving through the deployment of BESS especially in PV prolific distribution systems, where BESS are able to be recharged from solar power. Nevertheless, installation of BESS may also involve significant investment. Consequently, the feasibility of BESS as a potential solution for Distribution Network Operators (DNO) to defer network upgrades is subjected to an appropriate sizing, location and management of BESS. Therefore, determining the best locations, ratings and operation schedule of BESS for network upgrade deferral is essential.

While PV generation is environmentally friendly, many technical barriers to its grid integration persist. One of the concerns regarding high PV penetration is voltage rise. It has been noticed that in some specific parts of the network in Queensland, Australia, distribution voltage magnitude violates its upper limit defined by the standard AS 60038 [10]. To take care of such a problem, Queensland distribution utilities have adopted a guideline for small scale PV inverter connections, which are typically in the range of 30 kVA [11]. Based on this guideline, voltage is allowed to rise at the end of a feeder by 2%, if all the existing and proposed inverters are in operation. Therefore, if the recommended margin is breached, new connections of rooftop PV can be restricted, resulting in hindered growth of PV uptake by customers. Moreover, to mitigate potential voltage rise, the upcoming PV inverters are supposed to be operated at 0.9 power factor (0.9 lagging to 0.9 leading), which results in bigger inverters and additional line losses. BESS coupled with PV is considered as a key for system voltage regulation provided they are properly controlled. Therefore, the design of appropriate control strategies of BESS for system voltage regulation is of utmost importance.

For PV power smoothing, BESS needs to be operated in variable charge/discharge rates at different Depth-of-Discharge (DOD) levels. Generally, one full charge and discharge is treated as a full cycle, where the rated DOD level is 80-90% [12]. Any DOD levels less than 80% can be considered as micro-cycles. Usually, BESS are controlled in fixed charge and discharge rates for several applications. Due to the variable charging rates for PV power smoothing, BESS DOD levels can be less than their rated values. Hence, in photovoltaic applications, various micro-cycles besides full cycles can be observed in the state of charge history of a BESS [13].

Effective utilisation of usually costly lithium-ion BESS can be achieved by avoiding operation regimes that can cause fast degradation of cycle life. Ageing of lithium-ion batteries is related to the electro-chemical charge exchange between the electrodes (at the same temperature, current and without exceeding high and low voltage limits). Some other factors such as operating temperature, DOD levels and high charge-discharge current are also responsible for lithium-ion ageing as reported in literature [12] [14, 15]. Usually manufacturers specify lithium-ion battery life by cycles. If there are half cycles in the state of charge history of a BESS, two such half cycles age the battery as one full cycle. Therefore, both full and micro-cycles of a BESS utilised in PV applications are counted to calculate total full cycles [14]. Hence, BESS control algorithms should be designed in such a way that battery state of health is taken care of.

Since the uptake of distributed PV and BESS is on the rise, demand side management for voltage regulation is a future option for system operators. Researchers have investigated the prospective demand response schemes for better voltage regulation [16-18]. Currently, Demand Response Aggregators' (DRA) focus is on transmission side voltage support after a contingency situation. However, the aggregator's service can be utilised for distribution voltage support if required. In that case, coordination of PV, BESS and existing voltage control devices in a distribution system is essential; where optimisation based voltage control approaches are suitable.

Moreover, the developed voltage regulation methods require experimental validation under practical situations [19].

To sum up, BESS is a growing technology and can be very useful in tackling several technical problems arising from large PV penetration. Whilst the cost of BESS is showing a declining trend, the expense is still considerable. Therefore, careful sizing, siting and controller design for better utilisation of BESS are critically important. In addition, experimental validation of the developed BESS control approaches is also important to evaluate their performances in practical circumstances.

1.3 Objectives

The primary objective of this thesis is to develop approaches for effective sizing, siting and control methods of BESS for multiple applications, specifically peak shaving and voltage regulation of a distribution network under high PV penetration. The following specific objectives are addressed in this thesis.

1. To develop a generic framework that has the flexibility for deciding optimal size, site and charge/discharge schedule of BESS in distribution networks considering peak shave, load growth rate and PV penetration levels.

2. To investigate the maximum allowable export limits from prospective solar PV sources to a low voltage network without violating standard operating voltage limits.

3. To design an effective BESS control algorithm for prolongation of BESS life when used for voltage regulation within PV prolific distribution networks. The controller requires experimental validation through a Hardware-in-the-Loop (HIL) set up that involves a Real Time Digital Simulator (RTDS) and a dSPACE control board.

4. To propose a generic framework for distribution voltage regulation utilising battery energy storage through a coordinated effort of a system operator and a demand response aggregator. The performance of the proposed control method should be tested via HIL simulation under several loading situations.

1.4 Thesis Layout

This thesis is organised into seven chapters. Following this chapter, the rest of the thesis is organised as follows.

In Chapter 2, an overview of the key operation challenges with high solar PV penetration are discussed with relevant voltage regulation and inverter control standards. Then, the major BESS technologies and their grid applications are presented. In the next stage, a detailed literature review on voltage regulation methods and BESS control approaches are presented while the specific research gaps are identified.

In Chapter 3, firstly a generalised approach is proposed to model network upgrade deferral as a function of load growth rate, renewable generation penetration and peak shave fraction. The developed model is then used for the formulation of an optimisation problem, which benefits from multi-period power flow analysis to co-optimise battery size, location and charge/discharge profile for a pre-specified number of units to be deployed in a given distribution network. The proposed approach is further extended for voltage regulation and several case studies are performed using different networks under multiple practical and potential future scenarios.

In Chapter 4, the impact of prospective solar PV units on the voltage performance of a part of the Queensland low voltage distribution system is investigated. Then an allowable power export limit of a new PV inverter is determined by satisfying standard voltage margins. This limit is utilised to develop a rule based BESS control strategy, which ensures voltage rise mitigation in the studied network. This strategy is then applied to explore the implication of PV-BESS on voltage enactment of the network. Guidelines to determine the number of BESS units are also investigated through several case studies.

In Chapter 5, a new control method for BESS is proposed and experimentally validated to ensure elongated BESS life without compromising the distribution voltage regulation performance. The approach is based on the finite short term forecast of PV generation to attain forecast voltage trajectories. The forecast PV generation in conjunction with calculated feasible BESS charge-discharge trajectories is utilised to regulate voltage response over a finite time horizon. A receding horizon control scheme is achieved that significantly reduces the charge/discharge cycling of a BESS. The HIL setup comprising RTDS and dSPACE is utilised for practical validation of the proposed method under several load and PV profiles.

In Chapter 6, a generic approach of distribution voltage regulation utilising customers BESS is proposed. The approach is targeted to minimise the cost of customers that is associated with the BESS usage for voltage regulation in a system. An optimisation based model is developed that connects the interests of network operators and BESS owners through the help of demand response aggregators. The model is used to determine the optimal charging pattern of BESS to regulate system voltage under high PV situations. The controller performance is tested via HIL setup under several practical situations.

In Chapter 7, a summary of the thesis with some concluding remarks is provided. Recommendations for potential future research problems are also outlined.

Chapter 2 Literature Review: BESS and Technical Issues

In this chapter, at first the present status of worldwide solar PV and BESS uptake is discussed. In the next stage, a comprehensive literature review on the technical challenges of high PV proliferation in power systems is presented. Then, several applications of distributed BESS and their grid connection challenges are highlighted. Based on the discussions, appropriate research gaps are identified.

2.1 Solar PV and BESS Uptake Status

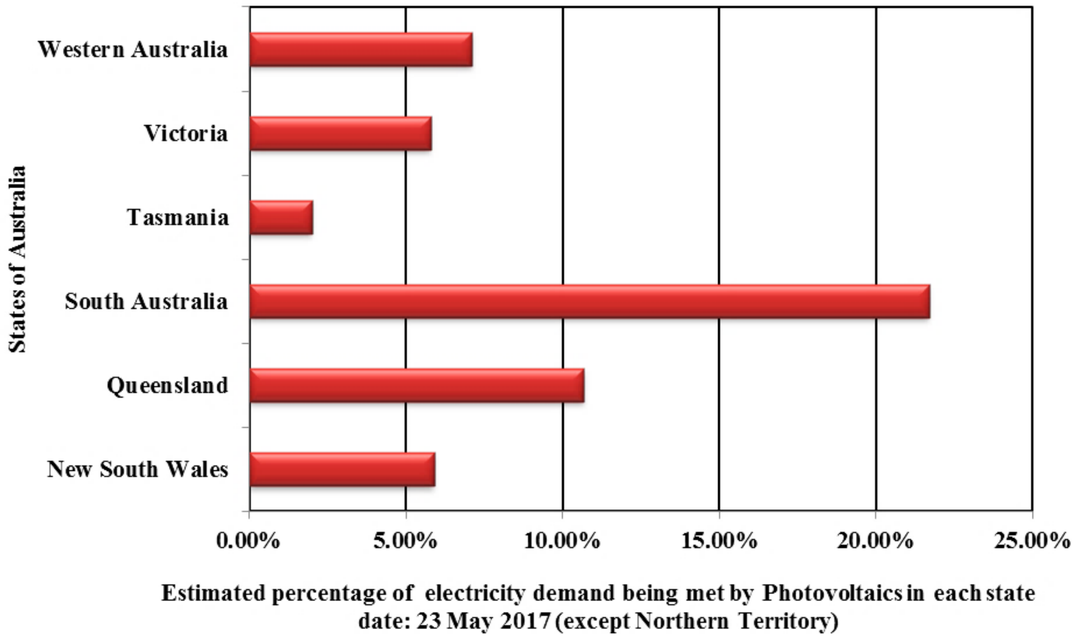

Figure 2.1 Percentage of demand being met by solar PV in each state of Australia [20]

Solar photovoltaic is a commonly used renewable energy resource and its global installation was 227 GW at the end of 2015 [20]. Like many other countries, the growth of solar PV in Australia has been rising due to several incentives such as small-scale technology certificates, commercial solar credits and feed-in-tariff schemes [21]. Small-scale technology certificates are provided to residential PV owners based on their PV size and locations and these certificates are sold to the fossil fuel based power producers in a spot market. Feed-in-tariff is another form of solar incentive that is a special tariff for feeding PV power back to a grid by solar users. The aforementioned inducements led to a high solar PV uptake within power systems of Australia. Figure 2.1 shows the recent percentage of electricity demand being met by solar PV in several states [20]. It can be observed that the percentages of demand served by PV generation in Queensland and

South Australia are almost 11% and 22% respectively. Such high PV penetration is advantageous in many ways, specifically for reducing carbon emissions and less usage of fossil fuels. Solar PV output is not dispatchable, unlike traditional synchronous generators of power systems. Therefore, system operators adjust the conventional generators output to balance the load with the overall generation including PV. Moreover, PV systems can rapidly change their output due to passing clouds. Therefore, large integration of this source introduces numerous technical challenges such as voltage rise, fluctuations and reverse power flow in electricity distribution systems [4].

The above technical challenges can be easily addressed by using small or large-scale battery based energy storage. Several economists have recently claimed that battery storage utilisation has a high value for end-users in order to efficiently manage behind-the-meter solar energy [22]. Therefore, a number of economic drivers such as wholesale arbitrage and ancillary services for battery storage are likely to be introduced in the near future with the help of aggregators. Reportedly, Germany and USA have installed a couple of megawatts of BESS in their respective power systems in 2015 and 2016. In Australia and Japan, several demonstration projects of grid-scale batteries have been undertaken in 2016 [23].

Battery energy storage technologies are maturing and offer unique advantages such as they can easily be scaled to suit many applications with high cycle efficiencies. Several analysts predict significant cost reduction of some battery technologies such as lithium-ion and flow-type prices, which are expected to drop considerably by 2020 [8]. Despite the declining trend in costs, BESS are still expensive and should be properly utilised for several grid applications. Subsequent sections review some of the existing literature on power distribution challenges due to high PV penetration and their solutions with BESS.

2.2 Challenges in Power Systems and Applications of BESS

The major challenges of power distribution systems due to high photovoltaic penetration and the applicability of BESS to resolve them are described as follows.

2.2.1 Challenges in Power Distribution Systems Due to High PV Penetration

i) *Change of Load Curve*

Photovoltaic power is only available in the daylight, while the hours of peak PV generation is not correlated with the hours of peak load. Typically, peak demand of a zone substation occurs in the evening when PV power is unavailable. Figure 2.2 presents a typical demand curve in California, USA with and without solar PV. It can be observed that a high PV output reduces the day time load. Therefore, the reformed load curve consists of a valley in the afternoon and a peak in the evening, which is known as ‘duck curve’ [24]. The system operators of South Australia have experienced similar duck curves in 2016 as illustrated in Figure 2.3.

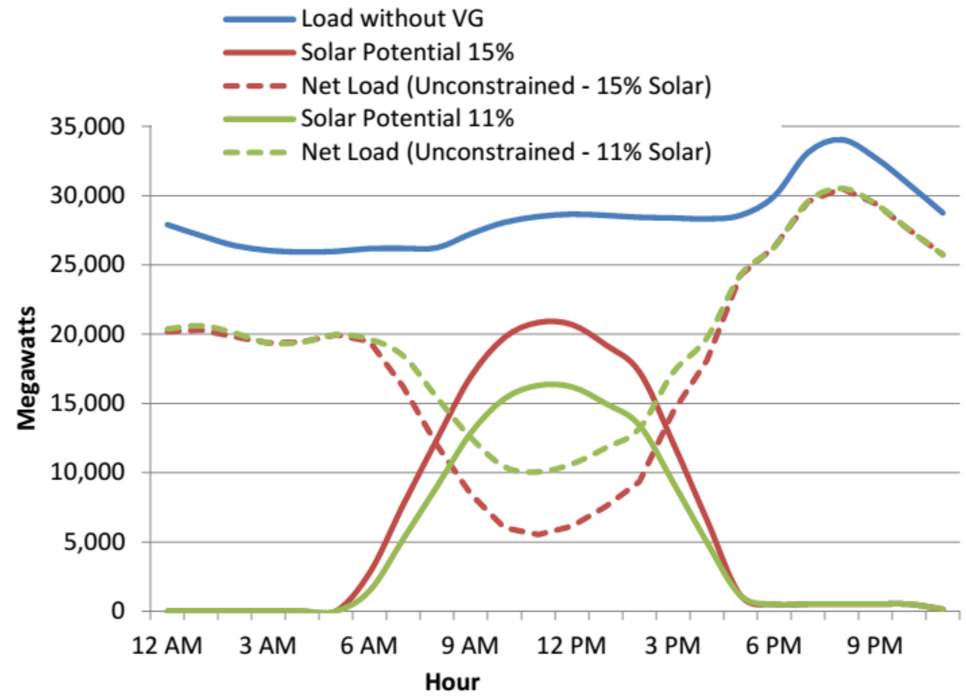

Figure 2.2 Original and net load profiles (California, USA) with 11% and 15% annual solar (on March 2013) [24]

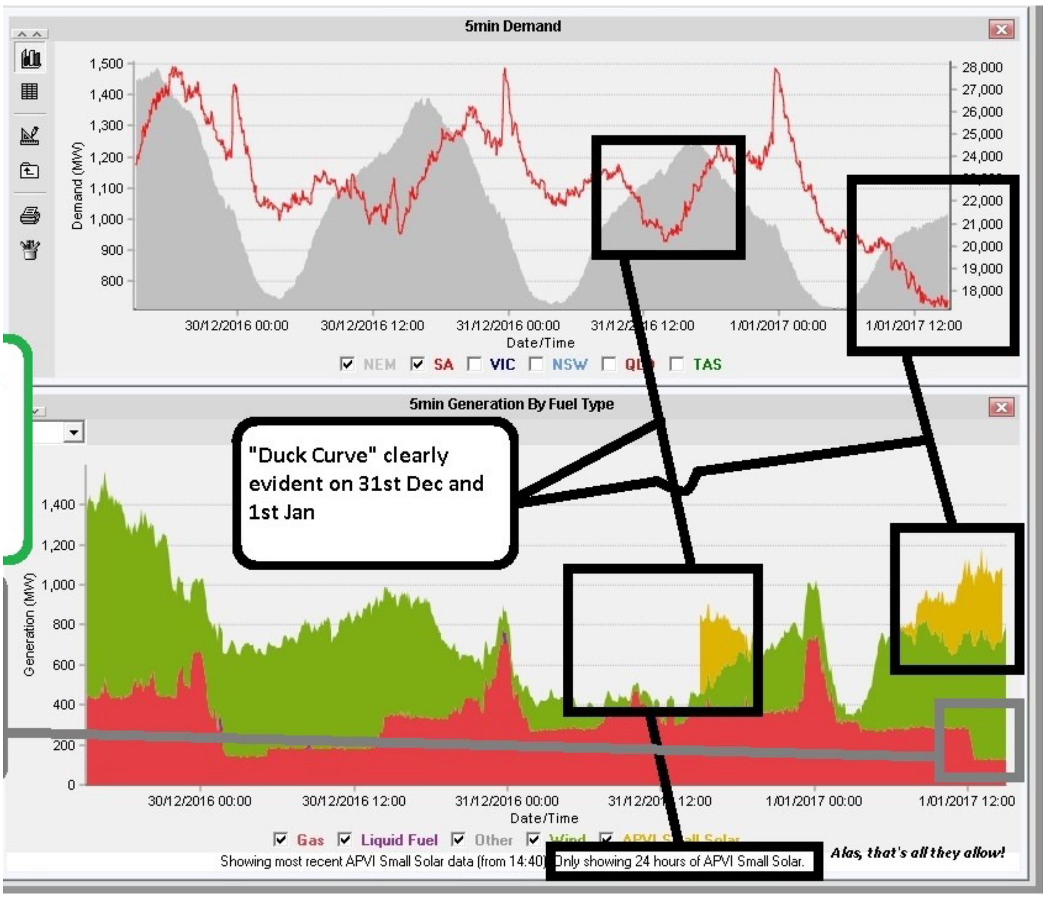

Figure 2.3 Duck curve experienced by South Australia system operator in 2016 [25]

With growing PV penetration, the difference between the lower and upper peaks of the net load curve increases. Reduction of load in the afternoon causes uneconomic operation of several base power plants under a wholesale market. In addition, the necessity of quick generation resources is evident to meet the evening peak due to the increased ramp in the load curves. Therefore, dispatchable generation sources are required to accommodate more solar PV in power systems.

ii) *Voltage Rise, Fluctuations and Reverse Power Flow*

Due to the high integration of solar PV, several technical challenges have arisen in planning and operation of distribution systems. The key issues include voltage rise, fluctuations and reverse power flow. Distribution network operators aim to deliver power to the customers at specified voltage levels (e.g. 120V or 230V or 240V). The service voltage should be maintained within acceptable ranges under changing load conditions depending on the respective system standards, which is known as Voltage Regulation (VR). Usually, distribution voltage regulation is performed by an On-Load Tap Changing Transformer (OLTC) at a substation, a fixed tap changer through a feeder, Step Voltage Regulators (SVR) and fixed capacitors.

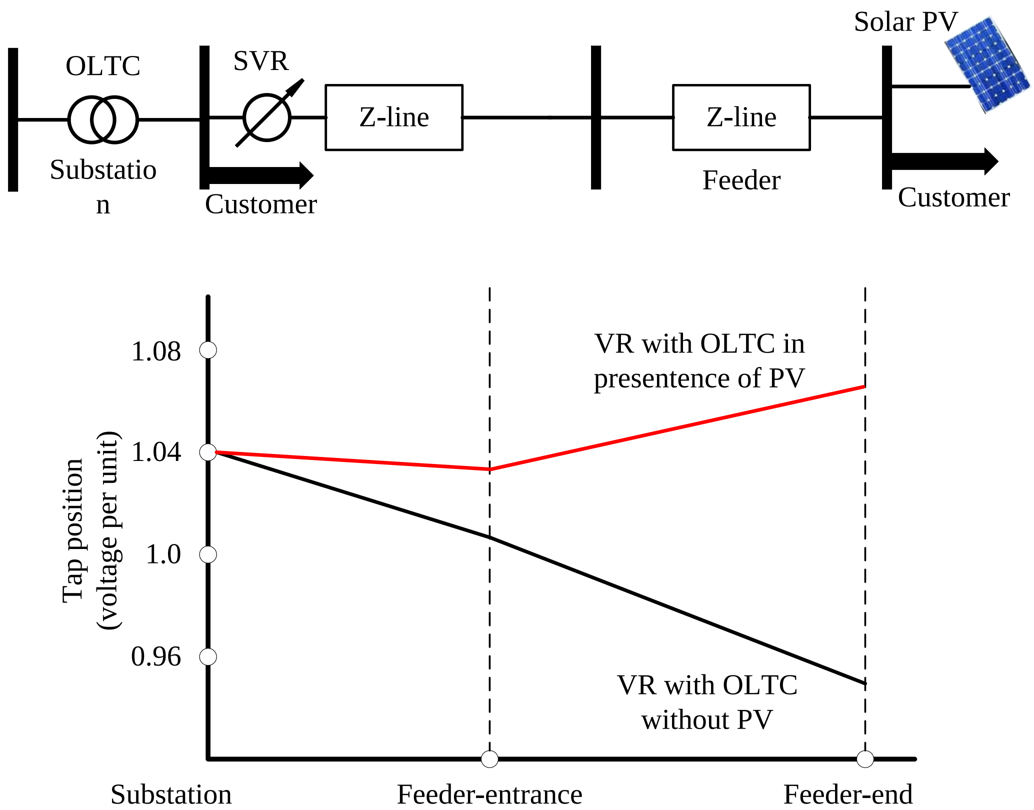

Figure 2.4 A typical radial distribution network with voltage regulation devices

Figure 2.4 presents the schematic diagram of a typical radial distribution feeder with voltage regulating equipment. Without any solar PV at the customer end, current flows from a distribution substation to loads causing a gradual voltage drop towards the feeder end. While solar PV is connected, if the output of PV exceeds local demand, surplus PV power is injected into the network. Therefore, the current flow direction is reversed, that causes voltage rise at the customer's point. Figure 2.4 presents the distribution feeder voltages with and without solar PV.

Unlike transmission systems, line transposition is rarely executed in distribution networks. Therefore, three phase distribution lines have unbalanced coupling and different voltage characteristics. Since the cross sectional area of distribution line conductors is much smaller than those of transmission lines, relatively higher resistance to reactance (R/X) ratios are observed in distribution systems. Therefore, voltage rise caused by reverse power flow from PV may propagate to upstream locations due to the mutual reaction of high R/X ratios of the lines and PV penetration levels in the respective feeders [26].

A number of research studies have been reported in literature regarding the impact analysis of high solar PV installation in power systems. In one of the first studies back in 1985, the impact of variable PV output due to passing clouds on distribution voltage is investigated [27]. In 1988, Public Service Company of Oklahoma system suggested keeping the PV penetration level within 15% to avoid serious consequences on voltage control and protection devices mainly due to reverse power flow [28]. The General Electric (GE) report released in 2003 investigated network voltage regulation, protection and transient stability under 40% PV penetration and concludes that such high PV penetration may cause false tripping and feeder voltage regulator malfunction [29]. In a report of National Renewable Energy Laboratory (NREL), voltage rise phenomenon is discussed, while PV penetration varies from 5% to 50% [26]. The mathematical presentation of voltage rise effect is described in [30]. This research indicates that the severity of the voltage rise is largely dependent on the network structure (tree/comb, mesh, rural/urban) and PV capacities.

Thomson and Infield in 2007 have presented the impact of distributed PV in balanced distribution networks, while the analysis focused on static effects on voltage rise, voltage dip, loss reduction, reverse power flow and mitigation of transformer loading [31]. From the simulation results, unacceptable voltage rise phenomenon is found for most of the PV installation cases. Several methodologies to examine voltage stability problem due to sudden PV power drop in unbalanced systems are established by Yan & Saha in 2012 [32]. A method of distribution voltage rise assessment from the bulk database with a relatively less computational burden is proposed by Alam et al in 2014 [33]. Notably, the existing literature indicates that high PV proliferation may cause serious consequences on system voltage regulation.

The standard practices for voltage regulation and PV interconnections in distribution networks are described in the following subsection.

2.2.2 Standards for Distributed PV System Integration

Several standards and guidelines for solar PV integration into a grid are already available providing recommended practices for small-scale distributed generators connection. The PV connection standards can be found in IEEE 1547, IEEE 929 and AS 4777 [10, 34, 35]. The standards provide information regarding PV interconnection to the grid such as installation, testing, protection, voltage/frequency ratings and response to disturbances. Guidelines for small scale inverters (<30 KVA) have recently been introduced in Queensland, Australia that contain further details of voltage requirements for old and new PV connections [11].

According to standards IEEE 1547 and AS 4777, small-scale PV systems are not allowed to operate for distribution voltage regulation. The recommended PCC voltage limits for PV connection are -12% to +10% of nominal value according to the IEEE 1547 and 929 standards. IEEE 929 has specified the recommended power factor of PV to be greater than 0.85 lagging/leading, while AS 4777 allows PV power factor variation from 0.95 lagging to 0.8 leading. Any violation of the aforementioned voltage and power factor ranges will cause disconnection of a PV system from the grid. The voltage and power factor ranges can vary based on standard practices in different power systems.

It is a utility's accountability to maintain their customers' voltage within an acceptable range. IEEE 1547 and ANSI C84.1 have described recommended practices for distribution voltage regulation [36]. The voltage regulation standards are specified for service and utilisation point voltages. Service point voltage is directly dependent on feeder voltage, which is equal to feeder voltage minus drops along the connecting line. Utilisation voltage is at the point of use where the outlet equipment is plugged in. IEEE 1547 and ANSI C84.1 have two types of voltage ranges, Range-A specifies voltages at normal operating conditions, while Range-B is specified for emergency operating conditions. The two ranges of voltage according to the standards are presented in Table 2.1.

Table 2.1 Voltage ranges according to ANSI C84.1 standard (percentage of nominal voltage) [36]

	Service		**Utilisation**	
	Min	Max	Min	Max
Range A (Normal)	-5%	+5%	-8.3%	+4.2%
Range B (Emergency)	-8.3%	+5.8%	-11.7%	+5.8%

Voltage fluctuations and flickers are other issues due to high PV penetration in distribution systems. Voltage flicker is referred to as a visible change in brightness of customers' lights due to rapid fluctuations. AS 4377 and IEEE 1453 have demonstrated the guidelines for PV-induced flicker, where short (10 mins) and long term (2 hours) flicker levels are defined [37, 38]. Short term flicker is calculated every 10 minutes and is defined by (2.1).

$$P_{st} = \sqrt{0.0314P_{0.1} + 0.0525P_1 + 0.0657P_3 + 0.28P_{10} + 0.08P_{50}} \tag{2.1}$$

where $P_{0.1}$, P_1, P_3, P_{10} and P_{50} indicate the flicker levels exceeded by 0.1%, 1%, 3%, 10% and 50% of the observation period respectively. Long term flicker level is calculated for 2 hours duration and defined by (2.2).

$$P_{lt} = \sqrt[3]{\frac{1}{12}P_{st}^3} \tag{2.2}$$

AS/NZS 61000-2012 specifies the short and long term flicker levels should be less than 1 and 0.65 respectively [37]. IEEE 1159 and the AS/NZS 61000 have also defined a voltage unbalance range, which is preferably less than 1% between the three phases [38]. Moreover, corrective measures should be taken if 2% unbalance limit is breached.

2.2.3 Grid Applications of BESS

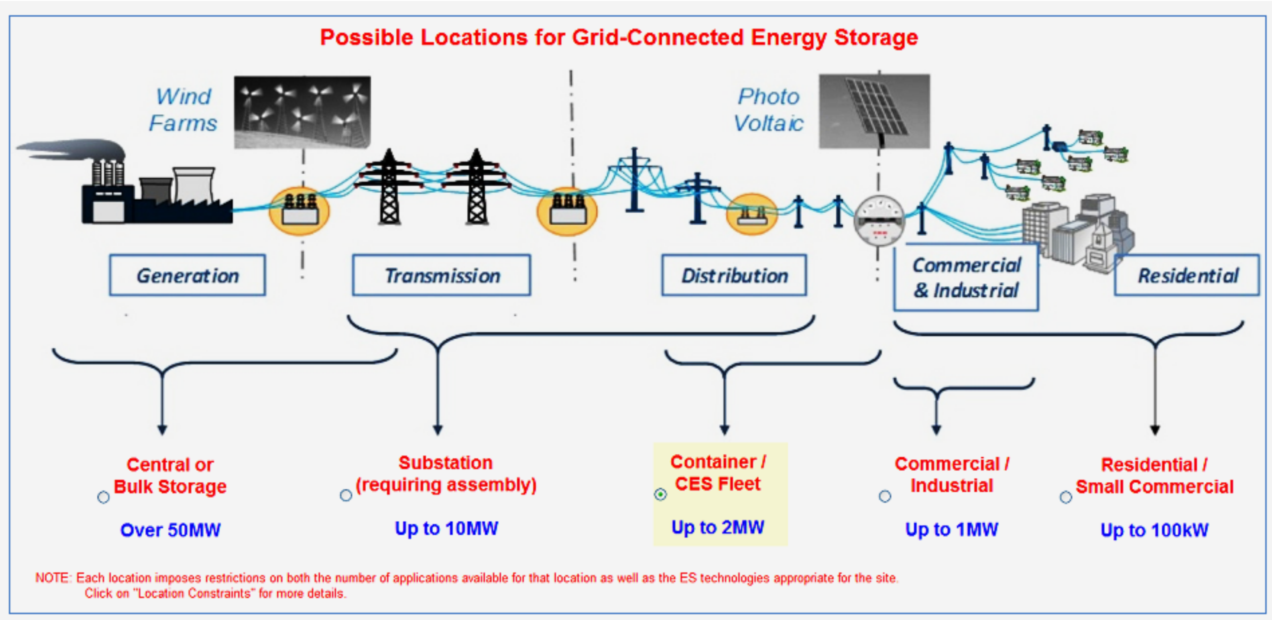

Figure 2.5 Potential locations for grid-connected energy storage [39]

Energy storage has a wide range of applications in power systems due to its unique capability; it can act as a controllable load as well as a generation source. Storage utilisation can be beneficial for a power grid depending on where they are located and how they are controlled. The potential location of different types of energy storage in power sectors have been reported in 2010 as illustrated in Figure 2.5 [39]. According to this report, the feasible sizes for energy storage are categorised into three classes. In the generation side, bulk energy storage of capacity up to 50 MW is suitable. For transmission and distribution network applications, storage size can vary within 2 MW-10 MW range. For commercial and industrial customers, small-scale storage up to 1 MW capacity is feasible, while residential storage capacity should be less than 100 kW. Compressed air and pumped hydro are feasible storage technologies for large-scale use in generation and transmission sectors. Battery-based energy storage systems or BESS are preferable for small-scale use in distribution networks.

In 2015, the Australian Renewable Energy Agency (ARENA) reported the potential applications of battery storage for power grids [23]. The major applications of grid connected BESS include load levelling, network upgrade deferral, power quality improvement and voltage support. Short descriptions of the above applications are as follows.

i) *Load Levelling*

Load Levelling refers to the process of charging a BESS in off peak demand and discharging in the peak time as presented in Figure 2.6. Therefore, peak demand of a network is reduced, which lessens the need for network capacity upgrade and high cost generation sources. It also helps levelling off-peak demand to handle reverse power flow in relevant situations. It is observed from Figure 2.6 that the peak point of the demand curve (P_{demand}) is decreased to a specified value (P_{max}), while the loading at off peak time is increased up to a level (P_{supply}).

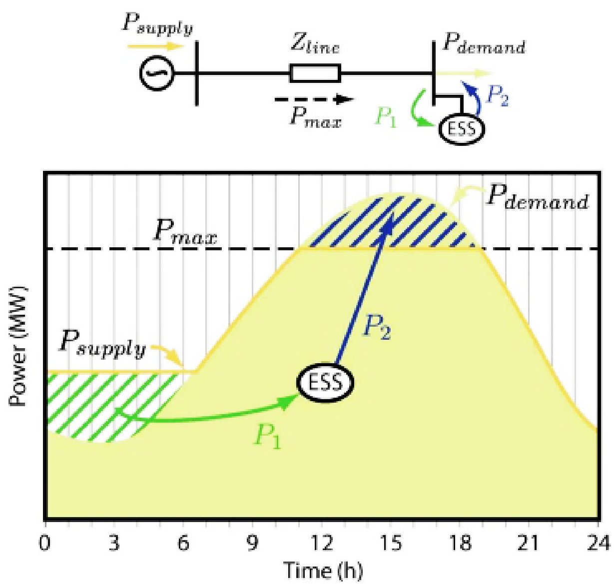

Figure 2.6 Load levelling applications with grid connected BESS [40]

ii) *Network Upgrade Deferral*

Electrical components of a power distribution system such as transformers, line conductors and protection equipment are designed to operate under maximum current ratings. Customers' peak demand gradually increases over time and it necessitates the periodic upgrading of system components. System upgrades involve significant investment, for which a customers' network charges may increase [9]. The system peak can be reduced by utilising BESS for a specified duration through which a network upgrade can be deferred. However, the effectiveness of such an approach hugely depends on the capital cost of the BESS installation. The cost of BESS mainly depends on associated materials and size. If the BESS size and technology are carefully chosen, network upgrade deferral through BESS can be financially viable.

iii) *Voltage Regulation*

High penetration of PV introduces reverse power flow, which may cause voltage regulation challenges in weak distribution networks due to long lines and high resistance [41]. BESS can be used to solve such problems by storing excess energy injected by PV units into a network. Therefore, BESS should be operated in such a way that it can adequately store surplus PV energy. The effective use of BESS to store variable PV power depends upon the applied control algorithms. Since BESS has a limited life-span, their appropriate control and management are crucial.

iv) *Energy Arbitrage*

Energy arbitrage is another application of BESS, which is basically charging BESS while the energy price is low and discharging at a high price. In deregulated markets, this application is attractive for residential and commercial customers since their electricity expenses can be reduced by a certain amount. If BESS are charged from solar PV, a further reduction of the customers' electricity charges is achieved. The arbitrage application is schematically shown in Figure 2.7.

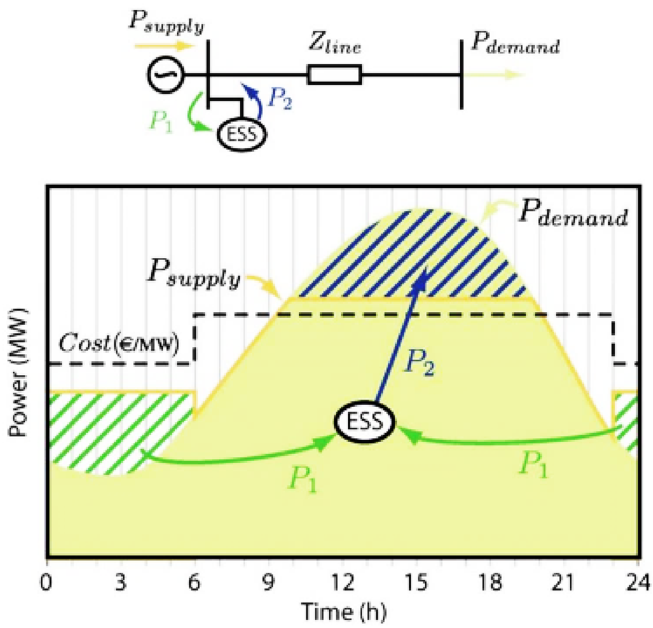

Figure 2.7 Energy arbitrage with BESS [40]

2.2.4 Overview of BESS Technologies

A typical BESS consists of a battery bank, a dc-dc bidirectional converter, an inverter and a control unit. Some common battery technologies are Lead-acid, Sodium-sulphur, Lithium-ion, Metal-air and Flow-type. Deep cycle batteries (e.g. Lead-acid, Lithium-ion etc.) are designed to regularly deep discharge and suitable for power system applications [22]. The main features of some BESS technologies are described as follows.

Lead-acid batteries are the oldest technology, which are appropriate for high power density applications (power quality, voltage regulation). Lead-acid is relatively cheaper than other technologies, the cost can be less than $170 per kWh [39]. The main disadvantages of Lead-acid include fewer life cycles, low energy density, high depth of discharge and environmental safety concerns [39].

Lithium-ion is the most advanced technology and is feasible for stationary and portable use. Lithium-ion type batteries have the highest energy density, which is appropriate for both short and long duration power system applications. Lithium-ion has a long life cycle, no memory effect, low self-discharge and the highest efficiency. However, this technology is more expensive than others. For instance, according to the recent reports, the cost of Lithium-ion in 2017 is approximately $300/kWh [8] [39]. The major disadvantages of Lithium-ion are- (i) they have capacity loss over time and (ii) their ageing is accelerated by high operating temperature.

Some other BESS technologies such as metal-air and flow types have high energy density and are suitable for utility side stationary applications such as load balancing, arbitrage, peak load shaving and so on. Flow type BESS are quick in response with reasonably good life cycles, however, their main limitation is the complicated structure (pumps, sensors, control units, secondary vessel) that restricts them for portable applications [23].

Figure 2.8 shows the co-related power ratings and discharge duration of different energy storage technologies. It can be seen from Figure 2.8 that Lead-acid and Lithium-ion BESS offer a wide range of operational flexibility with highest efficiencies. Both of them can be operated in a time range from minutes to hours with high power ratings.

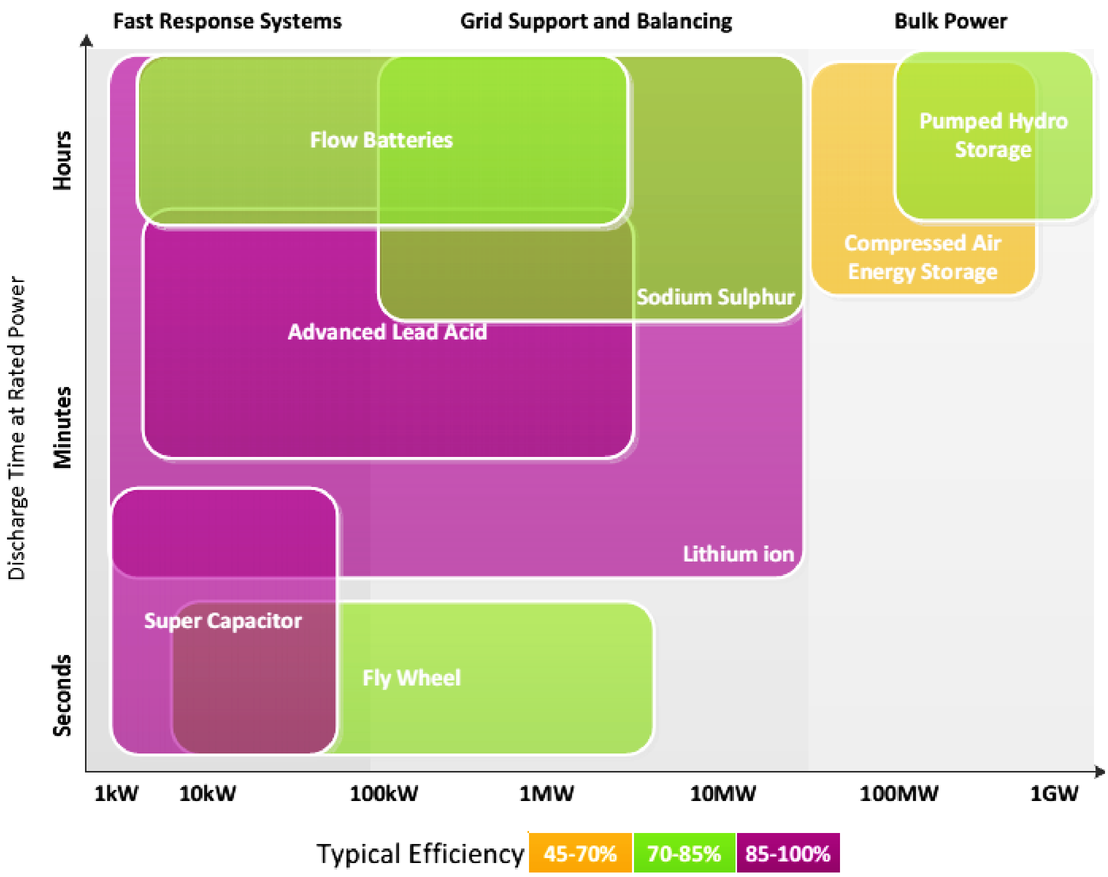

Figure 2.8 Energy storage technologies and their applications [23]

Super capacitors are fast responding storage, they are used with BESS for grid applications. Flywheel storage can be discharged within a few seconds at high power ratings, therefore, are mainly utilised in power system contingency situations.

Although several BESS technologies exist with relevant benefits, Lithium-ion BESS are more promising especially in photovoltaic applications due to their high life cycles and efficiency. In this thesis, Lithium-ion BESS are used for several case studies; however, the proposed methods are reproducible for any other types of BESS.

2.3 Research Gaps

In this section, specific research gaps are identified from the comprehensive literature review. The subsequent sections describe the research niches addressed in this thesis.

2.3.1 Appropriate Sizing, Siting and Operational Planning of BESS

BESS is a potential solution for DNOs to defer network upgrades as well as to regulate voltage by storing excess PV energy during off-peak periods. However, the feasibility of BESS utilisation for the two purposes is heavily reliant on their size, location and management. A number of optimisation-based approaches to determine the size and location of utility-scale BESS are reported in the literature. Suitable size and location of distributed generation are investigated from several perspectives such as reduction of generation cost [42, 43], reduction of loss [44] and better utilisation of PV power [45, 46]. Optimal sizing and siting of BESS for network upgrade deferral are determined in [47-50]. The techno-economic model of PV-battery [51] and life cycle based cost modelling of batteries [52, 53] are also reported, although these papers do not consider the impact of PV penetration levels on BESS placement.

Whilst significant studies exist on BESS sizing and siting for network upgrades, the main limitations of the existing literature include, firstly the problems of determining battery size, location and charging pattern are assumed as decoupled and therefore, treated as independent problems. Battery sizing depends on its day-ahead charge-discharge rate for a specific application. It also depends on the location of BESS, connected load and PV sources in a network. Costing, size, location and charging patterns of BESS are interrelated and should be optimised within a single framework in order to obtain a practically meaningful BESS allocation. Secondly, the existing literature does not provide any guidelines on the possible interaction between DNOs and retailers to employ BESS for a DNO's benefit.

Thirdly, the existing approaches treat the network upgrade deferral model as an economic input-output model. As a result, these models lack explicit dependence on factors such as load growth rate, PV penetration level, network size and structure, which characterise the distribution networks. Consequently, the existing approaches are usually devoid of the generalisation capability and the methodologies based on them are non-portable to other networks. Furthermore, the economic input-output network upgrade deferral models fail to capture the explicit technical dependence between the network upgrade deferral and the Optimal Power Flow (OPF), which is required to find an appropriate size and location of a BESS.

Therefore, in this thesis, *a generic model for distribution network investment deferral is developed considering peak shave, load growth rate, discount factor and PV penetration level for a specified planning horizon. The investment deferral model is used to formulate an optimisation problem to search for the most cost-effective sizing and placement of BESS units in order to defer system upgrades. The model is further improved for distribution voltage regulation and relevant case studies are performed under several load and PV scenarios.*

2.3.2 Investigation of the Maximum Export Limits of Residential PV Systems and an Effective BESS Control Strategy for Distribution Voltage Regulation

One of the concerning issues due to high PV penetration is reverse power flow, which can cause unacceptable voltage rise in distribution networks. A number of studies have been reported in the literature on voltage issues instigated by rooftop solar PVs [26, 30, 54-57]. The reason behind voltage rise phenomenon is investigated in [26, 30, 54], where reverse power flow is identified as the key factor. The severity of the voltage rise problem explicitly depends on the network line characteristics. There are 13 major distributors responsible for power networks in the National Electricity Market (NEM) of Australia [58]. Figure 2.9 presents the areas of power distributors within the NEM.

Figure 2.9 Distribution networks within the National Electricity Market [58]

It can be observed that Energex and Ergon Energy are the two main distributors in Queensland, who manage transporting electricity from the high voltage transmission network to low voltage customers. Due to the geographical distance, the load centres of the rural networks managed by Ergon Energy are dispersed. Therefore, the rural networks have two important features such as long line-length and high resistance to reactance ratios of distribution lines.

It has been noticed that in weak parts of the Queensland network, voltage magnitude violates its upper limit defined by AS 61000 [37]. To take care of this problem, distribution utilities have adopted a guideline for small scale PV inverter connections, which are typically in the range of 30 kVA [11]. Based on the guideline, voltage is allowed to rise at the end of a feeder by 2% if all the existing and proposed inverters are in operation. Therefore, if the recommended margin is breached, new connections of rooftop PV can be restricted, resulting in hindered growth of PV uptake by customers. Therefore, alternative solutions are required for effective voltage regulation instead of limiting PV capacities.

To resolve voltage regulation issues, one of the means could be the utilisation of battery energy storage. If batteries are integrated with PVs, they can absorb excess power when required. As a result, voltage performance of a network can be maintained within given specified limits. Along this line, several battery charging strategies are proposed in [55-57], which include the use of available battery capacity, ramp rate control and PV power smoothing respectively. It is to be mentioned that the existing PV units in Queensland are usually operated at unity power factor. However, to mitigate potential voltage rise, the upcoming PV inverters in Queensland are supposed to be operated at 0.9 power factor. Therefore, customers need to sacrifice some part of active power for PV operation at 0.9 power factor causing uneconomic resource management.

In accordance with the existing guideline, it is crucial to investigate the steady state voltage performance of the distribution networks in Queensland before permitting new PV inverter connections. If prospective PV inverters show a high risk of voltage regulation problems, the combination of PV and BESS can be utilised. However, the PV-BESS system must be adjusted in order to limit its power export to the network. Even though the export limit from a PV inverter has been mentioned in the present guideline, no detailed procedure to determine the limit is publicly available. To this end, *steady state voltage performance of a section of the Queensland low voltage distribution network is studied with a high share of PV units. Based on this investigation, the permissible export limit from a new PV unit is determined, which eliminates overvoltage issues. In the next stage, the export limit is utilised to control a BESS so that it can absorb sufficient energy from PV units keeping bus voltages within acceptable ranges. Then, the BESS control strategy is further modified for multiple functions such as peak shaving and load levelling.*

2.3.3 Controller Design and Hardware-in-the-Loop Validation for Prolongation of Battery Life in PV Applications

Existing research studies indicate that the voltage rise and fluctuation caused by distributed PV can be locally controlled for efficient and reliable system operation [11, 26]. There are two ways to locally solve the voltage issues [59, 60]. Firstly, zero export from a PV source to a network, however this approach is not economically desirable [59]. Another solution is to operate PV inverters in such a way that they consume reactive power from the distribution feeder to which the PV system is attached [60]. Such an operation increases the magnitude of current in the corresponding feeder and results in additional power losses. To this end, BESS is considered as the key solution for improving system voltage performance due to its active power absorbing/delivering capability and fast response [7]. Although BESS costs are declining, most commercially available BESS options are still expensive and therefore, they should be operated in a way that ensures their prolonged lifetime [12].

There has been substantial growth in research and development of BESS grid applications in recent years. Moving-average based strategies are adopted in literature to control PV and BESS for voltage regulation [61, 62]. The moving-average method at an instant calculates an average of successive PV data samples and continues for the next instances. Since this method does not take into account any short-term forecast, it often fails to detect sudden ramps in PV power production and the associated abrupt voltage rise at the Point of Common Coupling (PCC). Co-ordinated control [63, 64] and rule-based [65] strategies are used to manage distributed energy storage for voltage rise mitigation. These methods require frequent BESS discharge (with several depth-of-discharge lengths) due to PV variability. Therefore, the aforementioned methods [63-65] introduce numerous micro-cycles besides full cycles of a BESS, which is a stress factor for BESS service life. Model predictive control has been used for energy management of distributed PV and BESS for customers' benefit in [66, 67].

In a nutshell, the main limitations of the aforementioned BESS control approaches are - firstly, the existing moving-average based methods do not use short-term PV forecast and therefore often fail to promptly mitigate sudden voltage rise. Secondly, the existing BESS control approaches require frequent micro-cycles to alleviate voltage rise issue and hence, put additional stress on BESS cycle-life. Thirdly, the vast majority of voltage regulation and storage management techniques that exist in literature lack the essential steps of experimental validation of their proposed approaches under realistic conditions. Therefore, *this thesis proposes a real-time forecast-based receding horizon control approach (named as RTF control) for BESS, which decides an appropriate charge rate to mitigate voltage rise during high PV power production while* *simultaneously ensuring that the rapid cycling of the BESS system can be reduced. The performance of the proposed method is tested on the hardware-in-the-loop setup containing RTDS and dSPACE under several operating situations.*

2.3.4 Aggregator's Coordinated Multi-Objective Control of Distributed BESS

DNOs manage their system voltage by installing necessary equipment, which often involves high costs. Typically, distribution voltage regulation is performed by OLTC at substations, SVR along feeders and fixed capacitors. Since the existing OLTCs and SVRs are not designed for voltage regulation under reverse power flow, they may malfunction in the case of high PV availability. Previously, the PV inverters were not allowed to actively participate in voltage regulation. In recent times, a limited reactive VAR support is allowed for the prospective inverters as per the revised IEEE 1547 standard. Controlling the reactive power of PV inverters can be a solution to mitigate voltage issues [5]. The main limitation of such an approach is that bigger sized inverters are required to deliver a specific amount of active power at a non-unity power factor.

BESS is a key to regulating distribution network voltage by controlling its real and reactive power. BESS can be beneficial for demand side management due to their capability of charging and discharging [7]. With several analyst reports predicting a rapid progression of the global BESS market, BESS are expected for home energy management in forthcoming years [8]. The utilisation of BESS is beneficial for customers through energy arbitrage or demand response incentives, while network operators can control the same BESS for voltage management. Therefore, central control of the distributed BESS inverters is essential to coordinate multiple BESS for voltage regulation, while DRAs can play a vital role to accomplish such tasks [7]. Figure 2.10 presents a typical radial distribution network with several houses with PV and BESS units. The BESS units are able to communicate with a DRA through a network, while the DRA manages the sending and receiving of relevant data accessed by smart meters.

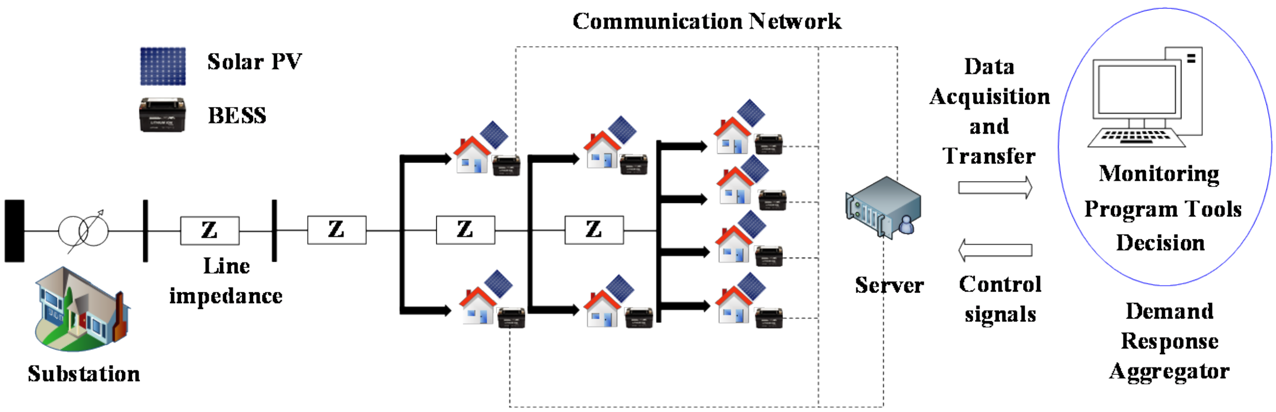

Figure 2.10 A typical control architecture of aggregating distributed resources

Recent studies indicate that DRAs can offer incentives to customers if allowing the load control for voltage regulation [58-62]. Direct load control is associated with minor inconvenience to customers. However, the use of PV and BESS enables indirect load control without causing much inconvenience to customers. The advantage of such methods is that customers can be benefitted from energy arbitrage or incentives. In addition, network operators can avoid installation of new voltage regulating devices by utilising aggregators' service through fixed term contracts.

Existing literature mostly focus on determining market policies of DRAs targeting maximum benefits from spot market [16-18]. Optimum voltage regulation through demand response is investigated, where BESS are utilised to flatten network voltage and control load disruption respectively [68, 69]. It is worth mentioning that such advanced voltage regulation methods require practical validation of their proposed approaches.

Some of the voltage control approaches that have used distributed inverter reactive power support are practically validated via HIL environment. The HIL simulation (combines RTDS and a test hardware) is performed for validation of voltage control approaches including droop control, PID and rule-based techniques in [70-74]. Voltage regulation is accomplished by reactive power control, where RTDS and dSPACE are used for realistic simulation in [75, 76]. Rule-based voltage control approach is validated using MATLAB and OPAL-RT based HIL set-up and a 34 node system is used for case studies in [77]. However, these approaches do not consider any optimum voltage regulation technique. Optimum voltage regulation using OLTC, plug-in electric vehicles and PV inverters is achieved and validated via HIL simulation using OPAL-RT, where the major concern is to maximise the energy delivery to electric vehicle owners in [19].

To sum up, as the uptake of BESS at the distribution level ramps up, their use for voltage regulation applications is frequently claimed as an option. Nevertheless, when customers leverage their BESS capacity for voltage regulation it comes at the expense of their planned arbitrage resulting in costs (disutility) to customers. The existing optimum voltage regulation approaches often do not directly take this into account. To meet this gap, *a generalised mathematical model for the cost of voltage regulation with BESS is formulated as a function of customers' disutility and system voltage, which are utilised to formulate an optimisation problem to search for feasible and cost-effective BESS charge-discharge trajectories. Therefore, distribution voltage is regulated through a coordinated effort of a system operator and a DRA, while a DNO pays to DRAs for their service via a short/long term contract unlike existing methods. The effectiveness of the proposed method is tested via HIL environment comprising RTDS and dSPACE through several practical cases.*

2.4 Summary

The key technical challenges due to prolific solar photovoltaic generation in power distribution systems are presented in this chapter. The major issues include the reformation of load curves, voltage rise, fluctuations and reverse power flow. A clear insight of the applicability of battery storage systems to resolve these issues is exhibited. Existing literature indicates several integration challenges of BESS for grid applications under substantial solar PV availability. The foremost challenges are related to – i) appropriate BESS sizing and siting ii) design of BESS controllers considering their lifetime iii) optimum voltage regulation framework with distributed BESS iv) practical validation of the developed BESS control methods. Based on the detailed literature review, four research gaps are identified.

To address the specific research gaps, a generic model for deciding appropriate sizes, locations and charging patterns of BESS for a network upgrade deferral through peak shaving will be developed. The model should offer network investment deferral using peak shave, load growth rate and discount factor for a specific planning horizon. The model will be further improved by incorporating voltage regulation constraints, while relevant case studies will be executed under several realistic PV and load profiles. Next, a detailed analysis will be accomplished on steady state voltage assessment of a segment of Queensland distribution network with a high share of solar PV. Based on the study, the allowable export limit from a new PV connection will be determined. Later, suitable BESS charging strategies will be proposed to improve voltage performance of unbalanced distribution networks. Afterward, a real-time forecast-based receding horizon control approach will be developed, which should be able to decide appropriate set points of BESS to mitigate voltage rise during high PV generation while simultaneously ensuring that the rapid cycling of BESS can be reduced. In the next stage, a generic voltage regulation tool with distributed BESS will be developed under a demand response framework. Both of the control methods will be practically validated via hardware-in-the-loop set-up.

Chapter 3 A Generic Approach of BESS Sizing and Placement for Distribution Network Management

Widespread deployment of distributed intermittent renewable generators, rapidly rising peak demand and reductions in the price of batteries instigate the use of BESS in power networks. While BESS can be advantageous to tackle several technical issues of distribution systems, the best possible sizing, location and usage govern the financial viability. The ratings of distribution network components such as transformers and lines are designed to match the maximum peak load specified for a planning horizon. Due to the ever growing peak demand, periodic reinforcement of system components is essential for reliable power delivery to customers. Clearly such solutions, usually termed as *network solutions*, involve considerable expenditure. An alternative is to device *non-network solutions* that defer or eliminate the need for network solutions. The use of BESS units, as a *non-network solution,* is a promising option provided they are properly sized, located and managed. Furthermore, the impact of reverse power flow caused by high photovoltaic generation can be nullified through BESS charging. Therefore, the best possible size, location and charging strategy of BESS are of utmost importance for a distribution network operator[1].

The existing approaches of determining an appropriate BESS sizing and siting are mainly focussed on network loss minimisation, while network upgrade deferral is treated as an economic input-output problem [45, 47, 49-51]. However, these approaches lack the capability of representing technical characteristics (e.g. thermal limit, peak shave, PV penetration etc.) of a network. In addition, they are not generic enough to be applicable to any distribution systems. Therefore, the need of a generic tool for a network upgrade with BESS persists, which considers several parameters such as peak shave, load growth rate, discount factor and PV penetration level [78]. The main contributions of this chapter are listed as follows.

(i) A model for net profit from investment deferral is proposed. The model expresses investment deferral as a function of peak load growth rate, peak shave, arbitrage and BESS size and

[1] This chapter has significant materials from the following articles published by the PhD candidate.

- S. R. Deeba, R. Sharma, T. K. Saha, D. Chakraborty and A. Thomas, "Evaluation of technical and financial benefits of battery-based energy storage systems in distribution networks," *IET Renewable Power Generation,* vol. 10, pp. 1149-1160, 2016.
- S. R. Deeba, R. Sharma, T. K. Saha and D. Chakraborty, "A tool to estimate maximum arbitrage from battery energy storage by maintaining voltage limits in an LV network," in *IEEE PES Asia-Pacific Power and Energy Engineering Conference (APPEEC)*, 2015, pp. 1-5.

location. As a result, unlike the existing techniques, the proposed approach provides sufficient flexibility to model the network upgrade deferral for any distribution networks and not just for the one considered in this thesis.

(ii) The investment deferral model is used to formulate an optimisation problem to search for the most cost-effective sizing and placement of BESS units in order to defer system upgrade. It also determines the optimum charging patterns of storage via multi-period optimal power flow analysis. Based on the results, a potential policy is proposed for interaction between a DNO and retailers so that batteries can be utilised to get energy arbitrage.

(iii) The proposed approach is applied to a section of an Australian distribution system. The effect of rooftop PV penetration level on the size, location and dispatch schedules of BESS is investigated.

(iv) The developed approach is further modified for voltage regulation by utilising BESS real and reactive power in distribution systems. The modified tool is applied to a Low Voltage (LV) system under various clustered load and solar PV profiles in a year. The modification of the proposed approach is targeted to easily estimate maximum yearly energy arbitrage and near optimum charging patterns of BESS for residential customers keeping all bus voltages within acceptable limits in a PV prolific distribution network.

In the subsequent sections, the proposed approaches and relevant case studies are thoroughly described. The nomenclature section in the end of the chapter explains all relevant variables, indices, sets and constants.

3.1 Problem Formulation

This section describes mathematical models of network upgrade deferral and power flow in a distribution system. These models are used in the formulation of the BESS sizing and location optimisation problem.

3.1.1 Modelling Network Upgrade Deferral

Expenditure for distribution network reinforcement is associated with distribution lines and power transformer costs. The time period before which network reinforcement may become necessary depends on the unutilised capacity of a network and the rate of peak load growth. A DNO has to foresee and plan for reinforcement before network components reach their thermal limits. If peak load increases, network components will steadily approach their thermal limits. Therefore, reduction in peak load has a direct impact on the prolongation of the lifetime of network components (e.g. distribution lines and transformers). Consequently, network reinforcement deferral entails peak shaving.

Assume that a network component l has a capacity of C_l and power flow through it during peak load is D_l. Thus, the number of years (y_1) required to reach C_l from D_l at a yearly peak load growth rate of g is given by (3.1) [79].

$$C_l = D_l \,.\, (1+g)^{y_1} \tag{3.1}$$

Taking logarithm of (3.1), y_1 can be written as

$$y_1 = \frac{\log C_l - \log D_l}{\log(1+g)} \tag{3.2}$$

Now assume that a DNO installs BESS units in a network to reduce the peak demand by ΔP_l. As a result, the new peak demand becomes ($D_l - \Delta P_l$). Let y_2 be the number of years required for component l to reach its maximum rating (C_l), then (3.1) takes the following form:

$$y_2 = \frac{\log C_l - \log(D_l - \Delta P_l)}{\log(1+g)} \tag{3.3}$$

It is to be noted that $y_2 > y_1$ and the number of deferred years to upgrade a network deploying BESS is ($y_2 - y_1$).

The network reinforcement cost (*expenditure*) consists of the capital cost of the transformer and feeder upgrade. The present value of future expenditure is given by (3.4) [79].

$$PresentValue_{original} = \frac{expenditure}{(1+d)^{y_1}} \quad ; d = \text{discount rate} \tag{3.4}$$

Accordingly, the present value of the expenditure after placing BESS is expressed as follows.

$$PresentValue_{new} = \frac{expenditure}{(1+d)^{y_2}} \tag{3.5}$$

Using (3.4) and (3.5), the change of the present value (ΔPW) of future expenditure is expressed by (3.6).

$$\Delta PW := PresentValue_{original} - PresentValue_{new} = expenditure \,.\, \left[\frac{1}{(1+d)^{y_1}} - \frac{1}{(1+d)^{y_2}}\right] \tag{3.6}$$

Reduction of (3.6) provides the following relationship between the deferred number of years ($y_2 - y_1$), peak shave fraction $\left(x = \dfrac{\Delta P_l}{D_l}\right)$ and ΔPW:

$$\Delta PW = expenditure \,.\, (1+d)^{-y_1} \,.\, \left\{1 - (1+d)^{-(y_2 - y_1)}\right\} \tag{3.7}$$

Furthermore, using (3.2) and (3.3), ($y_2 - y_1$) can be expressed by (3.8).

$$y_2 - y_1 = -\frac{\log(1-x)}{\log(1+g)} \;\; ; \; x = \frac{\Delta P_l}{D_l} \tag{3.8}$$

Finally, by substituting (3.8) in (3.7), an expression for the network upgrade deferral is obtained as follows:

$$\Delta PW(x, g) = K.\{1-(1-x)^{ab}\} \tag{3.9}$$

where $K =$ *expenditure.* $(1+d)^{-y_1}$, $a = \dfrac{1}{\log(1+g)}$ and $b = \log(1+d)$.

For a fixed ΔP_l (obtained from a given BESS capacity), $(y_2 - y_1)$ reduces with an increasing load growth rate. Therefore, in order for a BESS utilisation to be economically viable, it should reach cost parity within $(y_2 - y_1)$ years because network load will exceed its capacity C_l beyond this time interval.

Assume that the discount rate (d) is 3% and the peak load growth rate (g) varies up to 3% [80]. Consequently, the magnitude of ab is greater than 1. If peak shave fraction (x) is up to 5%, the higher order terms (2nd order and onward) of Taylor Series expansion of (3.9) can be neglected.

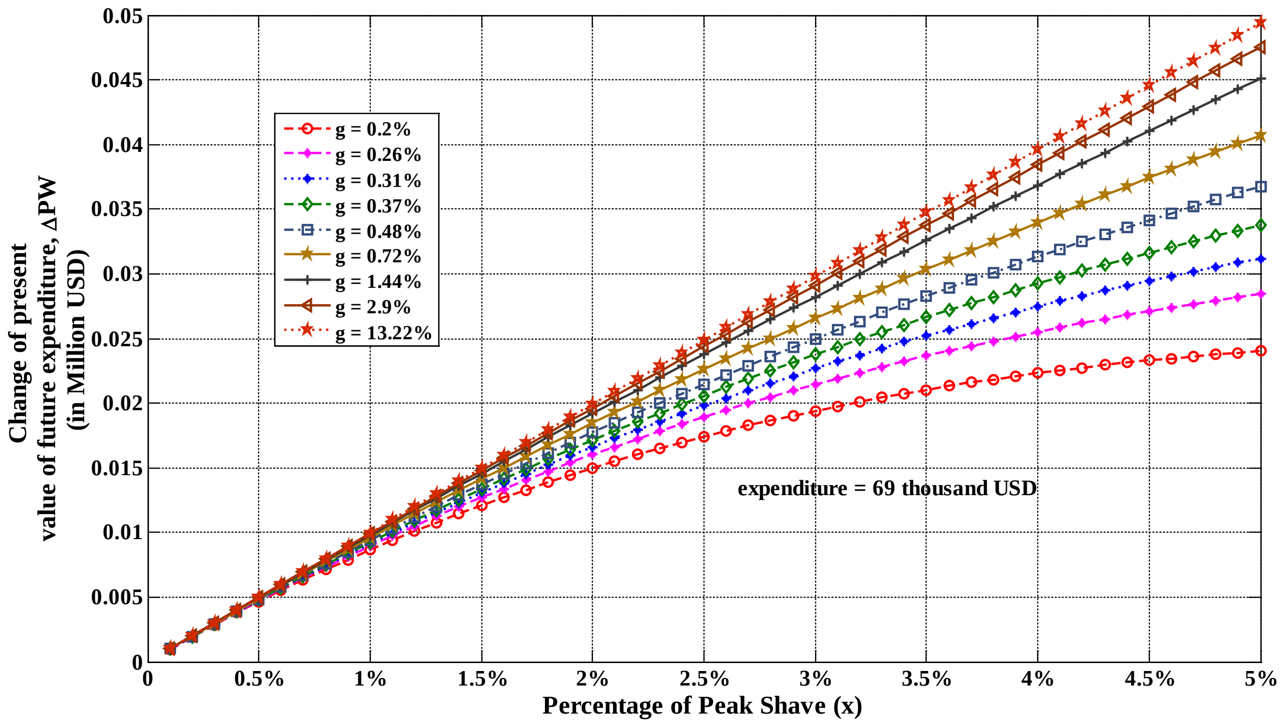

Figure 3.1 ΔPW vs. peak shave fraction (x) for different load growth rates (g) [78]

Figure 3.1 presents the correlation between ΔPW and x for different load growth rates. It is observed that if x varies up to 2.5%, the relationship between ΔPW and x is approximately linear at all load growth rates (g). However, ΔPW vs. x curves exhibit linear trends if growth rate is more than 0.48% and x varies up to 5%. Therefore, (3.9) is approximated as a linear function of x and g by taking the first order term of Taylor Series expansion, which is presented by (3.10).

$$\Delta PW(x, g) = K_1.x \quad ; K_1 = K.a.b \tag{3.10}$$

3.1.2 Power Flow Model for a Distribution Network

A distribution network is considered with u number of buses and indexed by the set N:=[1, 2, . . , u]. Let $\beta^{u \times u}$ be the susceptance matrix for the u bus system. Let the number of loads in the network be represented by s such that $s \leq u$ and at most one load is connected to each bus. Let H be the set of buses through which the network is connected to the grid such that $H \subseteq N$. A daily load profile is considered for the formulation, where demand data are given for every 30 minutes. Therefore, the time interval for each sample is given as Δt = 0.5 hour. A 24-hour optimal power flow (OPF) problem is formulated so that the proposed approach provides the flexibility to study several daily load curves separately or collectively as a part of annual data.

The active power import from the grid at j^{th} bus and n^{th} sampling instant is denoted by $P^G(j,n)$ and is limited by the following constraint.

$$P^{\min}(j) \leq P^G(j,n) \leq P^{\max}(j) \quad ;\forall \quad j \in H,\, n \in [1,48] \tag{3.11}$$

where $P^{\min}(j,n)$ and $P^{\max}(j,n)$ indicate the minimum and the maximum active power import limits respectively.

Furthermore, let the allocated locations for BESS installation in the system be indexed by P such that $P \subseteq N$, with at most one BESS permitted at each bus. The rate of charge and discharge of a BESS at n^{th} sample, which is located at j^{th} bus, is limited by the following inequalities:

$$r^{d\min}(j) \leq r^d(j,n) \leq r^{d\max}(j) \quad ;\forall \quad j \in P,\, n \in [1,48] \tag{3.12}$$

$$r^{c\min}(j) \leq r^c(j,n) \leq r^{c\max}(j) \quad ;\forall \quad j \in P,\, n \in [1,48] \tag{3.13}$$

where $r^d(j,n)$ and $r^c(j,n)$ represent the discharge and charge rates of BESS respectively. $r^{d\min}(j,n)$ and $r^{d\max}(j,n)$ present the minimum and the maximum discharge rates, while $r^{c\min}(j,n)$ and $r^{c\max}(j,n)$ present the minimum and the maximum charge rates respectively. The charge and discharge rates are defined by the absorbed and delivered power by the BESS in p.u. considering the network rated kVA as the base value.

BESS discharge and charge rates are equal to zero if j^{th} bus is not an allocated location for BESS. Therefore,

$$\left.\begin{array}{l} r^{d}(j,n) \\ r^{c}(j,n) \end{array}\right\} = 0 \quad ;\forall\, j \notin P \tag{3.14}$$

The balance of energy of the BESS located at j^{th} bus at a days end can be represented as

$$\sum_{n=1}^{48} \{r^{d}(j,n) - r^{c}(j,n)\}.\,\Delta t \le 0 \quad ;\forall\, j \in P \tag{3.15}$$

It is assumed that the BESS is operating at its rated voltage consistently. Moreover, the same charge and discharge efficiencies of the BESS are considered.

The state of charge is defined as the state of energy in a BESS at an instant, while it is modelled as (3.16) by using (3.15) and [46]. The state of charge of a BESS at n^{th} sampling instant can be obtained from (3.16).

$$SoC(j,n+1) = SoC(j,n) - \{r^{d}(j,n) - r^{c}(j,n)\}.\Delta t \quad ;\forall\, j \in P \tag{3.16}$$

where state of charge (SoC) is expressed in p.u. considering the rated kWh of BESS as the base value.

The network's active power flow constraint at j^{th} bus and at n^{th} sampling instant is expressed as follows.

$$\begin{aligned} P^{G}(j,n) + r^{d}(j,n) - r^{c}(j,n) - P^{d}(j,n) = \sum_{m=1}^{u} \beta(j,m)\{\theta(j,n) - \theta(m,n)\} \\ + P_{Loss}(n) \quad ;\forall\, j \in N \end{aligned} \tag{3.17}$$

where $P^{d}(j,n)$ indicates the net load (load minus PV) and $\theta(j,n)$ represents the voltage angle at j^{th} bus and n^{th} sampling instant. The power flow expression in (3.17) is known as dc load flow and is obtained after simplification of the fast decoupled load flow method [81]. Active power flow from j^{th} to m^{th} bus $\left(\sum_{m=1}^{u} \{\beta(j,m)\ \{\theta(j,n) - \theta(m,n)\}\right)$ is a linear function of bus voltage angle, $\theta(j,n)$. Time varying line loss is expressed by $P_{Loss}(n)$ and is estimated as 3% of total active power flow $P^{G}(j,n)$ of the system under consideration. The reactive power balance at j^{th} bus and at n^{th} sampling instant can be expressed by (3.18).

$$Q^{G}(j,n) + Q^{B}(j,n) - Q^{d}(j,n) = \mathrm{Im}\{V(j,n).\,I^{*}(j,n)\} \quad ;\forall\ j \in N,\, n \in [1,48] \tag{3.18}$$

where

$Q^{G}(j,n)$ = Reactive power import from grid

$Q^{B}(j,n)$ = Reactive power absorbed/ delivered by j^{th} BESS

$Q^{d}(j,n)$ = Reactive load at j^{th} bus

$I(j,n)$ = Injected current at j^{th} bus

Nevertheless, the developments in the ensuing sections assume that BESS is capable of exchanging active power only. This is consistent with the main objective of this work, which is to achieve network upgrade deferral through peak shaving. Consequently, the reactive power balance as shown in (3.18) is not included in the proposed model.

3.1.3 Formulation of the Objective Function

Having modelled the savings from network reinforcement deferral and technical constraints associated with distribution networks, the next task is to formulate an objective function that captures the trade-off between the savings earned by a DNO and expenditure due to the installation of BESS. This objective function is to be used in the formulation of a DNO's profit maximisation problem.

The profit earned by a DNO is governed by the difference of present value of future investment ($\Delta PW(x, g)$), benefit from energy arbitrage (X_{TOU}) and the capacity cost of BESS. That is, the net profit of a DNO over a $(y_2 - y_1)$ time period is given by

$$Net\ profit = \Delta PW\left(x,g\right) + X_{TOU} + Capacity\ Cost\ of\ \ BESS \tag{3.19}$$

In (3.19), the energy arbitrage that comes from Time of Use (TOU) electricity price is denoted by X_{TOU} and is expressed as

$$X_{TOU} = \begin{cases} 0 & ;\ \text{flat rate} \\ cycles.\sum\limits_{n=1}^{48}\sum\limits_{j=1}^{u}\{(r^{d}(j,n) - r^{c}(j,n)).\,price(n)\}; & \text{variable rate} \end{cases} \tag{3.20}$$

where *cycles* represents the number of charge/discharge cycles used from a BESS (maximum life cycle varies typically between 1800 to 2500 depending on the type of batteries [46]). In order to shave peak, the BESS units will typically charge during off-peak times from the grid and discharge during peak-times. Since the operation of BESS will potentially involve the purchase of power; a DNO may need to involve a retailer to purchase the required energy in order to charge a BESS [47]. Retailers can offer several electricity tariff schemes (i.e. flat rate or TOU) to their customers, which are controlled by policies set by regulatory frameworks. Nevertheless, the interaction between a retailer and a DNO is likely to vary from country to country. In this study, analyses are performed assuming the provision of X_{TOU} pricing in the regulatory framework.

Using (3.20), the net profit given by (3.19) can be expressed as

$$Net\ profit = \Delta PW(x,g) + J\left(r^d(j,n), r^c(j,n)\right) \tag{3.21}$$

where

$$J(r^d(j,n), r^c(j,n)) = \sum_{n=1}^{48}\sum_{j=1}^{u}\{cycles.(r^d(j,n)-r^c(j,n)).\,price(n)\} - \sum_{n=1}^{48}\sum_{j=1}^{u}\left(\frac{B_{cap}}{\eta}.\ r^d(j,n).\Delta t\right) \tag{3.22}$$

In (3.22), B_{cap} and η represent the capacity cost ($ per kWh) and round-trip efficiency of BESS. It is worth mentioning that efficiencies related to charge and discharge of a BESS are not considered, rather a round-trip BESS efficiency is used in this model. This is due to the fact that the optimisation tool is meant to estimate the sizing, siting and an expected scheduling of BESS, while roundtrip efficiency is able to serve the purpose. Summation of $r^c(j,n)/\eta$ over 24 hours (48 time samples) indicates the size of j^{th} BESS. For a given load growth rate, ΔPW depends only on peak shave fraction (x). The power delivered by BESS at the time of system peak directly contributes to the amount of peak shave. Assuming that a system peak occurs at n=v (at the v^{th} time sample), with $P^{\max}(j)$ and $P^G(j,v)$ expressed in per unit, x can be written as

$$x = \sum_{j \in H}(P^{\max}(j) - P^G(j,n)) \quad ;\forall\, n = v \tag{3.23}$$

The overall objective is to find such size and location for BESS that maximises net profit given by (3.21)-(3.22) while keeping in view the network constraints. Noting that for a particular load growth rate g and a chosen peak shave x, ΔPW is fixed. Therefore, in order to maximise the profit for an appropriate size and location of BESS, the following optimisation problem is to be solved for specified values of g and x:

$$\underset{\substack{r^d(j,n),\ r^c(j,n),\\ P^G(j,n),\ \theta(j,n)}}{Maximise} \quad J\left(x, g, r^d(j,n), r^c(j,n)\right) \tag{3.24}$$

Subject to

$$\begin{aligned} P^G(j,n) + r^d(j,n) - r^c(j,n) - P^d(j,n) = {} & \sum_{m=1}^{u}\left\{\beta(j,m).(\theta(j,n) - \theta(m,n))\right\} \\ & + P_{Loss}(n) \quad ;\forall\, j \in N \end{aligned} \tag{3.25}$$

$$\sum_{n=1}^{48}\{r^d(j,n) - r^c(j,n)\}.\,\Delta t \le 0 \quad ;\forall\, j \in P \tag{3.26}$$

$$P^{\min}(j) \le P^G(j,n) \le P^{\max}(j) \quad ;\forall\, j \in H,\ n \in [1,48] \tag{3.27}$$

$$r^{d\min}(j) \le r^{d}(j,n) \le r^{d\max}(j) \quad ;\forall \; j \in P,\, n \in [1,48] \tag{3.28}$$

$$r^{c\min}(j) \le r^{c}(j,n) \le r^{c\max}(j) \quad ;\forall \; j \in P,\, n \in [1,48] \tag{3.29}$$

$$SoC(j,n+1) = SoC(j,n) - \{r^{d}(j,n) - r^{c}(j,n)\}.\Delta t \;\; ;\forall \; j \in P,\, n \in [1,48] \tag{3.30}$$

$$SoC^{\min}(j) \le SoC(j,n) \le SoC^{\max}(j) \quad ;\forall \; j \in P,\, n \in [1,48] \tag{3.31}$$

where the minimum and maximum state of charge of BESS are denoted by $SoC^{\min}(j)$ and $SoC^{\max}(j)$ respectively.

Traditionally, OPF is static and can be independently solved at each time slot. However, the inclusion of BESS constraints expressed in (3.26) and (3.30) require optimisation across time. The problem defined in (3.25)-(3.31) is solved for 48 time samples in a day by using linear programming. That is, a multi-period OPF has been solved. The objective function is maximised to obtain feasible values of all variables, namely, $r^{d}(j,n)$, $r^{c}(j,n)$, $P^{G}(j,n)$ and θ (*j*, *n*). Day-ahead charge and discharge rates of BESS are obtained from the values of variables $r^{d}(j,n)$ and $r^{c}(j,n)$. Possible BESS locations presented by set *B* are given as initial inputs to solve the formulated problem. For a given j^{th} bus, if the optimisation results in zero values of the variables $r^{d}(j,n)$ and $r^{c}(j,n)$, that location is not chosen for BESS siting. Therefore, the best location of BESS is determined from the non-zero values of variables $r^{d}(j,n)$ and $r^{c}(j,n)$. Finally, the optimal size of BESS at j^{th} bus is calculated by using the following expressions.

$$\sum_{n=1}^{48} r^{c}(j,n).\Delta t / \eta \quad ;\forall \; j \in P \tag{3.32}$$

$$\sum_{n=1}^{48} r^{d}(j,n).\Delta t / \eta \quad ;\forall \; j \in P \tag{3.33}$$

It is to be mentioned that the sizing and siting optimisation of BESS for network upgrade deferral is a planning problem and should be executed offline. Therefore, the proposed optimisation based method is not meant to perform in real-time.

3.2 System Description and Simulation Cases

This section presents a brief description of the studied power system and simulation cases.

3.2.1 System Description

In this chapter, a segment of the primary distribution network from the Queensland, Australia, where the voltage level is 11 kV line-to-line is studied. It is connected to an infinite bus at node N631 as shown in Figure 3.2. The network has 869 nodes, 876 branches, 387 load buses and 3 voltage regulating transformers. Although the entire network is used in simulation to determine the best possible size and locations of BESS units, only nodes that are close to their capacity limit are highlighted in the schematic as shown in Figure 3.2. The total length of the network is 197 circuit-km. The total peak and base loads are 20 MW and 3 MW respectively. Table 3.1 shows the lengths of the heavily loaded feeders and the corresponding resistances and reactances. As shown in Table 3.1, the system feeders consist of different R/X ratios such as 0.5, 1.2, 2, 3, 4, 5, 8, 9, 12, 15 and 30. The wide variation in R/X ratios occurs due to different types of conductors.

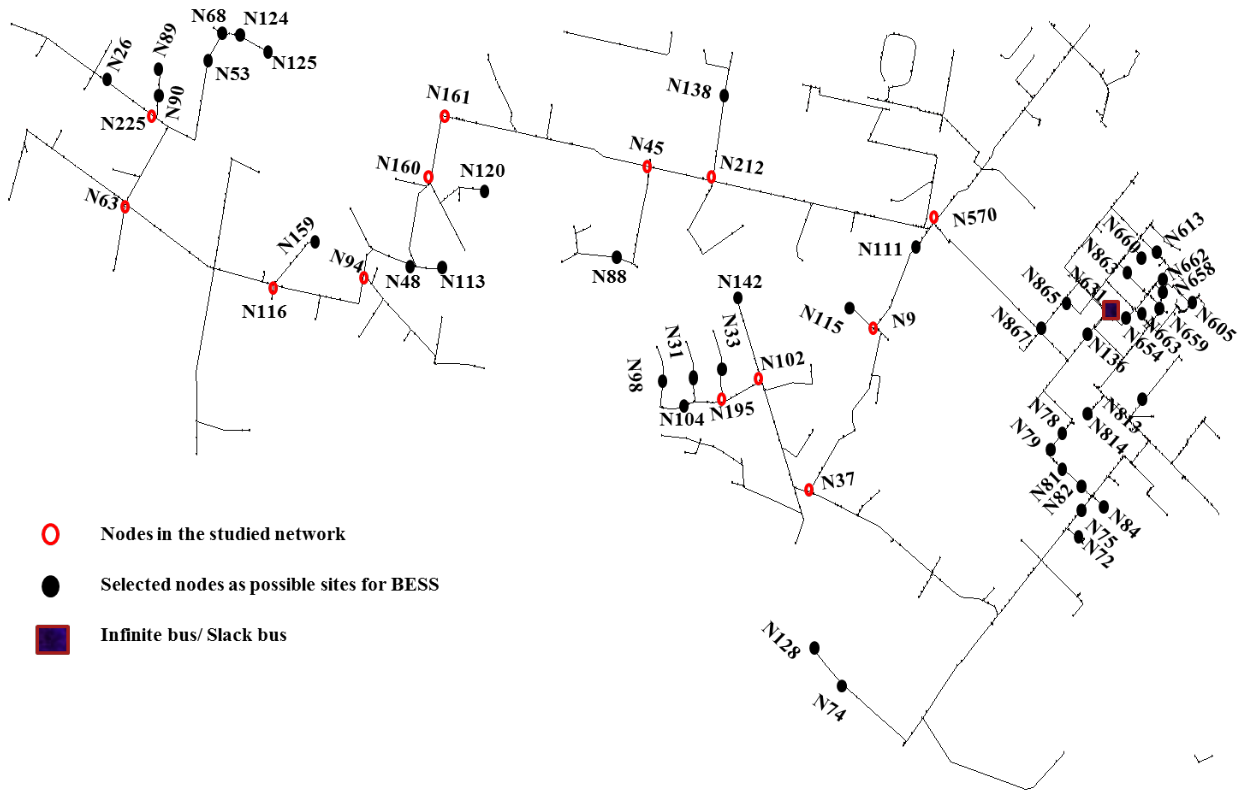

Figure 3.2 Schematic diagram of the studied 11-kV network [78]

Table 3.1 Line parameters of the heavily loaded feeders [78]

From Node	To Node	Line Length	R (Resistance/ unit length)	X (Reactance/ unit length)	R/X Ratio
N631	N654	0.21	0.06	0.16	0.38
N631	N136	0.05	0.06	0.16	0.38
N654	N663	0.16	0.17	0.33	0.52
N663	N659	0.24	0.56	0.38	1.47

N659	N658	0.29	0.56	0.38	1.47
N659	N605	0.29	0.56	0.38	1.47
N658	N662	0.30	1.90	0.38	5.00
N662	N613	0.24	0.56	0.38	1.47
N631	N863	0.30	1.90	0.38	5.00
N863	N660	0.24	0.56	0.38	1.47
N660	N613	0.16	0.17	0.33	0.52
N631	N865	0.16	0.17	0.33	0.52
N865	N867	0.30	1.90	0.38	5.00
N813	N814	0.30	1.90	0.38	5.00
N867	N570	1.50	0.56	0.38	1.47
N570	N111	0.06	0.45	0.37	1.22
N111	N9	0.93	0.17	0.33	0.52
N9	N115	0.35	4.10	0.42	9.76
N9	N37	1.80	0.17	0.33	0.52
N37	N102	0.98	0.73	0.38	1.92
N102	N142	0.86	0.73	0.38	1.92
N102	N195	0.40	0.73	0.38	1.92
N195	N33	0.40	0.73	0.38	1.92
N195	N104	0.40	0.73	0.38	1.92
N104	N31	0.35	0.73	0.38	1.92
N104	N98	0.25	0.73	0.38	1.92
N570	N212	2.70	0.37	0.35	1.06
N212	N45	0.65	0.29	0.35	0.83
N212	N138	0.30	1.50	0.42	3.57
N45	N88	1.62	1.78	0.39	4.56
N45	N161	2.30	0.55	0.44	1.25
N161	N160	0.68	1.50	0.42	3.57
N160	N120	0.65	12.50	0.41	30.49
N160	N48	0.88	0.56	0.44	1.27
N48	N113	0.32	1.78	0.39	4.56
N48	N94	0.79	1.97	0.39	5.05
N94	N116	1.16	0.56	0.37	1.51
N116	N159	0.48	1.50	0.42	3.57
N116	N63	1.85	0.56	0.37	1.51
N63	N225	0.48	1.50	0.42	3.57
N225	N90	0.48	1.50	0.42	3.57
N90	N89	1.85	0.56	0.37	1.51
N90	N53	1.85	0.56	0.37	1.51
N53	N68	1.85	0.56	0.37	1.51
N68	N124	1.85	0.56	0.37	1.51
N124	N125	1.85	0.56	0.37	1.51

N225	N26	1.85	0.56	0.37	1.51
N75	N74	3.75	0.56	0.37	1.51
N75	N72	3.75	0.56	0.37	1.51
N75	N84	3.75	0.56	0.37	1.51
N74	N128	0.48	0.56	0.37	1.51
N84	N81	0.48	0.56	0.37	1.51
N81	N82	0.48	0.56	0.37	1.51
N81	N79	0.48	0.56	0.37	1.51
N78	N79	0.48	0.56	0.37	1.51

3.2.2 Case Studies

Two case studies, namely, case study-1 and case study-2 are performed in Section 3.3. PV penetration level is defined as the ratio between PV capacity and base load in the network. Case study-1 involves a low PV penetration level (10%), which represents the current scenario. Case study-2 considers high PV penetration (40%) and captures the future growth in PV uptake whose possible locations are specified by the DNO. PV units are placed in 4 and 13 locations for case studies-1 and 2 respectively. Table 3.2 presents the peak load and PV capacity at each node for both cases. There are 42 heavily loaded nodes in the system and these sites are selected as possible options to place BESS. The possible BESS locations are highlighted in Figure 3.2 and listed in Table 3.2.

Table 3.2 Capacities and locations of PV Sources in the network for two case studies [78]

Node	Peak Load (kW)	PV Capacity (kW)		Index of Possible Location of BESS
		Case Study-1 (10% Penetration)	Case Study-2 (40% Penetration)	
N9	0	No PV	No PV	No
N26	50	30	30	B1
N31	10	No PV	10	No
N33	10	No PV	10	No
N37	0	No PV	No PV	No
N45	0	No PV	No PV	No
N48	100	40	40	B2
N53	50	40	40	B3
N63	0	No PV	No PV	No
N68	100	No PV	No PV	B4
N72	200	150	150	B5
N74	150	No PV	30	B6
N75	200	No PV	No PV	B7
N78	200	No PV	No PV	B8

N79	320	No PV	No PV	B9
N81	100	No PV	40	B10
N82	200	No PV	80	B11
N84	200	No PV	80	B12
N88	200	No PV	80	B13
N89	20	No PV	No PV	B14
N90	100	No PV	No PV	B15
N94	0	No PV	No PV	No
N98	50	No PV	No PV	B16
N102	0	No PV	No PV	No
N104	63	No PV	No PV	B17
N111	63	No PV	No PV	B18
N113	100	No PV	No PV	B19
N115	100	No PV	No PV	B20
N116	0	No PV	No PV	No
N120	100	No PV	No PV	B21
N124	100	No PV	No PV	B22
N125	200	No PV	No PV	B23
N128	63	No PV	No PV	B24
N136	100	No PV	No PV	B25
N138	63	No PV	No PV	B26
N142	63	No PV	No PV	B27
N159	500	No PV	No PV	B28
N160	0	No PV	No PV	No
N161	0	No PV	No PV	No
N195	0	No PV	No PV	No
N212	0	No PV	No PV	No
N570	0	No PV	No PV	No
N605	500	No PV	150	B29
N613	500	No PV	No PV	B30
N631	500	No PV	No PV	B31
N654	500	No PV	No PV	B32
N658	750	No PV	No PV	B33
N659	750	No PV	No PV	B34
N660	750	No PV	No PV	B35
N662	750	No PV	No PV	B36
N663	500	No PV	No PV	B37
N813	1000	No PV	340	B38
N814	500	No PV	No PV	B39
N863	750	No PV	No PV	B40
N865	750	No PV	No PV	B41
N867	750	No PV	No PV	B42

Table 3.3 shows the values of input parameters for solving (3.24)-(3.31), which are used in case studies-1 and 2. Based on the local trends, the peak load growth rate is considered as 0.48% for both studies [82]. The peak load growth rate depends on the economic and social situations of a particular place. By using the present ratings of network components and load growth rate, y_1 is calculated from (3.2). The typical cost to upgrade with new feeders is assumed as $70,000/km and transformer cost is $28,800 for a 100 kVA unit [79]. The value of *K* in (3.10) is calculated by using the parameters *g*, *a* and *b* as given in Table 3.3.

Table 3.3 Input parameters for case studies -1 and 2 [78]

Parameters	**Case Study - 1 and 2**
Feeder upgrade cost	US$ 70,000 per km [79]
100 kVA transformer cost	US$28, 800 [79]
K	$1159029.126
g	0.48%
x	4%
a	854
b	0.012837225
$r^{d\min}$, $r^{d\max}$	0, 0.008 p.u.
$r^{c\min}$, $r^{c\max}$	0, 0.008 p.u.
$P^{\min}$	0 p.u.
$P^{\max}$	1 p.u.
B_{cap} ($/kWh)	1000 (lithium-ion)
cycles	2000 (lithium-ion) [46]
SoC^{min}	0.3 [46]
SoC^{max}	0.9 [46]
$SoC(j, n=1)$	0.4 (initial state of charge)

Maximum charge/discharge rates of each battery are chosen in such a way that the total power flow through each line does not exceed the corresponding cable ratings. The case studies are performed for lithium-ion BESS considering a conservative capacity cost $1000 per kWh [46]. Usually, lithium-ion battery experiences capacity reduction over time depending on its depth-of-discharge. Along the line, the expected life cycle of lithium-ion is assumed to be 2000 in Sections 3.2 and 3.3. While solving (3.24)-(3.31), the initial state of charge for each BESS is assumed as 40% for both studies. The minimum and maximum limits of state of charge constraints are assumed as 30% and 90% respectively [46].

3.2.3 Load and PV Data

One-year load and PV data of the studied system are collected from a local DNO [82, 83]. This load data is used to generate 12 representative scenarios including peak, average and low load profiles for each of the four seasons (summer, winter, autumn and spring) [83]. A representative PV profile is selected, which involves periods of intermittent generation and is scaled for different PV locations based on their installed capacities. The 12 representative load profiles and day-ahead electricity price are shown in Figure 3.3. The optimisation problem (3.24)-(3.31) is individually repeated for each of the 12 load profiles for both cases using CPLEX solver in the Generic Algebraic Modelling System (GAMS) platform [84]. Full details of the simulation results are presented in Section 3.3.

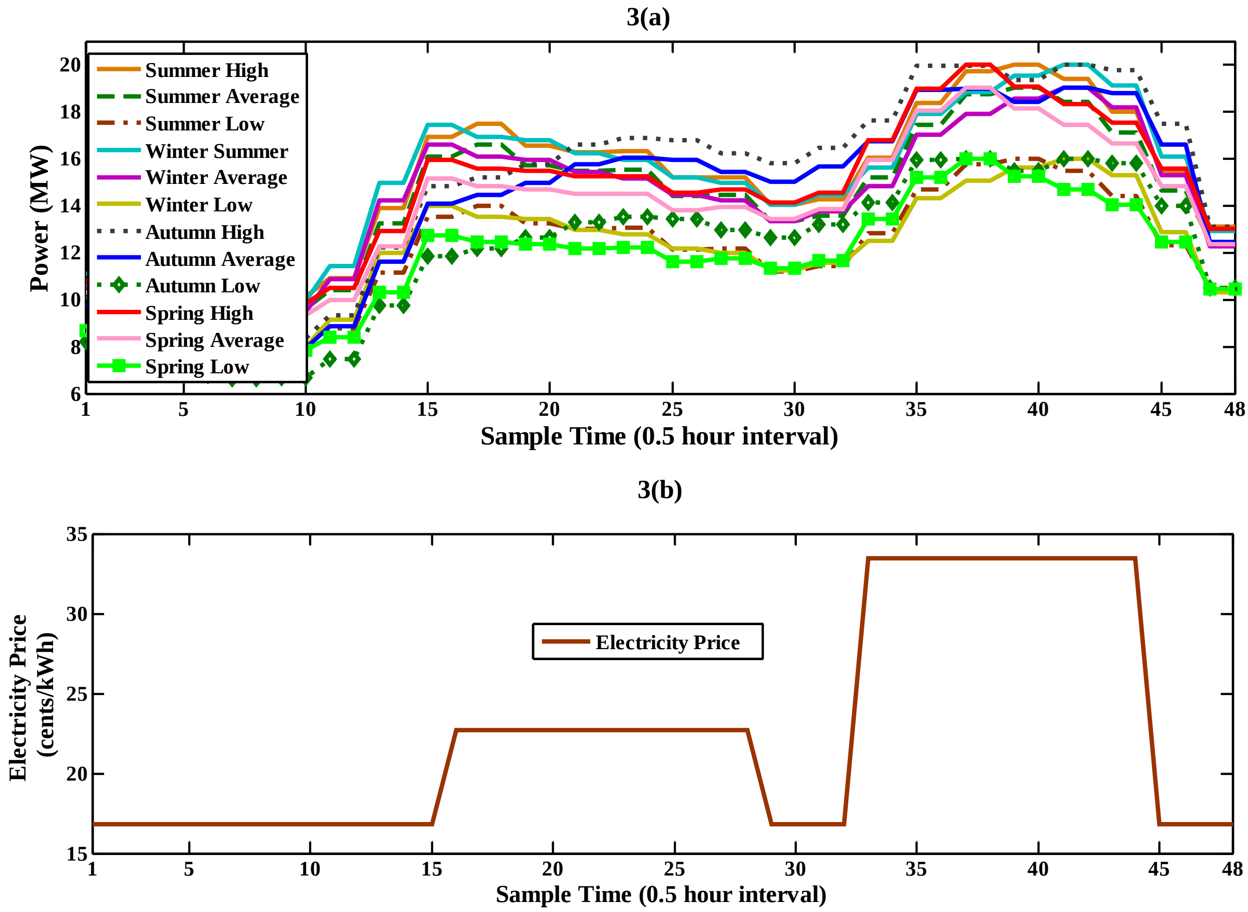

Figure 3.3 (a) Representative load profiles used in case studies (b) Day-ahead electricity TOU price [78]

3.3 Simulation Results and Analysis

This section presents simulation results for case studies-1 and 2. The effects of load growth rate and BESS capacity on network upgrade deferral are investigated and discussed. In the results of this section, BESS power is shown from the AC side of the inverter. This is because for a grid-connected BESS, the ac power exchange at the point of common coupling affects the overall power flow in a network. Therefore, the dc side power is not shown in the results.

3.3.1 Case Study – 1 (10% PV Penetration)

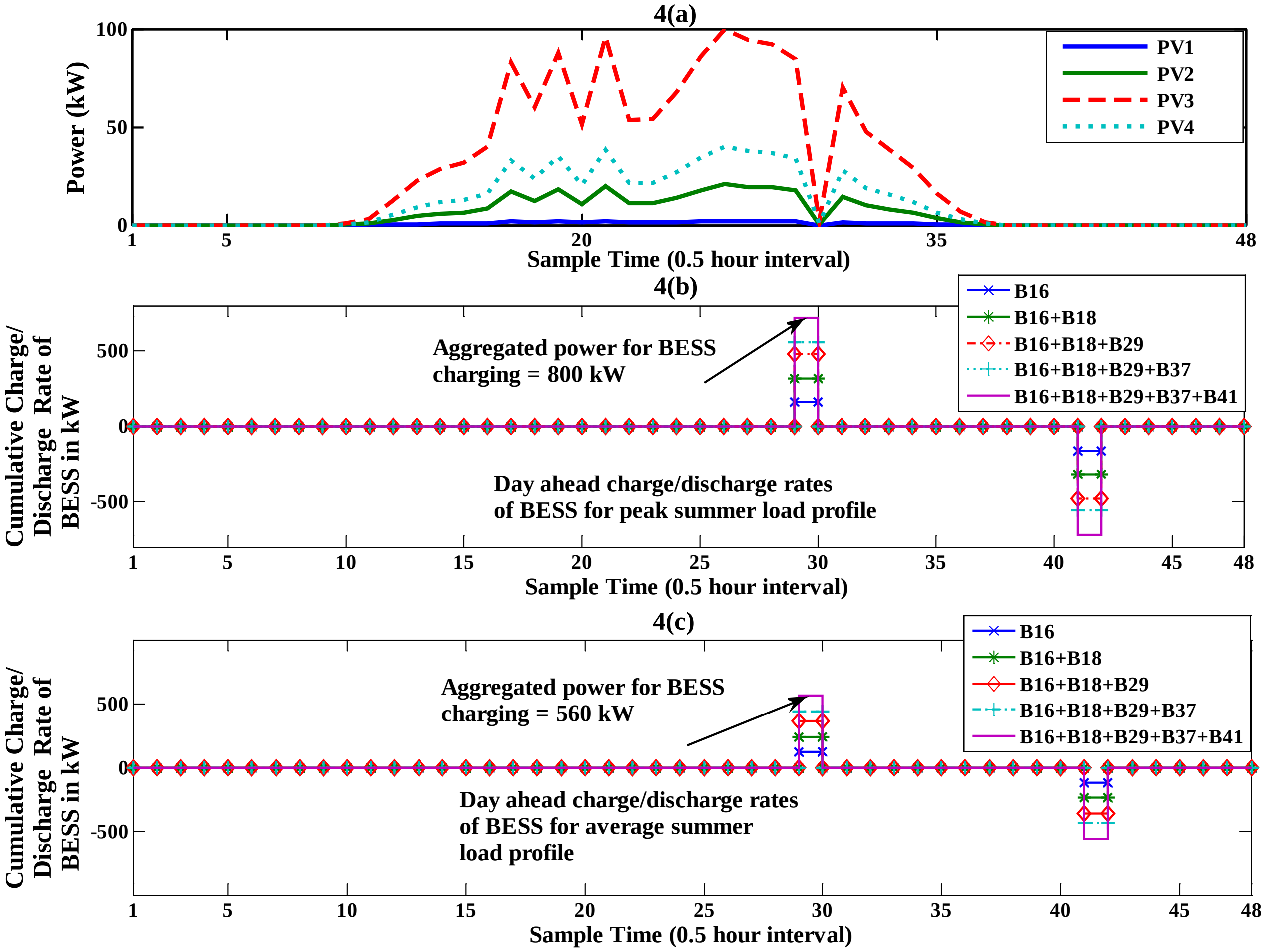

Figure 3.4 (a) PV power profiles for case study-1 (b) Day-ahead dispatch of BESS under peak summer load (c) Day-ahead dispatch of BESS under average summer load [78]

In this case, 4 PV sources with an aggregated capacity of 260 kW are utilised. Day-ahead power profiles of these sources are presented in Figure 3.4(a). Upon the application of (3.24)-(3.31), it is found that five BESS units are suitable to be placed in the network to shave the overall system peak by 4% with a load growth rate of 0.48%. Figures 3.4(b) and (c) present day-ahead dispatch rates of these BESS units for the peak summer and average summer load profiles respectively. It is observed from Figures 3.4(b) and (c) that all BESS units require approximately 0.5 hour charging at the 29th sampling instant for the respective load profiles, when PV output is high and the system is in a light load condition. The electricity price is the cheapest at the 29th sampling instant (Figure 3.3(b)). It can be noticed from Figure 3.4(b) that five BESS units deliver 800 kW at the 41st sampling instant under the peak summer load condition. Hence, 4% of the system peak is reduced by using five BESS units.

All storages are charged during the 29th sampling instant (14.00 to 14.30 hour) and the total stored energy is approximately 450 kWh. During this time, the total energy delivered by PV sources is 150 kWh. This amount is reasonably low, which is likely to serve only the loads connected to the buses with PV sources. Consequently, the solution of (3.24)-(3.31) has resulted in BESS locations that are different from the PV locations. It indicates that a low PV penetration level may have a reasonably small impact on BESS size and location with respect to network reinforcement deferral.

Table 3.4 summarises the results of case study-1. Five nodes are found as optimum locations for installing BESS. Individual capacities of these BESS units are calculated by (3.32) and (3.33) as shown in Table 3.4. The aggregated size of the 5 BESS units is found as 450 kWh to reduce the overall system peak by 4%.

Table 3.4 Optimum size and location of BESS in case study -1 (Bold text represents the final choice of BESS size) [78]

Load Profiles	Total Energy used from BESS (kWh)	Optimum Location for BESS units	BESS Index and corresponding sizes (kWh) for the locations in column-3		Aggregated size of all BESS (kWh)
Peak Summer	**450**	N98, N111, N605, N663 and N865	B16, B18, B29 and B41	180 kW and 100 kWh	450 (Total 5 BESS units)
Average Summer	350				
Low Summer	275				
Peak Winter	**450**				
Average Winter	300				
Low Winter	200				
Peak Autumn	**450**		B37	80 kW and 50 kWh	
Average Autumn	320				
Low Autumn	270				
Peak Spring	**450**				
Average Spring	300				
Low Spring	220				

3.3.2 Case Study – 2 (40% PV Penetration)

In case study- 2, the peak shave option is fixed to 4%, which is the same as case study-1. This assumption is taken to observe the effects of low and high PV penetration levels on BESS sizing and siting. There are 13 locations for PV (provided by the local DNO), which are used to represent a prospective future scenario. In this case, the aggregated PV capacity is considered as 4000 kW for 40% PV penetration. Simulations are executed by using input parameters given in Table 3.3.

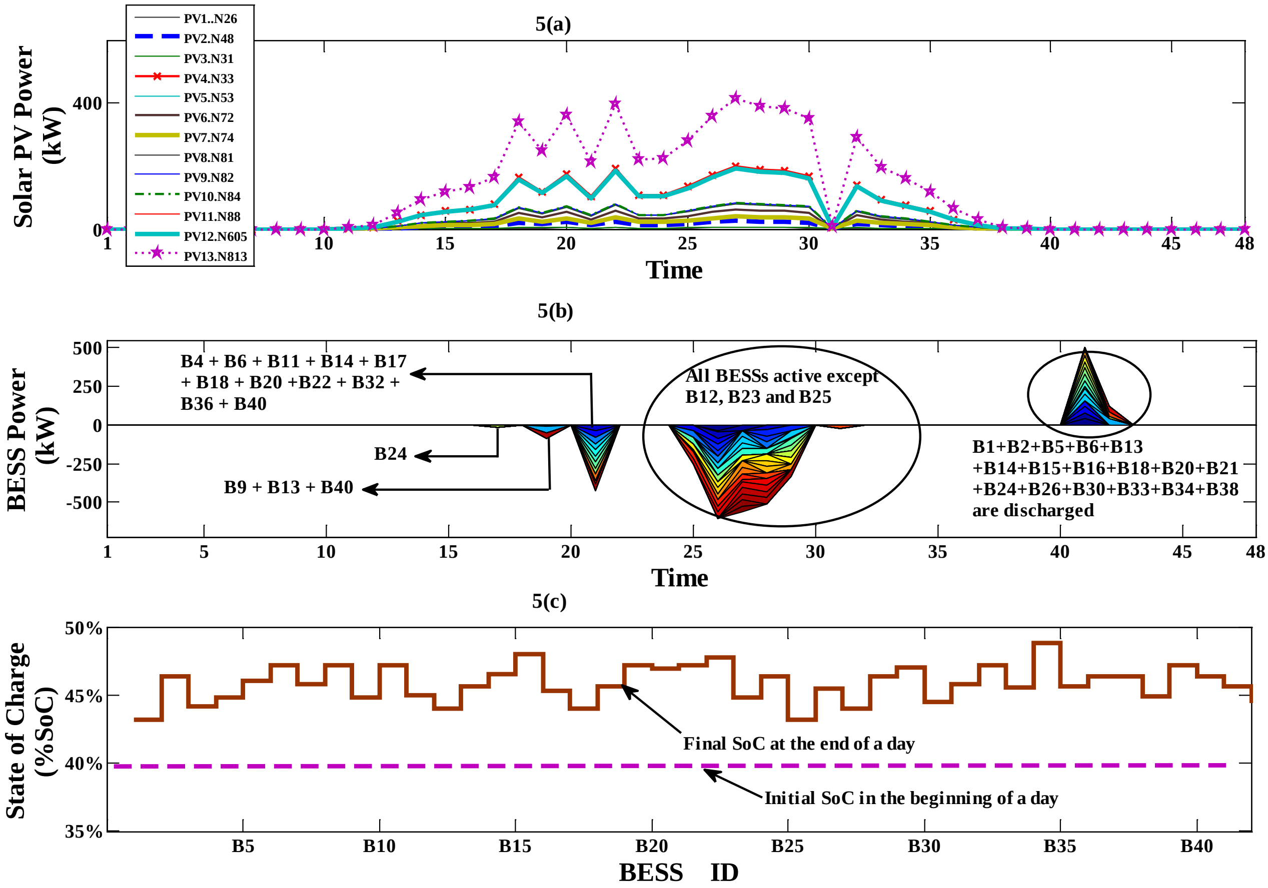

Figure 3.5 (a) PV power profile in case study-2 (b) Day-ahead dispatch of BESSs in case study-2 with peak summer load profile (c) Percentage of state of charge (%) of BESSs for peak summer load profile [78]

Out of 12 representative load profiles, peak summer is discussed as an example. The day-ahead PV profiles are shown in Figure 3.5(a). It is to be mentioned that initially 42 BESS units are taken into account for simulations. After solving (3.24)-(3.31), 39 BESS locations are obtained for the peak summer load profile. Figure 3.5(b) depicts the day-ahead dispatch schedule of these BESS units. It is observed from Figure 3.5(b) that 14 BESS units are charged in the morning for 120 minutes and 39 BESS units are charged in the afternoon for 180 minutes. It is also noticed from Figure 3.5(b) that 17 BESS units are discharged for 120 minutes at the peak-time.

It can be seen from Figures. 3.5(a) and (b) that locations of some of the BESS units are the same as that of PV sources. This is due to the charging of BESS units from PV sources during high PV generation under light load conditions. At that time, the BESS units store 4000 kWh of energy from PV. Therefore, excess PV power is better utilised in case study-2 compared to case study-1 (450 kWh in case-1).

Figure 3.5(c) presents the initial and final *SoC* for obtained BESS units (BESS ID are referred to in Table 3.2). The initial *SoC* is selected as 40% for all BESS units. It can be observed from Figure 3.5(c) that the final state of charge is higher than the initial value. It occurs due to the constraint in (3.26), which restricts the amount of charge stored in the BESS to greater or equal to the amount discharged in a day. The results are shown for the representative daily load and PV profiles, where BESS have sufficient space at a day end to charge in the next day. In case of some other daily load profiles, the BESS may be charged to such an extent that may restrict the BESS to charge again in the following day. This issue can be easily mitigated by modifying (3.26), where amount of charge stored in BESS units should be discharged on the same day so that they can be charged on the following day if necessary.

Detailed simulation results for 12 load profiles are shown in Table 3.5. It can be seen that the maximum BESS energy is found for peak summer load profile. Therefore, the outcomes corresponding to this load profile can be treated as the best possible size and location of BESS for case study-2. Thus, in total 39 BESS units are found as an optimum solution, whose aggregated capacity is 5,500 kWh. It is worth mentioning that in case study-1, 5 BESS units with an aggregated capacity of 450 kWh are obtained as an optimum solution. PV penetration in case-2 is considerably higher than that of case-1. Therefore, the amount of surplus energy from PV (which is stored in BESS) in case-2 is higher than that of case-1. As a result, for the same peak shaving, the aggregated size of BESS units in case study-2 is larger than that of case study-1. This can be attributed to the constraint expressed by (3.27), which limits the power drawn by a network from the connected grid. If the imported power from the connected grid drops below a limit due to high PV generation, a higher number of BESS units should be charged. Such a situation may arise if a network with substantial PV penetration, experiences very low demand during the daytime.

Table 3.5 Optimum size and location of BESS in case study -2 (Bold text represents the final choice of BESS size) [78]

<table>
<tr><th>Load Profiles</th><th>Total Energy used from BESS (kWh)</th><th>BESS Optimum Location</th><th colspan="2">BESS Index and Corresponding Size (kWh)</th><th>Aggregated capacity of all BESS (kWh)</th><th>Total peak shave</th></tr>
<tr><td>Peak Summer</td><td>5500</td><td rowspan="3">N26, N48, N53, N68, N72, N74, N75, N78, N79, N81,</td><td rowspan="3">B1-B3, B6, B9, B15 - B17, B20-B21, B29-B30, B33, B36, B41-B42</td><td rowspan="3">20 - 80</td><td rowspan="3"></td><td rowspan="3"></td></tr>
<tr><td>Average Summer</td><td>4900</td></tr>
<tr><td>Low Summer</td><td>3500</td></tr>
</table>

Peak Winter	**5400**	N82, N84, N88, N89, N90, N98, N104, N111, N113, N115, N120, N124, N125, N128, N136, N138, N142, N159, N605, N613, N631, N654, N658, N659, N660, N662, N663, N813, N814, N863, N865 and N867	B4-B5, B8, B10-B11, B13, B19, B22, B24, B26, B28, B31-B32, B34, B39	80 -160	5500 (total 39 BESS)	800 kW (4% of 20 MW)
Average Winter	3500					
Low Winter	2000					
Peak Autumn	**5400**		B7, B14, B27, B35, B37 - B38	200-300		
Average Autumn	3200					
Low Autumn	2700					
Peak Spring	**5400**		B18, B40	320-400		
Average Spring	3600					
Low Spring	2200					

Thus, it can be revealed that the optimum size and location of BESS vary with PV penetration levels. For higher PV, more BESS units are required to be deployed to store surplus PV energy. Therefore, when the PV penetration in a network proliferates, the required BESS capacity becomes higher for peak shaving and reverse power flow restriction.

3.3.3 Effects of Load Growth Rate and BESS Capacity on Network Upgrade Expenditure

This section investigates the impact of BESS size and load growth rate on network upgrade expenditure. Initially two PV penetration cases, 10% and 40% are considered in this context. Then, the penetration levels are varied from 5% to 45% to understand the maximum permissible PV penetration for economic deployment of BESS. For each case, net profit is determined using the proposed optimisation tool by varying the size of BESS (kWh) at different load growth rates. Peak shave is kept fixed for the aforementioned cases. A new constraint is added in the optimisation model, which limits the aggregated capacity of BESS. At a given peak shave, the duration of upgrade deferral depends only on load growth rate according to (3.8). If growth rate increases, a network quickly reaches its maximum capacity and therefore, upgrades deferral year decreases. If the duration of upgrade deferral is relatively smaller, BESS will be utilised for a period, which is less than its maximum lifetime. Henceforth, the number of *cycles* in (3.22) will also reduce. Table 3.6 presents network upgrade deferral year and the number of *cycles* for several load growth rates for 10% and 40% PV penetration cases at 4% peak shave.

Table 3.6 Network upgrade deferral year and BESS *cycles* at 10% and 40% PV penetration (peak shave = 4% or 800 kW) [78]

Peak load growth rate (g)	Upgrade deferral year for both 10% and 40% PV penetration cases	No. of BESS *cycles* used for two PV penetration cases
0.5	8.2	2000
1	4.2	1460
2	2.1	760
3	1.38	500

It can be observed from Table 3.6 that for a given load growth rate, upgrade deferral year is the same for both cases. Since the occurrence of peak load and PV do not coincide with each other, upgrade deferral year for a given peak shave is independent of PV penetration level. It is to be mentioned that the number of *cycles* shown in Table 3.6 is utilised to determine net profit using (3.22) for various BESS sizes.

Figures 3.6(a) and (b) present the required expenditure to upgrade the studied network with BESS for several peak load growth rates (g) at 10% and 40% PV penetration respectively. The actual cost to upgrade the network without BESS (referred to as 'actual w/o BESS') is estimated as \$1.2 million as described in Section 3.3.2. The studied load curve as shown in Figure 3.3(a) contains its peak for duration of half an hour and the peak shave is considered as 4% (800 kW). That is why the BESS capacity starts from 800kW×0.5h=400 kWh, so that it can be discharged for at least half an hour. It is observed from Figure 3.6(a) that if BESS capacity increases, upgrade expenditure also increases due to the rise in capital expenditure of BESS. However, the amount of expenditure with BESS is much smaller than 'actual w/o BESS' expenditure for 10% PV penetration.

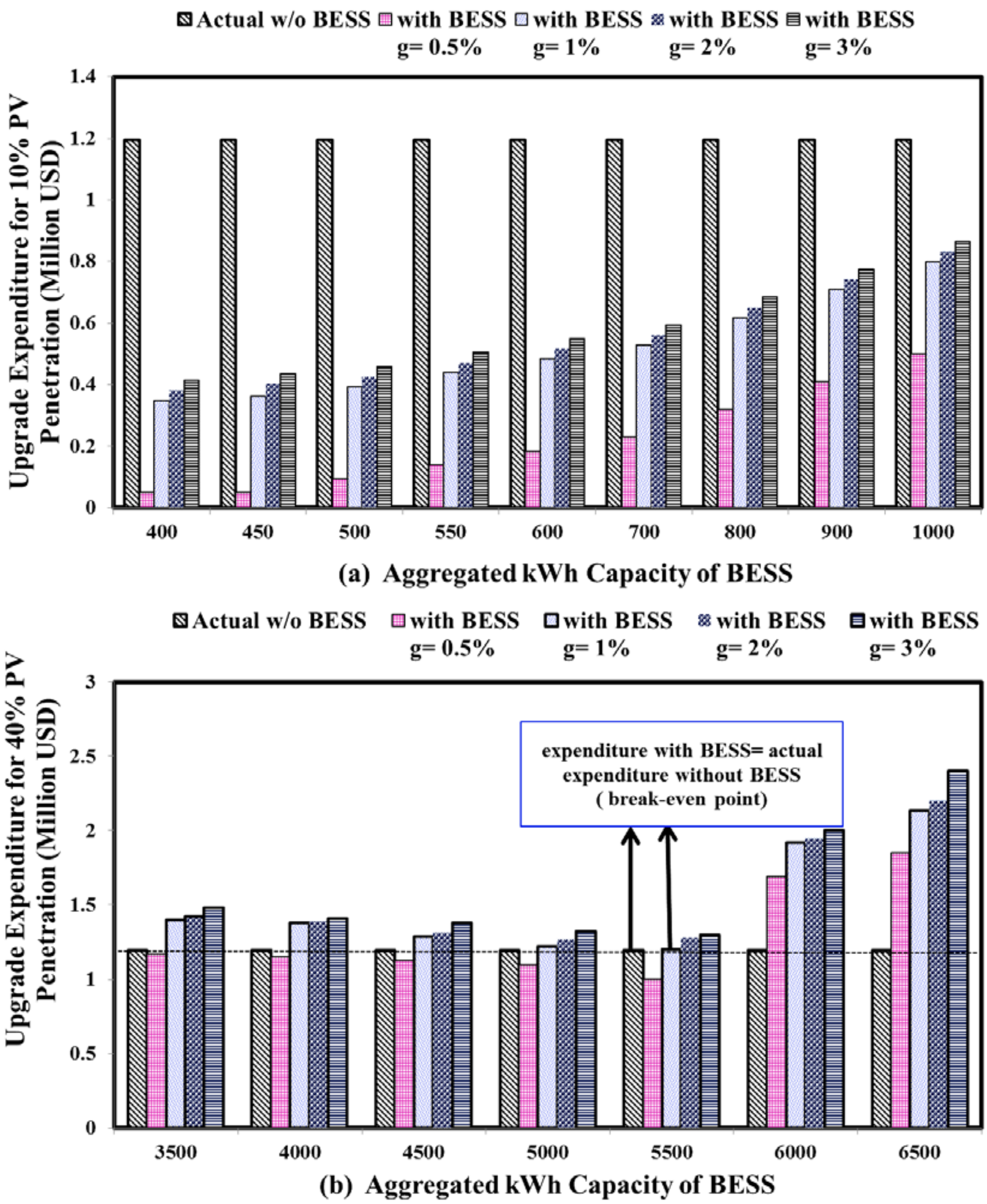

Figure 3.6 Network's upgrade expenditure vs. total kWh capacity of BESS for different g (a) 10% PV penetration (b) 40% PV penetration [78]

It is also noticed that for a given BESS capacity, if the load growth rate becomes higher, upgrade expense increases. This is because, for a given peak shave, the number of years for which the network upgrade may be deferred using BESS reduces as the load growth rate increases (according to (3.8)). Hence, the number of *cycles* also reduces causing relatively less TOU benefit as shown by (20). Therefore, net profit as expressed by (3.21) and (3.22) decreases when load growth rate increases.

At 40% PV penetration, more cumulative BESS capacity is required to store surplus PV energy. Hence, BESS capacity starts from 3,500 kWh as shown in Figure 3.6(b). It is observed that the network upgrade expenditures with BESS (capacity ranging from 3,500 to 5,500 kWh) are reasonably close to actual expenditure at 0.5% load growth rate. If BESS capacity is more than 5,500 kWh, upgrade expenditure exceeds ‘actual w/o BESS’ expenditure. Moreover, for smaller BESS capacity (< 5,500 kWh), upgrade expense also surpasses actual expenditure if load growth rate is higher than 0.5% (attributed to the reduction in the number of years for which the network upgrade may be deferred using BESS due to the increasing load growth rate). It is also noticed that for 1% load growth rate and BESS capacity of 5,500 kWh, network upgrade with BESS is as expensive as actual cost (referred to as the break-even point in Figure 3.6(b)).

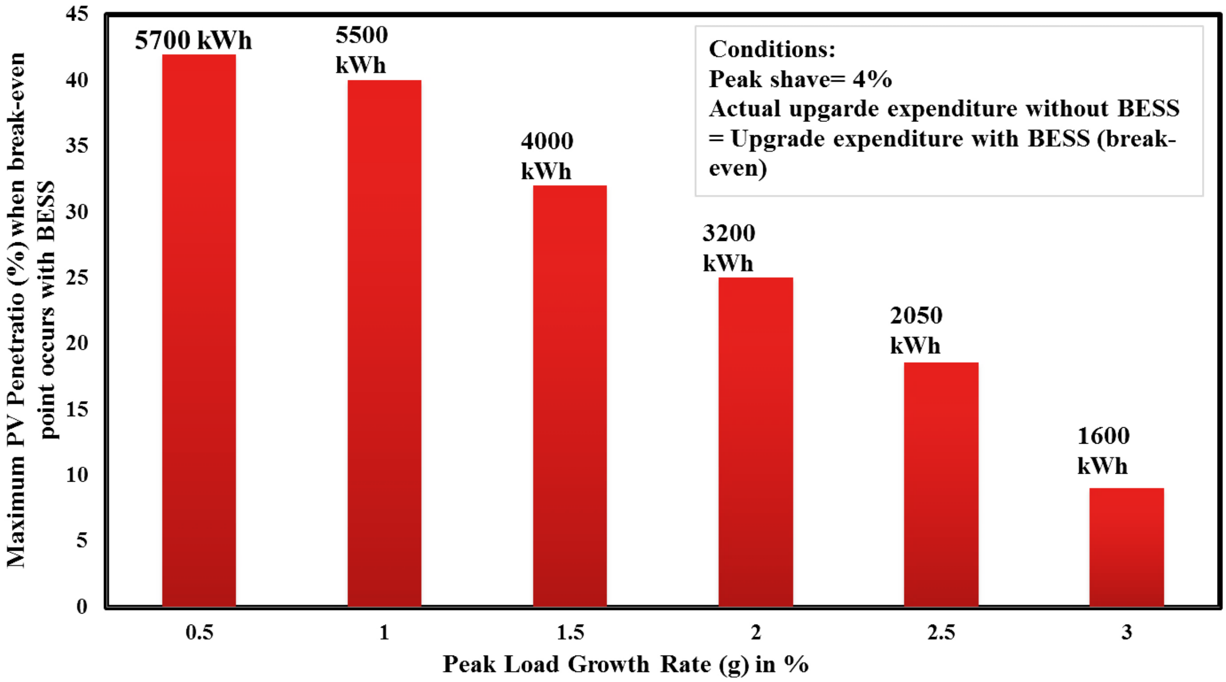

Figure 3.7 Maximum PV penetration at break-even point vs. peak load growth rate [78]

The level of PV corresponding to this point is called maximum permissible PV penetration for utilising BESS with financial viability. Figure 3.7 presents the maximum values of PV penetration for which financial viability (or break-even point) can be achieved for different load growth rates. Corresponding BESS capacities are also shown. It can be observed from Figure 3.7 that the maximum PV penetration and BESS capacity show declining trends as load growth rate increases at a given peak shave. As the load growth rate increases, network upgrade deferral year reduces at a given peak shave as shown in Table 3.6. Consequently, the values of *cycles* and net profit decrease. Therefore, a smaller BESS is permitted to reach the break-even point. Thus, with a smaller BESS, the permissible maximum PV penetration reduces with the increasing load growth rate for financial viability.

3.4 Extension of the Proposed Approach for Voltage Regulation

In this section, the proposed optimisation model as discussed in Section 3.1 is modified for the regulation of network voltage via both active and reactive OPF analysis. To achieve the required voltage regulation in LV distribution systems, the BESS owned by customers are utilised. It is worth mentioning that there are other voltage regulating devices in distribution systems. However, the model is developed to assess the potential benefits to customers by allowing their BESS for voltage regulation. Since a customer's main interest is to reduce their electricity bill, a new objective function is formulated in the modified model [85].

Let us assume a distribution network containing u number of nodes, which is defined by a set, N = [1, u]. Let $\beta^{u \times u}$ be the admittance matrix for u bus system. Active and reactive power flow at each bus of the system is modelled by (3.34) and (3.35) respectively [86].

$$\begin{aligned} & P^G(j,n) + r^d(j,n) - r^c(j,n) - P^d(j,n) = \\ & V_e(j,n) \sum_{\substack{k=1 \\ k\in N}}^{u} (G(j,k).V_e(j,n) - B(j,k).V_f(j,n)) + V_f(j,n) \sum_{\substack{k=1 \\ k\in N}}^{u} (G(j,k).V_f(j,n) \\ & + B(j,k).V_e(j,n)) \quad j \in N,\ n \in [1,24] \end{aligned} \tag{3.34}$$

$$\begin{aligned} & Q^G(j,n) - Q^d(j,n) = V_f(j,n) \sum_{\substack{k=1 \\ k\in N}}^{u} (G(j,k).V_e(j,n) - B(j,k).V_f(j,n)) - \\ & V_e(j,n) \sum_{\substack{k=1 \\ k\in N}}^{u} (G(j,k).V_f(j,n) + B(j,k).V_e(j,n)) \quad j \in N,\ n \in [1,24] \end{aligned} \tag{3.35}$$

where

$P^G(j,n)$ = Real power drawn from the grid via j^{th} node and n^{th} sampling instant

$Q^G(j,n)$ = Reactive power drawn from the grid via j^{th} node and n^{th} sampling instant

$P^d(j,n)$ = Net real power demand (load–solar PV) at j^{th} node and n^{th} sampling instant

$Q^d(j,n)$ = Reactive power demand by loads at j^{th} node and n^{th} sampling instant

$V_e(j,n)$ = Real part of complex voltage at j^{th} node and n^{th} sampling instant

$V_f(j,n)$ = Imaginary part of complex voltage at j^{th} node and n^{th} sample

$G(j,k)$ = Real component of the complex admittance matrix β

$B(j,k)$ = Imaginary component of the complex admittance matrix β

The objective function is the summation of day-ahead arbitrage benefits of all BESS in the system and defined by (3.36).

$$J = price(n).\sum_{j=1}^{u}\sum_{n=1}^{24}\{r^d(j,n) - r^c(j,n)\}.\,\Delta t \tag{3.36}$$

where J refers to the daily energy arbitrage from BESS and

$r^d(j,n)$ = Discharge rate of a battery at j^{th} node and n^{th} sampling instant

$r^c(j,n)$ = Charge rate of a battery at j^{th} node and n^{th} sampling instant

$price(n)$ = Day-ahead price of electricity at n^{th} sampling instant

Δt = Duration of a sample

The amount of energy stored in a BESS should be discharged by the end of a day so that it can be available for charging from solar power the following day. Therefore, a constraint for BESS energy management is formulated as

$$\sum_{n=1}^{24}\{r^d(j,n) - r^c(j,n)\}.\,\Delta t = 0 \tag{3.37}$$

Now, the proposed time-series optimisation model is given by (3.38) to (3.45).

$$\underset{\substack{r^d(j,n),\ r^c(j,n),\\ V_e(j,n),\ V_f(j,n),\ P^G(j,n)}}{Maximise} \quad J(r^d(j,n), r^c(j,n), price(n)) \tag{3.38}$$

Subject to

$$\begin{aligned} &P^G(j,n) + r^d(j,n) - r^c(j,n) - P^d(j,n) = \\ &V_e(j,n)\sum_{\substack{k=1\\k\in N}}^{u}(G(j,k).V_e(j,n) - B(j,k).V_f(j,n)) + V_f(j,n)\sum_{\substack{k=1\\k\in N}}^{u}(G(j,k).V_f(j,n) \\ &+B(j,k).V_e(j,n)) \quad j\in N,\ n\in[1,24] \end{aligned} \tag{3.39}$$

$$\begin{aligned} &Q^G(j,n) - Q^d(j,n) = V_f(j,n)\sum_{\substack{k=1\\k\in N}}^{u}(G(j,k).V_e(j,n) - B(j,k).V_f(j,n)) \\ &-V_e(j,n)\sum_{\substack{k=1\\k\in N}}^{u}(G(j,k).V_f(j,n) + B(j,k).V_e(j,n)) \quad j\in N,\ n\in[1,24] \end{aligned} \tag{3.40}$$

$$\sum_{n=1}^{24}\{r^d(j,n) - r^c(j,n)\}.\,\Delta t = 0 \tag{3.41}$$

$$V_{\min} \le \sqrt{V_e(j,n)^2 + V_f(j,n)^2} \le V_{\max} \tag{3.42}$$

$$P^{\min}(j) \le P^G(j,n) \le P^{\max}(j) \tag{3.43}$$

$$r^{d\min}(j) \le r^{d}(j,n) \le r^{d\max}(j) \tag{3.44}$$

$$r^{c\min}(j) \le r^{c}(j,n) \le r^{c\max}(j) \tag{3.45}$$

The objective function is to be maximised under all constraints described by (3.39)-(3.45). These constraints are considered to introduce the limits on variables i.e. voltage magnitude of all nodes, total active power flow in the network and battery discharge-charge rates. In order to estimate the energy arbitrage from batteries, the non-linear optimisation task is resolved with COUENNE solver [87]. COUENNE is an open source solver and uses IPOPT for the solution of non-linear problems. The proposed optimisation tool is solved for day-ahead charge/discharge patterns of BESS (r^d (j, n), r^c (j, n)), real and imaginary parts of node voltages (V_e (j, n), V_f (j, n)), total real and reactive power (P^G (j, n), Q^G (j, n)) flow at each sampling instant.

3.4.1 Investigations

3.4.1.1 Description of the Studied LV Network

The studied network for voltage regulation with BESS as shown in Figure 3.8 is radial in nature and contains a primary feeder and 6 secondary feeders [26]. The network is connected to an infinite bus through a power transformer facilitated with an on-load tap changer (OLTC). The network resembles a radial distribution network located in the USA. The total length of the primary feeder is 9.66 km and the length of the secondary feeder can vary between 60 to 160 meters. The R/X ratio of the secondary feeder is assumed to be reasonably high. Seven residential customers are supposed to be connected to feeder x1. The maximum load for each customer is 10 kW. The line-to-line voltage levels of primary and secondary feeders are 12.5 kV and 240 V respectively [26]. Each secondary feeder has approximately 0.3 MW lumped load. It is assumed that each customer owns a 4 kW PV system. There is an step voltage regulator (SVR) at node N3 to control primary feeder voltage in the network.

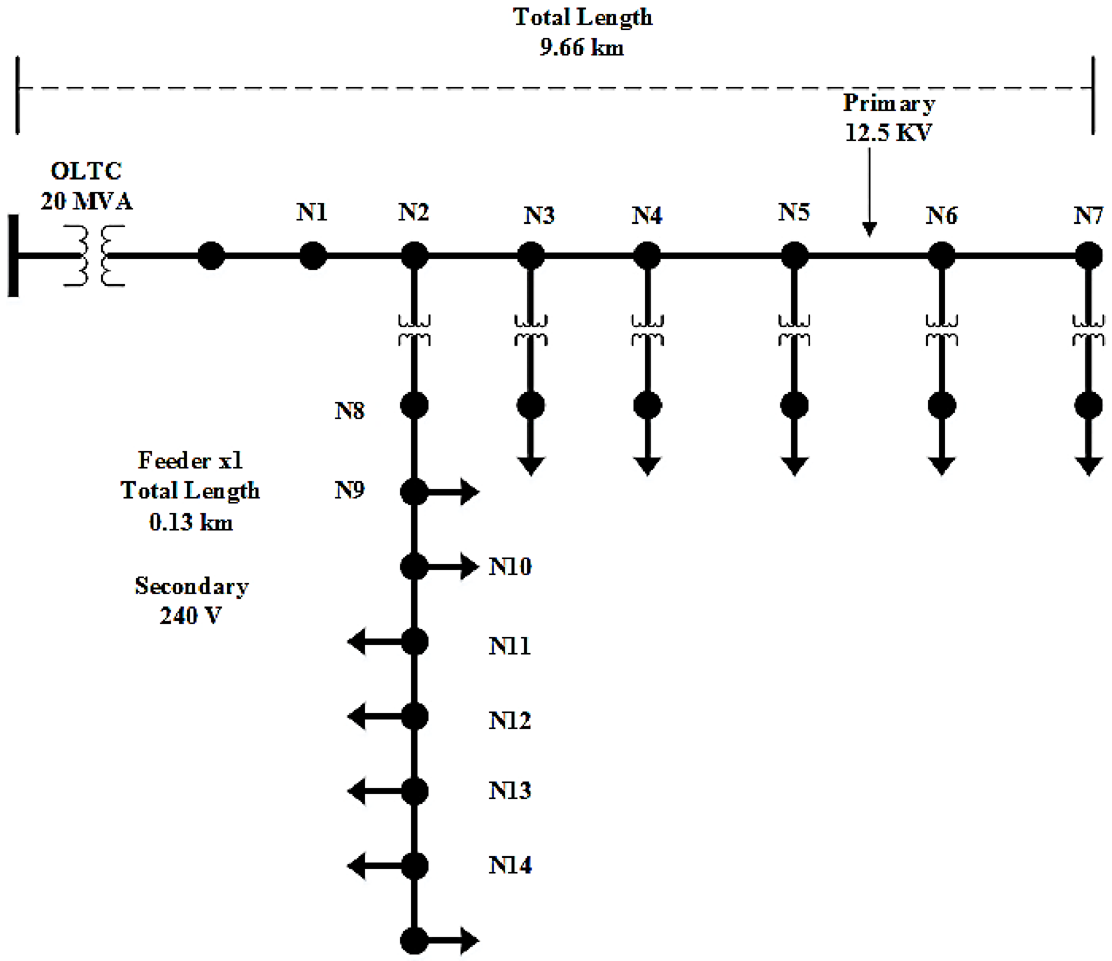

Figure 3.8 Schematic diagram of the studied radial distribution network [85]

3.4.1.2 Simulation Scenarios

PV power output data from the University of Queensland solar system [88] over a one year period is studied and used in this section. It is well known that PV output follows a seasonal pattern. Therefore, clustering PV output based on seasonal variation is more practical instead of considering 365 daily profiles (for a year). Clustering can provide more compact information about PV patterns, which ultimately control BESS charge-discharge rates. Besides, clustering reduces computational burden. Therefore, PV output data is categorised by using k-means clustering method, which is discussed in Section 3.4.2. Then, the average load profile of each season is collected and studied [83]. If the number of load and PV profiles are α and λ respectively, the possible number of net load patterns is $\alpha \times \lambda$. To reduce the number of load patterns, the correlation co-efficient of each PV cluster with seasonal daily irradiance is determined [88]. If the correlation coefficient between a PV cluster and a seasonal daily irradiance pattern is very high (>0.8), the respective PV cluster is utilised to determine the net load of the corresponding season.

In the next stage, the voltage problem is identified with a very low demand and high PV output in the x1 feeder. Lithium-ion BESS are connected to PV units and the proposed OPF is solved for all clustered load scenarios. Finally, the maximum yearly energy arbitrage is estimated by taking a weighted average of daily arbitrage values of all load and PV profiles under study. Figure 3.9 shows a block diagram of the proposed analysis.

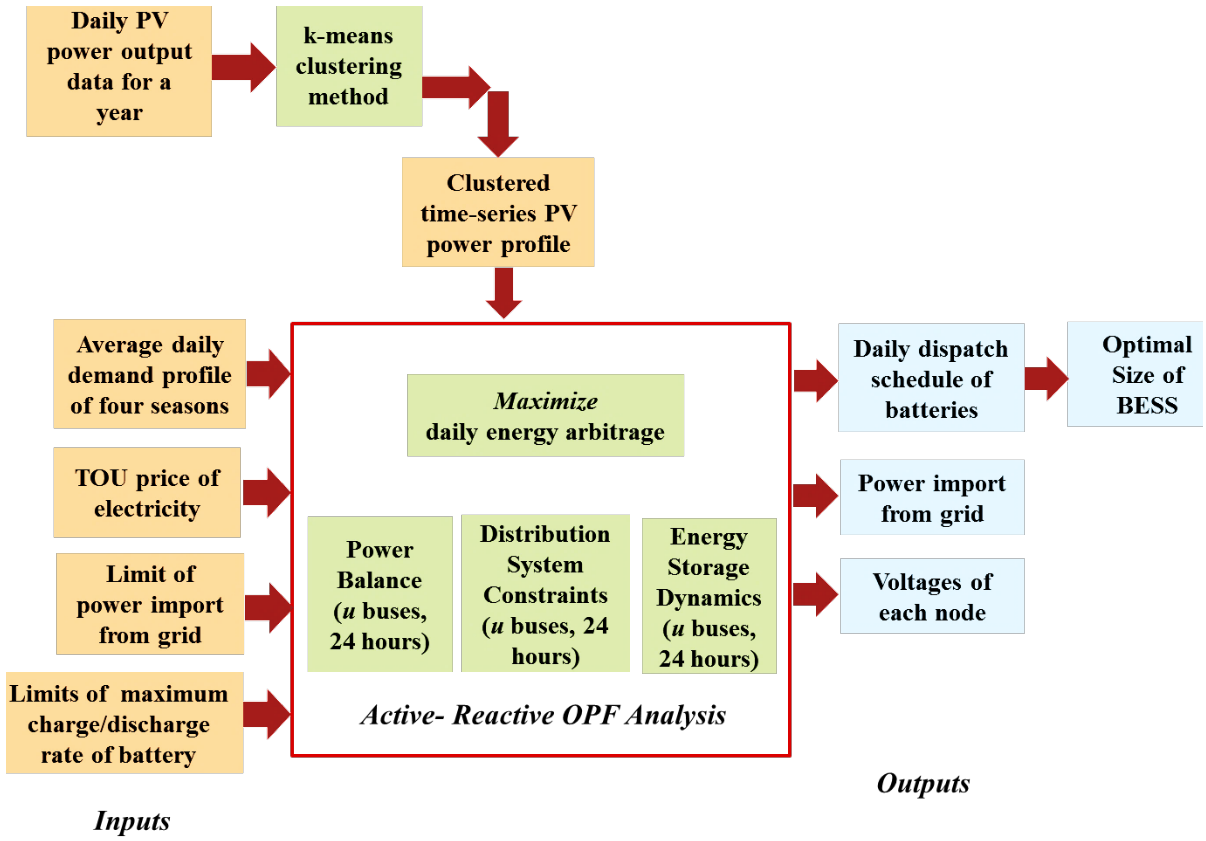

Figure 3.9 Block diagram of the proposed analysis [85]

3.4.2 Results and Discussions

This section presents the categorised solar PV profiles through k-means clustering algorithm and the relevant results from the proposed voltage regulation approach.

3.4.2.1 Categorising PV Output using k-means Clustering

Several tools for time series data clustering have been reported in the literature [89]. One of them is k-means method, which provides fast computation. The k-means [89] technique is an iterative algorithm, which first determines the centroid of each cluster. Then it minimises the sum of distances between data points and the centroid of a cluster, summed over all clusters iteratively. The objective function (F) to minimise in this algorithm is as follows.

$$F = \sum_{i=1}^{c} \sum_{p=1}^{o} \left\| D_p - S_i \right\|^2 \tag{3.46}$$

where $p \in \{1,2,3,\ldots,o\}$ and $i \in \{1,2,3,\ldots, c\}$. D_p represents o number of data points, while S_i , presents c number of cluster centroids. The cluster centroids are updated iteratively until F is minimised.

To identify the optimum number of clusters, an objective function (*OF*) is defined as

$$OF = \sum_{c} \sum_{j} \left\| Y_{i,j} - \gamma_i \right\| \tag{3.47}$$

where $Y_{i,j}$ is the j^{th} data point of the i^{th} cluster and γ_i is the centroid of the i^{th} cluster. The total number of clusters is presented by c.

The k-means algorithm is applied to categorise PV power output. Figure 3.10(a) shows time-series profiles of a 4 kW PV system for a year. Figure 3.10(b) presents the value of the objective function computed using (3.47) for different cluster numbers. It is observed that as the number of clusters increases, the value of objective function decreases. After a definite cluster number, the magnitude of objective becomes almost constant. By observing Figure 3.10(b), ten clusters are selected for the studied data set of solar PV. The time series profiles of all the ten clusters are presented in Figure 3.10(c).

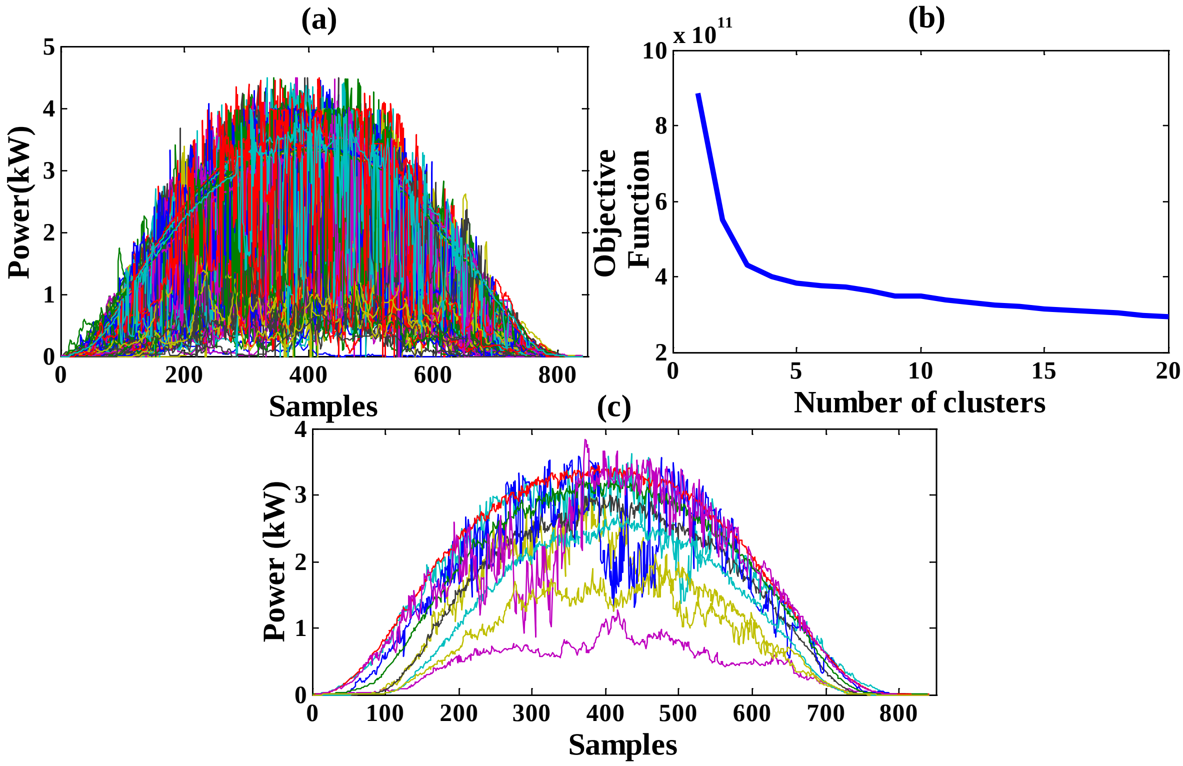

Figure 3.10 (a) Studied time-series PV power profile in a year (b) Determining optimum number of cluster (c) Time series pattern of 10 optimum clusters [85]

It can be observed from Figure 3.10(c) that more than 800 samples are obtained in each cluster. The optimisation tool needs 24 samples instead of 800. Therefore, it is required to reduce the number of samples in each cluster. It is achieved by taking an average of 34 data samples at each hour of a cluster. Figure 3.11 presents the compact PV output clusters. In the next step, all clustered PV profiles are compared with seasonal solar irradiation patterns. Table 3.7 presents the correlation co-efficient of each PV cluster with their corresponding seasonal irradiation profiles.

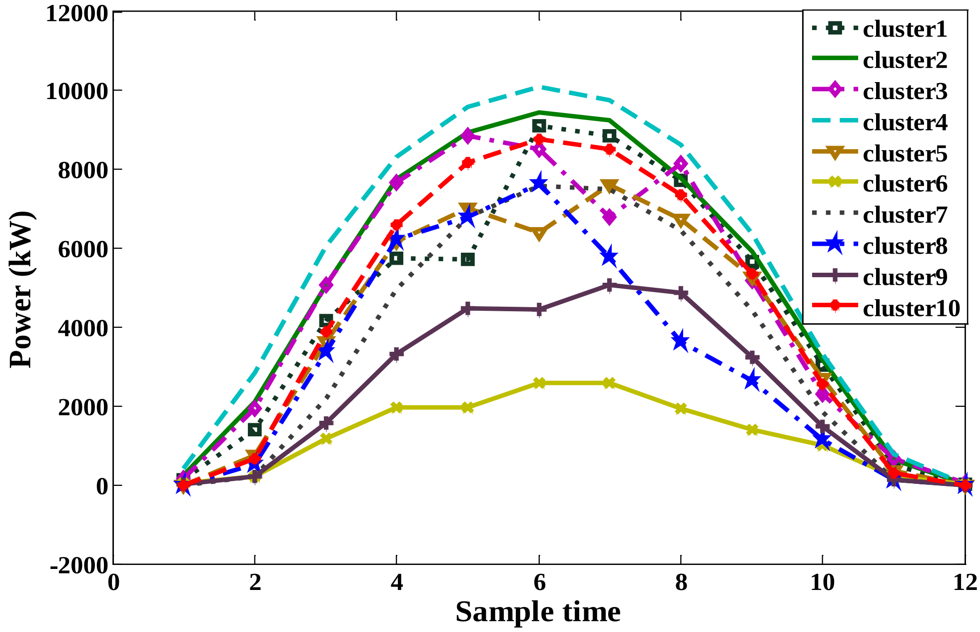

Figure 3.11 Compact PV output clusters [85]

Table 3.7 Correlation co-efficient of PV clusters with seasonal irradiance [85]

Cluster Name	Seasonal Irradiance	Correlation co-efficient
Cluster1	Spring	0.9373
Cluster2	Spring	0.9420
Cluster3	Summer	0.9702
Cluster4	Summer	0.9647
Cluster5	Winter	0.8291
Cluster6	Summer	0.9654
Cluster7	Autumn	0.9476
Cluster8	Winter	0.9156
Cluster9	Autumn	0.9577
Cluster10	Spring	0.9213

It is observed from Table 3.7 that clusters 3, 4 and 6 are highly correlated with summer irradiation profiles. Clusters 5 and 8 are represented as winter PV profiles. Clusters 1, 2 and 10 are represented by spring PV profile. Clusters 7 and 9 are matched with the autumn season. Figure 3.12 shows the net load profiles (load minus solar PV) of all seasons with corresponding PV clusters. It is found from Figure 3.12 that the net load profiles in winter cluster-2 and autumn cluster-1 are negative, which implies that rooftop PV systems are supplying active power to the grid.

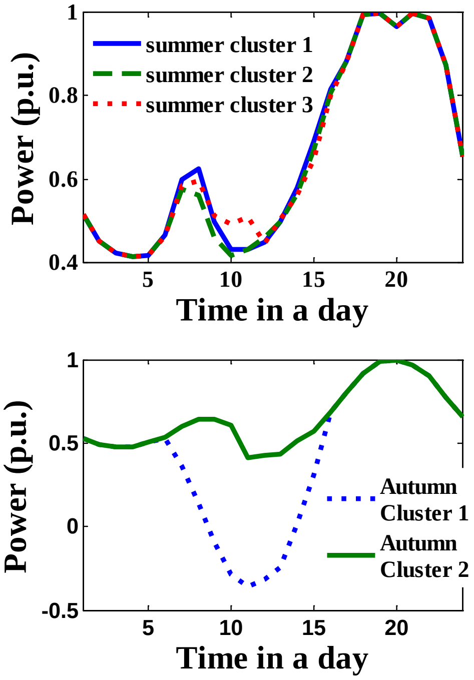

Figure 3.12 Load profiles of all seasons subtracting corresponding PV output clusters [85]

3.4.2.2 Case Study-1: Identification of Voltage Problem Due to PV

The studied power system and the proposed formulation are modelled in GAMS platform [84]. All loads in the system are modelled as constant power loads. Each customer has a PV unit and they are modelled as negative loads. Very light load profiles at node N11, N12, N14 and N15 are considered at the noon. In the next stage, an optimal power flow is performed without any battery storage to search for the minimum cost of energy. If the voltage limits are considered ±5% of the nominal voltage magnitude, the optimisation does not converge. Therefore, node voltage limits are selected as ±10% of the nominal voltage and it is found from OPF results that there are some locations in the system which experience reasonably high voltage at noon. The voltage profile of each bus from the OPF analysis is presented in Figure 3.13. It is observed from Figure 3.13 that customers experience voltage rise at peak PV time at some sites in the secondary distribution feeder x1. Customers located at N11 and N14 locations experience high voltage situation. This occurs due to a reverse power flow at the corresponding nodes at noon. In case of large PV capacity, these voltage rise situations may deteriorate.

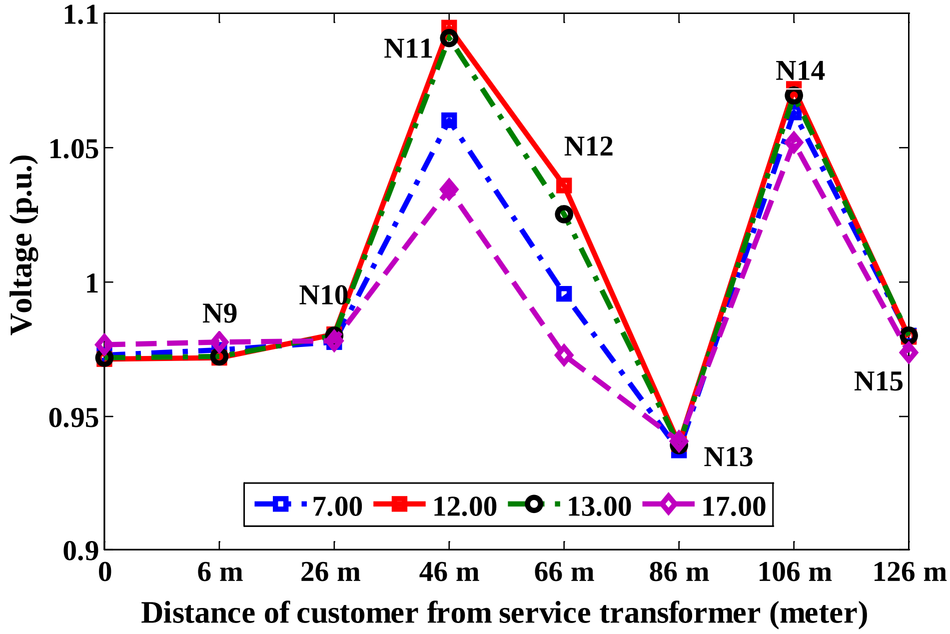

Figure 3.13 Voltage magnitudes of nodes in the secondary feeder [85]

3.4.2.3 Case Study-2: Node Voltages with PV and Batteries

It is observed from case study-1 in subsection 3.4.2.2 that the voltage rise problem is prominent at nodes N11 and N14. That is why if BESS are used at these two locations, local voltage issues can be mitigated. However, the voltage problem may occur in other nodes depending on customer load and PV power profiles. Therefore, each PV unit is assumed to be supported by a battery. In this case, the upper and lower limits of voltage are selected as ±5% of the nominal voltage magnitude. The proposed tool is executed to attain the maximum value of the objective function described by (3.38) to (3.45). The optimum charge/discharge schedule of batteries is obtained from the result. Figure 3.14 shows a day-ahead charging pattern of a BESS for a light load and high PV power case.

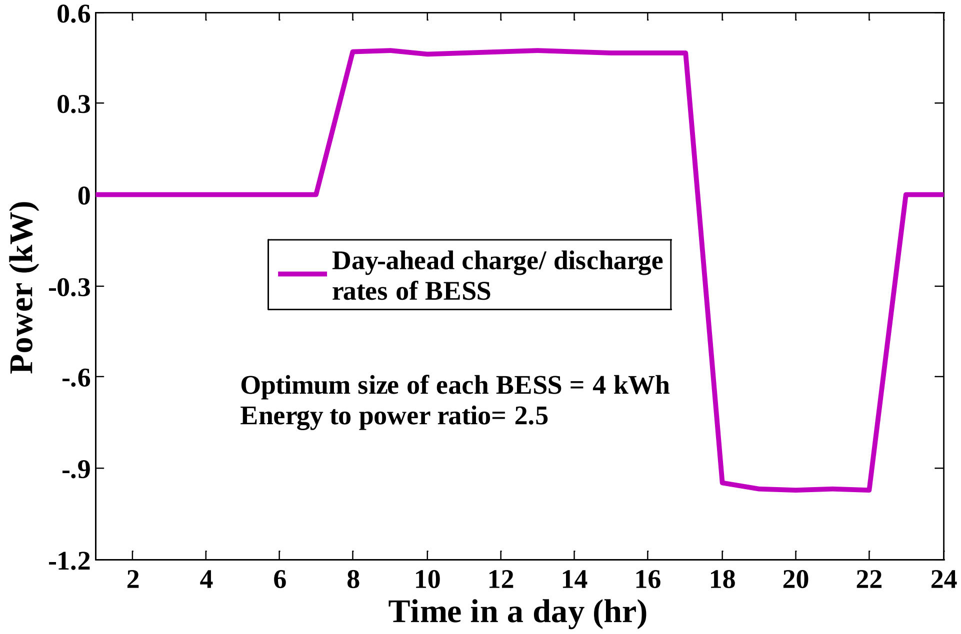

Figure 3.14 Charge-discharge schedules of a BESS in case study-2 [85]

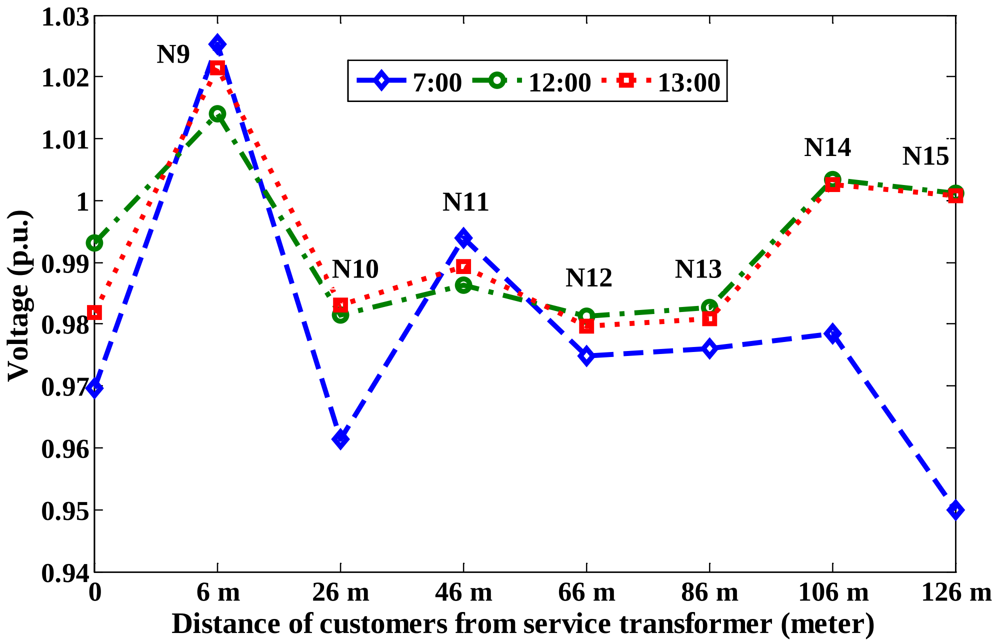

Figure 3.15 Voltage magnitude at each location of the LV feeder [85]

It is observed that the BESS charging rate increases with PV power increase. After a certain level, the charge rate becomes fixed and then it sharply falls to zero. Batteries are discharged for 5 hours in the night time. It is determined from the charging pattern that the suitable size of BESS is 6 kWh by considering 80% round-trip efficiency. The rated power of each BESS unit is 1.2 kW (approximately). Figure 3.15 presents voltage magnitude of each node after placing BESS in the secondary feeder at three different times of day. It is observed from Figure 3.15 that all node voltages remain within ±5% limit of the nominal secondary voltage.

3.4.2.4 Yearly Arbitrage Benefits and Pay-back Time of PV-BESS

The optimal power flow results in ten individual Daily Arbitrage Benefits (DAB) for different seasons in a year. Then the yearly arbitrage benefit is calculated by taking the weighted average of each DAB. Table 3.8 presents all DABs of corresponding load profiles. It is observed that by using a 6 kWh battery with a 4 kW PV unit, a customer can achieve a yearly arbitrage of around $380. It is assumed that off-peak electricity price is 16 cents/ kWh and peak price is 40 cents/kWh [16]. The BESS has utilised 1 cycle per day, which leads to the use of 365 cycles per year. Therefore, if the cycle-life of BESS is 2500, it can be operated for almost 6.5 (i. e. 2500/365) years.

Table 3.8 DAB for each load profile and yearly DAB [85]

Load and PV Cluster	DAB (US$)	Number of days when similar load pattern occurs, ς	Weightage, (DAB $\times\varsigma$ /365)	Yearly Arbitrage (365$\times \sum$ (DAB $\times$ ς /365)
Summer: C1	1.32	29	0.1049	479 US$ (approximately)
Summer: C2	1.39	31	0.1138	
Summer: C3	1.18	40	0.1292	
Winter: C1	1.51	68	0.2812	
Winter: C2	1.41	17	0.0655	
Autumn: C1	1.37	50	0.1874	
Autumn: C2	1.13	40	0.1241	
Spring: C1	1.19	26	0.0847	
Spring: C2	1.21	36	0.1191	
Spring: C3	1.32	28	0.1013	

Figure 3.16 presents yearly cash flow for a PV-BESS and for a PV only unit. The payback period of PV-BESS depends on their capital costs of installation. Usually, BESS cost is associated with both kW and kWh ratings. Residential BESS does not require high kW ratings, hence, comes with a low cost package. Furthermore, BESS costs are likely to be significantly reduced in the upcoming years. On that note, it is assumed that a PV-BESS system is purchased by customers considering the capital cost of BESS $570 per kWh over 15 years period [8]. It is worth mentioning that the proposed methods in Sections 3.1 and 3.4 are generic and applicable for any price of BESS. Therefore, the results presented in this thesis are indicative in nature. The merit of the proposed methods does not change due to the variation the of BESS price. The study considers the time of use price scheme of electricity only, feed-in-tariff for PV is not taken into account. The annual inflation rate is considered 4%.

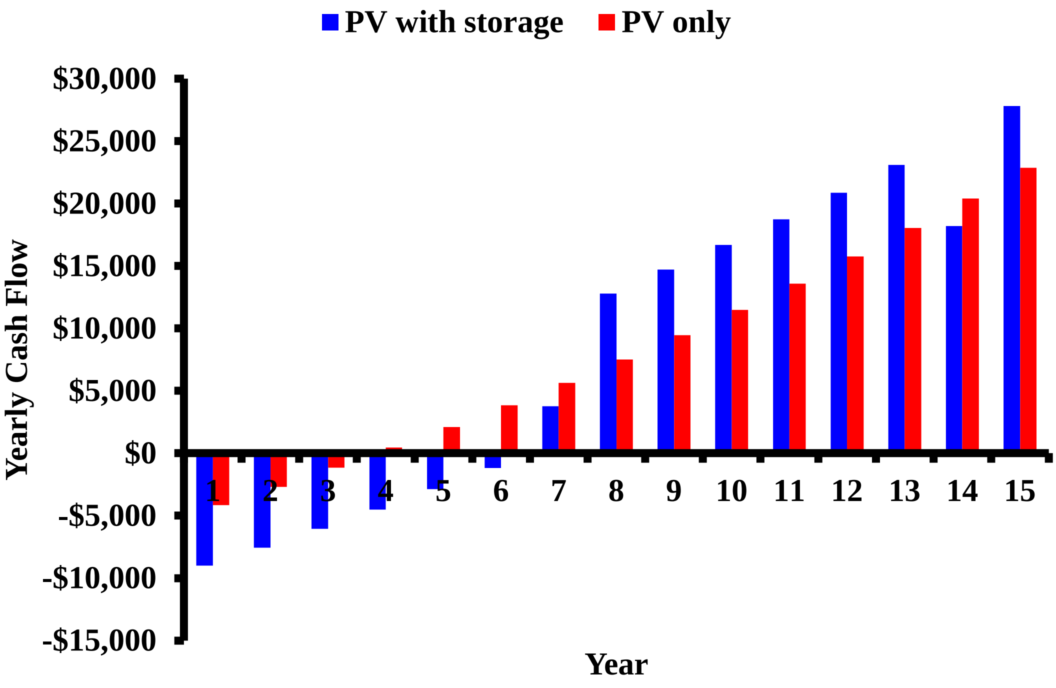

Figure 3.16 Yearly Cash Flow for PV user and PV-BESS user [85]

It is observed from Figure 3.16 that cash flow is positive at the 5th year for only PV system users. A PV-BESS system is likely to have a positive cash flow at the 7th year. Therefore, payback time of a PV-BESS unit is closer to only PV. However, yearly energy savings with PV-BESS is much higher than a PV without battery. The total electricity costs savings with PV-BESS for 15 years is about $25,429. This saving considers battery replacement cost every 7 years. In contrast, the total bill savings for only PV unit for the same time frame is $20,755. Therefore, a customer may achieve more benefits with PV-BESS than only PV unit in the long run. At the same time, network voltage problems caused by large PV penetration are mitigated. So, the proposed tool can estimate optimum dispatch of battery systems while maintaining expected voltage limits at the customers' end.

3.5 Summary

In this chapter, a mathematical tool is developed to defer network upgrade investment using BESS via an active optimal power flow framework. The developed tool is applied to a segment of a distribution network in Queensland, Australia. Results show that the proposed model is able to evaluate proper sizing, siting and the day-ahead dispatch schedule of BESS in a PV dominated power system. The required size of BESS increases if the PV penetration level is substantial. Network reinforcement with the optimally allocated BESS is an economic option for a DNO rather than upgrading components. Declining costs of BESS indicates that network reinforcement with BESS is a promising option to DNOs. The analyses in this chapter also show the necessity of a third party for the possible interaction between DNOs and customers, where aggregators can play an important role.

It is found that a network upgrade with BESS is less expensive in a low load growth rate region than that of a high load growth rate region. To achieve financial viability with BESS, the permissible maximum PV penetration decreases with an increase in the load growth rate. The proposed model can evaluate the optimum BESS capacity and location for any networks while maintaining technical and financial viability. The proposed tool will be utilised in the upcoming chapters of this thesis to select a suitable capacity and location of BESS in a network.

In many LV distribution networks, voltage rise caused by PV is a severe problem, where a BESS system can be a potential solution. However, initiatives to integrate BESS are limited mainly due to their high capital costs and lifetime limitations. The analysis in this chapter gives an insight towards an optimum selection and utilisation of BESS to mitigate voltage rise issues. In the case of large PV integration in residential networks (>5 kW for each customer), the voltage problem may deteriorate, which require larger BESS. At least one charge/discharge cycle is required every day in this study, while more cycles can be used to fulfil further objectives, such as ramp rate control of PV output. In that case, the lifetime of BESS may be reduced.

The analyses in this chapter indicate that the suitable control features of multi-functional BESS need to be developed and tested under numerous operating conditions. To this end, a detailed investigation on the voltage performance of residential feeders is required with high PV penetration based on the local standards. The maximum permissible feed-in limit by a solar PV should be determined from the assessment, which will be accomplished in the next chapter.

3.6 Nomenclature

Indices

i, *j*, *k*, *m*	Bus indices
n	Sample index

Inputs (as constants)

expenditure	Total reinforcement cost
d	Discount rate
g	Peak load growth rate (called as load growth rate)
x	Peak shave fraction
cycles	Number of used charge/discharge cycles of a BESS
price (*n*)	Day ahead price of electricity

B_{cap}	Cost of BESS ($/kWh)
η	BESS efficiency
$SoC^{\min}(j)$	Minimum BESS state of charge at j^{th} bus
$SoC^{\max}(j)$	Maximum BESS state of charge at j^{th} bus
$P^{\min}(j)$	Minimum active power drawn from grid via j^{th} bus
$P^{\max}(j)$	Maximum active power drawn from grid via j^{th} bus
$P^{d}(j, n)$	Net active power demand (load minus solar PV) at j^{th} bus
$Q^{d}(j, n)$	Reactive power demand at j^{th} bus
$r^{d\min}(j)$	Minimum discharge rate of j^{th} BESS
$r^{d\max}(j)$	Maximum discharge rate of j^{th} BESS
$r^{c\min}(j)$	Minimum charge rate of j^{th} BESS
$r^{c\max}(j)$	Maximum charge rate of j^{th} BESS
V_{min}	Minimum voltage limit
V_{max}	Maximum voltage limit

Sets

N	Set of total buses in a network
P	Set of possible BESS locations
β	Susceptance matrix
G	Real component of the complex admittance matrix β
B	Imaginary component of the complex admittance matrix β
H	Set of buses through which the network is connected to the grid

Variables

$P^{G}(j, n)$	Active power drawn from grid via j^{th} bus
$Q^{G}(j, n)$	Reactive power drawn from grid via j^{th} bus
$V(j, n)$	Voltage at j^{th} bus
$V_{e}(j, n)$	Real part of complex voltage at j^{th} node and n^{th} sampling instant
$V_{f}(j, n)$	Imaginary part of complex voltage at j^{th} node and n^{th} sample
$I^{*}(j, n)$	Complex conjugate of injected current from j^{th} bus
$r^{d}(j, n)$	Discharge rate of j^{th} BESS
$r^{c}(j, n)$	Charge rate of j^{th} BESS
$SoC(j, n)$	State of charge of j^{th} BESS at n^{th} sampling instant

$Q^{B}(j, n)$	Reactive power absorbed/ delivered by j^{th} BESS

Chapter 4 Distribution Voltage Performance and BESS Control Strategies to Facilitate High Photovoltaic Penetration

It is well documented that distribution networks in Australia are facing voltage regulation challenges due to large amounts of renewable generation [32, 82, 90]. Therefore, several points of existing guidelines for solar PV connections have recently been renewed, which have led to a reduction of PV usage [91]. To this end, the utilisation of BESS has the potential to facilitate the growth of solar PV in power systems[2].

Having analyses of appropriate BESS sizing for peak shaving and voltage regulation applications, this chapter investigates the steady-state voltage performance of a distribution system under substantial PV penetration. A typical section of the Queensland distribution network is analysed to understand the impact of existing and probable solar PV on system voltage rise characteristics. Based on this study, the allowable export limit from a prospective PV connection that alleviates unacceptable voltage rise in the network is determined. This export limit is utilised to develop suitable BESS control strategies for better voltage regulation.

4.1 Background

4.1.1 Analysis of Voltage Rise Phenomenon

A radial distribution feeder is assumed with rooftop PV units at each bus as presented in Figure 4.1. Without PV units, power flows from the distribution transformer to the loads and voltage magnitude drops along a feeder [55]. However, the power flow direction is opposite (load to distribution transformer) if PV output exceeds local demand. The reverse active power flow in a network causes voltage rise, which is illustrated in Figures 4.2(a) and (b).

[2] This chapter has significant materials from the following articles published by the PhD candidate.

- S. R. Deeba, R. Sharma, T. K. Saha and A. Thomas, "Investigation of Voltage Performance of an LV Distribution Network for Improving Rooftop Photovoltaic Uptake in Australia", *IEEE Power and Energy Society General Meeting,* Boston, MA, U.S., 17 - 21 July, 2016.
- S. R. Deeba, "A Battery Management Approach to Improve Steady State Voltage Performance of an LV Distribution Feeder", *Australasian Universities Power and Energy Engineering Conference*, Brisbane, Australia, 25-28 September, 2016.
- S. R. Deeba, R. Sharma and T. K. Saha, "Coordinated Control of Multi-Functional Battery Energy Storage System in an Unbalanced Network", *Australasian Universities Power Engineering Conference,* Perth, Australia, 28 September – 1 October, 2014.

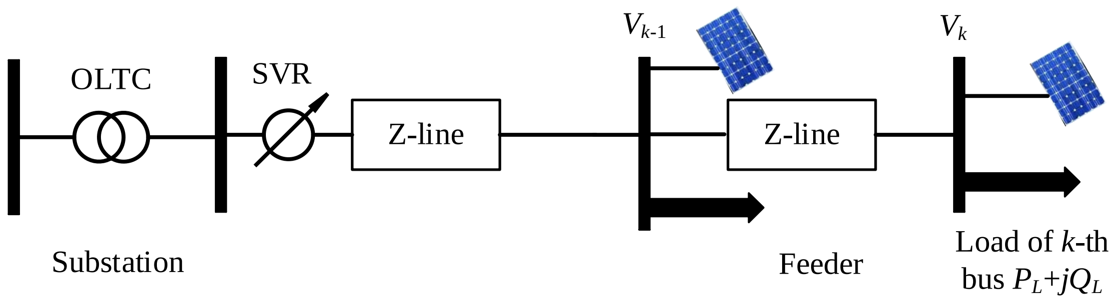

Figure 4.1 A radial distribution feeder with solar PV

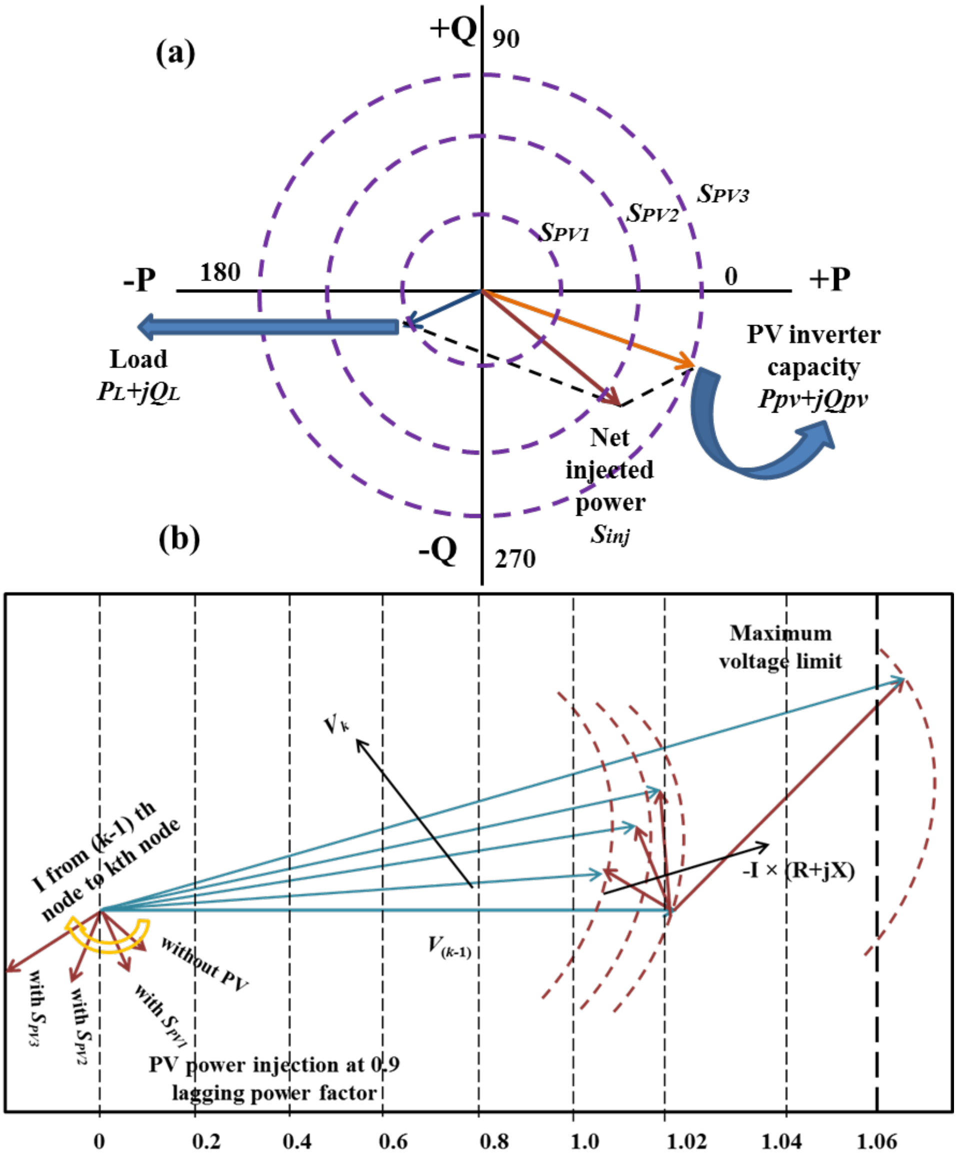

Figure 4.2(a) PQ diagram of the operating point of a PCC at 0.9 lagging power factor (b) Vector diagram of the k^{th} node voltage for various PV outputs [55, 92]

A four quadrant PQ (where P and Q are real and reactive power respectively) diagram is shown in Figure 4.2(a). The 1st and 4th quadrants in the PQ diagram present the active power injection from the PV source to PCC (connection point of a PV and a network) [55]. If a PCC is operated in the 1st and 4th quadrants, it acts as a source. On the other hand, a PCC operating in the 2nd and 3rd quadrants behaves like a load. The +Q and –Q axes imply reactive power source and sink respectively. Let the load at a feeder end bus (denoted by k) be P_L+jQ_L. The net injected power is presented by S_{inj}. The PCC is operating in the P-source and Q-sink mode in Figure 4.2(a). Furthermore, a controllable PV inverter output can be varied along the loci of S_{PV1}, S_{PV2} and S_{PV3}. Figure 4.2(b) shows a vector diagram of the k^{th} node voltages (V_k) for various PCC operating points. Current from the $(k\text{-}1)^{th}$ (upstream location) to the k^{th} node is represented by I. The vector diagram shows that V_k may exceed the 1.06 p.u. limit although PCC is operating at lagging power factor.

The existing and upcoming PV inverters may cause high reverse power flow in light loading situations in a network. It is to be mentioned that the existing rooftop PV units in Queensland until recently have usually operated at unity power factor. However, to mitigate potential voltage rise, the future PV inverters in Queensland are required to be operated at power factors from 0.9 lagging to 0.9 leading [91]. However, voltage rise could violate the allowable limits even though inverters are operated at power factors less than unity.

Now to resolve this problem, existing guidelines in Queensland have recommended limiting the PV power export up to a specified boundary [91]. If BESS are utilised to restrict power export to a pre-defined limit, the prospective inverters can comply with the connection guideline. Therefore, it is crucial to assess the maximum allowable active power export limit for new PV inverters to resolve the voltage rise issue. Even though the export limit is mentioned in the present guidelines, no detailed method is publicly available to determine the maximum export limit from a PV inverter. Once the export limit is determined, it can be used to control the associated PV-BESS units [92].

4.1.2 BESS Topology

The BESS topology consists of a battery bank, a dc-dc bi-directional converter and an inverter [93]. BESS is considered as a shunt device while integrated to a network. BESS performs like a load while charging and as a passive source of generation while discharging. A schematic diagram of BESS with its connection at the PCC is illustrated in Figure 4.3. Two control units are assumed for a BESS: External Control Unit (ECU) and Inverter Control Unit (ICU). ECU utilises a user-defined control scheme and generates appropriate real and reactive power set points for the ICU of the BESS. The ICU tunes the relevant parameters of an inverter to follow the given set points by the ECU for BESS operation.

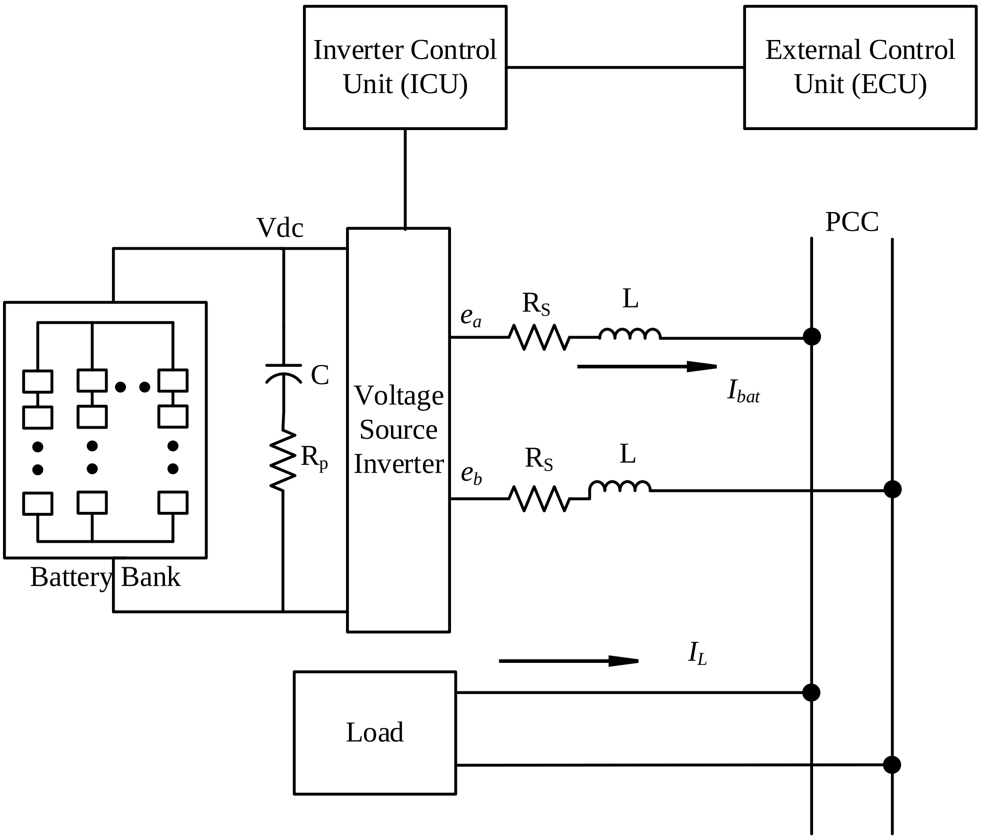

Figure 4.3 Schematic diagram of the BESS topology

4.2 Voltage Performance of an LV Distribution Network under High PV Penetration

In the following sub sections, the voltage performance of an LV network under high solar PV situations is described.

4.2.1 Network Description

A schematic diagram of a section of the Queensland distribution network is shown in Figure 4.4. There are 186 nodes and 114 load buses in the network. The rated line-to-line voltage of the feeders is 0.415 kV. The network is connected to an 11 kV system through a 315 kVA transformer. There is a mix of residential and commercial loads in the system under study. High penetration of PV is observed in the residential feeder F_1. Thereby, the voltage performance of this feeder is analysed as an example case. Currently, there are seven PV units in the feeder F_1. More PVs are likely to be connected in the near future. To investigate the effect of new PV connections on the voltage performance, three PV units are incorporated in bus N_{17}. The node (N_{17}) is located at the furthest end from the distribution transformer and the new PV connection at this site requires detailed voltage assessment.

Usually, distribution lines are periodically upgraded and line impedances are changed after renovation with new conductors. As a consequence, resistance to reactance ratios (R/X) of overhead lines in the studied network are reasonably high (R/X>5). All of the system components i.e.

transformer, feeders, constant power loads and solar PVs are modelled in PSS®SINCAL platform, which is widely used by distribution utilities in Australia [94].

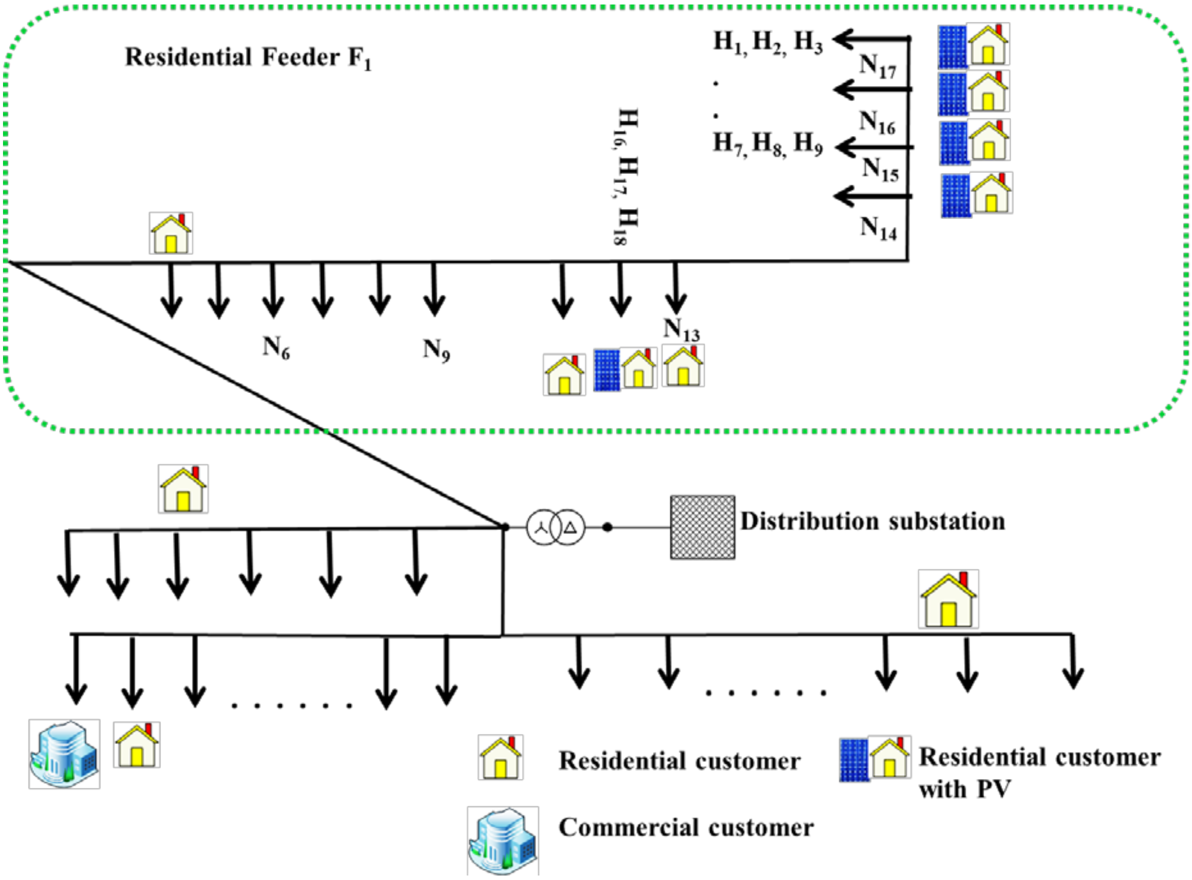

Figure 4.4 Schematic diagram of the studied distribution system [92]

Figure 4.5 illustrates customers' load and PV power profiles used in Section 4.2 [83, 95]. There are seven load patterns for residential customers. Amongst them, profiles A1, A2 and A3 represent light loading scenarios (less than 1 kW) in a year. Since reverse power flow occurs when PV generation exceeds load demand, the aforementioned light load profiles are considered for PV connected customers. This assumption is made to simulate a concerning voltage performance scenario. Other load profiles such as A4, A5, A6 and A7 are used for customers without a PV unit. Available PV capacities in the network are 3kW, 5kW and 6kW.

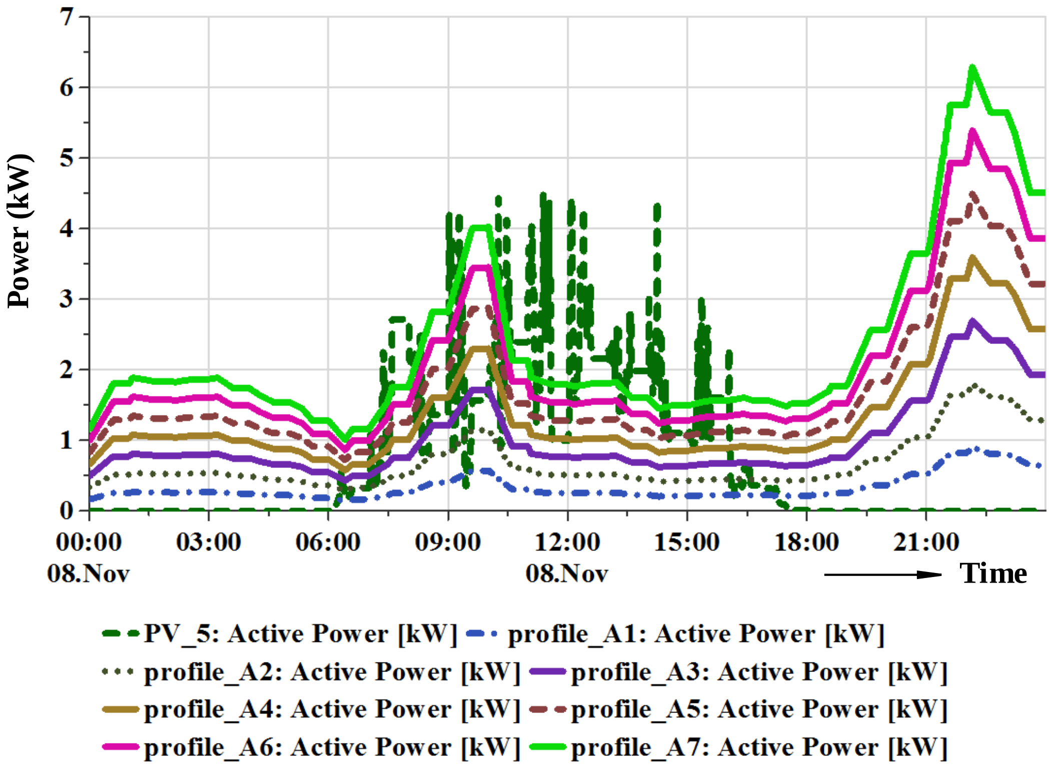

Figure 4.5 Residential customers load and PV power profiles [92]

It is to be remembered that the existing PV inverters are operating at unity power factor and upcoming inverters will be operated at 0.9 lagging to leading power factor. A PV profile, which corresponds to maximum output power and rapid fluctuations, is considered as an example case to understand the voltage rise phenomenon [95]. The selected profile is being scaled for the three aforementioned capacities of PV units. A PV power pattern (PV_5) for a 5 kW unit is also shown in Figure 4.5.

Table 4.1 presents the locations of all the existing and proposed PV units in the feeder F_1. It is observed from Table 4.1 that there are a total of ten rooftop PV units in the feeder (existing and proposed), which are unequally distributed to all three phases.

Table 4.1 Rooftop PV connection to households in feeder F_1 [92]

House	PV unit Capacity (kW)	Connected to Node	Connected to Phase
H_1-H_3	5	N17	L123 (all)
H_5	3	N16	L2
H_9-H_{11}	5	N15	L123
H_{16}	3	N12	L2
H_{28}	6	N8	L2
H_{38}	3	N4	L3

4.2.2 BESS Control Strategy

A rule based control strategy for BESS is adopted to mitigate the voltage rise effect caused by high PV power availability. It is assumed that the proposed strategy is implemented in the external control unit of a BESS. The ECU is connected to a supervisory control centre through a communication channel, which can be monitored by a system operator. Figure 4.6 presents a flow chart of the considered BESS control scheme.

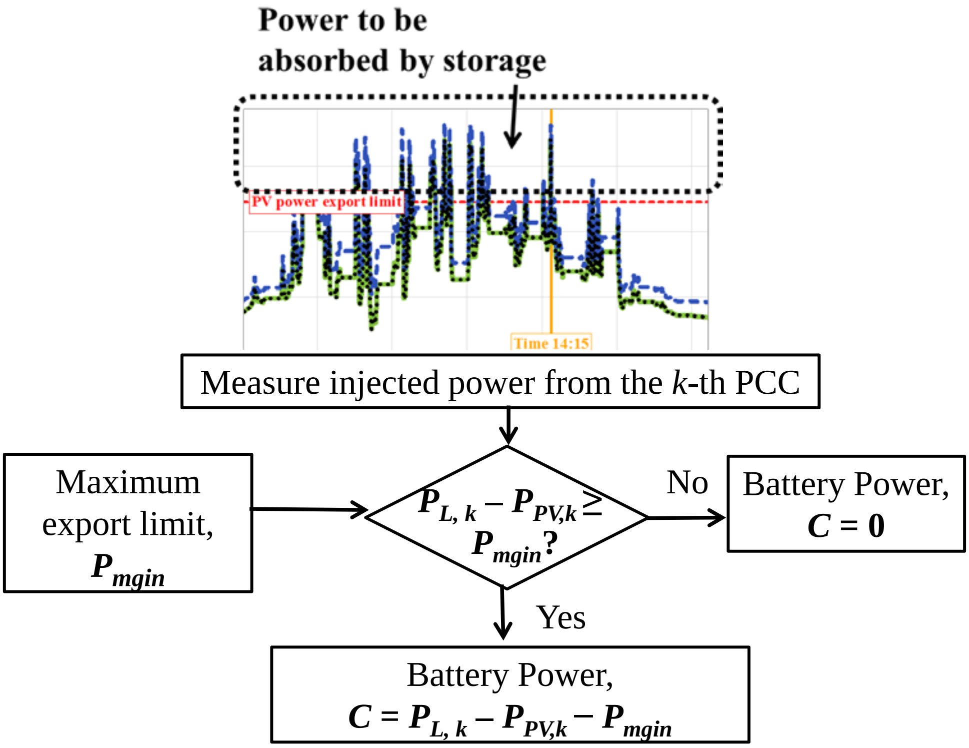

Figure 4.6 The proposed charging scheme for BESS [92]

A BESS starts charging from solar PV if power injection from a PCC to a network exceeds a specified boundary, which is selected by the supervisory system. Let the maximum allowable power export be P_{mgin} for k^{th} PCC. Let the load and PV output be represented by $P_{L,k}$ and $P_{PV,k}$ respectively. A decision making strategy for BESS is selected, which is able to limit power injection from the k^{th} PCC ($P_{L,k}$ – $P_{PV,k}$) by an allowable margin P_{mgin}. If the injected power exceeds P_{mgin} , BESS charge rate is determined by (4.1).

$$C = (P_{L,k} - P_{PV,k} - P_{mgin,k}) / \eta ; \eta = \text{charging effeciency} \tag{4.1}$$

Otherwise, BESS power is set to C = 0. The energy stored in the BESS can be discharged if required, when load is more than a certain value. Nevertheless, the voltage rise phenomenon is alleviated by only charging BESS. Therefore, BESS discharging is not considered in this section.

4.2.3 Results and Discussions

The proposed BESS control strategy is applied to the studied network under the PSS®SINCAL environment. In this subsection, the simulation results to determine the maximum allowable PV export limits for acceptable voltage performance are presented.

4.2.3.1 Investigating the maximum export from the prospective rooftop PV connections

In the first stage of simulation, voltage performance of the studied network is observed with seven existing PV units in feeder F_1. It is found from the load flow study that the bus voltages of N15, N16 and N17 experience around 104% of the nominal voltage (240 V) at some instants in a day. Therefore, these locations are selected as candidate buses to scrutinise their voltage performance under reverse power flow scenarios. In the next stage, new PV units each with 3 kW capacity are connected at node N17. Notably, the PV inverters are assumed to be charged at 0.9 lagging power factor. Figure 4.7 illustrates active power export to the network from the proposed PV units (3 kW), which are connected to all three phases (L1, L2 and L3) of node N17. The associated reactive power flow is also presented in Figure 4.7. Corresponding node voltage profiles are depicted in Figure 4.8.

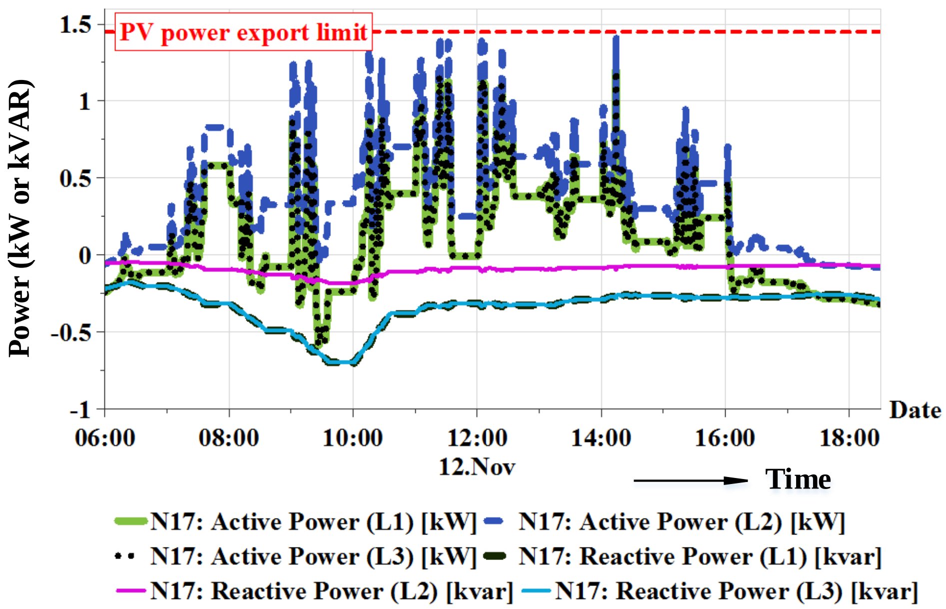

Figure 4.7 Active power injection from node N17 with new PV inverters (3 kW capacity each) [92]

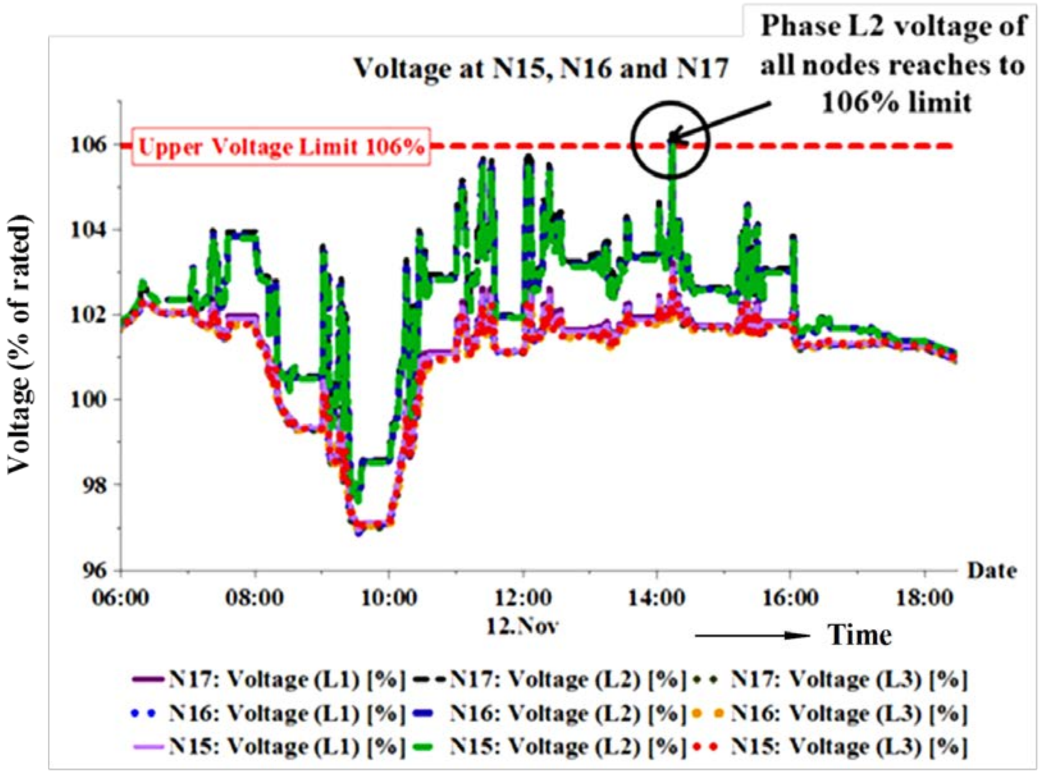

Figure 4.8 Voltage performance of the studied buses with new PV inverters (3 kW capacity) [92]

It is observed from Figures 4.7 and 4.8 that at all phases of node N17 are exporting high active power at lagging power factor at the time instant 14:15. As a result, the voltage of phase L2 of nodes N15, N16 and N17 reach 106% at time 14:15. Alternatively, it can be said that the feeder end voltage rises by 2% due to prospective PV connections, which marginally complies the connection guideline.

It is noticed that active power export from phases L1, L2 and L3 of node N17 at the time 14:15 are 1.25 kW, 1.5 kW and 1.25 kW respectively. It causes the candidate bus voltages to reach 106% of their rated magnitude. Therefore, the maximum active power export limit from each phase of nodes N17 to N16 can be considered as 1.5 kW for the current PV penetration level in the network. If PV power injection increases, the voltage increases at PCC.

Now the capacities of new PV units are increased to 5 kW for customers H_1, H_2 and H_3 connected to node N17. Figure 4.9 presents power injection from each phase of node N17 with such a high PV penetration.

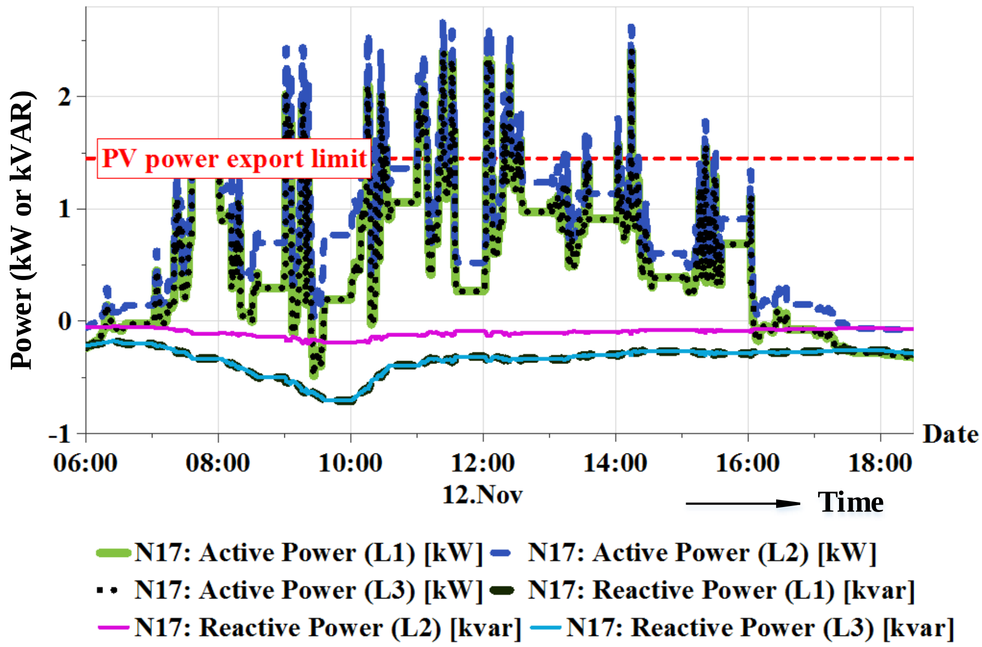

Figure 4.9 Active power export from nodes N17 to N16 for the proposed 5 kW PV connection [92]

It is observed that significant active power is exported and reactive power is absorbed from node N17 during the day between 7:00 and 17:00. Therefore, it can be said that the PCC at node N17 is working in Q-sink mode. Corresponding voltage magnitudes at buses N15, N16 and N17 are presented in Figure 4.10. It is noticed that the proposed PV units with 5 kW capacity cause voltage rise at phase L2 of candidate buses. The voltage magnitudes of the aforementioned buses become 107.5% at the time instant 14:15 for the studied PV power profile. Furthermore, the voltage rise issue could be prolonged in the case of a clear sunny summer day.

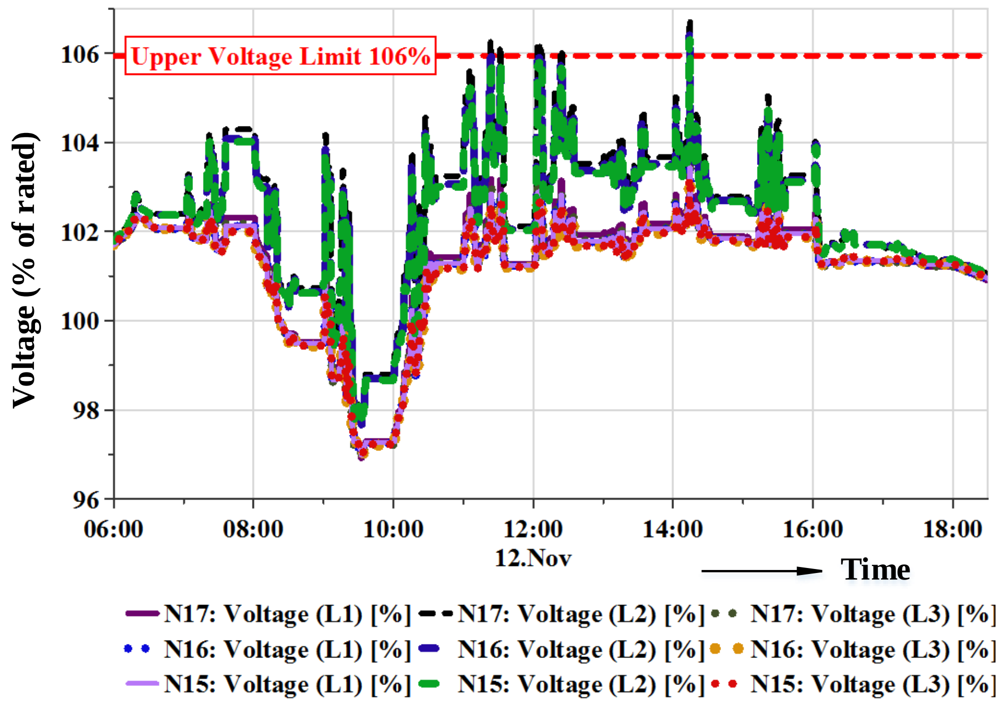

Figure 4.10 Voltage profiles at nodes N15, N16 and N17 for the proposed 5 kW PV connection [92]

The above case studies show that PV operation less than unity power factor of the prospective 5 kW PV units does not necessarily help to resolve the voltage rise issue in the studied section of the network. In such a scenario, the proposed inverters with bigger capacities i. e. more than 3 kW will not comply with the voltage standards. Therefore, the customer's application for a PV connection above 3 kW capacity may not be approved resulting in restriction to the growth of solar PV. To resolve this issue, the high PV power export should be limited by utilising a device such as BESS. The injected power at a PCC, which exceeds the 1.5 kW limit can be stored in a BESS. Hence, customers can use bigger PV units with BESS storage without creating undesirable voltage rise. The utilisation of BESS can help customers in a number of ways; firstly, additional PV capacity offers more benefits through electricity cost reduction. BESS can also be utilised during rainy days while PV power is unavailable. Moreover, an appropriate BESS utilisation under time of use pricing can help customers in achieving energy arbitrage.

4.2.3.2 Observation of Voltage Profiles with PV and BESS

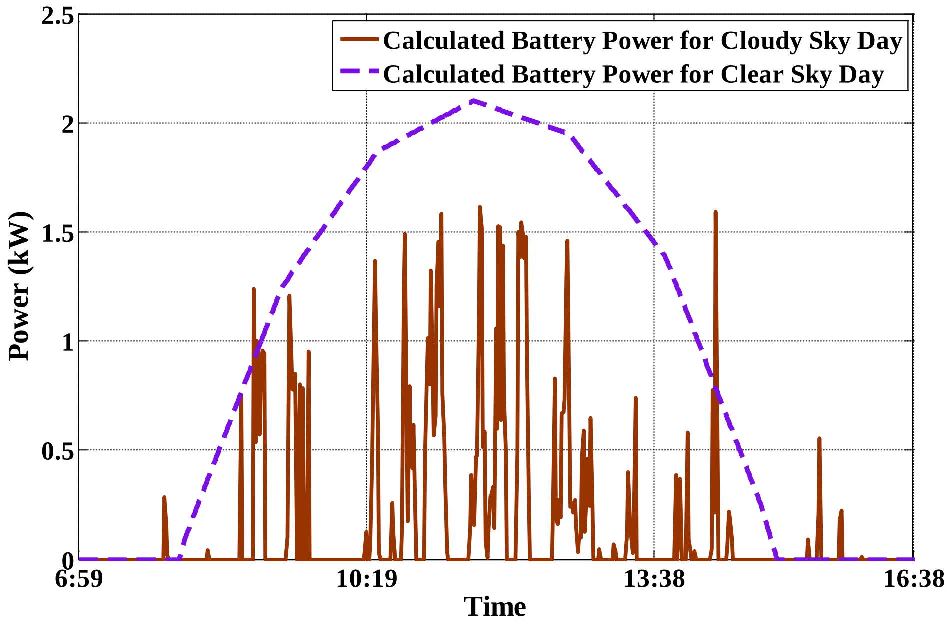

Figure 4.11 BESS output power using the proposed strategy [92]

A user-defined BESS model in PSS®SINCAL is used to execute the proposed control strategy. The model consists of battery banks, a bi-directional converter and an inverter. Charge/discharge rates of BESS depend on the set points of the user-defined controller in ECU. A desired charging rate is provided to the ECU set point and the inverter controller (i. e. ICU) tries to track this reference value. Figure 4.11 presents charging rate (kW) of BESS during the day for two PV power profiles i.e. cloudy and clear sky days. The desired BESS power (C) is calculated by using the proposed control scheme as described in Section 4.2.2. When the injected power from a PCC exceeds 1.5 kW margin, BESS controller is set to a charge rate as calculated using (4.1). The charging efficiency of

BESS management system is considered to be 80%. It can be observed that the maximum value of C is 2.1 kW for a clear sky day. The capacity of BESS is determined by calculating the area under the clear sky profile, which is 10 kWh for each customer. In the case of a cloudy day, there is a rapid fluctuation in BESS charging rate with the proposed control scheme. Advanced BESS technologies such as Lithium-ion BESS can handle this fluctuation and perform up to 10 years .

Customers H_1, H_2 and H_3 are being connected with three individual PV and BESS units and their voltage profiles are observed. Figure 4.12 shows the voltage magnitudes of all phases at nodes N15, N16 and N17. It can be observed that all node voltages reside within 106% of their rated value.

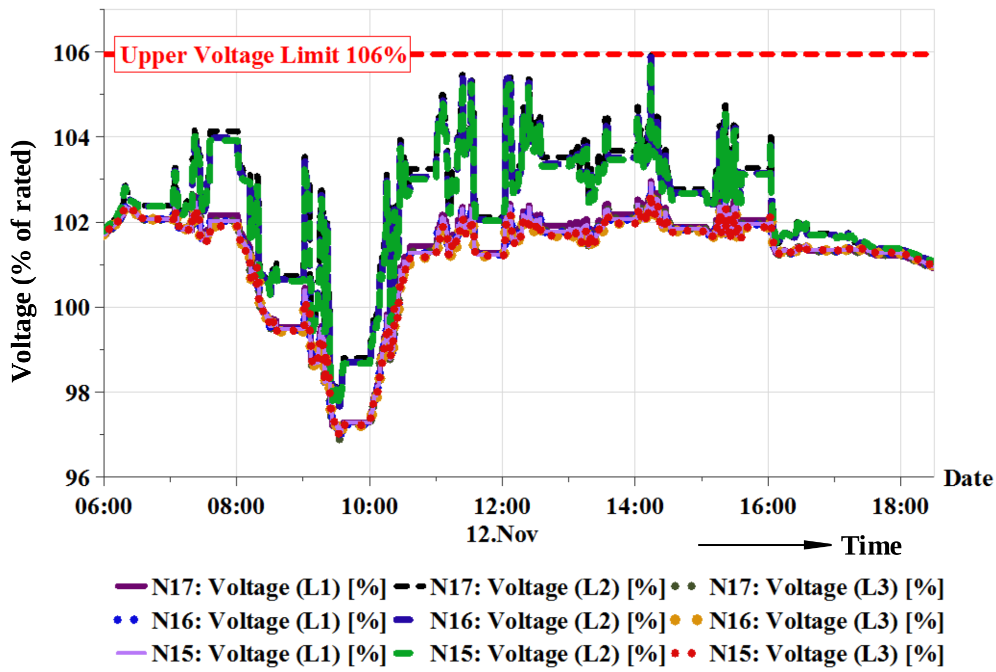

Figure 4.12 Voltage profiles of the candidate buses with PV and BESS [92]

Figure 4.13 illustrates the injected power from node N17 with controlled BESS units. It is observed that active power is exported from bus N17 between the time 7:50 and 15:00. It is also found that power injection with controlled BESS does not exceed the limit of 1.5 kW during this time period.

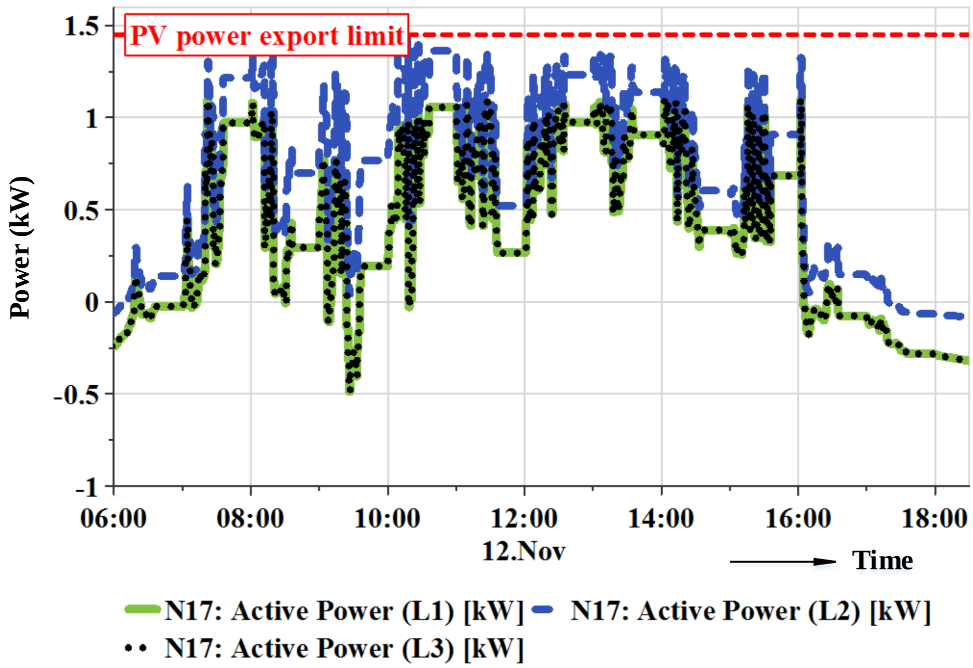

Figure 4.13 Active power export from node N17 to N16 with PV and BESS [92]

Figure 4.14 shows the *SoC* of a BESS connected to H_1 customer at node N17. It is observed that *SoC* reaches to 10% from its initial *SoC* at around 16:00 hrs. The BESS connected to customers H_2 and H_3 also shows a similar *SoC* pattern since their load and PV profiles are similar. With the proposed control strategy, BESS will be charged from solar PV. If BESS is charged from a grid, there is an associated expenditure for a customer. However, a similar amount of expenditure is reduced when the BESS are discharged. The distribution utilities can offer an incentive to promote PV-BESS system among the customers. Since BESS allows customers to accommodate more PV, it can be economically beneficial for them in the long run.

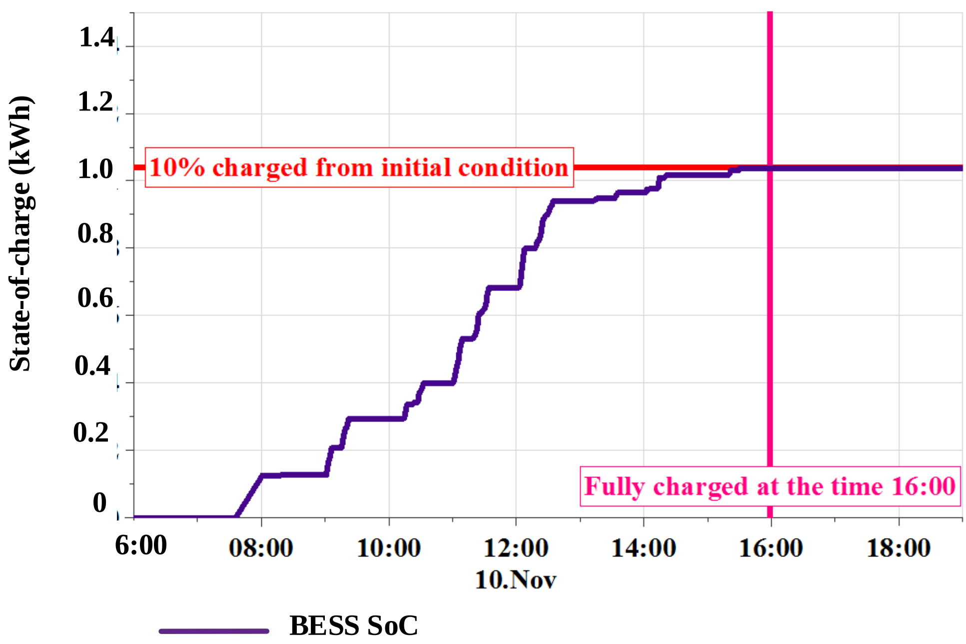

Figure 4.14 State of charge (kWh) of a controlled BESS unit [92]

4.3 A BESS Management Approach to Improve the Steady State Voltage Performance of Distribution Networks

In this section, the rule-based BESS management strategy described in Section 4.2 is further improved to maintain the standard voltage limits in an LV network. The proposed strategy can reduce the fluctuations of the BESS charge rate under variable PV output. The total capacity of a BESS is used for two purposes. Firstly, x% of the capacity is dedicated to peak shifting. The rest of the capacity is utilised for storing surplus PV energy. The effectiveness of the proposed approach is observed at different PV output conditions. Finally, the required number and locations of BESS are investigated [96]. The proposed BESS control strategy and simulation results are described in the following subsections.

4.3.1 BESS Control Strategy

4.3.1.1 Capacity Determination

BESS are utilised for two applications: system peak reduction and voltage rise mitigation. The BESS are charged in the daytime if the PV export exceeds a specified limit. Any violation of the condition causes no charging of the BESS during the day. The system peak for a residential feeder occurs in the evening, which implies BESS can be discharged in the evening. To ensure daily peak shaving, at least 30% of a BESS capacity is charged in the night. The maximum charge/discharge rate (C_{max}) is determined by using (4.2).

$$C_{max} = (P_{PV\,max} - P_{L\,min} - P_{mgin}) / \eta \tag{4.2}$$

P_{PVmax} = Maximum PV output

P_{Lmin} = Minimum demand at PCC

P_{mgin} = Active power export limit from a PCC

η = Charge/discharge efficiency of a BESS

4.3.1.2 Multi-Mode Operation of a BESS

In the proposed approach, ECU generates an appropriate reference signal for inverter action and delivers it to the ICU. The external controller is user-defined and is designed to operate in 3 (three) modes. ECU is set to Mode-A if the connected PV output is zero, while PCC is operated at its maximum loading (P_{Lmax}) or PCC voltage (V_{PCC}) violates its lower limit (V_{LO}). If PV output exceeds the maximum export limit, ECU operates in Mode-B. Mode-C is selected if PV has no output and V_{PCC} is above a limit V_{MD}. If none of the above situations occur, the BESS operates in an idle state.

4.3.1.3 Decision-Making Strategies of ECU

In **Mode-A**, ECU of a BESS generates a discharge signal for its ICU. If P_{PV} is zero, while V_{PCC} is less than V_{LO} or connecting load is more than P_{Lmax}. BESS charge rate (C_A in kW) is calculated by (4.3). In this operating mode, the BESS are discharged for almost 1.5 to 2 hours in the evening. The minimum state-of-charge of a BESS is chosen as 10% of its maximum capacity.

$$C_A = SoC_{av} / D, \text{ if } P_{PV} = 0, P_L \geq P_{L\,max} \text{ or } V_{PCC} \leq V_{LO} \tag{4.3}$$

D = Total discharge time

SoC_{av}= Available state-of-charge of a BESS (kWh)

P_L = Real power of the connected load

P_{Lmax} = Maximum limit of the real part of the load

In **Mode-B**, BESS are charged from the surplus PV energy. A PV output profile in the case of a clear sky day is considered to generate a standard BESS charging profile. A standard charge rate (C_{STD}) is determined by using (4.4).

$$C_{STD} = -\begin{cases} P_{PVclear} - P_L - P_{mgin}, & (P_{PVclear} - P_L) \geq P_{mgin} \\ 0 & \text{, otherwise} \end{cases} \tag{4.4}$$

$P_{PVclear}$ = PV output for a clear sky day

P_L= Household demand

The ECU calculates the charge rate (C_B) of a BESS by using (4.5).

$$C_B = -\begin{cases} P_{PV} - P_L - P_{mgin}, & \text{if } (P_{PV} - P_L) \geq P_{mgin} \ \& \ SoC_{av} \leq 100\% \\ 0 & \text{, otherwise} \end{cases} \tag{4.5}$$

In the next step, ECU compares C_B and C_{STD}. If the absolute error is more than 50%, ECU sets the charge rate as C_{STD}.

A BESS is charged at a fixed rate (C_C) for almost 4 hours in operating **Mode-C** during the night time while demand is reasonably low. The calculated charge rate is defined by (4.6).

$$C_C = -0.3 \times SoC_{max} / 4, \text{ if } P_{PV} = 0 \ \& \ V_{PCC} \geq V_{MD} \tag{4.6}$$

SoC_{max} = Maximum state-of-charge of a BESS in kWh

4.3.2 Simulation Results

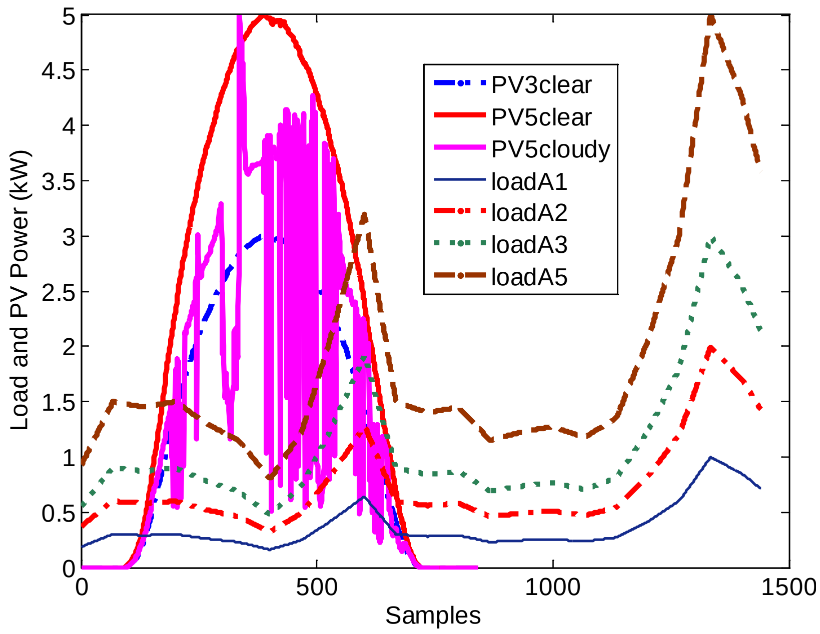

Figure 4.15 Day-ahead load and rooftop PV power profiles of residential customers [96]

A typical segment of the Queensland LV network as described in Section 4.2.1 is utilised for case studies. Figure 4.15 presents the load and PV power profiles of customers used in this section. PV power profiles for both sunny and cloudy days are collected from the UQ solar database and scaled for 3 and 5 kW units [95]. 'PV3clear' and 'PV5clear' represent the clear sky PV profiles for 3 kW and 5 kW systems respectively. 'PV5cloudy' presents the output profile of a 5 kW unit for a cloudy day. Four load profiles of the residential customer have also been presented in Figure 4.15, while 'loadA1' stands for a light loading scenario (<1 kW) [83]. To understand the voltage performances at high PV power situation, 'loadA1' profile has been chosen for houses H_1 to H_9 of the studied network.

By using the above load and PV profiles, the maximum PV export limit is determined. All the components of the studied network are modelled in the PSS®SINCAL software platform. Then, the export limit is used for the proposed BESS controller in 4 case studies. In case study–1, a BESS is integrated to phase L2 of node N17 and the network voltage performance is studied for a clear sky day. In case study- 2, BESS performance is observed under a variable PV power profile. The required number of BESS units with increasing PV penetration is examined in case studies 3 and 4.

4.3.2.1 Determination of the Maximum PV Export Limit

An upper voltage limit V_{UP} is considered to be 106% in this study. It is obtained from the analysis in Section 4.2 that studied bus voltages exceed V_{UP}, if surplus PV output at node N17 is more than 1.5 kW. This is taken as the value of P_{mgin} to control BESS units.

4.3.2.2 Case Study-1: Performance of a BESS for a Clear Sky Day

The node voltages of phase L2 of the studied feeder are more sensitive to PV and BESS connection because of the unbalanced line characteristics. Therefore, a BESS unit is connected to phase L2 of node N17 to control the respective PV export in case study-1. The maximum power and energy capacities of the BESS are selected as 4kW and 16 kWh respectively. The real and reactive power flow and the BESS output (BESS_clear) are presented in Figure 4.16. Figure 4.17 shows the day-ahead voltage profiles of the studied nodes with BESS. It is observed from Figures 4.16 and 4.17 that the BESS is charged during the night for 4 hours when the PCC voltage is above 100%. It stops charging while BESS *SoC* reaches 40% of its maximum capacity. The initial *SoC* of the BESS is considered as 10% of its nominal value. Figure 4.18 shows the day long *SoC* of the BESS unit in kWh.

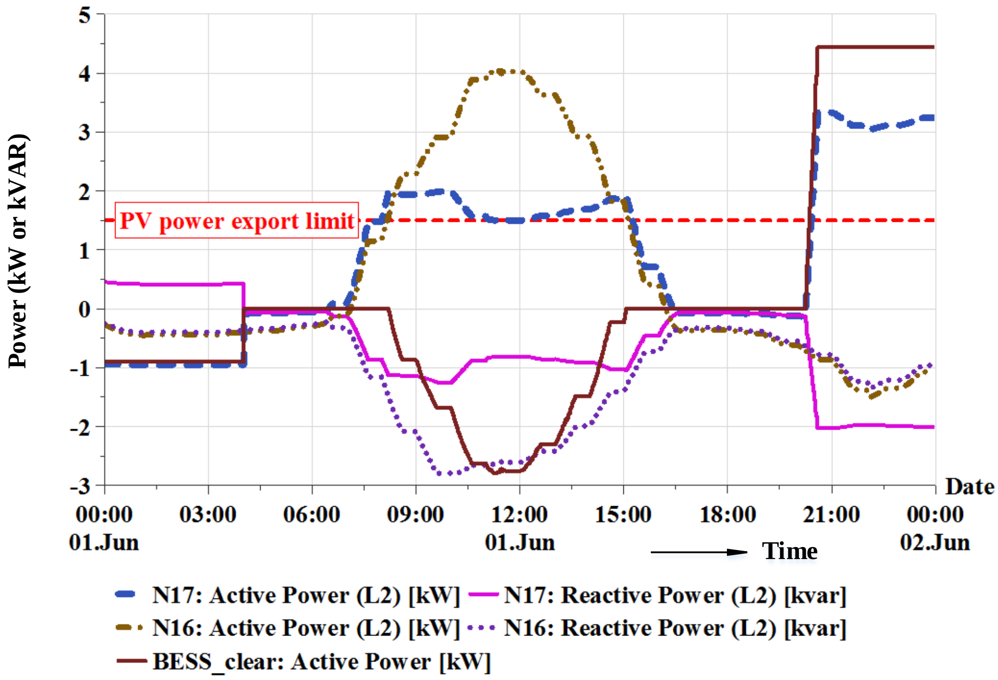

Figure 4.16 Active and reactive power flow at the node N17 with a BESS [96]

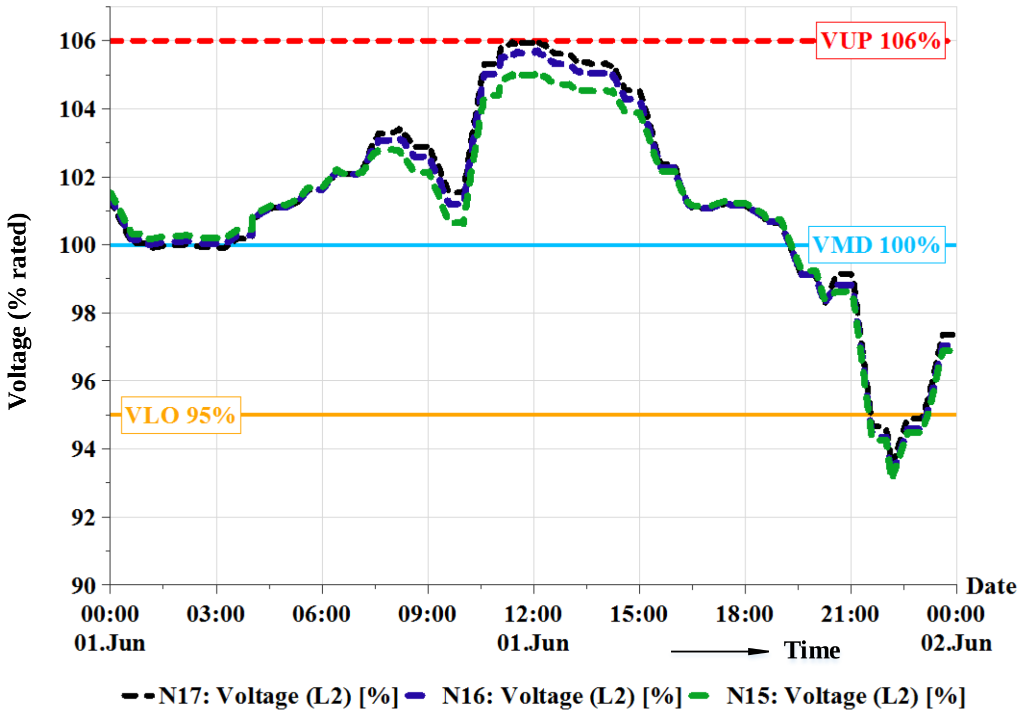

Figure 4.17 Day-ahead voltage profiles with PV and BESS in case – 1 [96]

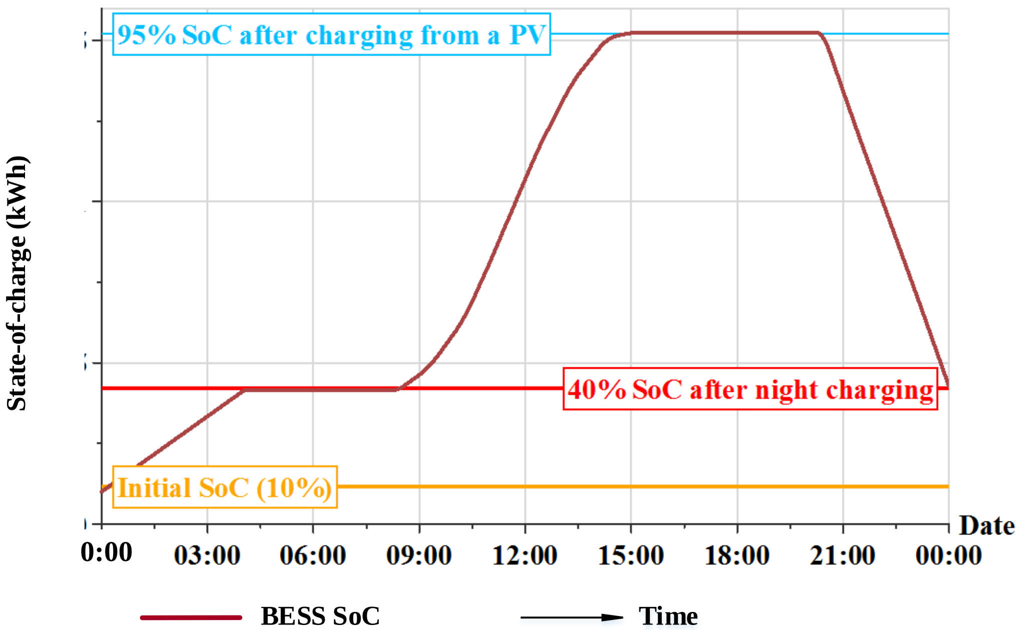

Figure 4.18 State of charge of a BESS connected to node N17 [96]

It is also found from Figures 4.16, 4.17 and 4.18 that the BESS is charged when PV export exceeds the specified limit (1.5 kW). It is also observed that the BESS absorbs the surplus PV energy starting from 8:40 to 15:00 hrs. The *SoC* of the BESS reaches 95% of its maximum capacity (i.e. 16 kWh) at 15:00 hrs. The BESS starts discharging in the evening when PV output is zero, while the load exceeds 0.75kW or PCC voltage goes below 95% of the nominal value

It is noticed from Figure 4.17 that the PCC voltage is maintained within the 106% limit during high PV generation time. It is also found that the voltage performance has been improved in the evening by using the proposed control scheme.

4.3.2.3 Case Study-2: BESS Performance for a Cloudy Day

Figure 4.19 presents the net power flow and the output of the BESS connected at phase L2 of node N17 on a cloudy day.

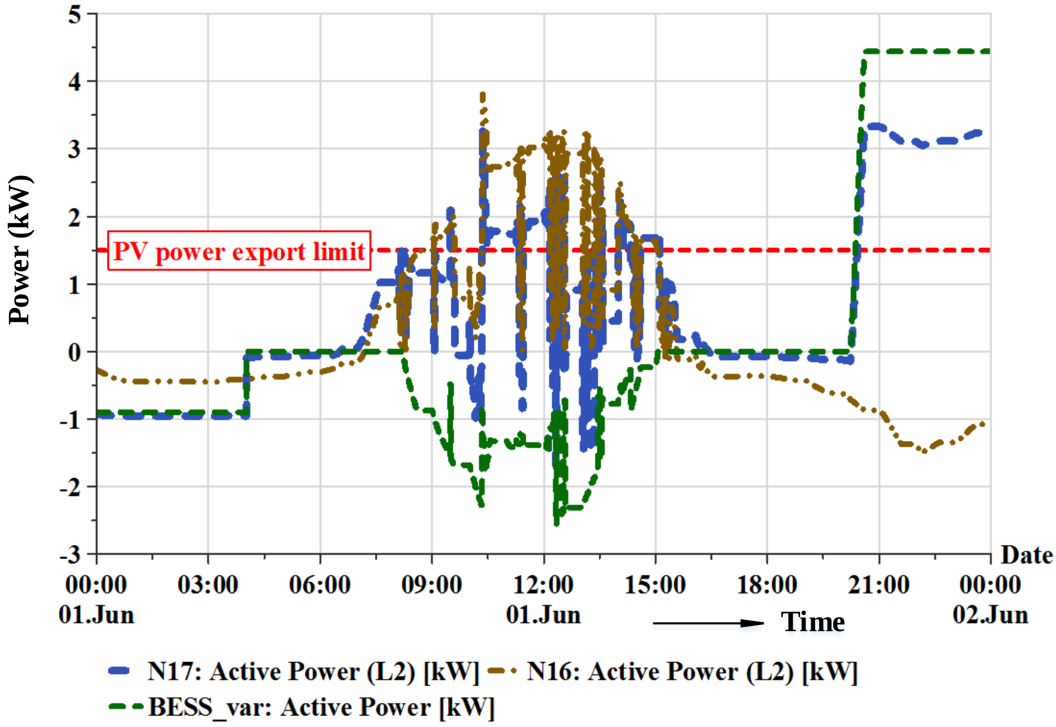

Figure 4.19 BESS output and net power at node N17 on a cloudy day [96]

It is observed that BESS is charged overnight at a constant rate, while BESS output experiences a small fluctuation under solar PV. In the evening, BESS is discharged at a constant rate, which helps to reduce the overall peak of feeder F_1. The state-of-charge of the BESS and the corresponding bus voltage profiles are presented in Figures 4.20 and 4.21 respectively. It is found that the studied BESS is charged to 75% of the rated capacity from PV on a cloudy day maintaining the voltage rise limit. However, the feeder voltage remains below the V_{LO} limit in the evening for case -2.

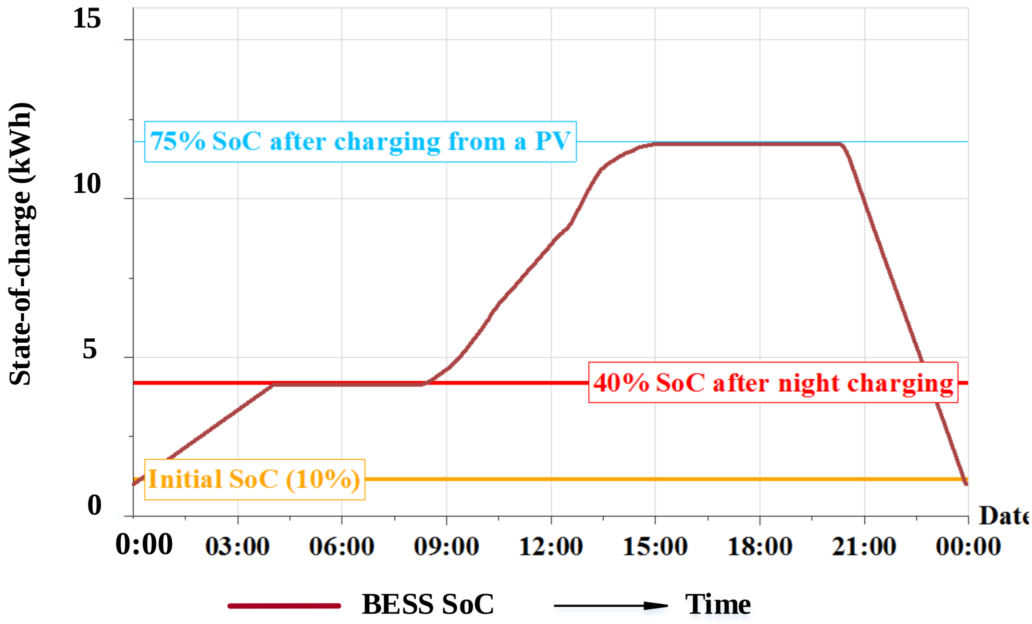

Figure 4.20 BESS SoC on a cloudy day

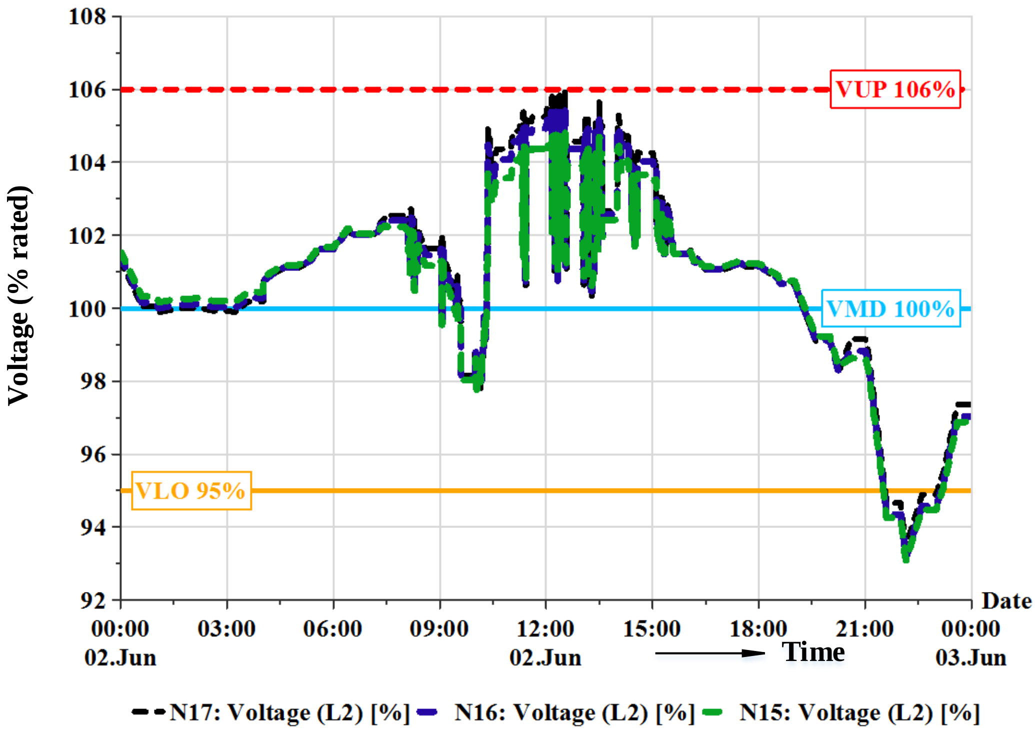

Figure 4.21 Voltage profiles of the studied buses with BESS on a cloudy day [96]

4.3.2.4 Case Study-3: Two New PV Units in the Phase L2

Two new PV inverters are allocated to phase L2 of nodes N14 and N17. There is only one BESS unit connected to node N17-L2. Figure 4.22 shows the voltage profiles of the feeder end nodes from N14 to N17.

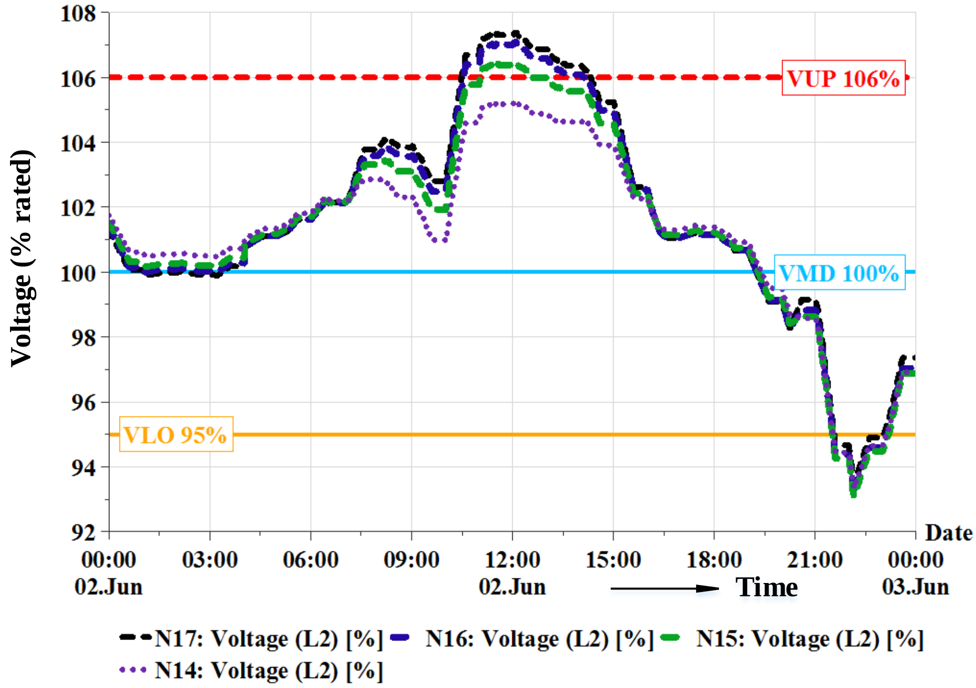

Figure 4.22 Voltage profiles of the studied buses in case study-3 without a BESS at N17 - L2 [96]

It is observed that the voltage magnitudes of the three feeder end nodes (N15, N16, and N17) have violated the 106% limit. Therefore, more than one BESS is required to resolve the voltage rise. Two BESS units are placed on phase-L2 of nodes N16 and N17 respectively. Then the voltage performance of the studied nodes is captured in Figure 4.23. It is observed that the voltage rise of the network can be resolved with two batteries if there are four PV units connected to the four feeder-end locations.

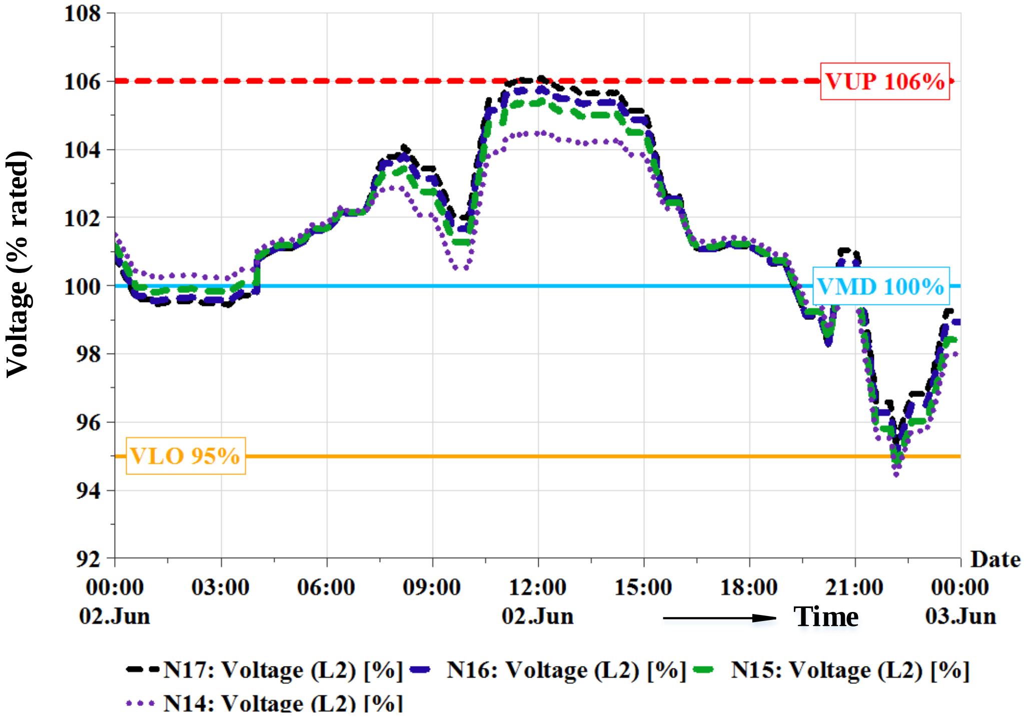

Figure 4.23 Voltage profiles of the studied nodes with two BESS units [96]

4.3.2.5 Case Study-4: Three New PV Units Connected to the Phase L2

In this case study, three new PV inverters are connected to nodes N13, N14 and N17 respectively. Therefore, there are five PV units in total connected to phase L2. It can be observed from the bus voltages that even though two BESS units are connected at N16 and N17, the voltage margin is violated during mid-noon as depicted in Figure 4.24.

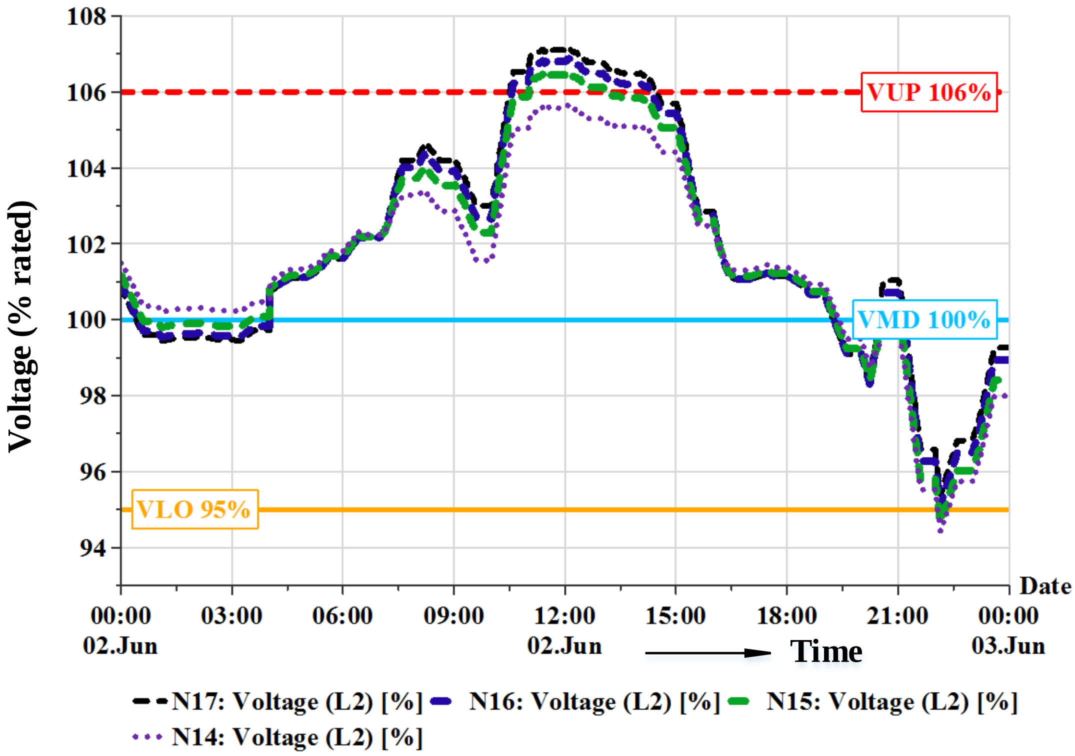

Figure 4.24 Voltage limit violation at the studied buses in case study –3 [96]

To resolve this problem, another BESS unit is placed at node N15-L2 and the voltage performance of the concerned nodes is again observed. Now, in total three BESS are connected to locations N15, N16 and N17. It is to be mentioned that all BESS units are of 16 kWh capacities and the whole PV-BESS package is installed by customers. Such PV-BESS users can be provided incentives through solar rebates or time of use pricing from the respective utility. Figure 4.25 illustrates the voltage profiles of the studied locations. It is observed that with the three BESS units, the network voltage is limited to within 106%.

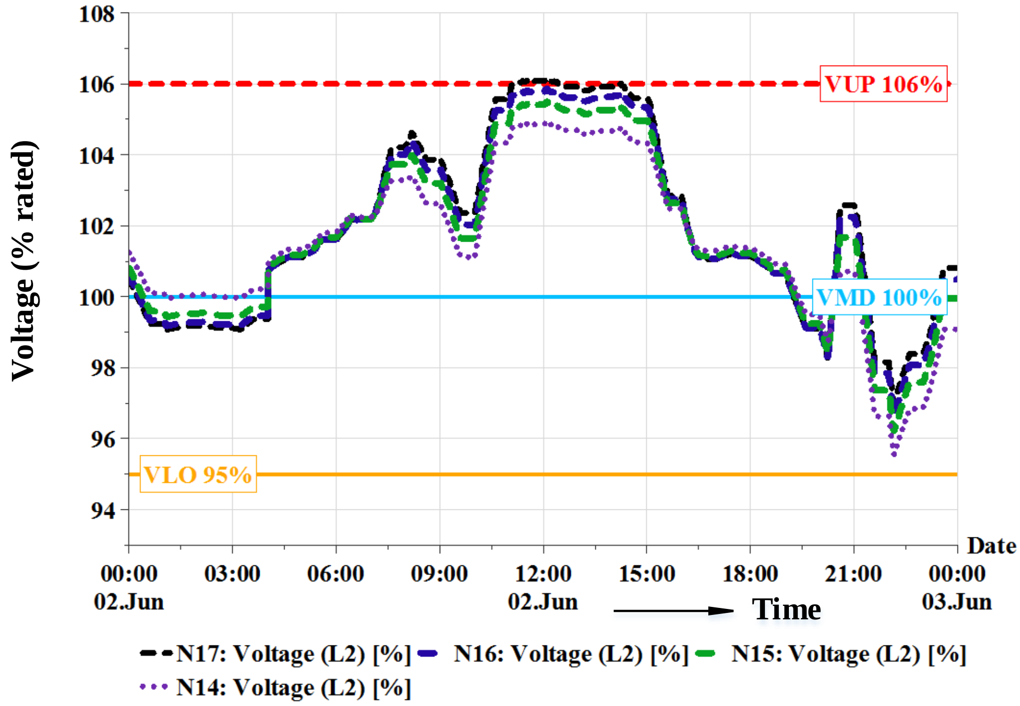

Figure 4.25 Voltage performance of the feeder end nodes in case study – 4 [96]

In this case, three BESS units altogether have participated in the overall peak shaving of the network. Therefore, the voltage profiles in the evening have been improved. The day-ahead power flow at the corresponding buses is presented in Figure 4.26.

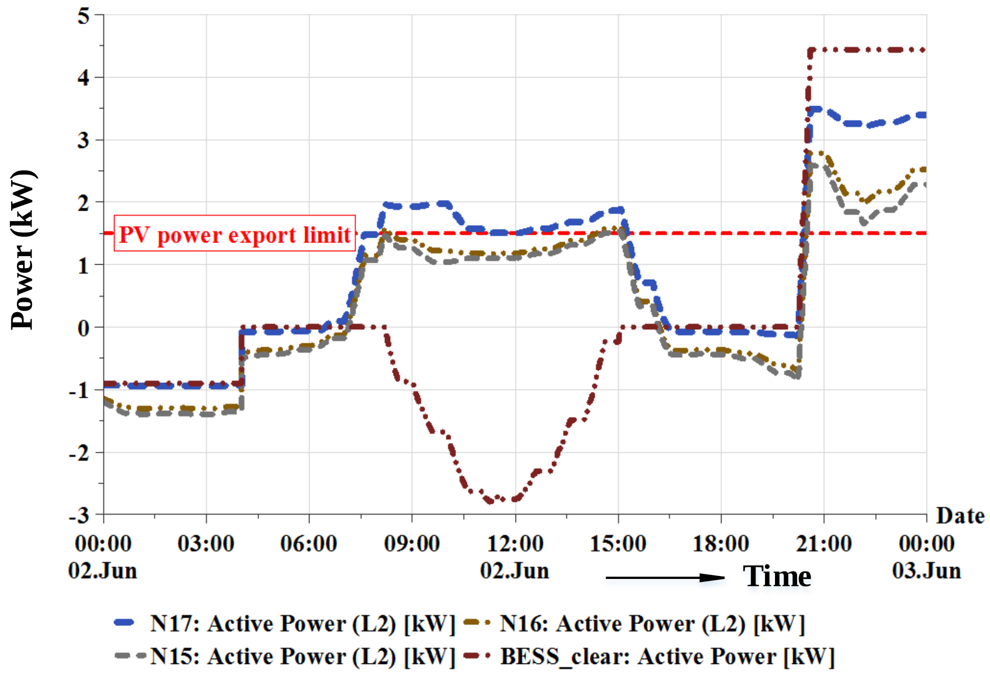

Figure 4.26 Net power flow at the studied nodes with three BESS in case study – 4 [96]

It can be observed from the four case studies that the considered network can accommodate more PV resources if a number of BESS units are connected to the appropriate locations. With higher PV penetration, the required number of BESS increases. In case study-1, three PV units are connected sequentially to the last three nodes of feeder F_1. Results show that the voltage rise can be mitigated by connecting a single BESS to N17-L2 in case study-1. The number of PV units is increased in the subsequent case studies. Case study-4 shows that if there are five PV units on phase L2, three BESS units are required to mitigate the over-voltage phenomenon. Therefore, it can be summarised that if there are n number of PV units connected in a phase of the studied LV feeder, (n-2) BESS units can be used to alleviate unacceptable voltage rise, where n represents a positive integer number.

4.4 Coordinated Control of Multi-functional BESS

In this section, three important applications of BESS namely, peak shaving, load levelling and voltage regulation are coordinated using a control approach. The proposed approach is based on measurements of current magnitudes at PCC and comparing them with predefined limits. The load forecast is also utilised to calculate two vectors for deciding charge and discharge operation of a BESS. The proposed approach is applied to the IEEE-37 nodes system in MATLAB-Simulink environment [97, 98].

4.4.1 Methodology

In the proposed approach, ECU (Figure 4.3) of a BESS takes seven inputs. These are actual and forecast load current, bus voltage, power flow direction, state of charge of a BESS, upper and lower current limits. Using these inputs, ECU sets separate commands for charge and discharge of BESS. Upper and lower current limits of a feeder load are specified by a DNO based on their desired operational requirements. For the given upper and lower limits of load current, the summation of charge and discharge energy of a BESS in a day should fulfil the expressions in (4.7) – (4.10).

$$\sum_{m=1}^{M} q_m = 0 \tag{4.7}$$

Hence,

$$\sum_{m=1}^{M} q_{charge} = \sum_{m=1}^{M} q_{discharge} \tag{4.8}$$

For k^{th} node,

$$\sum_{m=1}^{M} q_{discharge} = \sum_{m=1}^{M} |I_{L\ forecasted,m} - I_{L\,upper,m}| U_{dg,m} \Delta t_m \tag{4.9}$$

$$\sum_{m=1}^{M} q_{charge} = \sum_{m=1}^{M} |I_{Lforecasted,m} - I_{Llower,m}| U_{chg,m} \Delta t_m \tag{4.10}$$

where

m = Sampling indices

q_m = Total charge stored/released (Ampere-hour)

q_{charge} = Amount of charge stored in BESS

$q_{discharge}$ = Amount of charge released from BESS

$I_{L\ forecasted,m}$ = Load current forecast at k^{th} bus and m^{th} sampling instant

$I_{L\,upper,m}$ = Upper limit of load current at k^{th} bus and m^{th} sampling instant

$I_{L\,lower,m}$ = Lower limit of load current at k^{th} bus and m^{th} sampling instant

Δt_m = Sampling period

M = No. of total samples in a day

U_{dg} = Decision vector for discharge

U_{chg} = Decision vector for charge

BESS charge and discharge depends on the state (0 or 1) of two parameters, U_{dg} and U_{chg}. If $I_{Lforecasted} < I_{Lupper}$, $U_{dg} = 0$ and BESS is not discharged. If $I_{Lforecasted} \geq I_{Lupper}$ and U_{dg} =1, BESS starts discharging. Again, if $I_{Lforecasted} > I_{Llower}$ and U_{chg} =0, BESS is not charged. If $I_L \leq I_{Llower}$ and U_{chg} =1, the BESS is charged. ECU controls the selection of I_{Lupper} and I_{Llower} based on the forecast of daily load curve.

A rule-based priority control strategy is proposed and designed to achieve three aforementioned functionalities. A BESS can have two modes of operation that are power and voltage control modes. BESS examines the direction of power flow and decides its mode of operation. BESS operates in voltage control mode if reverse power flow occurs at a bus where BESS is connected. Otherwise, it operates in power control mode. Figure 4.27 shows a flow chart of the proposed operation scheme.

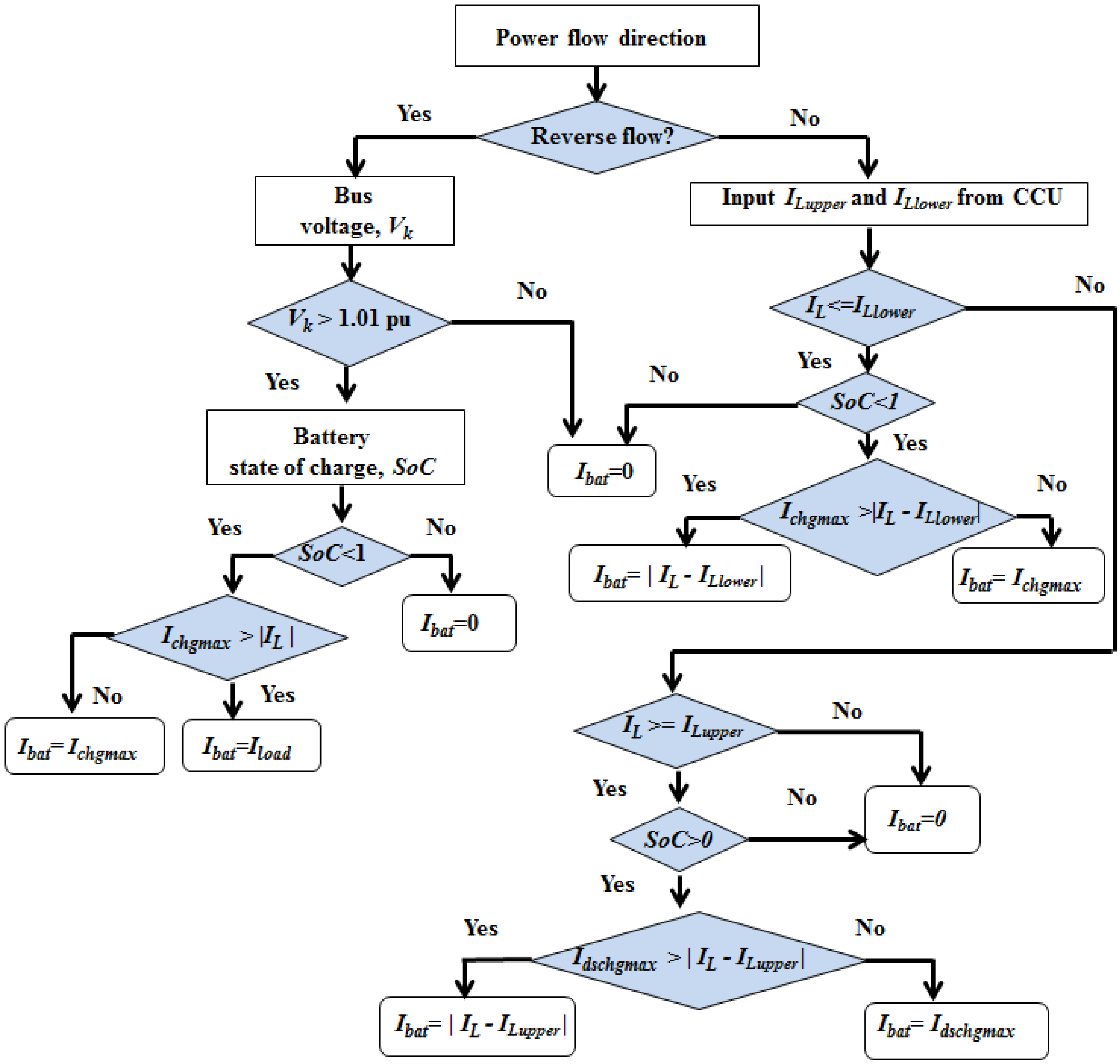

Figure 4.27 Flow chart of the proposed methodology [99]

4.4.1.1 Power Control Mode

In this mode, BESS is discharged when demand is high and charged when demand is low. ECU continuously checks load current I_L. As soon as I_L exceeds I_{Lupper}, U_{dg} is set to 1 and U_{chg} is set to 0. State of charge (SoC) of the BESS needs to be within 0 to 100% for the control operation. If BESS is discharged with its maximum current; it may not supply energy according to its expected time duration. Therefore, it is essential to control charge and discharge rates of BESS for satisfactory operation. If load current exceeds I_{Lupper}, discharge current of BESS can be expressed as, $I_{bat} = I_L - I_{Lupper}$. If the difference exceeds the BESS current rating, it is discharged with its maximum discharge current, $I_{bat} = I_{dschgmax}$ and peak shaving is achieved. Since I_L varies with time, consequently BESS discharge current varies.

When I_L falls below I_{Llower}, U_{chg} is set to 1 and U_{dg} is set to 0. Hence, BESS is charged by the current, $I_{bat} = I_L - I_{Llower}$. If the rate exceeds BESS current capacity, BESS is charged with its maximum charge rate, $I_{bat} = I_{chgmax}$. During light load conditions, BESS current is controlled to ensure a minimum load level in a system.

4.4.1.2 Voltage Control Mode

In this mode, BESS controller checks the PCC voltage. If bus voltage exceeds a certain limit (V_{PCC}), BESS is charged from the grid. As a consequence, the effect of reverse power flow is nullified. Charging current is given by, $I_{bat} = I_L$. If reverse flow current is greater than BESS current capacity, charging current is maintained as $I_{bat} = I_{chgmax}$.

4.4.2 Results and Discussions

The proposed BESS control scheme is applied to the IEEE-37 bus system under realistic load and PV power profiles collected from the UQ solar database [100]. Figure 4.28 illustrates the IEEE-37 bus network and the locations of PV and BESS. The detailed data of the network is provided in Appendix A1.

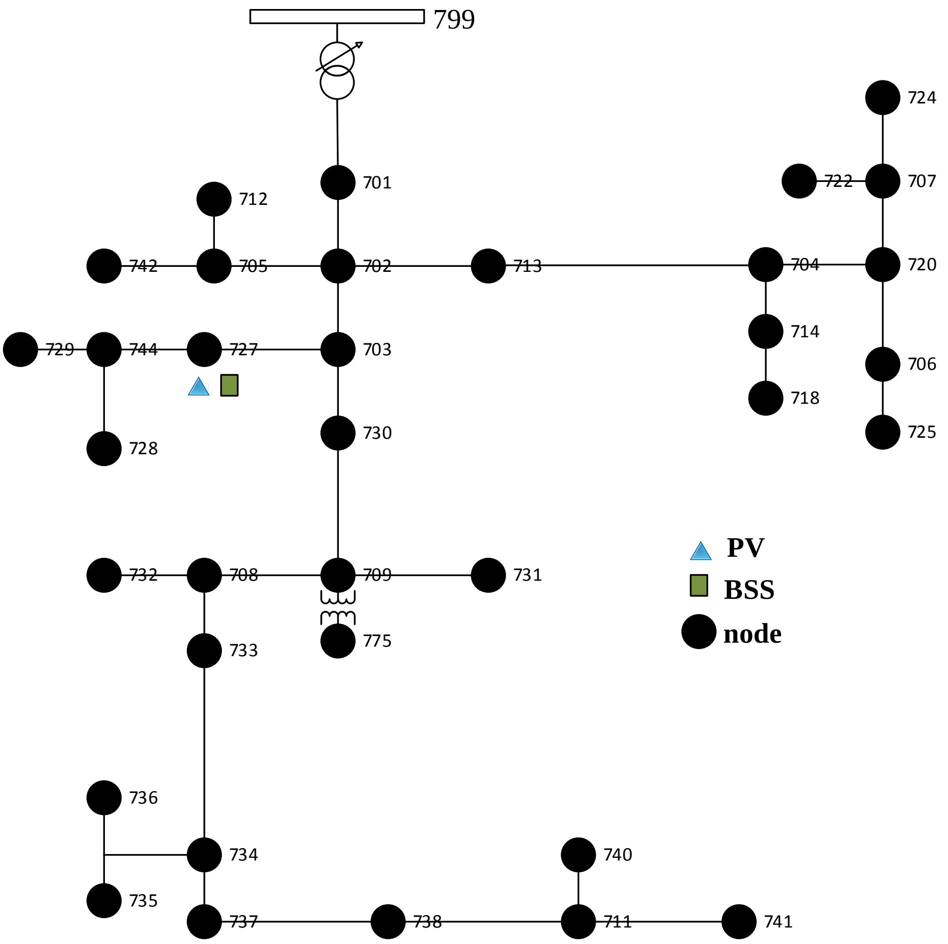

Figure 4.28 IEEE-37 node distribution system with PV and BESS [97-99]

Figure 4.29(a) shows the daily load profile of one phase of bus 727 with integrated PV. Figure 4.29(b) depicts a closer look of net load variation due to PV. It is observed from Figures 4.29(a) and (b) that due to the variable PV output, net load profile shows more fluctuations than actual during the day. Reverse active power flow occurs from 7:00 to 14:00 hr, which implies active power is being injected to the network from bus 727. The BESS at PCC is triggered for charging during this event.

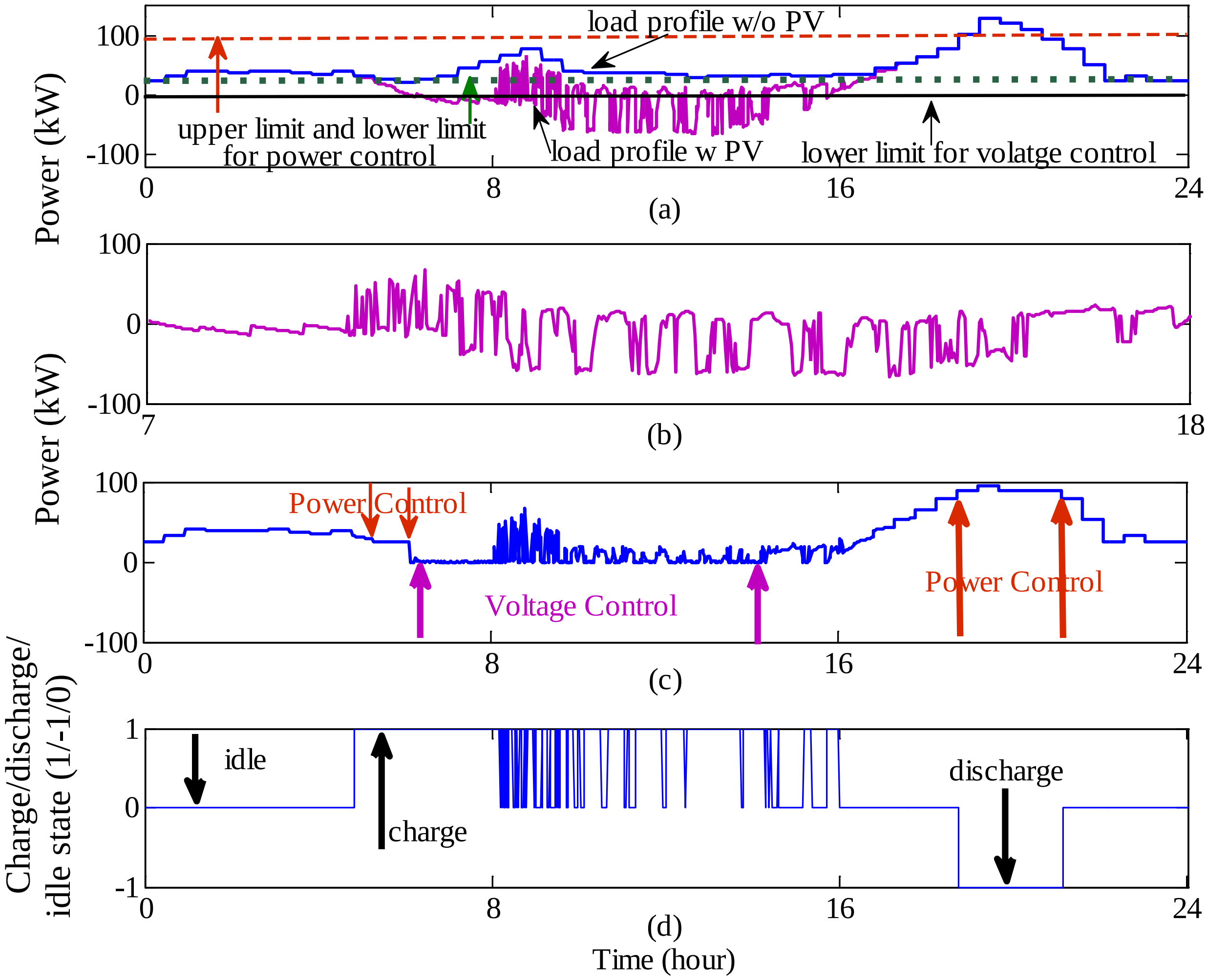

Figure 4. 29 Daily load profile with and without PV; (b) Zoomed in view of (a); (c) Load profile with integrated BESS; (d) Charge/discharge/idle states of BESS [99]

Figure 4.29(c) presents an improved load profile with BESS, while Figure 4.29(d) demonstrates the charge/discharge situations of the studied BESS. It can be seen from Figure 4.29(c) that BESS is operated in both voltage and power control modes. The BESS is utilised for load levelling from 5:00 to 6:30 hour. Voltage rise issue is mitigated using the BESS from 8:00 to 14:30 hour. Peak shaving is achieved from 18:00 to 22:00 hour. It is reflected from Figure 4.29(d) that the BESS changes its state from charging to idle very frequently as PV power fluctuates every minute.

The BESS control approach utilised in this section is heavily reliant on the load current and node voltage limits. Even if reverse power flow does not occur and the load current exceeds the specified limit in the day time, the BESS may start discharging. Therefore, both charge and discharge of the BESS may happen in the day time. The life-time of a BESS is impacted by its discharge operation that needs to be further investigated to design an appropriate control method for voltage regulation through BESS.

4.5 Summary

In this chapter, the voltage rise problem due to high PV penetration in a typical distribution network from Australia is investigated under various load and PV profiles. It is found that the network voltage exceeds the allowable boundary even if the future PV inverters are operated at less than unity power factor. To address this problem, a tool is proposed to determine the maximum power injection by prospective PV units, which satisfies operating voltage limits. It is found that the maximum power export limit for a new PV inverter in the studied network is 1.5 kW at 0.9 lagging power factor. However, this limit may vary from one network to the other depending on the PV penetration levels and network structures. For a radial feeder, the maximum export limit for prospective inverters tends to decrease with an increase in PV penetration level. If PV inverters are operated at leading power factor, the export limit is likely to be reduced.

BESS is considered as a means to store excess energy from a PV that causes voltage rise. Accordingly, a BESS charging strategy is proposed and applied. Results imply that the proposed BESS charging scheme can control the PCC voltage within an acceptable limit. However, a rapid fluctuation in the BESS charging is observed. This fluctuation is later reduced through setting additional rules in the BESS control strategy. The capacity of a BESS is utilised to reduce the overall peak of a feeder. Results show that (n-2) BESS units are required if n number of PV units are connected in a phase of the studied LV feeder. Low voltage problem at the feeder end during the evening is also alleviated with the proposed scheme.

In the next stage, the desired control features of a BESS obtained from the analyses are utilised to coordinate multiple functions namely peak shaving, load levelling and voltage regulation. The main limitation of the obtained control features is that the charge-discharge profiles of BESS are not smooth due to variable PV power. This shortcoming may affect the performance of BESS. Another limitation of the proposed strategies is that it is devoid of a feed-back loop. Therefore, bouncing in BESS charge/discharge power may happen, which can be resolved through a closed-loop control method. From the above analyses, it is revealed that a prudent control of BESS is required to reduce fluctuations of its charge and discharge modes in photovoltaic applications. To address this issue, a new control algorithm will be developed and practically validated in the next chapter. The developed control algorithm should be closed loop, which reduces the chance of bouncing of BESS power.

Chapter 5 Prolongation of Battery Life in Photovoltaic Applications

In this chapter, a real-time forecast-based receding horizon control approach for BESS is proposed, which decides an appropriate charge rate to mitigate voltage rise during high PV power production while simultaneously ensuring that the rapid cycling of BESS systems can be reduced. The major contributions are listed as follows[3].

(i) PV power is forecast for a finite horizon window at an instant based on previous PV power measurements. Forecasted PV power trajectories are used to estimate the future voltage response trajectories by numerically solving load flow at each sampling instant over the selected finite time horizon. The proposed RTF (Real-Time Forecast-Based) controller searches for an appropriate charge-discharge trajectory for BESS to maintain the PCC voltage within acceptable limits by using an iterative method. The main advantage of this approach is that it perceives and integrates future trends of a PV output in the control system operation unlike the moving-average method in the literature, and therefore, can resolve a sudden violation of upper voltage margin [61, 62].

(ii) Receding horizon control can smooth a BESS charge-discharge rates depending on the horizon window length. The proposed RTF strategy only charges a BESS during high PV generation and discharges while the lower voltage margin at the PCC is violated. Therefore, the chance of frequent use of BESS cycles during voltage rise events is reduced and hence the life of BESS can be prolonged. The cycle-life degradation of the studied BESS with RTF control scheme is analysed and compared with an existing rule-based approach [99].

(iii) The performance of the proposed method is tested in Hardware-in-the-Loop (HIL) setup comprising RTDS and dSPACE controller board under several realistic situations. The proposed RTF control scheme is applied to a distribution system that is modelled in RTDS [101] environment. The charge/discharge trajectories obtained from the RTF approach are passed onto respective BESS inverter controllers as a reference signal by means of a dSPACE board.

5.1 System Modelling and Hardware-in-the-Loop Setup

The IEEE-13 nodes feeder is considered as a test distribution system and is implemented in the RTDS environment [97]. RTDS modelling is based on Electromagnetic Transient Programming

---

[3] This chapter has significant materials from the following article by the PhD candidate, which is provisionally accepted subject to revision in the journal of IET Renewable Power Generation..

- S. R. Deeba, R. Sharma, T. K. Saha and F. Calderon, "Prolongation of Battery Life in Photovoltaic Applications: Controller Design and Hardware-in-the-Loop Validation," *IET Renewable Power Generation*, 1st revision is submitted on 6th May, 2017.

(EMTP) simulations, therefore, enables accurate high-fidelity modelling of the power systems [101]. In addition, RTDS models are suitable for understanding the real-time performance of system components since the models behave akin to an actual system. The following subsections describe the BESS model, studied system and HIL experimental setup.

5.1.1 BESS Modelling

An equivalent circuit based model that accurately captures the current-voltage characteristics of a lithium-ion battery is used and presented in Figure 5.1(a).

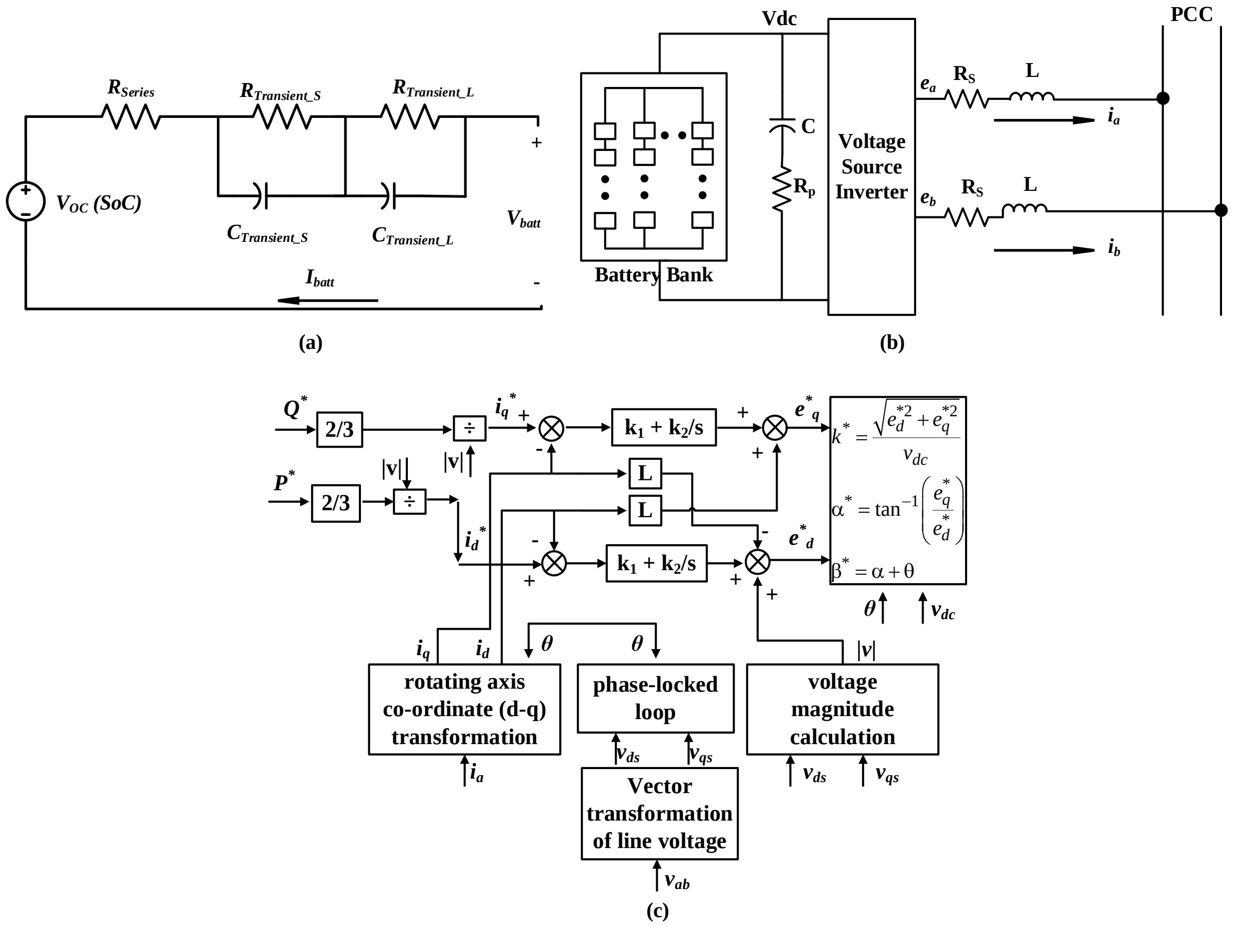

Figure 5.1 Battery energy storage system modelling (a) An equivalent circuit-based Lithium-ion battery model (b) Schematic diagram of a grid-connected BESS (c) BESS inverter control

The model parameters for a polymer lithium-ion battery are extracted from its pulse discharge characteristics at 20°C temperature [102]. The non-linear open-circuit voltage, series resistance and capacitance are functions of *SoC* (State of Charge) as presented in (5.1)-(5.6) [102].

$$V_{OC}(SoC) = -1.031e^{-35.SoC} + 0.2156\times SoC - 0.1178\times SoC^2 + 0.3201\times SoC^3 + 3.685 \tag{5.1}$$

$$R_{Series}(SoC) = 0.1562\times 2^{-24.37\,SoC} + 0.07446 \tag{5.2}$$

$$R_{Transient\_S}(SoC) = 0.3208e^{-29.14\,SoC} + 0.04669 \tag{5.3}$$

$$C_{Transient\_S}(SoC) = -752.9e^{-13.51\,SoC} + 703.6 \quad (5.4)$$

$$R_{Transient\_L}(SoC) = 6.603e^{-155.2\,SoC} + 0.04984 \quad (5.5)$$

$$C_{Transient\_L}(SoC) = -6056\,e^{-27.12\,SoC} + 4475 \quad (5.6)$$

The $SoC(k)$ of a battery bank at k-th sampling instant depends on its previous state $SoC(k\text{-}1)$ and is expressed as follows [102].

$$SoC(k) = SoC(k-1) - \eta\, I_{batt}(k)\Delta t \quad (5.7)$$

where, $I_{batt}(k)$ is the charge/discharge current in the battery bank at the k^{th} sampling instant and Δt represents the sampling period. The parameter η implies the charge/discharge efficiency.

For a value of *SoC* at an instant, the open circuit voltage governs the cell terminal voltage V_{batt}. If *SoC* becomes zero, the cell voltage reaches its minimum level 2 V. The *SoC* operational limit is chosen as 20%-100% because the battery modelling as per (5.1)-(5.6) is valid in this range [102]. Nevertheless, the approach presented in this thesis is applicable for other *SoC* operational limits depending upon the type of battery storage used.

Figure 5.1(b) shows a block diagram of a BESS, which includes a battery bank and a voltage source inverter [103]. To get sufficient dc power, 150 battery cells (0.85 Ah) are connected in series and such 1200 units are connected in parallel. The battery stacks are connected to a bi-directional DC-DC boost converter to match the grid voltage. The output of the dc converter is connected to a grid-tied DC/AC inverter. The inverter contains power electronic switches operated by controlled pulse-width-modulating wave. The inverter topology consists of a Voltage Source Converter (VSC) and two-level bridge blocks.

The inverter controller as shown in Figure 5.1(c) comprises a Phase Locked Loop (PLL), rotating axis coordinate (d-q) transformation blocks and a current regulator [103]. PLL determines a phase angle (θ) by using PCC voltage to synchronise the inverter with the grid. The inverter controller is given real (P^*) and reactive power (Q^*) reference signals for tracking. The P^* and Q^* are used to yield direct (i_d^*) and quadratic (i_q^*) parts of inverter reference current. The reference and measured current signals (i_d^*, i_q^*, i_d, i_q) are passed to a current regulator, which uses a PI (proportional k_1 and integral k_2) controller to produce VSC voltages (e_d^* and e_q^*). The inverter voltage is expressed by (5.8)-(5.9) [103].

$$e_d^* = k^*.v'_{dc}.\cos(\alpha^*) \quad (5.8)$$

$$e_q^* = k^*.v'_{dc}.\sin(\alpha^*) \tag{5.9}$$

The inverter topology allows continuous variation of parameters k^* and α^* as shown in Figure 5.1(c) so that the BESS produces sufficient power to track its reference trajectory. L is a design parameter in BESS inverter model, which represents the output filter inductance between voltage source inverter and the PCC (see Figure 5.1(b) and (c)). Table 5.1 presents the values of L and inverter controller parameters. The values of proportional and integral gains of the control circuit are tuned through a trial and error method. The value of L is calculated by considering 10% ripple in the output current. The detailed calculation of L is included in Appendix A2.

Table 5.1 Design parameters of the BESS inverter

Parameters	**Value**
Proportional gain, k_1	1.5
Integral gain, k_2	58.823
Inductance, L	5×10^{-5} H

5.1.2 Distribution System under Study and HIL setup

Line-to-line voltage of the IEEE-13 nodes network (shown in Figure 5.2(a)) is 4.16 kV, which is regulated by an OLTC connected between nodes N632 and N650 [97, 104]. The 4.16 kV network is connected to a 115 kV system through a 5 MVA transformer. The network has overhead and underground lines with unbalanced characteristics. Both single and three phase lines with high resistance to reactance ratios (R/X) exist in the system. There are spot and distributed loads modelled as constant power, impedance and current loads. The detailed data of the network is provided in Appendix A3.

A schematic diagram of the RTDS-dSPACE HIL setup is shown in Figure 5.2(b). RTDS comprises of both hardware and software parts. The analog input/output ports of Gigabit Transceiver cards are used with voltage levels ranging from -10V to +10V. The software platform RSCAD is utilised to model necessary components such as unbalanced impedance, single and three phase loads, transformer, solar PV and BESS.

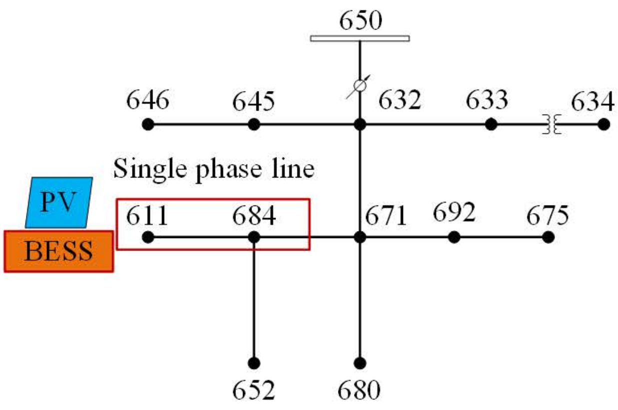

(a)

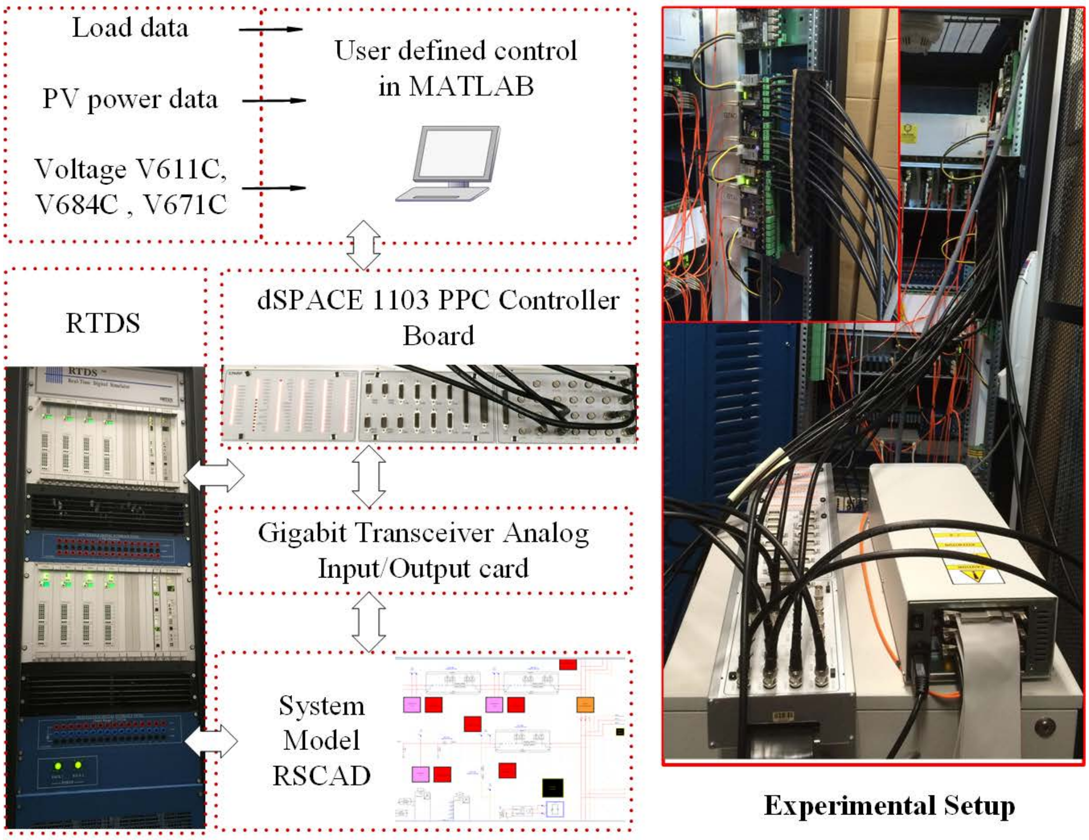

(b)

Figure 5.2 System Modelling (a) IEEE-13 nodes distribution system (b) Schematic diagram of RTDS-dSPACE HIL setup [97, 104]

Rapid control prototyping system dSPACE is interfaced with RTDS through their analog channels [105]. The dSPACE has a processor unit (DS1103), which is interfaced with a host computer through a PCI card and a TX/RX optical link. The proposed BESS control algorithm (discussed in Section 5.2) is designed in MATLAB-Simulink software [106]. The RTDS power-flow results are accessed via GTAI/O cards. The analog signals of the RTDS network is then processed to digital using ADC channels of dSPACE and is utilised in MATLAB to generate control signals for a BESS. The controller outputs from MATLAB are then passed on to the BESS model in RSCAD via DAC channels of the dSPACE.

5.2 Proposed Control Algorithm

The proposed RTF scheme determines the charge/discharge rates of a BESS in three steps. At each sampling instant the values of system variables including node voltage, phase current, load and PV power are measured. In reality, the system states can be measured by smart meters. The measured data is used to forecast the future PV power trajectory by using a persistence method as discussed below [107]. Then, the forecasted PV power trajectories are utilised to forecast the respective node voltage trajectories by solving load-flow at each sampling instant. Then, based on the future system voltage response for a specified horizon (T), the controller produces BESS charge/discharge trajectories.

5.2.1 PV Forecast using a Persistence Method

The PV power is forecast using a method of diminishing derivative persistence [107], by which the forecast first sample assumes the difference of PV power, be the same as one sample back. The subsequent samples consider weights of the derivative from the last m samples. A PV output at k^{th} sampling instant being $P_{PV}(k)$, the forecast of the next T samples is expressed by (5.10)–(5.13) [107].

$$P_{PV}(k+1) = P_{PV}(k) + (P_{PV}(k) - P_{PV}(k-1)) \tag{5.10}$$

$$P_{PV}(k+2) = P_{PV}(k+1) + \frac{(P_{PV}(k) - P_{PV}(k-2))}{2} \tag{5.11}$$

$$\vdots$$

$$P_{PV}(k+T-1) = P_{PV}(k+T-2) + \frac{(P_{PV}(k) - P_{PV}(k-T+1))}{2^{T-1}} \tag{5.12}$$

$$P_{PV}(k+T) = P_{PV}(k+T-1) + \frac{(P_{PV}(k) - P_{PV}(k-1))}{T} \tag{5.13}$$

The above method is applied to a PV power profile to understand the forecast accuracy at different horizon lengths. Figure 5.3(a) shows the actual and forecast PV power for several horizon lengths (T = 5, 10 and 15 samples). The sampling interval can be chosen from seconds to minutes depending on the data availability. The forecasting horizon of up to 15 samples is chosen based on discussions with local DNOs in Queensland for the coordinated scheduling of PV and BESS.

Figure 5.3(b) shows the % errors of PV forecast at different horizon lengths. It is observed that the error increases with the increasing horizon. The positive error implies overestimation of PV power, while negative error means the opposite. It is found from Figures 5.3(a) and (b) that forecasting error is high when there is a sharp drop in PV power. However, when PV power rises, the error remains within 15% for all values of T.

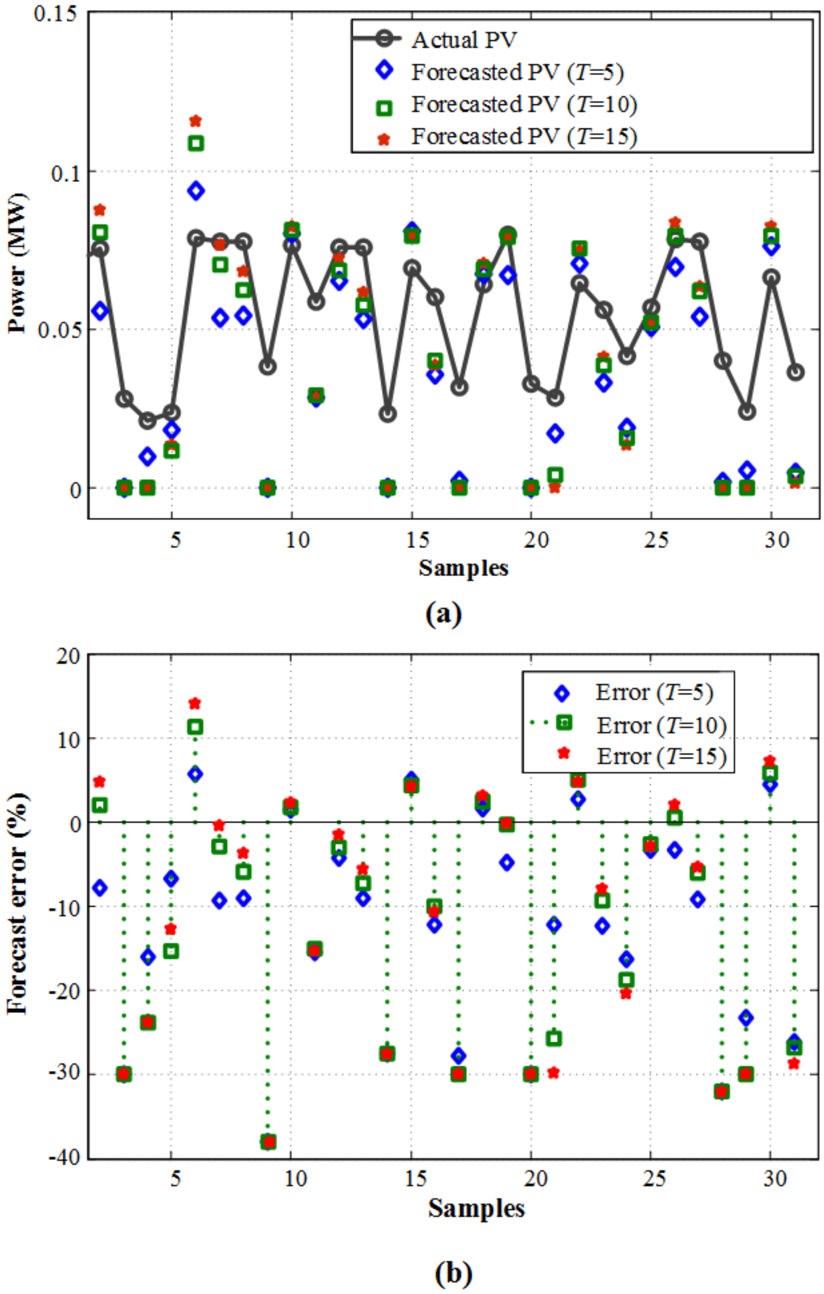

Figure 5.3 PV power forecasting (a) Actual and forecasted PV power for different forecast horizon lengths (b) Forecast error for several horizon lengths

Regardless of forecasting techniques, the forecast accuracy tends to deteriorate with the rise in PV variability. Forecast accuracy also tends to worsen with longer forecast horizon. Based on the analysis of the persistence-based method, it is found that the forecasting accuracy of up to 85%-95% can be achieved for the worst cases (e.g. cloudy days). Improvements in the accuracy may be achieved through alternative forecasting methods, however, the main focus of this work is to utilise a forecast algorithm to improve scheduling of BESS for voltage regulation and smoothing charge/discharge cycling.

5.2.2 Forecasting of Voltage Trajectories

The forecast PV power in Subsection 5.2.1 is used to estimate future voltage response of the network over the horizon length of T samples. The nodes at close proximity to PV units are highly influenced by PV generation. Therefore, the voltage trajectories of those nodes are forecast for a specified horizon window. A generalised expression of the load-flow problem for an N-node system is presented by (5.14)-(5.15) [108].

$$P_{Gn}(k) + P_{PVn}(k) - P_{BESSn}(k) - P_{Ln}(k) = V_n(k)\left[\sum_{p=1}^{N} V_p(k) Y_{pn} \cos\{\theta_{pn} + \delta_p(k) - \delta_n(k)\}\right] \quad (5.14)$$

$$Q_{Gn}(k) - Q_{BESSn}(k) - Q_{Ln}(k) = -V_n(k)\left[\sum_{p=1}^{N} V_p(k) Y_{pn} \sin\{\theta_{pn} + \delta_p(k) - \delta_n(k)\}\right] \quad (5.15)$$

where

n, p = Bus indices

k = Sampling index

P_{Gn} = Infinite bus active power

Q_{Gn} = Infinite bus reactive power

P_{Ln} = Real load at nth node

Q_{Ln} = Reactive load at nth node

P_{PVn} = Active power of PV at nth node

P_{BESSn} = BESS active power at nth node

Q_{BESSn} = BESS reactive power at nth node

V_n = Voltage magnitude at nth node

Y_{pn} = Magnitude of system admittance matrix

θ_{pn} = Angle of system admittance matrix

δ_p, δ_n =Voltage angles

The solution of the above load-flow problem provides voltage magnitudes and angles of N number of buses. With the PV power forecast at k^{th} sampling instant, for given values of P_{Ln}, Q_{Ln}, Y_{pn} and θ_{pn}, expressions (5.14)-(5.15) are iteratively used to determine the node voltage trajectories for the horizon length T. The proposed RTF controller utilises the forecast voltage trajectories over the horizon length T to determine appropriate BESS charge/discharge trajectories so that satisfactory voltage performance is achieved. The following subsection describes the proposed algorithm to determine BESS charge/discharge rates.

5.2.3 Trajectory of BESS Charge/Discharge

The forecast PV power and the respective node voltage trajectories as described in Section 5.2.2 are used to determine an appropriate charge/discharge rate of a BESS. Figure 5.4 shows a flow chart of the proposed RTF control strategy for selecting BESS charge/discharge rates ($P_{BESS}(k)$) for the network voltage regulation. The controller is set to yield BESS discharge signal only if PV power is unavailable. To detect the availability of PV power, the controller checks the average PV output for the last *m* samples (e.g. m = 20 in this study). If this average value is zero, BESS power is positive indicating a discharge operation, whereas, the non-zero value implies a charge or an idle operation.

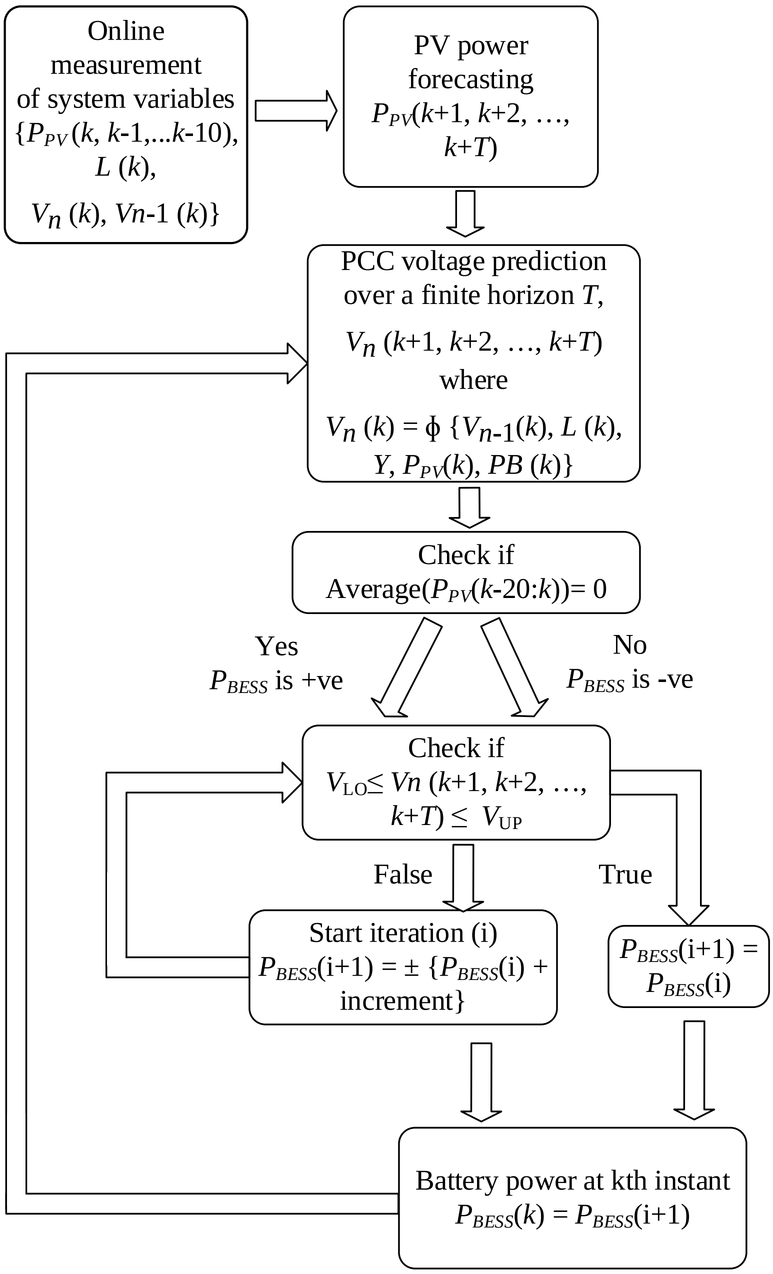

Figure 5.4 Flowchart of the proposed RTF control strategy

In the next stage, the forecast voltage magnitudes of PCC for T samples are checked. If the PV power is unavailable and PCC voltage is below the lower limit V_{LO}, the controller starts searching for a discharge rate for the BESS. The searching method is an iterative process that increases BESS power with a fixed increment. This search continues until an appropriate discharge rate is found so that the PCC voltage resides above V_{LO} for the upcoming T samples.

If the PV power is available and the PCC voltage exceeds the upper limit V_{UP} at any instance within the horizon window (k, k+1… k+T), the controller searches for a charge rate to maintain the voltage within the V_{LO} and V_{UP} limits. If PCC voltage does not violate any limits, the BESS remains in an idle mode. Based on the local DNO standard, the lower and upper voltage margins for the network are -10% and +6% of the nominal value (i.e. 0.9 p.u. and 1.06 p.u.). However, the values of V_{LO} and V_{UP} for the RTF controller are set at 0.95 p.u. and 1.05 p.u. respectively, which are slightly lower than the standard limits. It ensures that the controller action occurs before the system voltage reaches its boundary values.

In a real-time online implementation, at each sampling instant k, based on the current measurement, BESS power trajectory $P_{BESS}\,(k+1), \ldots, P_{BESS}\,(k+T)$ is determined. Then, $P_{BESS}\,(k+1)$ is applied to the actual BESS and the rest of the trajectory is discarded. The process is repeated at each sampling instant with the updated PV and voltage measurements. The forecast PV and respective voltage response depend on the current state measurement and hence provides a degree of robustness to modelling error and uncertainty.

5.2.4 Proposed Algorithm vs. One-step Ahead Rule-based Method

The proposed RTF controller is compared with an existing one-step ahead rule-based approach [99]. The existing rule based method selects charging or discharging of a BESS based on specified current and voltage limits. In line with that approach, a BESS is charged if net power (demand−PV power) at the PCC goes below a given threshold, while it is discharged if the net load exceeds that limit during voltage rise (>1.05 p.u.). Since this strategy is reliant on the specified net-load limit, both charge and discharge operations are involved in the smoothing of variable PV output. Unlike the one-step ahead rule-based approach, the proposed control scheme resolves voltage rise by only charging a BESS. A comparison of the proposed control scheme with the one-step ahead rule-based approach is discussed in Section 5.3.2.

5.3 HIL Simulation Results

The proposed approach is validated using the HIL setup comprising of RTDS and dSPACE as described in Section 5.1.2. To understand the network voltage rise under high PV penetration, a PV source with a capacity of 100 kW is connected to node N611. This node is chosen to consider the effect of voltage rise propagation from the feeder end node to the upstream locations. Then, the impact of the proposed BESS control scheme on the voltage performance is investigated. The power and voltage results are obtained in per unit (p.u.) quantities from the load flow solution. However, BESS power is expressed in kW obtained by multiplication of the p.u. value with corresponding base quantity. The size of BESS unit installed at N611 is determined using an approach presented in [85]. This approach establishes the size of a BESS such that the relevant customer's profit is maximised under time of use pricing scheme while simultaneously resolving the network voltage rise. Table 5.2 presents the peak and off-peak demand of the customers at node N611 and capacities of PV and BESS.

Table 5.2 Customer's demand and capacities of PV and BESS

Parameters	**Value**
Peak load, L611	120 kW
Off-peak load, L611	80 kW
PV capacity	100 kW
BESS capacity	100 kW, 300 kWh

PV data for a year is collected from the University of Queensland Solar website [109]. The annual load data of a typical Australian distribution network is accessed from the Australian Energy Market Operator (AEMO) website [83]. Both PV and load data are scaled down to appropriate values to match the specifications of the 13-bus network. Specific values of PV power in kW are shown in the simulation results.

The proposed BESS control strategy is tested under two representative PV power profiles - cloudy and clear sky days in case studies 1 and 2 respectively. The cycle-life degradation of a BESS is also estimated for two approaches- with the proposed RTF scheme and with a one-step ahead rule-based method. Later on, yearly degradation of the BESS cycle-life is estimated using year-long PV and load profiles. The subsequent sections present the simulation results and relevant discussions.

5.3.1 Implementation of the Proposed RTF Method on the HIL Setup

The proposed method outlined in Figure 5.4 is validated using hardware-in-the-loop setup. The simulation model of the 13-bus system including PV and BESS (Figure 5.2(a)) is implemented on RTDS. The control algorithm is implemented in MATLAB/Simulink and is executed on the dSPACE processor board. RTDS and dSPACE sampling rates are 50μs and 80 ms, respectively. PV and load data are concurrently fed to both RTDS and dSPACE. At each sampling instant, the control algorithm in dSPACE, on the basis of PV forecast trajectory, determines an appropriate feasible BESS charge/discharge profile that delivers permissible voltage profile trajectory over the horizon length *T*. The PV forecasts, at each sampling instant, are based on the model expressed in (5.10)-(5.13). In contrast, BESS power and node voltage trajectories are based on the solution of load flow equations (5.14 - 5.15) sequentially multiple times in each sampling instant (as per the iterative loops shown in Figure 5.4).

5.3.2 Case Study-1: Cloudy Day PV Profile

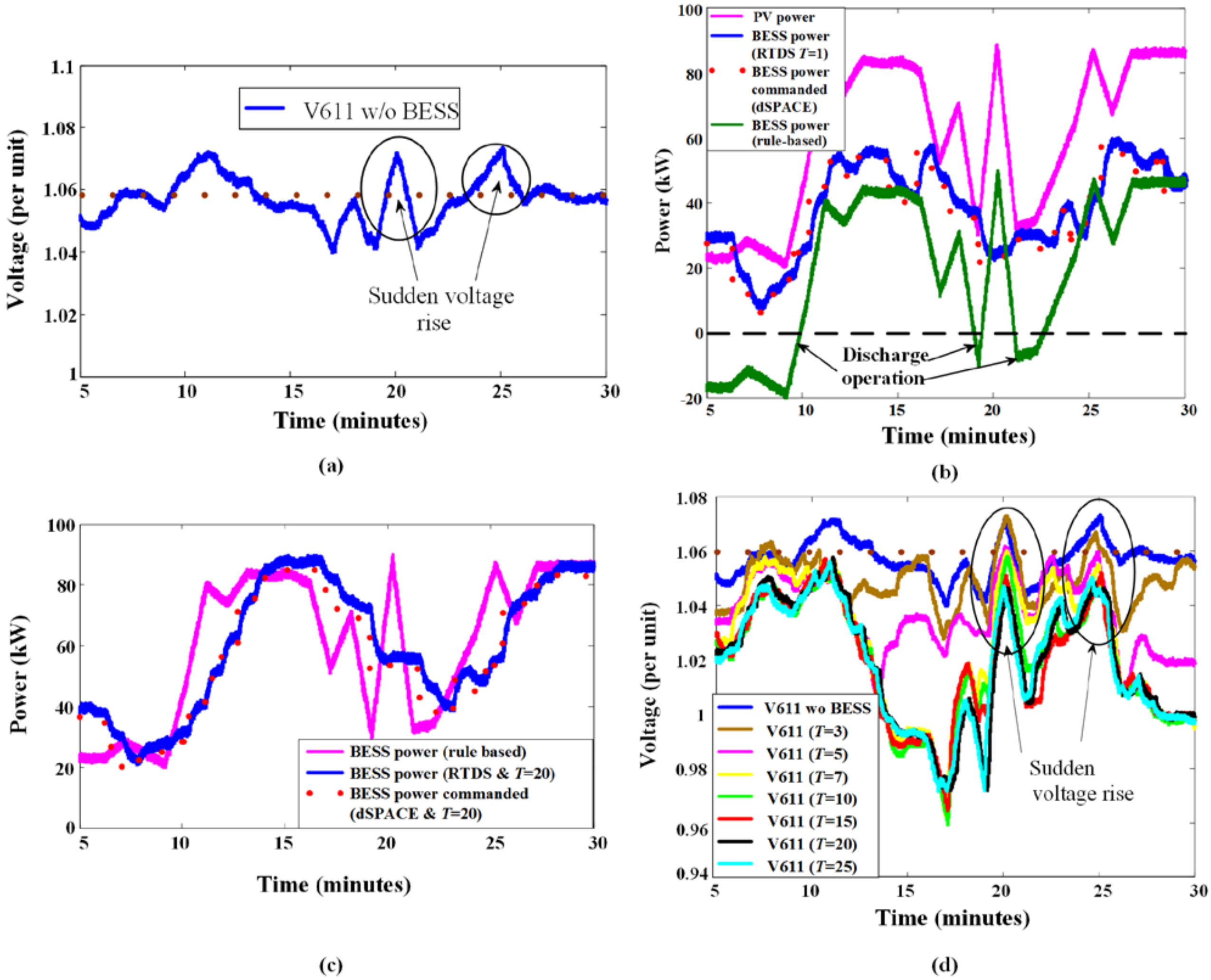

Figure 5.5 Response of a BESS on a variable PV power day (a) Voltage rise at PCC (N611) due to PV but without a BESS (b) BESS power with the proposed RTF control scheme vs. BESS power for one-step ahead rule-based algorithm (c) BESS power command in dSPACE and actual BESS power (RTDS) with the RTF approach for a long forecast horizon (d) PCC voltage performance with a BESS under the RTF control at different forecast horizons

Figure 5.5(a) presents PCC voltage without any BESS under a cloudy day PV profile for 25 minutes duration. It is observed that voltage rise occurs at several instants such as at 10th, 20th and 24th minutes. Notably, PCC voltage exceeds 1.06 p.u. at the 10th minute and the over voltage lasts for 3-4 minutes duration. At the 20th minute, PCC voltage again rises from 1.05 p.u. and exceeds 1.06 p.u. Afterward, PCC voltage falls below 1.06 p.u. and suddenly rises again due to the fluctuation of PV power. To maintain the voltage within an acceptable upper boundary, a BESS is placed at N611.

Figure 5.5(b) shows the studied PV profile and the BESS response for one-step ahead rule-based controller [99]. As discussed in Section 5.2.4, the charge-discharge of BESS relies on a net-load limit, which is chosen as 40 kW for the studied network. It is observed from Figure 5.5(b) that the BESS is charged if the net-load goes below 40 kW and discharged when net load exceeds 40 kW. It is evident from the result that with the rule-based controller, BESS charge and discharge events frequently occur, which can deteriorate its life-cycle.

Figure 5.5(b) also presents the BESS power command from Simulink and actual BESS power in RTDS using the proposed RTF method. The horizon length is considered as T = 1 sample to forecast PV power and system voltage as expressed in equations (5.10)-(5.15) in Sections 5.2.1 and 5.2.2. It is observed that the proposed RTF scheme ensures smooth BESS charging. It is also found that there is a rapid fluctuation in PV power between the 15th and 20th minutes, while BESS power with the proposed RTF control (at horizon length, T = 1) does not fluctuate with PV. If the forecast horizon length is increased to T = 20, RTF controller can foresee upcoming voltage rise events in 20 samples and the charge rate is accordingly increased as depicted in Figure 5.5(c). It is observed from Figure 5.5(c) that the BESS model in RTDS successfully follows the charging trajectory as commanded from dSPACE. However, a delayed response (330ms) is noticed for the actual BESS in RTDS due to the difference in response time of the two hardwares (RTDS and dSPACE) as well as a communication delay.

Figure 5.5(d) presents the PCC voltage profiles with BESS under different forecast horizons (T = 3, 5, 7, 10, 15, 20, 25 samples). If the horizon is smaller than T=5, BESS is unable to maintain its PCC voltage within the upper limit. The sudden rise of PV power between the 15th and 20th minutes causes a sudden voltage rise at the PCC. The abrupt change in PCC voltage is better forecast with the longer horizon ($T \geq 5$), for which the standard voltage margin is retained. It is also found that if the forecast horizon is too long ($T \geq 7$), voltage rise issue is solved but a high ramp in the voltage profile is introduced. The reason of the high ramp is - as the forecast horizon increases, the RTF controller increases the BESS charge rate. The higher charge rate drops down the PCC voltage and creates a higher voltage ramp. Noticeably, voltage profiles are almost similar for T = 20 and 25. It implies that horizon lengths of T > 20 do not significantly improve controller performance. Therefore, a forecast window [k+1: k+5] is sufficient to maintain the PCC voltage within permissible limits.

5.3.3 Case Study-2: Clear-sky PV Profile

5.3.3.1 BESS Charging

In case study-2, the effectiveness of the proposed RTF control approach is investigated under a clear-sky PV profile. Figure 5.6 presents the BESS response and PCC voltage profiles for different forecast horizon windows. It is observed from Figures 5.6(a) and (b) that the BESS power gradually increases and follows the pattern of PV power. Since the PV profile is linear for a small duration of time, the proposed scheme can almost accurately foresee the future trends of PV power. BESS power command produced by the RTF scheme in dSPACE also gradually increases with different forecast horizon length as depicted in Figure 5.6(b). It is noticed that for a clear-sky profile, BESS power commands do not significantly vary with longer forecast horizons.

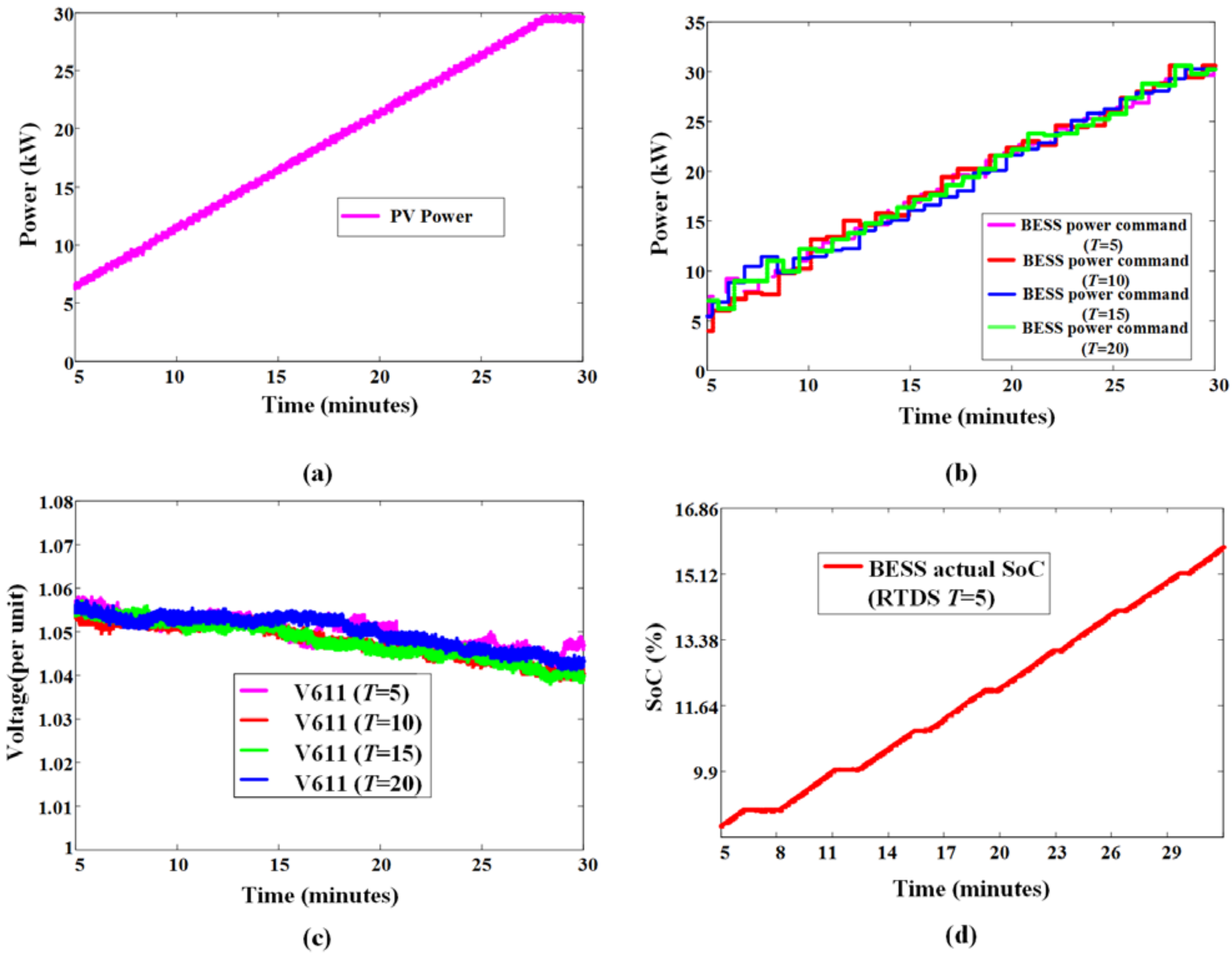

Figure 5.6 The proposed RTF controller response in a clear-sky day (a) The studied PV profile (b) BESS power command (dSPACE) for different horizon lengths (c) PCC voltage (RTDS) for different forecast horizon lengths (d) BESS %SoC in RTDS for T=5

Figure 5.6(c) shows voltage profiles of N611 with a BESS at different values of *T*. It is found that the voltage magnitude of N611 resides below the upper limit for all values of *T*. BESS state-of-charge (%SoC) is shown in Figure 5.6(d) and is increased to 16% from the initial value due to 25 minutes charging.

5.3.3.2 BESS Discharging

The BESS is set to its discharge mode if the specified voltage limit in the RTF controller (V_{LO} = 0.95 p.u.) is breached. Figure 5.7(a) presents the load profile of the respective feeder of PCC during the evening peak and the BESS discharge power. It is found that BESS discharge power gradually decreases. The PCC voltage profiles for several forecast horizons are shown in Figure 5.7(b). It is observed that for all forecast horizons (*T*), PCC voltage is improved and resides above 0.9 p.u.

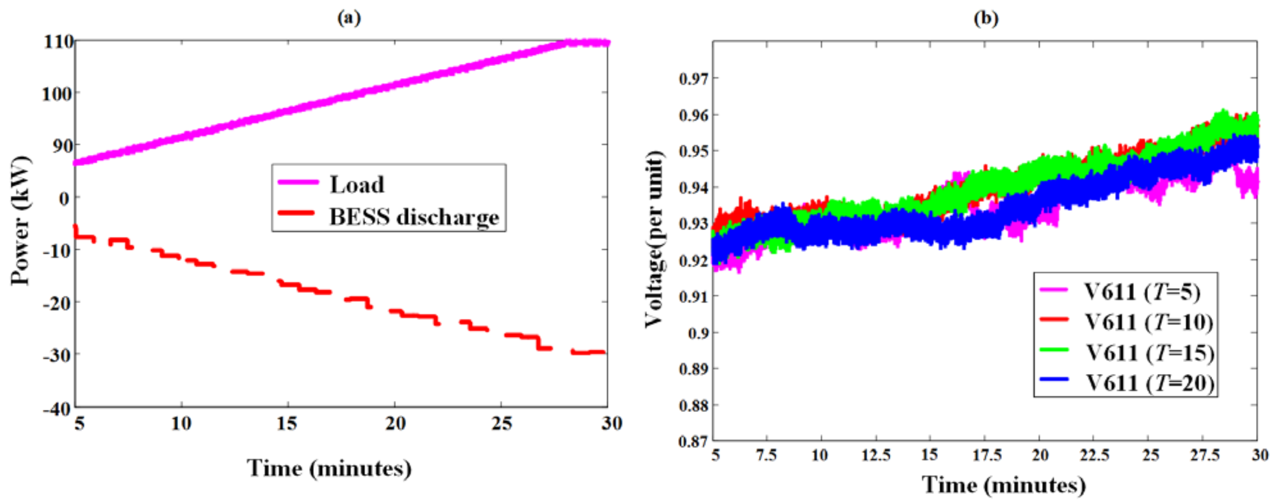

Figure 5.7 BESS discharge performance in low voltage situation (a) Load of node N671 and the discharge profile of BESS at N611 (b) PCC voltage while BESS discharging

5.3.3.3 BESS Cycle-Life Degradation

The cycle-life refers to the total number of charge/discharge cycles that a BESS can provide before its capacity is reduced to 80% of nominal value. A battery lifespan is highly influenced by its DOD, charge rate and temperature [12]. Typically, BESS life cycle varies between 1800 and 2500 depending on the type of batteries [46]. If one full cycle is related to 80% DOD, the discharge of a lithium battery less than 80% is considered as a micro-cycle [13].

The one-step ahead rule-based scheme as discussed in Section 5.3.2 for PV power smoothing introduces numerous micro-cycles in its *SoC* history. Therefore, the calculation of cycle-life degradation due to such micro-cycles needs to be performed. A numeric expression of degradation of BESS due to the incurred cycles/micro-cycles is given by (5.16) [13].

$$DMC = \sum_{w=1}^{M} \frac{Cycle \text{ of } S_w}{A \times (S_w)^B} \times 100\% \; ; Cycle \text{ of } S_w = \begin{cases} 0.5 \text{ if } S_w < 80\% \\ 1 \text{ if } S_w \geq 80\% \end{cases} \tag{5.16}$$

where *DMC* implies the degradation factor for *M* cycles and S_w is the DOD range of the *w*-th cycle. The parameters, *A* and *B* are computed using lithium-ion pulse discharge characteristics and found as *A*=2873.1 and *B*= –1.483 respectively [12].

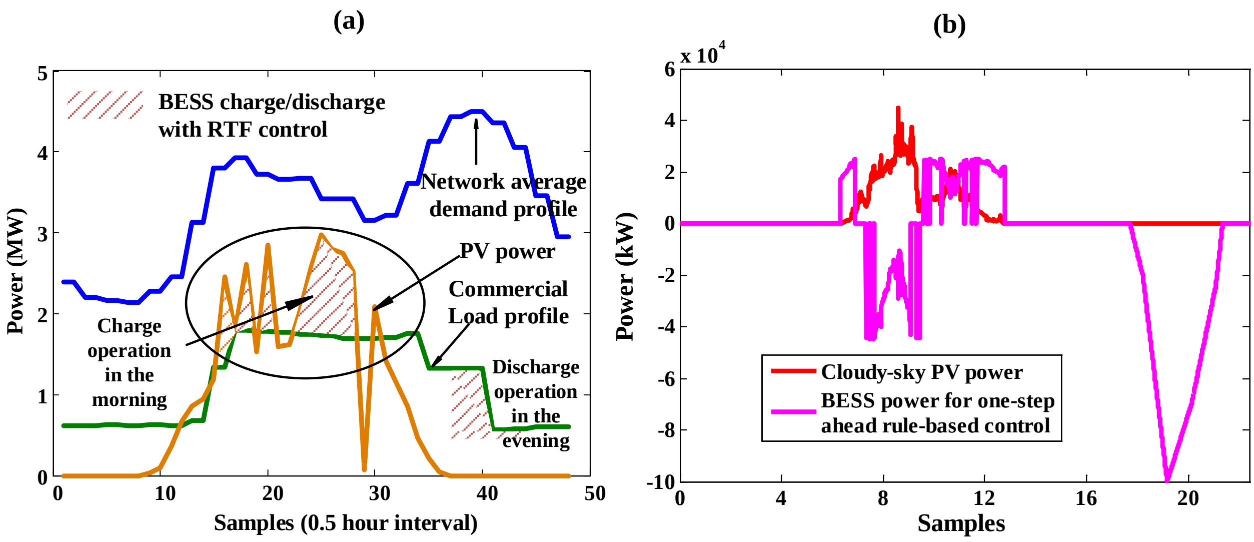

Figure 5.8 Day-ahead charge-discharge schedule of a BESS with the RTF scheme and with a rule-based approach (a) day-ahead PV-BESS power schedule under the proposed RTF control scheme (b) BESS charge/discharge with a one-step ahead rule-based control for a variable PV profile

The proposed RTF control ensures that a BESS does not discharge if voltage rise occurs during high PV. Additionally, the proposed controller smooths the output of a BESS. Therefore, a very few micro-cycles are detected in the case of RTF controlled BESS. A typical day-ahead charge-discharge schedule with the proposed approach is illustrated in Figure 5.8(a). The PCC experiences a voltage less than 0.95 p.u. in the evening as system peak occurs in that period. Therefore, the proposed RTF control discharges BESS in the evening peak period most of the days in a year. At night, network voltage resides within the upper and lower limits. As a consequence, usually it is not required to discharge a BESS any time of a day other than the evening peak. BESS partial discharge in the day time occurs only if the solar PV is unavailable and the system voltage is below the permissible lower limit of 0.95 p.u. (which could be due to the higher power consumption by customers during the day). Such situations lead to the occurrence of a few micro-cycles in a year.

To calculate the BESS cycle-life degradation under an existing rule-based approach, BESS charge/discharge profiles are observed at several PV-load scenarios for one year duration. BESS charge-discharge curves for the rule-based approach of a variable PV day are presented in Figure 5.8(b). It is noticed that with the rule-based approach, BESS are discharged at several DOD levels (10%-70%) due to PV variability. The BESS is again discharged at its rated DOD (90%) during the evening peak. Therefore, a degradation factor due to micro-cycles needs to be calculated along with the full cycle count.

The BESS cycle-life degradation is calculated using (5.16) for the proposed approach and also for the rule-based approach. The results are presented in Table 5.3. It is found that yearly degradation of BESS cycle-life due to the incurred micro-cycles with rule-based control is 8.9%. It is also noticed that about 4,000 micro-cycles occur yearly while using the rule-based algorithm. In contrast, the proposed RTF scheme uses a very few micro-cycles (only 70) in a year. For the annual PV and load datasets used in the simulation, situations requiring micro-cycling arise only 70 times. Therefore, compared to the existing rule-based approach (yearly degradation 8.9%), the developed RTF scheme gives a much smaller degradation per year (0.4%) due to the incurred micro-cycles without compromising its control performance. With the proposed method, the best-case micro-cycle occurrence in a day is found to be 0, whereas the worst-case micro-cycle occurrence is found as 1 per day. Therefore, the best possible micro-cycle occurrence in a year is 0 and the worst possible number of occurrences is 365.

Table 5.3 Partial degradation of BESS cycle-life due to micro-cycles

<table>
<tr><th colspan="2">Items</th><th>Values</th></tr>
<tr><td rowspan="5">One-step ahead rule-based approach</td><td>Micro-cycles</td><td>3 (daily best)
12 (daily worst)
4000 (yearly)</td></tr>
<tr><td>Full cycles</td><td>265 (yearly)</td></tr>
<tr><td>Depth-of-Discharge (DOD)</td><td>10 – 70% (micro-cycle)
80 – 90% (full cycle)</td></tr>
<tr><td>Yearly degradation due to incurred full-cycles</td><td>6.63%</td></tr>
<tr><td>Yearly degradation due to incurred micro-cycles</td><td>8.9%</td></tr>
<tr><td></td><td>Total degradation per year</td><td>15.53%</td></tr>
<tr><td rowspan="5">Proposed RTF scheme</td><td>Micro-cycles</td><td>0 (daily best)
1 (daily worst)
70 (yearly)</td></tr>
<tr><td>Full cycles</td><td>~265 (yearly)</td></tr>
<tr><td>Depth-of-Discharge (DOD)</td><td>< 80% (micro-cycle)
80 – 90% (full cycle)</td></tr>
<tr><td>Yearly degradation due to incurred full-cycles</td><td>6.63%</td></tr>
<tr><td>Yearly degradation due to incurred micro-cycles</td><td>0.4%</td></tr>
</table>

	Total degradation per year	7.03%

For both control schemes, yearly cycle-life degradation due to the full cycles is found as 6.63%. It is to be mentioned that yearly degradation of 0.4% due to the micro-cycles implies that 0.4% of the maximum cycle-life will be lost per year. However, the total degradation calculated for both full and micro cycles for the RTF method is 7.03%. It indicates that if the BESS has 2500 maximum cycles, almost 175 (=2500×0.0703) cycles will be used per year. Therefore, with the proposed RTF method, maximum 14 (=2500/175) years BESS life can be obtained. However, the BESS life is also affected by other factors e.g. operating temperature and self-discharge, which are not considered in this calculation. In contrast, by using the rule-based control scheme, the achievable maximum BESS life time is 6.5 years, which is much less than that of using the RTF method.

5.4 Summary

In this chapter, a generic forecast-based receding horizon control approach is proposed and experimentally validated for prolongation of BESS lifetime without compromising distribution voltage performance. The key findings of this work are as follows:

- The use of short-term forecasting of PV generation in the proposed method can deliver substantial benefits for the prolongation of BESS life when used in voltage regulation in distribution networks. The cycle-life degradation of BESS is significantly reduced by using the proposed RTF control approach compared to the traditional one-step ahead rule-based technique.
- An increase in the forecast horizon length generally tends to improve the BESS cycling and voltage regulation performance. However, the benefits through the use of longer horizons tend to gradually diminish due to the combined effect of increasing forecast error and increased computation burden. Nevertheless, this limitation can be partially addressed through the use of better forecasting methods such as methods based on the use of a sky-camera.
- Latency is observed between the BESS power command (dSPACE) and the actual BESS response (RTDS) in hardware-in-the-loop simulation. This latency causes no noticeable effect on the control operation because the period associated with the frequency of the PV variations is much longer than the latency associated with the HIL set-up.

The proposed method controls individual BESS for PCC voltage regulation simultaneously reducing the rapid cycling of BESS. As the use of BESS proliferates in residential sectors, their aggregated use for system voltage regulation is considered as an option. In the next chapter, a generic optimum voltage regulation framework for BESS aggregators will be developed and experimentally validated.

Chapter 6 Coordinated Multi-Objective Control of Distributed BESS Units

The utilisation of BESS is beneficial for customers through energy arbitrage and demand response incentives. The growing use of solar PV leads to an increase in the uptake of BESS in the residential sector. Distributed BESS are suitable for system voltage regulation if they are centrally controlled. To accomplish such tasks, demand response aggregators (DRA) can play a vital role. To this end, establishing a central control method to coordinate the distributed BESS for voltage regulation is essential [5, 68].

When customers leverage their BESS capacity for voltage regulation, it comes at the expense of their planned arbitrage resulting in costs to customers termed as *disutility*. The existing optimum voltage regulation approaches often do not directly take this into account [17, 69, 73]. The main objective of this chapter is to explicitly model this phenomenon and develop a control scheme to optimise the overall benefit to customers. The major contributions are listed as follows.

(i) A generic mathematical model for the cost of voltage regulation with BESS is formulated as a function of ‘disutility’ and system voltage. Customers’ disutility is expressed as a non-linear function of BESS dispatch, whilst the expression is generalised for any customers.

(ii) The customers’ disutility and DRA’s cost models are utilised to formulate an optimisation problem to search for feasible and cost-effective BESS charge-discharge trajectories so that ‘disutility’ is minimised ensuring acceptable system voltage. Therefore, distribution voltage is regulated through a coordinated effort of a DNO and a DRA, while DNOs pay to DRAs for their service via a short/long term contract, unlike existing voltage regulation methods.

(iii) The effectiveness of the proposed method is validated via hardware-in-the-loop simulations involving RTDS and dSPACE. The experiment is conducted under variable PV power profiles for several hours to test the performance of the BESS control scheme.

In the subsequent sections, the proposed control algorithm and relevant simulation results are presented. The indices, variables and parameters used in this chapter are provided in the nomenclature in the last section.

6.1 Proposed Control Algorithm

In this section, generalised mathematical expressions of a distribution system with PV and BESS are formulated and then the control variables are identified. In the next stage, an optimisation problem is developed and its solution method is described.

6.1.1 Power Flow Model

A radial distribution network with n number of buses is considered and presented by the set $N := [N_1, N_2, N_3, \ldots, N_n]$. Let L be the set of load buses in the network, where $L := [L_1, L_2, L_3, \ldots, L_p]$. The set of BESS connected nodes is represented by B, where $B := [B_1, B_2, B_3, \ldots, B_m]$. The network admittance is represented by the matrix $Y^{n\times n}$. Let H be the set of the buses through which the network is connected to the grid such that $H \subseteq N$.

If a particular node does not have a load that consumes real or reactive power or does not have a PV or BESS, the corresponding variables are set to zero. The active power (P_{Bi}) and reactive power (Q_{Bi}) of BESS are considered as the control variables, where $i \in [1, \ldots, n]$. The state variables include real (P_{gi}) and reactive power (Q_{gi}) of the infinite bus. Voltage magnitudes (V_i) and angles (δ_i) of all the nodes are also considered as state variables. The state variables are presented by a set $Z_i := [P_{gi}, Q_{gi}, V_i, \delta_i]$, while the voltage magnitude and angle of the slack bus are known and not included in the state vector. The real and reactive power flow problems at i^{th} node of a balanced three phase system can be expressed by (6.1) – (6.2) [108].

$$P_{gi} + P_{PVi} + P_{Bi} - P_{li} = \sum_{j=1}^{n} |V_i||V_j||Y_{ij}| \cos(\theta_{ij} + \delta_j - \delta_i) \tag{6.1}$$

$$Q_{gi} + Q_{PVi} + Q_{Bi} - Q_{li} = -\sum_{j=1}^{n} |V_i||V_j||Y_{ij}| \sin(\theta_{ij} + \delta_j - \delta_i) \tag{6.2}$$

It is to be noted that the expressions of network parameters and all the variables are presented in the nomenclature in Section 6.5.

6.1.2 Disutility to Customers

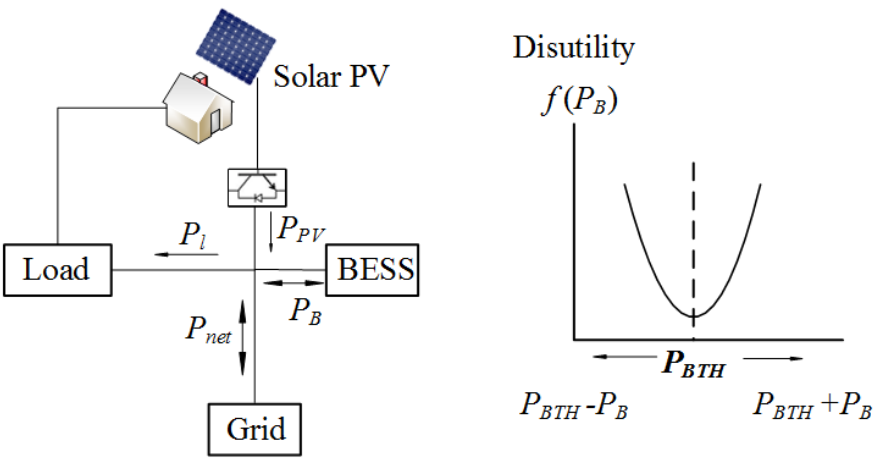

Figure 6.1 Threshold BESS output and customer’s disutility modelling

Feed-in-tariff is a popular form of incentive that is a rate paid to electricity consumers for feeding solar power back to the grid [3]. Without any solar feed-in-tariff scheme, a potentially economic option can be to store the excess PV energy in a BESS during the day and utilising the stored energy when solar power is not available. To this end, an economic charging rate (P_{BTHi}) of BESS at i-th sampling instant can be expressed by (6.3).

$$P_{BTHi} = P_{li} - P_{PVi} \;\; ; \forall\, i \in [1, n] \tag{6.3}$$

where, P_{Li} and P_{PVi} indicate the customer's load and PV power respectively at i-th sampling instant and shown in Figure 6.1. If the load is higher than PV output, the sign of P_{BTHi} is positive which indicates discharging of BESS. The negative sign of P_{BTHi} indicates charging of BESS when PV is higher than load.

Any change in the threshold charge/discharge rate (P_{BTHi}) for the network voltage support will impose costs or disutility to customers. A BESS charge rate higher than P_{BTHi} implies charging from the grid, while a charge rate less than P_{BTHi} means exporting power to the grid. Discharging BESS is directly associated with its lifetime. Any discharge rate above P_{BTHi} implies quick discharge, which gradually diminishes the BESS lifetime. BESS discharging at a smaller rate than P_{BTHi} implies a slower discharge for which BESS may not be available for charging when required. If higher BESS power is commanded, the consumer will experience more disutility and vice versa. To address the above phenomenon, the disutility of customers by using BESS is modelled as a quadratic function of BESS power and expressed by (6.4).

$$f(P_{Bi}) = \mathrm{a}_1 (P_{Bi} - P_{BTHi})^2 \, ; \; \forall\, i \in [1, n] \tag{6.4}$$

where a_1 is a constant that implies disutility convex coefficient and its value depends on the cost of BESS generation (in $/kW) for network voltage support. The quadratic disutility function is illustrated in Figure 6.1. The role of f is to impose a cost on the loss of consumer's quality of service, and the subsequent optimisation of the proposed method is supposed to balance that against the other needs (discussed in Section 6.1.3).

6.1.3 Optimisation Problem Formulation

The input data for the problem are P_{PVi}, Q_{PVi}, P_{li}, Q_{li}, V_j and δ_j, where $i \in [1, \ldots, n]$ and $j \in H$. The above inputs can be measured via smart meters. Given a specific choice of the control variables P_{Bi} and Q_{Bi}, there is (n×2) number of unknowns, which can be determined from the (n×2) power flow equations, assuming a solution exists.

i) *Objective Function*

Let J be a function that models the cost to the relevant stakeholders (consumer and DNO). The formulated cost function is given by (6.5).

$$J(P_{Bi}, P_{gi}, Q_{Bi}, V_i) = f(P_{Bi}) + \alpha |V_i - 1|^2 + \beta P_{gi}^2 + \gamma Q_{Bi}^2 \quad ; \forall\, i \in [1, n] \tag{6.5}$$

The first term of the cost function is consumer's disutility as explained in subsection 6.1.2. The second term helps in keeping the bus voltage close to unity by choosing a large value of the voltage penalty factor α. A reasonable value of β should be chosen to keep the third term of (6.5) in order to maintain the peak demand of the total network as low as possible. Keeping the bus voltages near unity is in the interest of voltage regulation and is consistent with peak shaving. The fourth term of the cost function is to penalise reactive power injection from the BESS for voltage regulation. Distribution voltage regulation can be attained by controlling both real and reactive power of the BESS inverters. Currently, BESS are comprised of four quadrant inverters enabling the flexibility of using a limited amount of reactive power besides real power. The reactive power penalty factor γ should be reasonable enough so that BESS can utilise its reactive power within allowable limits since there are restrictions on power factors of inverters in many power systems.

In reality, the cost function and associated variables change every sampling instant. The objective is to minimise the cost of a DRA and decide the BESS operation instantly. Therefore, time dependence has been omitted in the problem formulation.

ii) *Limits on Total Power Flow in a Network*

Constraints (6.6) and (6.7) are formulated to control the total real and reactive power flow. This will impose limits on the power import from the grid and reduce the overall cost to retailers. Maintaining peak power drawn from the grid within acceptable limits reduces the chance of transformer overloading, therefore, is consistent with the interests of a DNO.

$$P_{gi\,\min} \le P_{gi} \le P_{gi\,\max} \quad ; \forall\, i \in [1, n] \tag{6.6}$$

$$Q_{gi\,\min} \le Q_{gi} \le Q_{gi\,\max} \quad ; \forall\, i \in [1, n] \tag{6.7}$$

iii) *BESS Capacity Constraints*

The state of charge (*SoC*) implies the percentage of available energy in a BESS at an instant with respect to its maximum capacity. If *SoC* of a BESS is y%, it requires (100–y)% of its rated energy to be completely charged. Voltage regulation may require both charge and discharge operations. Therefore, BESS *SoC* is continuously monitored by a DRA, which can be accomplished through the use of smart meters. The required amount of energy (E_{avi} kWh) for full charging of a BESS from the present state at i^{th} node is expressed by (6.8).

$$E_{avi} = (1 - SoC_i)\,.\, E_{i\,\max} \quad ; \forall\, i \in [1, n] \tag{6.8}$$

where the maximum BESS capacity at i^{th} node is denoted by E_{imax} (kWh)

Then, the maximum limits of real and reactive power of BESS at an instant are expressed by (6.9)–(6.10).

$$P_{Bi\max} = \frac{E_{avi}}{T_{VR}} \;\; ; \forall\, i \in [1, n] \tag{6.9}$$

$$Q_{Bi\max} = \tan\{\cos^{-1}(p.f.)\} P_{Bi\max} \;\; ; \forall\, i \in [1, n] \tag{6.10}$$

where T_{VR} indicates the possible duration for voltage regulation and is given as an input by DRAs. Reactive power limit at an instant is calculated based on the power factor (*p.f.*) standards for small scale BESS inverters defined by IEEE 1547. These two limits expressed in (6.9) and (6.10) are utilised to formulate the following constraints.

$$P_{Bi\min} \le P_{Bi} \le P_{Bi\max} \;\; ; \forall\, i \in [1, n] \tag{6.11}$$

$$Q_{Bi\min} \le Q_{Bi} \le Q_{Bi\max} \;\; ; \forall\, i \in [1, n] \tag{6.12}$$

The value of P_{Bimin} and Q_{Bimin} can be 0 or equal to -P_{Bimax} and -Q_{Bimax} respectively depending on the DRA's choice.

iv) *Node Voltage Constraints*

The voltage of the BESS connected nodes are controlled within standard limits and expressed by (6.13).

$$V_{\min} \le V_i \le V_{\max} \;\; ; \forall\, i \in [1, n] \tag{6.13}$$

v) *BESS Inverter Size*

The real and reactive power of BESS must be selected in such a way that can reside under the inverter's maximum capacity limit as expressed by (6.14).

$$(P_{PVi} + P_{Bi})^2 + Q_{Bi}^2 \le S_{\max}^2 \;\; ; \forall\, i \in [1, n] \tag{6.14}$$

where, S_{max} implies the maximum VAR capacity of the BESS inverter.

Now, the goal is to pick P_{Bi} and Q_{Bi} that minimises J and for which the corresponding P_{gi}, Q_{gi}, V_i, δ_i (obtained from power flow equations) satisfy the relevant inequality constraints expressed by (6.1)-(6.2), (6.6) – (6.7) and (6.11) – (6.14).

A decision vector $x := [P_{Bi}, Q_{Bi}, P_{gi}, Q_{gi}, V_i, \delta_i]^{\mathrm{T}}$, which is a concatenation of the control and exogenous signals. The load-flow equations (6.1) and (6.2) are expressed in the form of $g(x) = 0$. An inequality in the form of $a \le x \le b$ is equivalent to $x - b \le 0$ and $-x + a \le 0$. Therefore, all the inequality constraints in (6.6) – (6.7) and (6.11) – (6.14) are compactly represented as $h(x) \le 0$. The expression of the inequality constraints is given by (6.15).

$$h(x) = \begin{bmatrix} A_h . x - b_h \\ C_h . x^2 - S_{\max}^2 \end{bmatrix} \tag{6.15}$$

A_h, B_h and C_h for a two node system with a single BESS are represented as follows.

$$A_h = \begin{bmatrix} 1 & 0 & 0 & 0 & 0 & 0 \\ -1 & 0 & 0 & 0 & 0 & 0 \\ 0 & 1 & 0 & 0 & 0 & 0 \\ 0 & -1 & 0 & 0 & 0 & 0 \\ 0 & 0 & 1 & 0 & 0 & 0 \\ 0 & 0 & -1 & 0 & 0 & 0 \\ 0 & 0 & 0 & 1 & 0 & 0 \\ 0 & 0 & 0 & -1 & 0 & 0 \\ 0 & 0 & 0 & 0 & 1 & 0 \\ 0 & 0 & 0 & 0 & -1 & 0 \end{bmatrix} \qquad b_h = \begin{bmatrix} P_{B\max} \\ -P_{B\min} \\ Q_{B\max} \\ -Q_{B\min} \\ P_{g\max} \\ -P_{g\min} \\ Q_{g\max} \\ -Q_{g\min} \\ V_{\max} \\ -V_{\min} \end{bmatrix} \qquad C_h = \begin{bmatrix} 1 \\ 1 \\ 0 \\ 0 \\ 0 \\ 0 \end{bmatrix}$$

Once the constraints are rewritten as $g(x) = 0$ and $h(x) \leq 0$, the goal is to pick x that solves the following optimisation problem expressed by (6.16) and (6.17)

$$\underset{x}{\text{minimise}}\ J(x) \tag{6.16}$$

$$\text{Subject to} \quad \begin{cases} g(x) = 0 \\ h(x) \leq 0 \end{cases} \tag{6.17}$$

The cost and inequality constraints are convex functions of x, while the equality constraints are non-linear and non-convex [106]. Therefore, a suitable solution method is required to solve the problem for optimum solutions at every sampling instant.

6.1.4 Solution Method

The non-convexity of the problem as described in Section 6.1.3 is caused by the non-linear equality constraints originating from power flow equations. Therefore, the convex problem needs to be approximated by a linear equality. The simplest approach is chosen for this purpose, this is called Jacobian Linearisation around an operating point of the state [110].

For Jacobian linearisation, let x_0 be a nominal operating point. Let $\Delta x = x - x_0$ so that the equality constraint can be linearised to $g(x_0) + \nabla g(x_0) \Delta x = 0$, which is expressed by (6.18).

$$A_h \ \Delta x \ = \ b_h \tag{6.18}$$

where $A_h = \nabla g(x_0)$ and $b_h = -g(x_0)$

Now, the problem can be defined by (6.19) and (6.20).

$$\tilde{J}(\Delta x) := J(x_0 + \Delta x) \tag{6.19}$$

$$\tilde{h}(\Delta x) := h(x_0 + \Delta x) \tag{6.20}$$

Based on the aforementioned definitions, the formulated problem can be updated to the following form.

$$\underset{\Delta x}{\text{minimise}} \ \tilde{J}(\Delta x) \tag{6.21}$$

Subject to the constraints as expressed by (6.22) and (6.23)

$$A_h \ \Delta x = b_h \tag{6.22}$$

$$\tilde{h}(\Delta x) \leq 0 \tag{6.23}$$

The convexity of J and h ensures that the respective $\tilde{J}$ and $\tilde{h}$ are convex, which makes (6.21)-(6.23) a convex problem. A simple heuristic method namely log-barrier interior point is used to search the optimum set point of the above problem [111]. The searching starts with a point x_0 such that it satisfies $g(x) = 0$, which is accomplished through root finding. Then the resulting solutions are checked to ensure no violation of constraints. If any constraint is violated, the real and reactive powers are increased sequentially, until a feasible point is found.

6.2 System Modelling and HIL Experiment

The proposed control method is applied to the IEEE-13 nodes distribution network, which is modelled in RTDS platform [101]. The detailed modelling of the system components is described in Chapter 5. PV and BESS units are placed at node 611 to observe the network voltage regulation performance with the proposed scheme. The single phase feeder connecting nodes 671, 684 and 611 is chosen as the area of a DRA for voltage regulation. Therefore, the proposed algorithm is implemented on the selected feeder of the total network. Figure 6.2 presents the schematic diagram of the system with locations of PV, BESS and DRA.

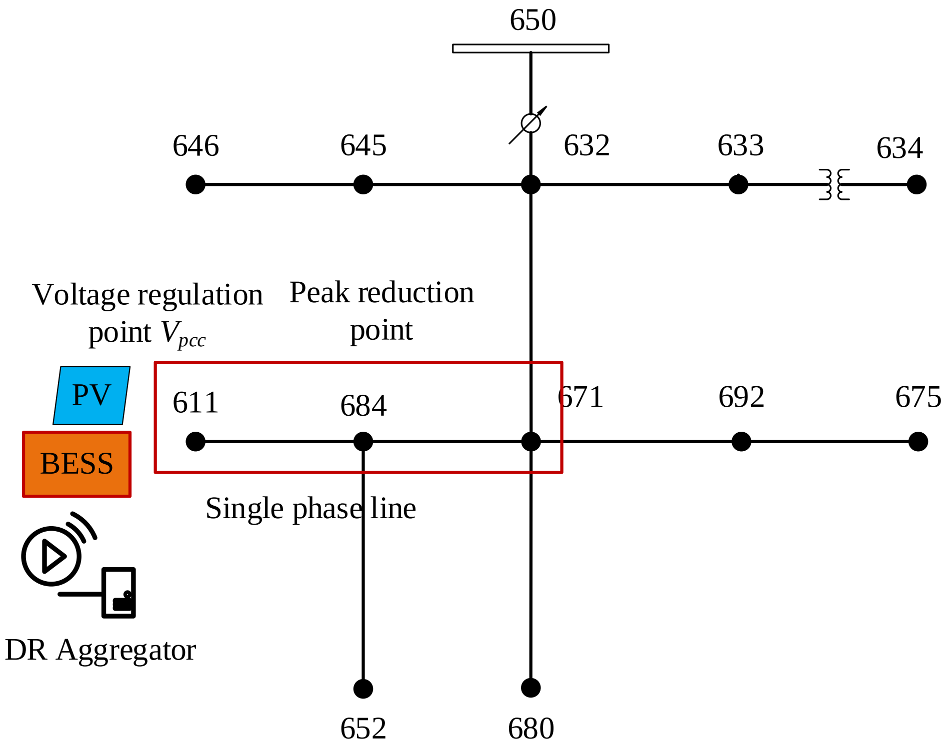

Figure 6.2 Schematic diagram of the IEEE-13 nodes feeder with PV, BESS and DRA

The state-of-charge $SoC(k)$ of a BESS at k-th sampling instant depends on its previous state $SoC(k–1)$ and is expressed by (6.24) [102].

$$SoC(k) = SoC(k-1) - \eta.\, I_{batt}(k).\, \Delta t \tag{6.24}$$

where $I_{batt}(k)$ is the charge/discharge current in the battery bank at the k^{th} sampling instant and Δt represents the sampling period. The parameter η implies BESS charge/discharge efficiency. The protection circuit of BESS ensures that the $SoC(k)$ is being operated within SoC_{min} and SoC_{max} limits. The detailed modelling of the BESS in RTDS platform is discussed in Chapter 5.

Hardware-in-the-loop simulation is performed using RTDS and a dSPACE controller board as shown in Figure 6.3. A detailed description of the set-up is provided in Chapter 5. The proposed BESS control approach is implemented in MATLAB Simulink software platform and the respective C-code is downloaded to dSPACE. While running the power flow of the RTDS network, all node voltage magnitudes, angles and real-reactive power flow through lines can be obtained.

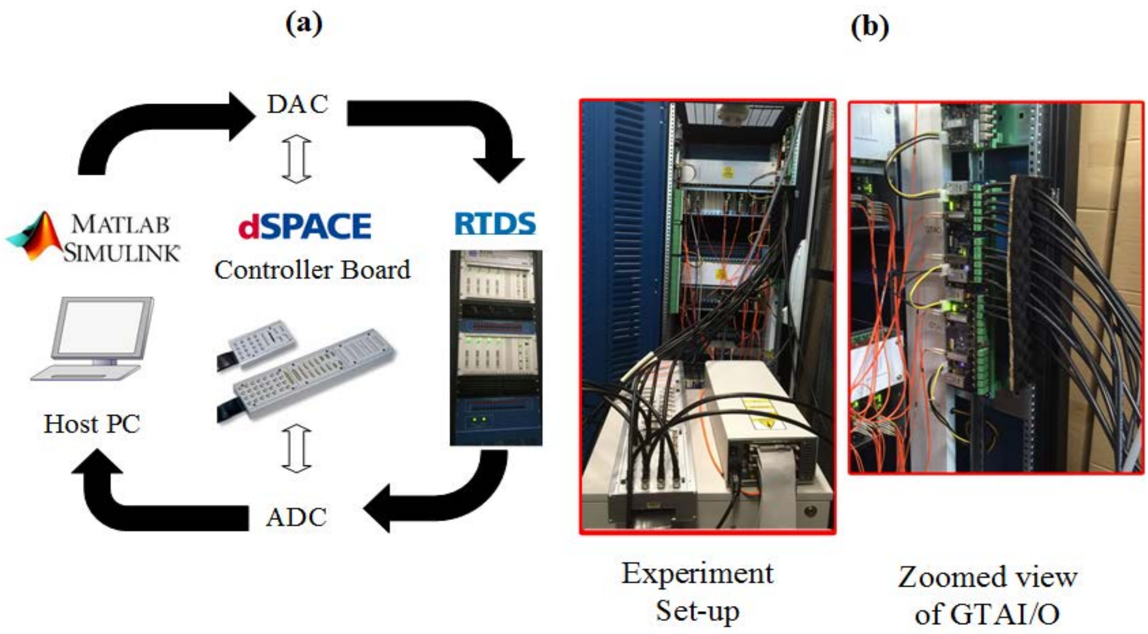

Figure 6.3 (a) Schematic diagram of the hardware-in-the-loop set-up (b) Experimental set-up

The analog data from the RTDS power flow simulation is accessed via a GTAO card and entered into the dSPACE control device through RG6 cables. The analog signals from the RTDS network is processed to digital using ADC channels of dSPACE and then is utilised in the proposed control algorithm to generate appropriate control signals for a BESS. The controller outputs from dSPACE are then passed on to the BESS model in RTDS via DAC channels. It is worth mentioning that the signals of RTDS and dSPACE are properly scaled before transporting to match the voltage levels ranging from -10V to +10V of the input/output ports of Gigabit Transceiver Input/output (GTI/O) cards of RTDS.

The sampling period of the Simulink program is selected in such a way that the control algorithm can execute within the sampling interval. If the execution time is more than the sampling period, the program cannot be run in real time. The distribution network runs in RTDS at a 50μs sampling rate, while the Simulink program is executed in a few seconds.

6.3 Results and Discussion

The performance of the developed control algorithm is evaluated through several simulation scenarios. In the beginning, a base case load flow of the IEEE-13 node system is simulated. Then, two case studies are performed with a BESS placed at node 611. The performance of BESS controller is scrutinised under different values of voltage penalty factor, α in case studies 1 and 2 respectively. The impact of different parameter values on the controller performance is also investigated. The values of the parameters of the proposed controller are presented in Table 6.1. All the values related to voltage and power are provided in p.u. considering the base power of the system as 1000 kVA.

Table 6.1 Parameter values in case studies-1 and 2

Parameters	**Value**
SoC_{min}	10%
SoC_{max}	90%
V_{min}	0.94 p.u.
V_{max}	1.055 p.u.
P_{gmin}	-5 p.u.
P_{gmax}	5 p.u.
S_{max}	1 p.u.

The subsequent sections explain the detailed results and relevant discussions.

6.3.1 Base Case (Voltage Regulation without BESS)

The base case simulation is performed with a PV unit at node 611 and without any BESS in the network. A variable PV power profile for 7.5 hours is considered, while loads remain consistent at 118 kW. The PV power rises to 120 kW in the mid-noon, which causes a reverse active power flow at PCC. Figure 6.4(a) shows the profiles of PV power and customer's load. The variable PV output causes voltage fluctuations at nodes 611 and 684 as shown in Figure 6.4(b). It can be observed that PCC voltage exceeds the upper limit (1.055 p.u.) at around noon time due to high PV generation. Therefore, a window of the PV power profile from 8:30 to 17:30 has been chosen to test the proposed BESS controller in case studies-1 and 2.

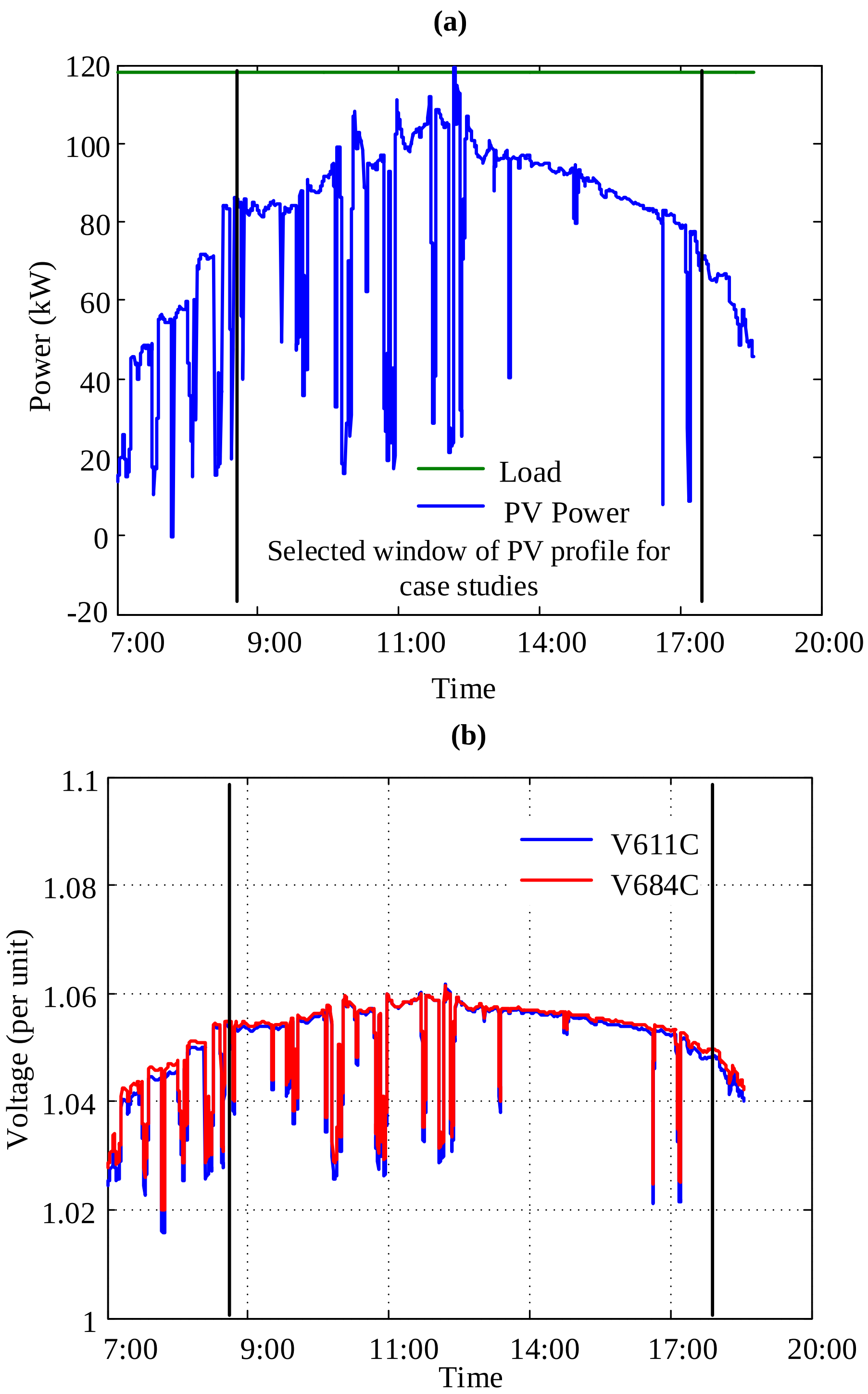

Figure 6.4 (a) Solar PV output and load profiles at PCC (b) Voltage profiles of the studied nodes (Base case)

6.3.2 Case Study-1 (with BESS and a Positive Value of α)

The values of the parameters a_1, α, β and γ for case study-1 are given in Table 6.2. These values are chosen arbitrarily and are varied in Section 6.3.4 to understand the impact of the parameters on controller performance.

Table 6.2 Proposed control parameter values in case study-1

Parameters	**Value (x10^{-6} \$)**
a_1	1000000
α	10000
β	10
γ	10000

The disutility convex coefficient a_1 is selected sufficiently large as can be seen in Table 6.2. This is to match per unit conversion of the respective variables. Higher values of disutility coefficient imply costlier BESS operation for customers, which imposes more cost to the aggregators. The voltage penalty factor is chosen as a large value to restrict voltage deviation from unity. The weight on β has been kept low to relax the peak power flow of the network while the weight on reactive power penalty γ is chosen reasonably large so that it does not end up using much reactive power of BESS.

In case study-1, a BESS is connected to node 611 and the proposed controller performance is examined. The real and reactive powers of the BESS and respective PV and load profiles are presented in Figure 6.5(a). It is observed that the BESS is charged at a variable rate from 8:30 until 10:00 hrs and then it starts discharging for a while. The charge-discharge continues for the rest of the day. As presented in Figure 6.5(b), the voltage magnitudes of nodes 611 and 684 also reside within 0.94 to 1.055 p.u. limits for the studied duration.

(a)

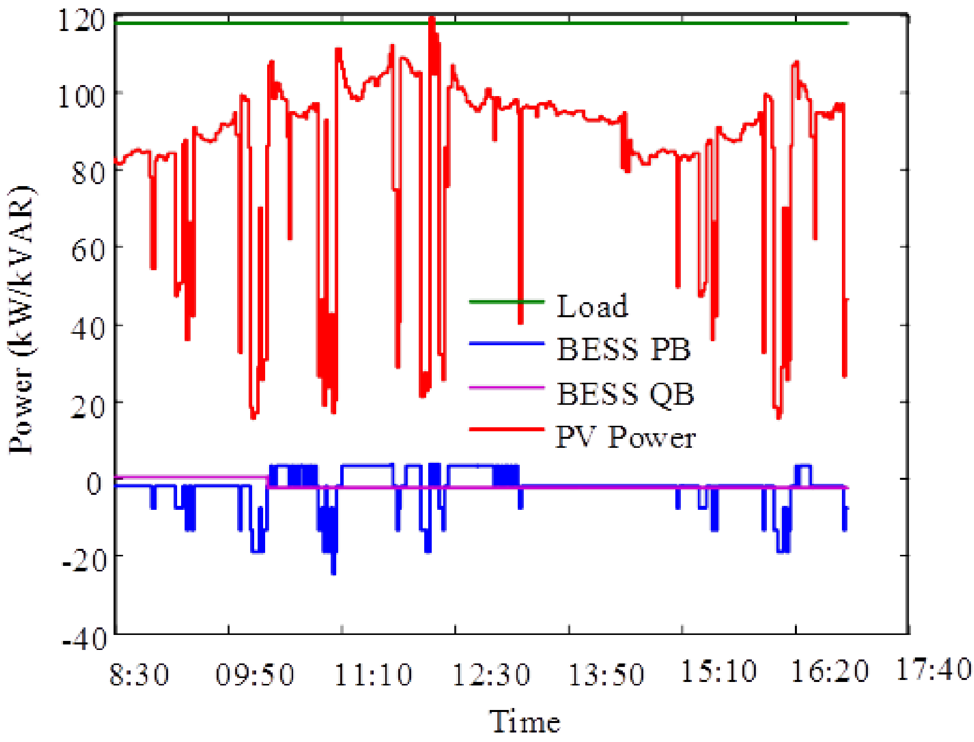

(b)

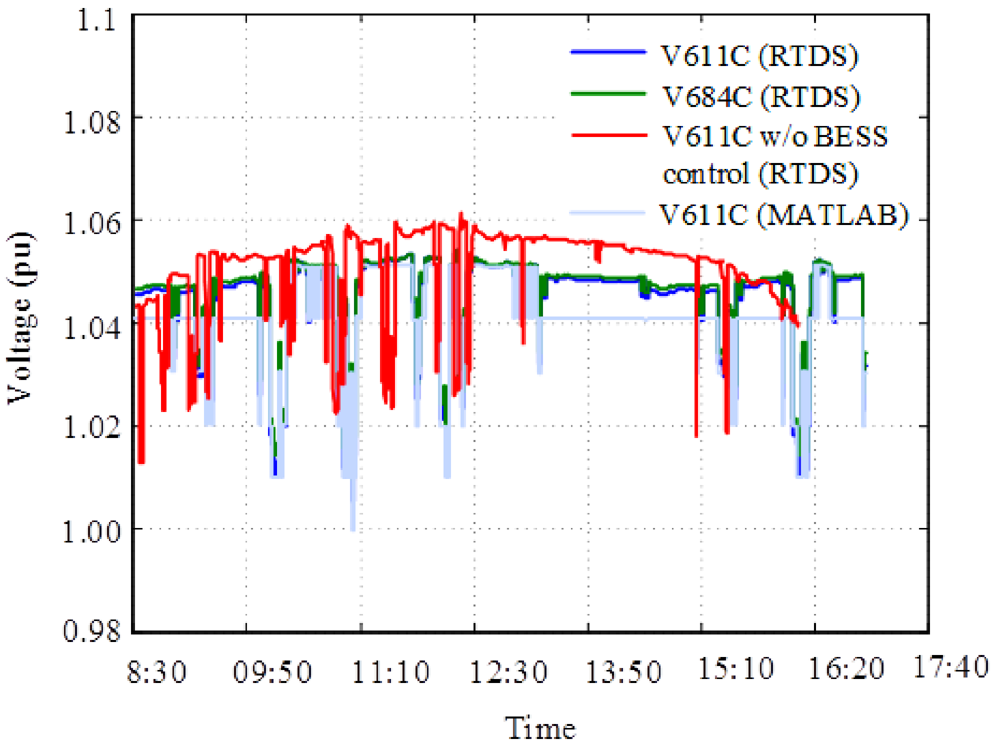

Figure 6.5 Case study-1 with a positive value of α (a) PV, load and BESS power at PCC (b) Voltage profiles of the studied nodes

It can be seen from Figures 6.5(a) and (b) that if PV output rapidly rises and results in a higher voltage (>1.055 p.u.) at the studied nodes, the BESS is discharged at such a rate that it regulates the voltage closer to the upper limit (1.055 p.u.). This is due to the high value of parameter

a_1, which imposes a higher cost for increasing BESS charge rate. Therefore, instead of charging at a high rate, the proposed control algorithm decides to discharge BESS at a low rate keeping the voltage within specified limits. It is also observed from Figure 6.5(b) that the predicted voltage at node 611 by the proposed method in MATLAB mostly matches the actual node voltage in RTDS, which indicates a reasonable accuracy of the problem formulation.

6.3.3 Case Study-2 (with BESS but No Voltage Penalty, α = 0)

In case study-2, no voltage penalty is considered, this means the value of parameter α is set to 0, while other parameters remain the same as case study-1. The real and reactive powers of BESS and respective node voltages are displayed in Figures 6.6(a) and (b) respectively. It can be observed from Figure 6.6(a) that the proposed control algorithm decides to charge the BESS at a fixed rate for the studied duration. Therefore, the voltage profiles of nodes 611 and 684 are maintained within permissible limits as shown in Figure 6.6(b). It can also be observed that the node voltages are close to 1.04 p.u. most of the time.

In case study-2, the PCC voltages at a few sampling instants are more close to unity compared with the case study-1 (where a positive voltage penalty factor is used). The BESS has used a fixed charge rate (25kW) for voltage regulation in case study-2, which leads to an expensive BESS operation than that of case study-1. Because of the consistent charge rate of BESS, the PCC voltages are close to 1.0 p.u. at a few sampling instances. Therefore, the load flow with higher BESS power is more responsible for such a situation rather than the voltage penalty factor.

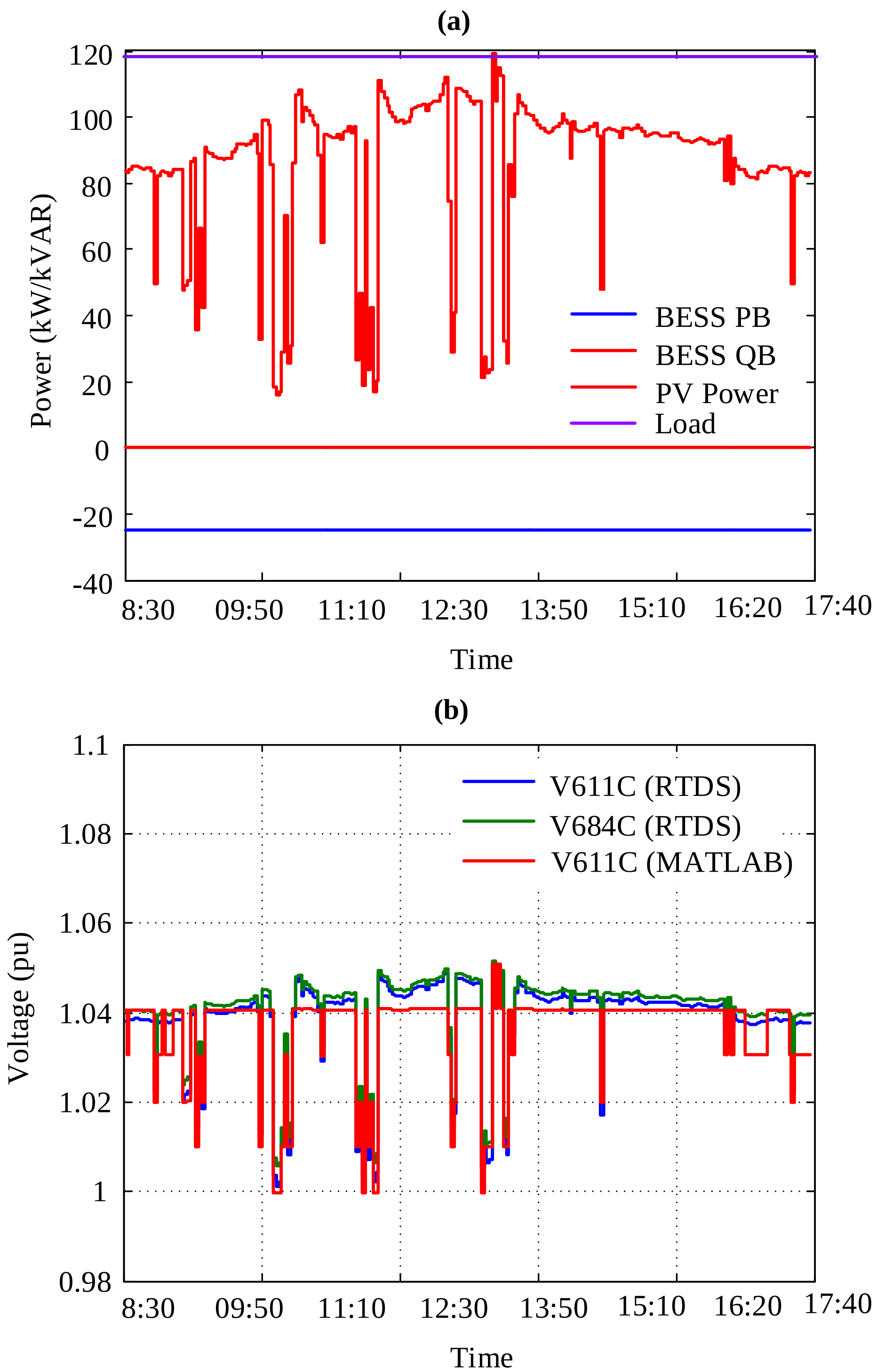

Figure 6.6 Case study-2 with a zero value of α (a) PV, load and BESS power at PCC (b) Voltage profiles of studied nodes

6.3.4 Comparing the Operating Regions of Case Studies 1 and 2

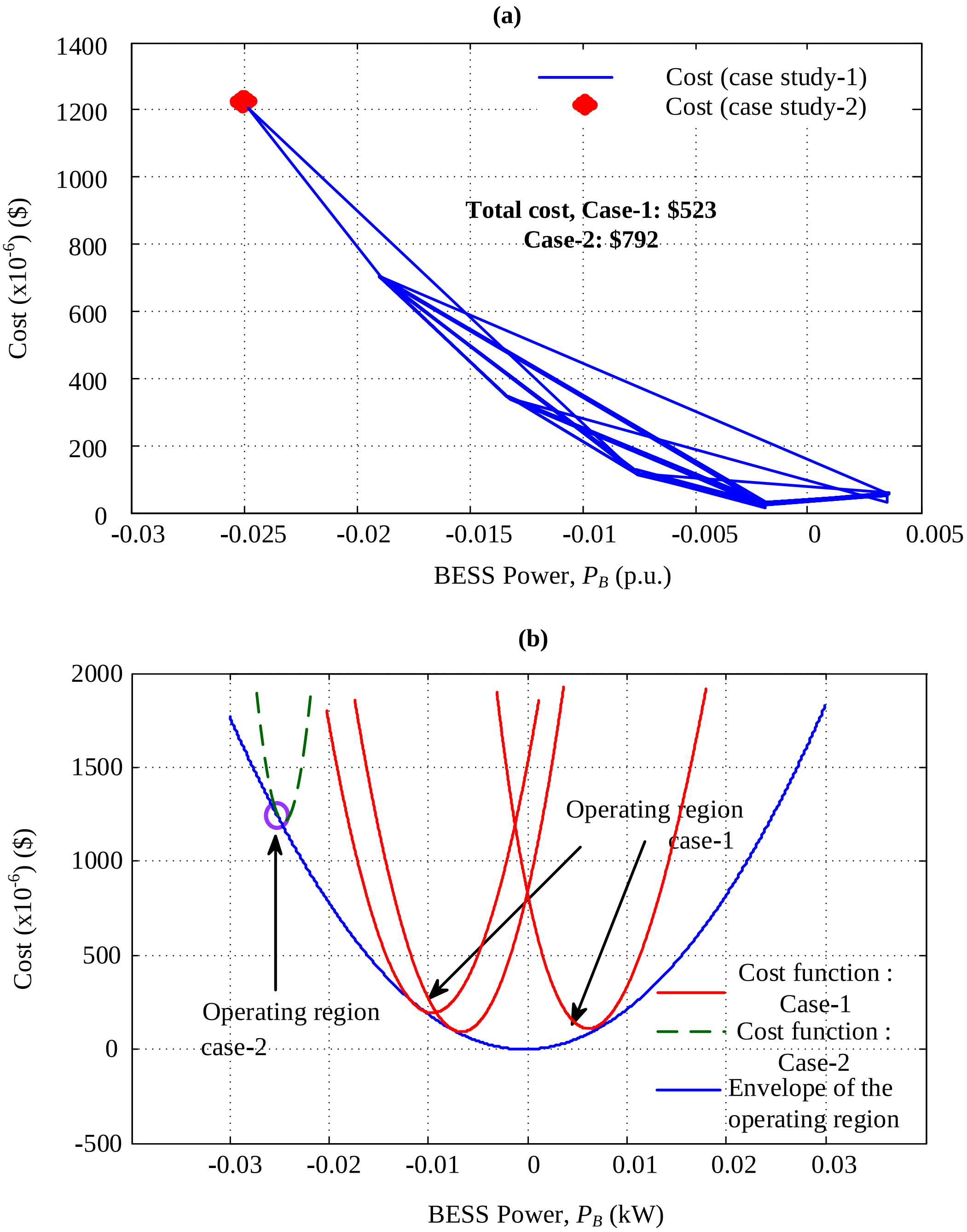

Figure 6.7 Operating regions of BESS in both cases

Figures 6.7 (a) and (b) show the costs of a DRA for two operating situations in case studies 1 and 2. It is observed that the DRA costs for both case studies are positive values. The total cost varies between \$0.5 and \$1200, while BESS power varies from 0.005 to 0.025 p.u. in case study-1. It is calculated that the total cost of the DRA is \$523 for the studied profile in case study-1, while the cost is \$792 in case study-2. Hence, it can be said that voltage penalty in case study-1 causes less operational cost for the DRA.

In case study-1, the BESS is charged and discharged at various rates and hence, the operating region is wider than that of case study-2 as presented in Figure 6.7. The BESS is operating at a fixed point in case study -2, which is much costlier than all operating points of case-1. Thus, the DRA experiences more expensive operation of BESS in case study-2. With the variations of PV power, the threshold BESS charge rate varies as expressed in (6.3). Therefore, load disutility curves can be drawn at each P_{BTHi} point as illustrated in Figure 6.7(b). An increase in BESS power magnitude requires higher costs. Therefore, the envelope of the operating regions of the BESS at different charge/discharge rates shows a parabolic trend.

The controller performance is further checked for different values of parameters, a_1, α, β and γ. Table 6.3 shows the BESS charge/discharge power and PCC voltage for two set points. It is observed that at a given load and PV, the value of a_1 controls the charge/discharge rates of the BESS. The disutility co-efficient a_1 represents the monetary value of using 1 p.u. BESS power for voltage regulation. Therefore, if the value of a_1 decreases, charge/discharge rates of the BESS increase. If BESS are charged for voltage regulation as per set point -1 in Table 6.3, a zero value of the reactive power is observed. For a smaller value of a_1 at set point-2, the BESS discharges and absorbs reactive power. The value of reactive power penalty factor (γ) is smaller in case-2 than that of case-1, which provides flexibility to utilise BESS reactive power. For the two set points, power flow penalty factor (β) is chosen a small value to ensure convergence of the optimisation problem.

Now, the disutility co-efficient a_1 is determined by the DRA looking at the customers' actual disutility for BESS utilisation in voltage regulation. From the value of disutility function, the DRA decides the payable amount to a customer. The total cost of a DRA can be utilised to calculate the charge of a DNO for their network voltage correction.

Table 6.3 Analysis of controller parameters impact on BESS performance

Set point-1 (P_l =118 kW, P_{PV} =100kW)				
Parameters	a_1	α	β	γ
Values (x10^{-6} $)	1000000	1000	10	20000
Variables	P_B	Q_B	V_{611}	δ_{611}
Results (p.u.)	-0.02	0	1.041	3.13
Set point-2 (P_l =118 kW, P_{PV} =100kW)				
Values	10000	100	0	200
Variables	P_B	Q_B	V_{611}	δ_{611}
Results (p.u.)	0.04	-0.005	1.052	4.5

6.4 Summary

In this chapter, an optimisation problem is formulated and solved for least cost operation of customers PV and BESS ensuring system voltage regulation. The resultant BESS charge-discharge trails are utilised to control actual BESS in RTDS, while practically validating the proposed method. Results confirm that the proposed method can successfully regulate the system voltage within given specified limits. Several control parameters namely disutility coefficients and voltage and reactive power penalty factors are introduced. The choice of controller parameters highly influences the total cost of DRA and the performance of BESS. The obtained values of the total cost from the analyses help to determine the payable amount to customers by DRA for participating in demand response. The total cost of the DRA for voltage regulation service is to be paid by the DNO. The major findings of the chapter are as follows:

(i) It is found that imposing a penalty on PCC voltage variation in the proposed controller reduces the total cost of DRAs.

(ii) Both charge and discharge operations happen in case study-1, while case study-2 is limited to only charging BESS at a high rate. It is found from results that BESS operation in case-1 is more cost effective than that in case-2.

(iii) If the disutility function is more convex, the higher charge/discharge rates of BESS are required. The proposed BESS controller tries to keep the PCC voltage close to unity and alleviates the risk of over voltage.

The hardware-in-the-loop simulation results provide an insight about the performance of the proposed controller in real-time. The control method is able to utilise actual BESS in a network for voltage regulation provided that communication between the local and central controller is secured. It is found that multiple stakeholders' involvement (e. g. customers and DNOs) is lucrative for DRAs. Customer's behaviour can play a vital role to model their 'disutility' for permitting BESS in system voltage regulation. If customers are risk aversive, more convex disutility for utilising their BESS can be found, while risk takers have less disutility. In the future works, the potential advantages for a DNO by using the proposed method will be analysed in detail.

In the next chapter, the concluding remarks and future direction of this research will be discussed.

6.5 Nomenclature

i, j	Bus indices

Sets

N	Set of total buses
L	Set of load buses
H	Set of infinite bus
B	Set of BESS connected buses
x	State vector

Parameters

n	Total number of nodes
p	Number of loads
m	Number of BESS connected nodes
$Y^{n\times n}$	Bus admittance matrix
θ	Bus admittance angles
η	BESS efficiency
α	Voltage penalty factor
β	Active power flow penalty factor
γ	Reactive power penalty factor of BESS
a_1	Disutility convex co-efficient
V_{min}	Minimum voltage magnitude in p.u.
V_{miax}	Maximum voltage magnitude in p.u.
T_{VR}	Possible duration for voltage regulation

Exogenous variables (in p.u.)

P_l	Active power demand
Q_l	Reactive power demand
P_{PV}	Active power from solar PV
Q_{PV}	Reactive power from solar PV
P_{gmin}	Minimum active power drawn from grid
P_{gmax}	Maximum active power drawn from grid
E_{imax}	Maximum kWh capacity of BESS
P_{Bmin}	Minimum active power of BESS

P_{Bmax}	Maximum active power of BESS
Q_{Bmin}	Minimum reactive power of BESS
Q_{Bmax}	Maximum reactive power of BESS
S_{max}	Maximum VAR capacity of the BESS inverter
P_{BTH}	Threshold active power of BESS
SoC	State-of-charge of BESS
SoC_{min}	Minimum state-of-charge of BESS
SoC_{max}	Maximum state-of-charge of BESS

State variables (in p.u.)

P_g	Active power drawn from grid
Q_g	Reactive power drawn from grid
V	Bus voltage
δ	Bus voltage angle

Actuation variables (in p.u.)

P_B	Active power of BESS
Q_B	Reactive power of BESS

Chapter 7 Conclusions and Recommendations for Future Works

7.1 Conclusions

In this thesis, several technical tools and control methods have been developed for BESS to facilitate additional solar PV while maintaining satisfactory operation of distribution systems. Comprehensive investigations are carried out for better utilisation of solar PV and BESS in accordance with the existing standards. The proposed control approaches are experimentally validated using hardware-in-the-loop setup to realise their practical performance. In this chapter, the main contributions of this thesis are reviewed and some conclusions are drawn.

In Chapter 2, the major technical issues caused by proliferated PV in power distribution systems and their existing solutions are outlined. The technical challenges due to high PV penetration include load curve reformation and voltage regulation, for which BESS are considered as an impending solution. The state of the art literature survey is carried out on existing tools for the allocation and control of BESS for peak shaving and voltage regulation purposes. Despite quite a few existing and ongoing studies, the present approaches on determining appropriate BESS allocation for peak shaving and voltage regulation are devoid of a few important factors that characterise a distribution system. Furthermore, the BESS control approaches should consider the cycling effect to prolong their life span in photovoltaic applications.

In Chapter 3, BESS is utilised for peak shaving as well as network upgrade deferral for a specific planning horizon for the benefit of distribution network operators. Due to the ever growing peak demand and the uncorrelated occurrence time of PV and maximum load, distribution network operators require periodic reinforcement of their networks involving significant investment. BESS is a potential technology to defer system upgrades provided it is properly sized, located and managed. The existing tools of BESS sizing and siting mainly focussed on loss minimisation and lack explicit dependence on several factors such as, peak shave, load growth rate and PV penetration level that portray a distribution system. Consequently, the approaches so far are not generic enough to be portable to other networks.

To address this niche, a generic tool to determine appropriate sizing, siting and operational planning of distributed BESS is developed. The proposed model expresses the net profit from network upgrade deferral with BESS as a function of peak load growth rate, peak shave fraction and arbitrage. The net profit model is utilised to formulate an optimisation problem to co-optimise

BESS sizing, siting and day-ahead dispatch. A potential policy is also proposed for interaction between a DNO and retailers so that BESS can be utilised to get energy arbitrage. The developed tool is applied to a segment of a Queensland network and the appropriate size, locations and dispatch schedule of multiple BESS are obtained through several case studies.

The analyses in Chapter 3 indicate that system upgrades with optimally allocated BESS is an economic choice for a DNO rather than upgrading transformers and lines. The cost of BESS and the electricity price plays a vital role for a DNO to achieve financial benefit. It is found that network upgrade with BESS is less expensive in a low load growth rate region than that of a high load growth rate region. The required size of BESS increases with growing PV penetration level. To attain financial viability with BESS, the permissible PV penetration decreases with an increase in the load growth rate. The proposed tool can be helpful to network operators in deciding the optimum BESS capacity and location for any networks while maintaining technical and financial viability.

The developed tool is further modified in Chapter 3 for distribution voltage regulation by utilising the real and reactive power of BESS and applied to a low voltage network. The modified tool utilises the k-means clustering method to categorise year-long solar PV power data into a few seasonal cluster profiles. By using the representative PV profiles, the proposed method is able to promptly determine appropriate real and reactive power dispatch schedules of BESS to achieve maximum energy arbitrage from the time of use electricity price, while maintaining acceptable system voltage. The enactment of the modified tool is verified through several case studies, which results in the desired BESS size to be 6 kWh for a customer with a 4 kW PV in the studied network. The payback time of PV-BESS is found to be close to only PV. However, the utilisation of PV-BESS provides relatively more financial benefits to customers in the long run compared to PV only. This investigation also shows that demand response incentives need to be offered to customers for utilising BESS with PV.

Having analyses of the suitable BESS sizing for peak shaving and voltage regulation applications, the steady-state voltage performance of a distribution system under substantial PV penetration is investigated in Chapter 4. The voltage rise phenomenon is described first in light of the existing standards. Then, a typical segment of the Queensland distribution network is analysed to understand the impact of existing and probable solar PV on the system voltage rise characteristics. The network voltage exceeds an allowable margin in reverse power flow cases even if the future PV inverter's reactive VAR is controlled. To mitigate this problem, a methodology is proposed to determine maximum power injection by prospective PV units, which satisfies operating voltage limits. It is found that the maximum active power export limit for a new PV inverter in the studied network is 1.5 kW at 0.9 lagging power factor. However, this limit may vary from one network to the other depending on the PV penetration level and line characteristics. If PV penetration increases in a feeder, the permissible export limit tends to decrease. This export limit is utilised to develop suitable BESS control strategies for better voltage regulation.

The proposed control scheme can maintain the PCC voltage within acceptable boundaries with rapid fluctuations in BESS charge rates. This fluctuation is further reduced through additional rule settings in the control strategy. The main limitation of the obtained control features is that the charge-discharge profiles of BESS are not smoothened. The analyses direct that a prudent BESS control algorithm is required to reduce fluctuations of its charge and discharge modes in photovoltaic applications.

To this end, a real-time forecast-based receding horizon control approach (named as RTF approach) is proposed in Chapter 5, which determines the appropriate charge and discharge profiles for BESS to mitigate voltage rise during high PV generation while simultaneously ensuring that the rapid cycling of BESS is reduced. The proposed control approach is based on PV power forecast for a finite time horizon at an instant using the previous PV measurement. The PV forecast is utilised to estimate the future voltage response trajectories by numerically solving load flow at each sampling instant over the selected time horizon. The proposed RTF controller searches for appropriate BESS charge/discharge trajectories through an iterative process to maintain the PCC voltage within acceptable limits. The novelty of this approach is that it perceives and integrates future trends of a PV output in the control system operation, which facilitates the mitigation of sudden voltage rises. Utilisation of receding horizon control is able to smooth BESS charge-discharge rates depending on the horizon window length. The designed controller reduces risk of rapid BESS cycling during voltage rise events and hence the life of BESS is prolonged.

The proposed RTF control scheme is implemented in Simulink and applied to a radial system modelled in RTDS platform. The charge and discharge trajectories obtained from the RTF approach are passed onto respective BESS inverter controllers in RTDS as reference signals by means of a dSPACE board. Therefore, the performance of the proposed method is verified in HIL setup under several realistic PV and load scenarios. The major findings from the experimental results include, the short-term forecast of PV power and network voltage in the proposed approach is beneficial in foreseeing prospective voltage rise events. It is therefore, able to fix appropriate set points of BESS dispatch within the horizon window. Hence, the proposed RTF method promptly regulates the PCC voltage of a distribution system. BESS discharge operation under variable PV output is substantially reduced by using the RTF approach. Therefore, the cycle-life degradation of BESS is significantly lessened compared to a traditional one-step ahead rule-based technique.

As the use of BESS proliferates in residential sectors, their aggregated use for system voltage regulation is regarded as an option, provided that they are centrally controlled. If customers enable their BESS capacity for system voltage regulation, it comes at the expense of their planned arbitrage causing costs to them. In Chapter 6, this phenomenon is modelled and a control approach is developed from a DRA's perspective. A mathematical model for the cost (termed as 'disutility') of customers due to BESS utilisation for voltage regulation is developed. The 'disutility' model is utilised to articulate the total costs of a DRA, which includes voltage and peak load restrictions. The customers' disutility and DRA's cost models are utilised to establish an optimisation-based tool to search for feasible and cost-effective BESS charge-discharge trajectories so that 'disutility' is minimised ensuring acceptable system voltage. The developed tool is able to regulate distribution voltage through a coordinated effort of a DNO and a DRA, while DNOs pay DRAs for their service via a short/long term contract.

The effectiveness of the proposed method is practically validated via hardware-in-the-loop set-up. The experiment is conducted under variable PV power profiles for several hours to test the performance of the BESS control scheme. The proposed tool is able to successfully coordinate multiple stakeholders' interests through DRAs maintaining satisfactory system voltage regulation. The values of DRA's costs can be utilised to evaluate the demand response incentives payable to customers. Besides, the payable amount by DNOs can also be calculated for providing them voltage regulation services. It is found that multiple stakeholders such as customers and DNOs involvement can be cost-effective for DRAs. Customers' behaviour can play a vital role to model their 'disutility' for permitting BESS in system voltage regulation. If customers are risk aversive, additional disutility for utilising their BESS can be found, while less disutility is expected for risk takers.

7.2 Recommendations

Although significant research work has been performed in this thesis, there are still a number of unresolved issues, which are highlighted below.

i) Since network augmentation is more important in the primary distribution side than the secondary, the BESS sizing and siting tool is established for the balanced three phase network on the primary side. The tool can be further extended for unbalanced networks to evaluate an appropriate BESS size and site.

ii) The proposed RTF control method can be implemented with practical BESS hardware for photovoltaic applications. Lithium-ion BESS has been used for the case studies in this thesis. The developed methods can also be tested and verified for other BESS technologies.

iii) An increase in the forecast horizon length in the proposed RTF method inclines to improve BESS life expectancy and voltage regulation performance. However, the benefits over the use of longer horizons are likely to be steadily reduced due to the combined effect of higher forecast error and computation burden. However, better forecasting techniques such as methods involving sky-camera can be utilised to address the limitation.

iv) One of the aims of demand response aggregators is to make profits from market participation, which is not the focus of this thesis. Separate analyses are required to establish appropriate market policies for DRAs to provide services to DNOs and customers.

List of References

[1] AEMO, "National Electricity Forecasting Report," 2016, Available: http://www.aemo.com.au/Electricity/National-Electricity-Market-NEM/Planning-and-forecasting/-/media/080A47DA86C04BE0AF93812A548F722E.ashx [Accessed: 1-Jan.-2017]

[2] "Solar PV Status", Available: http://pv-map.apvi.org.au/analyses [Accessed: 20-Feb.-2017]

[3] "Overview of Feed in Tariffs Australia," Available: http://www.aph.gov.au/About_Parliament/Parliamentary_Departments/Parliamentary_Library/pubs/rp/rp1314/QG/Tariffs [Accessed: 20-Jan.-2017]

[4] M. J. E. Alam, "Grid integration of solar photovoltaic resources: impact analysis and mitigation strategies", PhD Thesis, University of Wollongong, 2013.

[5] N. Mahmud and A. Zahedi, "Review of control strategies for voltage regulation of the smart distribution network with high penetration of renewable distributed generation," *Renewable and Sustainable Energy Reviews*, vol. 64, no., pp. 582-595, October, 2016.

[6] "How to get the most out of your solar PV system."Available: http://www.solarchoice.net.au/blog/homes-energy-usage-patterns-after-installing-solar-pv-system [Accessed: 20-Feb.-2017]

[7] K. C. Divya and J. Østergaard, "Battery energy storage technology for power systems—An overview," *Electric Power Systems Research*, vol. 79, no. 4, pp. 511-520,2009.

[8] "As energy push accelerates, battery costs set to plunge 60%," Available: http://www.computerworld.com/article/2977655/sustainable-it/as-energy-push-accelerates-battery-costs-set-to-plunge-60.html. [Accessed: 20-Feb.-2017]

[9] "How are electricity prices set in Australia", Available: http://www.rba.gov.au/foi/disclosure-log/pdf/101115.pdf [Accessed: 27-Nov.-2015]

[10] "IEEE Standard for Interconnecting Distributed Resources with Electric Power Systems," *IEEE Std 1547-2003*, pp. 1-28, 2003.

[11] Energex and Ergon Energy, "Standard for Small Scale Parallel Inverter Energy Systems up to 30 kVA," Available: https://www.ergon.com.au/__data/assets/pdf_file/0005/198698/STNW1170- Connection-Standard-for-Micro-EG-Units.pdf [Accessed: 15-Aug.-2016]

[12] J. Jaguemont, L. Boulon, P. Venet and Y. Dub *et al*, "Lithium-Ion Battery Aging Experiments at Subzero Temperatures and Model Development for Capacity Fade Estimation," *IEEE Transactions on Vehicular Technology*, vol. 65, no. 6, pp. 4328-4343, 2016.

[13] M. J. E. Alam and T. K. Saha, "Cycle-Life Degradation Assessment of Battery Energy Storage Systems Caused by Solar PV Variability," *in proc. IEEE Power and Energy Society General Meeting (PESGM)*, Boston, MA, USA, 17-21 July, 2016.

[14] M. Ecker, N. Nieto and S. Käbitz *et al.*, "Calendar and cycle life study of Li(NiMnCo)O2-based 18650 lithium-ion batteries," *Journal of Power Sources*, vol. 248, pp. 839-851, 2014.

[15] R. B. Wright, C. G. Motloch and J. R. Belt *et al.*, "Calendar- and cycle-life studies of advanced technology development program generation 1 lithium-ion batteries," *Journal of Power Sources*, vol. 110, no. 2, pp. 445-470, August 2002.

[16] J. Leithon, T. J. Lim, and S. Sun, "Battery-Aided Demand Response Strategy Under Continuous-Time Block Pricing," *IEEE Transactions on Signal Processing*, vol. 64, no. 2, pp. 395-405, 2016.

[17] N. G. Paterakis, O. Erdinç, A. G. Bakirtzis, and J. P. S. Catalão, "Optimal Household Appliances Scheduling Under Day-Ahead Pricing and Load-Shaping Demand Response Strategies," *IEEE Transactions on Industrial Informatics*, vol. 11, no. 6, pp. 1509-1519, 2015.

[18] J. Wan, R. Zhang, X. Gui, and B. Xu, "Reactive Pricing: An Adaptive Pricing Policy for Cloud Providers to Maximize Profit," *IEEE Transactions on Network and Service Management*, vol. 13, no. 4, pp. 941-953, 2016.

[19] M. A. Azzouz, M. F. Shaaban, and E. F. El-Saadany, "Real-Time Optimal Voltage Regulation for Distribution Networks Incorporating High Penetration of PEVs," *IEEE Transactions on Power Systems*, vol. 30, no. 6, pp. 3234-3245, 2015.

[20] "Live Solar PV", Available: http://pv-map.apvi.org.au/live [Accessed: 23-May.-2017]

[21] "Solar Incentives", Available: http://www.aemo.com.au/Electricity/National-Electricity-Market-NEM/Planning-and-forecasting/-/media/080A47DA86C04BE0AF93812A548F722E.ashx [Accessed: 29-May.-2017]

[22] "Energy Storage for Power Systems Applications: A Regional Assessment for the Northwest Power Pool (NWPP)."Available: http://www.pnl.gov/main/publications/ [Accessed: 22-Jun.-2015]

[23] AECOM, "Energy Storage Study",Available: http://arena.gov.au/assets/2015/07/AECOM-Energy-Storage-Study.pdf [Accessed: 20-May.-2016]

[24] NREL, "Overgeneration from Solar Energy in California: A Field Guide to the Duck Chart", Available: http://www.nrel.gov [Accessed: 1-May.-2017]

[25] "South Australia-'Duck Curve' ", Available: http://www.wattclarity.com.au/2017/01/sa-electricity-demand-at-new-years-exhibiting-the-duck-curve-affliction/ [Accessed: 21-June.-2017]

[26] Y. Liu, J. Bebic, B. Kroposki, J. d. Bedout, and W. Ren, "Distribution System Voltage Performance Analysis for High-Penetration PV," in *IEEE Energy 2030 Conference,* Atlanta, USA, 17-18 Nov., 2008.

[27] S. M. Chalmers, M. M. Hitt, J. T. Underhill, P. M. Anderson, P. L. Vogt, and R. Ingersoll, "The Effect of Photovoltaic Power Generation on Utility Operation," *IEEE Transactions on Power Apparatus and Systems,* vol. PAS-104, no. 3, pp. 524-530, 1985.

[28] W. T. Jewell, R. Ramakumar, and S. R. Hill, "A study of dispersed photovoltaic generation on the PSO system," *IEEE Transactions on Energy Conversion,* vol. 3, no. 3, pp. 473-478, 1988.

[29] "DG Power Quality, Protection and Reliability Case Studies Report," Available: http://www.localpower.org/documents/reporto_nrel_powerquality.pdf [Accessed: 1-May.-2017]

[30] A. Canova, L. Giaccone, F. Spertino, and M. Tartaglia, "Electrical Impact of Photovoltaic Plant in Distributed Network," *IEEE Transactions on Industry Applications,* vol. 45, no. 1, pp. 341-347, 2009.

[31] M. Thomson and D. G. Infield, "Impact of widespread photovoltaics generation on distribution systems," *IET Renewable Power Generation,* vol. 1, no. 1, pp. 33-40, 2007.

[32] R. Yan and T. K. Saha, "Investigation of Voltage Stability for Residential Customers Due to High Photovoltaic Penetrations," *IEEE Transactions on Power Systems,* vol. 27, no. 2, pp. 651-662, 2012.

[33] M. J. E. Alam, K. M. Muttaqi, and D. Sutanto, "An Approach for Online Assessment of Rooftop Solar PV Impacts on Low-Voltage Distribution Networks," *IEEE Transactions on Sustainable Energy,* vol. 5, no. 2, pp. 663-672, 2014.

[34] "IEEE Recommended Practice for Utility Interface of Photovoltaic (PV) Systems", IEEE Std 929-2000, 2000.

[35] Australian StandardTM Grid connection of energy systems via inverters," AS 4777-2005 Standard, 2005.

[36] "American national standard for electric power systems and equipment : voltage ratings (60 hertz)", National Electrical Manufacturers Association, 2006.

[37] "Electromagnetic compatibility (EMC) - Testing and measurement techniques - Power quality measurement methods," AS/NZS 61000.4.30:2007, ed-2007.

[38] "IEEE Recommended Practice for Monitoring Electric Power Quality," IEEE Std 1159-2009, ed-2009.

[39] KEMA, "ES-Select™ Documentation and User's Manual," Available: http://www.sandia.gov/ess/ESSelectUpdates/ES-Select_Documentation_and_User_Manual-VER_2-2013.pdf [Accessed: 1-May.-2016]

[40] S. Vazquez, S. M. Lukic, E. Galvan, L. G. Franquelo, and J. M. Carrasco, "Energy Storage Systems for Transport and Grid Applications," *IEEE Transactions on Industrial Electronics,* vol. 57, no. 12, pp. 3881-3895, 2010.

[41] S. S. AlKaabi, V. Khadkikar, and H. H. Zeineldin, "Incorporating PV Inverter Control Schemes for Planning Active Distribution Networks," *IEEE Transactions on Sustainable Energy,* vol. 6, no. 4, pp. 1224-1233, 2015.

[42] R. A. Jabr, S. Karaki, and J. A. Korbane, "Robust Multi-Period OPF With Storage and Renewables," *IEEE Transactions on Power Systems,* vol. 30, no. 5, pp. 2790-2799, 2015.

[43] S. Wogrin and D. F. Gayme, "Optimizing Storage Siting, Sizing, and Technology Portfolios in Transmission-Constrained Networks," *IEEE Transactions on Power Systems,* vol. 30, no. 6, pp. 3304-3313, 2015.

[44] L. Ochoa, A. Keane, and G. Harrison, "Minimizing the reactive support for distributed generation: Enhanced passive operation and smart distribution networks," in *2012 IEEE Power and Energy Society General Meeting*, San Diego, USA, 22-26 July 2012, pp. 1-1.

[45] F. Capitanescu, L. F. Ochoa, H. Margossian, and N. D. Hatziargyriou, "Assessing the Potential of Network Reconfiguration to Improve Distributed Generation Hosting Capacity in Active Distribution Systems," *IEEE Transactions on Power Systems*, vol. 30, no. 1, pp. 346-356, 2015.

[46] N. Jayasekara, P. Wolfs, and M. A. S. Masoum, "An optimal management strategy for distributed storages in distribution networks with high penetrations of PV," *Electric Power Systems Research,* vol. 116, no., pp. 147-157, 2014.

[47] H. A. Gil and G. Joos, "On the Quantification of the Network Capacity Deferral Value of Distributed Generation," *IEEE Transactions on Power Systems,* vol. 21, no. 4, pp. 1592-1599, 2006.

[48] M. F. Shaaban, Y. M. Atwa, and E. F. El-Saadany, "DG allocation for benefit maximization in distribution networks," *IEEE Transactions on Power Systems,* vol. 28, no. 2, pp. 639-649, 2013.

[49] P. Siano, L. F. Ochoa, G. P. Harrison, and A. Piccolo, "Assessing the strategic benefits of distributed generation ownership for DNOs," *IET Generation, Transmission & Distribution,* vol. 3, no. 3, pp. 225-236, 2009.

[50] A. S. A. Awad, T. H. M. E.-. Fouly, and M. M. A. Salama, "Optimal ESS Allocation for Load Management Application," *IEEE Transactions on Power Systems,* vol. 30, no. 1, pp. 327-336, 2015.

[51] N. Eghtedarpour and E. Farjah, "Distributed charge/discharge control of energy storages in a renewable-energy-based DC micro-grid," *IET Renewable Power Generation,* vol. 8, no. 1, pp. 45-57, 2014.

[52] M. Bortolini, M. Gamberi, and A. Graziani, "Technical and economic design of photovoltaic and battery energy storage system," *Energy Conversion and Management,* vol. 86, no., pp. 81-92, 2014.

[53] B. Battke, T. S. Schmidt, D. Grosspietsch, and V. H. Hoffmann, "A review and probabilistic model of lifecycle costs of stationary batteries in multiple applications," *Renewable and Sustainable Energy Reviews,* vol. 25, no., pp. 240-250, 2013.

[54] R. Tonkoski, D. Turcotte, and T. H. M. E.-. Fouly, "Impact of High PV Penetration on Voltage Profiles in Residential Neighborhoods," *IEEE Transactions on Sustainable Energy,* vol. 3, no. 3, pp. 518-527, 2012.

[55] M. J. E. Alam, K. M. Muttaqi, and D. Sutanto, "Mitigation of Rooftop Solar PV Impacts and Evening Peak Support by Managing Available Capacity of Distributed Energy Storage Systems," *IEEE Transactions on Power Systems,* vol. 28, no. 4, pp. 3874-3884, 2013.

[56] M. J. E. Alam, K. M. Muttaqi, and D. Sutanto, "A Novel Approach for Ramp-Rate Control of Solar PV Using Energy Storage to Mitigate Output Fluctuations Caused by Cloud Passing," *IEEE Transactions on Energy Conversion*, vol. 29, no. 2, pp. 507-518, 2014.

[57] A. Ellis, D. Schoenwald, J. Hawkins, S. Willard, and B. Arellano, "PV output smoothing with energy storage," in *38th IEEE Photovoltaic Specialists Conference*, Austin, USA, 3-8 June, 2012, pp. 1523-1528.

[58] "2014 Annual Distribution Benchmarking Report", Available: https://www.aer.gov.au/ [Accessed: 10-Nov.-2014]

[59] R. Tonkoski, L. A. C. Lopes, and T. H. M. El-Fouly, "Coordinated Active Power Curtailment of Grid Connected PV Inverters for Overvoltage Prevention," *IEEE Transactions on Sustainable Energy,* vol. 2, no. 2, pp. 139-147, 2011.

[60] E. Demirok, P. C. Gonz, K. H. B. Frederiksen, D. Sera, *et al.*, "Local Reactive Power Control Methods for Overvoltage Prevention of Distributed Solar Inverters in Low-Voltage Grids," *IEEE Journal of Photovoltaics,* vol. 1, no. 2, pp. 174-182, 2011.

[61] Q. Huang, J. Z. Kang, S. G. Tesfahunegn, Ø. Ulleberg, P. J. S. Vie, and T. M. Undeland, "PV Fluctuation Balancing Using Hydrogen Storage – a Smoothing Method for Integration of PV Generation into the Utility Grid," *Energy Procedia*, vol. 12, pp. 1015-1022, 2011.

[62] T. D. Hund, S. Gonzalez, and K. Barrett, "Grid-Tied PV system energy smoothing," in *IEEE Photovoltaic Specialists Conference (PVSC)*, Honolulu, USA, 20-25 June, 2010.

[63] K. T. Tan, P. L. So, Y. C. Chu, and M. Z. Q. Chen, "Coordinated Control and Energy Management of Distributed Generation Inverters in a Microgrid," *IEEE Transactions on Power Delivery*, vol. 28, no. 2, pp. 704-713, 2013.

[64] X. Liu, A. Aichhorn, L. Liu, and H. Li, "Coordinated Control of Distributed Energy Storage System With Tap Changer Transformers for Voltage Rise Mitigation Under High Photovoltaic Penetration," *IEEE Transactions on Smart Grid*, vol. 3, no. 2, pp. 897-906, 2012.

[65] T. Zhang, S. X. Chen, H. B. Gooi, and J. M. Maciejowski, "A Hierarchical EMS for Aggregated BESSs in Energy and Performance-based Regulation Markets," *IEEE Transactions on Power Systems*, vol. PP, no. 99, pp. 1-1, 2016.

[66] J. Li, Z. Wu, S. Zhou, H. Fu, and X. P. Zhang, "Aggregator service for PV and battery energy storage systems of residential building," *CSEE Journal of Power and Energy Systems*, vol. 1, no. 4, pp. 3-11, 2015.

[67] F. Adamek, M. Arnold, and G. Andersson, "On Decisive Storage Parameters for Minimizing Energy Supply Costs in Multicarrier Energy Systems," *IEEE Transactions on Sustainable Energy*, vol. 5, no. 1, pp. 102-109, 2014.

[68] I. D. d. C. Mendaza, I. G. Szczesny, J. R. Pillai, and B. Bak-Jensen, "Flexible Demand Control to Enhance the Dynamic Operation of Low Voltage Networks," *IEEE Transactions on Smart Grid*, vol. 6, no. 2, pp. 705-715, 2015.

[69] Y. Xu and L. Tong, "Optimal Operation and Economic Value of Energy Storage at Consumer Locations," *IEEE Transactions on Automatic Control*, vol. 62, no. 2, pp. 792-807, 2017.

[70] G. F. Lauss, M. O. Faruque, K. Schoder, C. Dufour, A. Viehweider, and J. Langston, "Characteristics and Design of Power Hardware-in-the-Loop Simulations for Electrical Power Systems," *IEEE Transactions on Industrial Electronics*, vol. 63, no. 1, pp. 406-417, 2016.

[71] M. Cupelli, M. d. P. Carro, and A. Monti, "Hardware in the Loop implementation of a disturbance based control in MVDC grids," in *IEEE Power & Energy Society General Meeting*, Denver, USA, 26-30 July, 2015.

[72] P. C. Kotsampopoulos, F. Lehfuss, G. F. Lauss, B. Bletterie, and N. D. Hatziargyriou, "The Limitations of Digital Simulation and the Advantages of PHIL Testing in Studying Distributed Generation Provision of Ancillary Services," *IEEE Transactions on Industrial Electronics*, vol. 62, no. 9, pp. 5502-5515, 2015.

[73] B. Palmintier, B. Lundstrom, S. Chakraborty, T. Williams, K. Schneider, and D. Chassin, "A Power Hardware-in-the-Loop Platform With Remote Distribution Circuit Cosimulation," *IEEE Transactions on Industrial Electronics,* vol. 62, no. 4, pp. 2236-2245, 2015.

[74] M. Rezkallah, A. Hamadi, A. Chandra, and B. Singh, "Real-Time HIL Implementation of Sliding Mode Control for Standalone System Based on PV Array Without Using Dumpload," *IEEE Transactions on Sustainable Energy,* vol. 6, no. 4, pp. 1389-1398, 2015.

[75] O. Samuelsson, S. Repo, R. Jessler, J. Aho, M. Kärenlampi, and A. Malmquist, "Active distribution network : Demonstration project ADINE," in *2010 IEEE PES Innovative Smart Grid Technologies Conference Europe (ISGT Europe),* Gothenburg, Sweden, 23-24 june, 2010.

[76] P. Sivachandra, P. Venkatesh and S. Balamurugan, "A new real time approach using dSPACE R&D controller board for reactive power control by SVC in autonomous wind-diesel hybrid power systems," *International Journal of Engineering, Science and Technology,* vol. 3, no. 5, pp. 30-45, 2011.

[77] H. Hooshyar, F. Mahmood, L. Vanfretti, and M. Baudette, "Specification, implementation, and hardware-in-the-loop real-time simulation of an active distribution grid," *Sustainable Energy, Grids and Networks,* vol. 3, no., pp. 36-51, 2015.

[78] S. R. Deeba, R. Sharma, T. K. Saha, D. Chakraborty, and A. Thomas, "Evaluation of technical and financial benefits of battery-based energy storage systems in distribution networks," *IET Renewable Power Generation,* vol. 10, no. 8, pp. 1149-1160, 2016.

[79] Z. Wang, C. Gu, F. Li, P. Bale, and H. Sun, "Active Demand Response Using Shared Energy Storage for Household Energy Management," *IEEE Transactions on Smart Grid,* vol. 4, no. 4, pp. 1888-1897, 2013.

[80] "Central bank discount rate", Available: http://www.indexmundi.com/australia/central _bank_discount_rate.html [Accessed: 1-Nov.-2014]

[81] Y. Riffonneau, S. Bacha, F. Barruel, and S. Ploix, "Optimal Power Flow Management for Grid Connected PV Systems With Batteries," *IEEE Transactions on Sustainable Energy,* vol. 2, no. 3, pp. 309-320, 2011.

[82] Energex, "Distribution annual planning report (volume-I)" Available: https://www.energex.com.au [Accessed: 27-Jul.-2015]

[83] "Daily Actual Operational Demand Update", Available: http://www.nemweb.com.au /Reports/CURRENT/Operational _Demand /ACTUAL_UPDATE/ [Accessed: 10-Mar.-2015]

[84] "Generic Algebraic Modelling System (GAMS)" Available: https://www.gams.com [Accessed: 15-Jun.-2015]

[85] S. R. Deeba, R. Sharma, T. K. Saha, and D. Chakraborty, "A tool to estimate maximum arbitrage from battery energy storage by maintaining voltage limits in an LV network," in *Power and Energy Engineering Conference (APPEEC),* in *IEEE PES Asia-Pacific*, Brisbane, Australia, 15-18 November, 2015, pp. 1-5.

[86] A. Gabash and P. Li, "Active-Reactive Optimal Power Flow in Distribution Networks With Embedded Generation and Battery Storage," *IEEE Transactions on Power Systems,* vol. 27, no. 4, pp. 2026-2035, 2012.

[87] "COUENNE solver in GAMS", Available: https://www.gams.com/latest/docs/solvers/couenne/index.html [Accessed: 15-Jun.-2015]

[88] "Live Solar Data", Available: http://solar.uq.edu.au/ [Accessed: 1-Mar.-2015]

[89] T. Warren Liao, "Clustering of time series data—a survey," *Pattern Recognition,* vol. 38, no. 11, pp. 1857-1874, 2005.

[90] R. Yan, "Impact of Photovoltaic Integration on Voltage Variation of Electricity Distribution Network," 2012.

[91] Energex and Ergon Energy, "Connection Standard Small Scale Parallel IES up to 30kVA," Available: https://www.ergon.com.au/__data/assets/pdf_file/0005/198698/STNW1170-Connection-Standard-for-Micro-EG-Units.pdf. [Accessed: 1-Dec.-2016]

[92] S. R. Deeba, R. Sharma, T. K. Saha, and A. Thomas, "Investigation of voltage performance of an LV distribution network for improving rooftop photovoltaic uptake in Australia," in *2016 IEEE Power and Energy Society General Meeting (PESGM)*, Boston, USA, 17-21 July, 2016, pp. 1-5.

[93] I. Serban and C. Marinescu, "A look at the role and main topologies of battery energy storage systems for integration in autonomous microgrids," in *12th International Conference on Optimization of Electrical and Electronic Equipment*, Brasov, Romania, 20-22 May, 2010, pp. 1186-1191.

[94] "PSS®SINCAL", Available: http://www.siemens.com/ [Accessed: 10-Oct.-2016]

[95] "Live Solar Data", Available: http://solar.uq.edu.au/ [Accessed: 10-Mar.-2015]

[96] S. R. Deeba, "A battery management approach to improve steady state voltage performance of an LV distribution feeder," in *Australasian Universities Power Engineering Conference*, 25-28 Sept., 2016, Brisbane, Australia, pp. 1-6.

[97] W. H. Kersting, "Radial distribution test feeders," in *IEEE Power Engineering Society Winter Meeting*, Columbus, USA, 28 Jan.-1 Feb., 2001, pp. 908-912.

[98] "IEEE 37-Bus Feeder" Available: https://ewh.ieee.org/soc/pes/dsacom/testfeeders/ [Accessed: 10-Mar.-2015]

[99] S. R. Deeba, R. Sharma, and T. K. Saha, "Coordinated control of multi-functional battery energy storage system in an unbalanced network," in *Australasian Universities Power Engineering Conference (AUPEC),* 28 Sept.-1 Oct., 2014, pp. 1-6.

[100] "Proof of Concept Residential Energy Monitoring Program Final Report", Available: http://www.energyrating.gov.au/document/proof-concept-residential-energy-monitoring-program-final-report [Accessed: 10-Mar.-2017]

[101] "RTDS Technology", Available: https://www.rtds.com/ [Accessed: 10-Apr.-2016]

[102] C. Min and G. A. Rincon-Mora, "Accurate electrical battery model capable of predicting runtime and I-V performance," *IEEE Transactions on Energy Conversion,* vol. 21, no. 2, pp. 504-511, 2006.

[103] C. Schauder and H. Mehta, "Vector analysis and control of advanced static VAr compensators," *IEE Proceedings C - Generation, Transmission and Distribution,* vol. 140, no. 4, pp. 299-306, 1993.

[104] "IEEE 13-Bus Feeder" Available: https://ewh.ieee.org/soc/pes/dsacom/testfeeders/ [Accessed: 10-Mar.-2015]

[105] "dSPACE 1103 PPC control board", Available: https://www.dspace.com/en/inc/home/products/hw/singbord/ppcconbo.cfm [Accessed: 24-Apr.-2016]

[106] "MATLAB Simulink" Available: http://au.mathworks.com/, [Accessed: 24-Apr.-2016]

[107] R. S., M. N and M. Blackman, "Model-based Control of Utility-Scale Wind Turbines," *Control & Intelligent Systems,* vol. 45, no. 1, 2017.

[108] J. D. Glover, M. Sharma, and T. Overbye, "Power System Analysis and Design", Cengage Learning, 2012.

[109] "Live UQ Solar Data" Available: http://solar-energy.uq.edu.au/ [Accessed: 5-Oct.-2016]

[110] Y. Bo and L. Wei, "Homogeneous observers, iterative design, and global stabilization of high-order nonlinear systems by smooth output feedback," *IEEE Transactions on Automatic Control,* vol. 49, no. 7, pp. 1069-1080, 2004.

[111] Y. Xihui and V. H. Quintana, "Improving an interior-point-based OPF by dynamic adjustments of step sizes and tolerances," *IEEE Transactions on Power Systems,* vol. 14, no. 2, pp. 709-717, 1999.

[112] S. V. Araujo, P. Zacharias and R. Mallwitz, " Highly efficient single-phase transformerless inverters for grid-connected photovoltaic systems", IEEE Transactions on Industrial Electronics, vol. 57 , no. 9 , pp. 3118-3128, 2010.

Appendices

Appendix A1: IEEE 37 Nodes Radial Network Data

The following network information has been taken from [97, 98].

a) Line Segment Data

From Node	To Node	Length(feet)	Configuration
701	702	960	722
702	705	400	724
702	713	360	723
702	703	1320	722
703	727	240	724
703	730	600	723
704	714	80	724
704	720	800	723
705	742	320	724
705	712	240	724
706	725	280	724
707	724	760	724
707	722	120	724
708	733	320	723
708	732	320	724
709	731	600	723
709	708	320	723
710	735	200	724
710	736	1280	724
711	741	400	723
711	740	200	724
713	704	520	723
714	718	520	724
720	707	920	724
720	706	600	723
727	744	280	723
730	709	200	723
733	734	560	723
734	737	640	723
734	710	520	724
737	738	400	723
738	711	400	723
744	728	200	724
744	729	280	724
775	709	0	XFM-1
799	701	1850	721

b) Underground Cable Data

Configuration	Phasing	Cable	Spacing ID
721	A B C	1,000,000 AA, CN	515
722	A B C	500,000 AA, CN	515
723	A B C	2/0 AA, CN	515
724	A B C	#2 AA, CN	515

c) Underground Line Spacing (515)

<table>
<tr><td>Spacing ID</td><td>515</td></tr>
<tr><td>Type</td><td>Three-Phase, 4 Wire</td></tr>
<tr><td>Figure</td><td>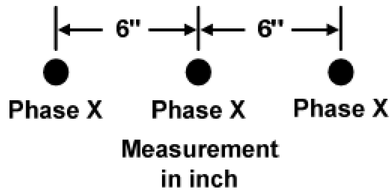
</td></tr>
</table>

d) Transformer Data

	KVA	KV-high	KV-low	R - %	X - %
Substation:	2,500	230 D	4.8 D	2	8
XFM -1	500	4.8 D	.480 D	0.09	1.81

e) Load Data

Node	Load	Ph-1	Ph-1	Ph-2	Ph-2	Ph-3	Ph-4
	Model	KW	KVAR	KW	KVAR	KW	KVAR
701	D-PQ	140	70	140	70	350	175
712	D-PQ	0	0	0	0	85	40
713	D-PQ	0	0	0	0	85	40
714	D-I	17	8	21	10	0	0
718	D-Z	85	40	0	0	0	0
720	D-PQ	0	0	0	0	85	40
722	D-I	0	0	140	70	21	10
724	D-Z	0	0	42	21	0	0
725	D-PQ	0	0	42	21	0	0
727	D-PQ	0	0	0	0	42	21
728	D-PQ	42	21	42	21	42	21
729	D-I	42	21	0	0	0	0
730	D-Z	0	0	0	0	85	40
731	D-Z	0	0	85	40	0	0
732	D-PQ	0	0	0	0	42	21
733	D-I	85	40	0	0	0	0
734	D-PQ	0	0	0	0	42	21
735	D-PQ	0	0	0	0	85	40
736	D-Z	0	0	42	21	0	0
737	D-I	140	70	0	0	0	0
738	D-PQ	126	62	0	0	0	0
740	D-PQ	0	0	0	0	85	40
741	D-I	0	0	0	0	42	21
742	D-Z	8	4	85	40	0	0
744	D-PQ	42	21	0	0	0	0
Total		727	357	639	314	1091	530

Appendix A2: BESS Model Parameters Tuning [112]

The required inductance of the output filter is determined by considering the condition when the ripple of the output current reaches its maximum value [112]. The factor representing such an instant is dependent on the modulation factor, which is determined by using expression (A2.1).

$$\Delta I_{factor}(M,t) = \sin(w_g, t) - M \sin^2(w_g, t) \tag{A2.1}$$

where M presents the voltage gain of the circuit (output voltage/input voltage) and w_g implies the grid angular frequency.

The output filter inductance L is designed by using the following expression considering a limit for the ripple of output current (ΔI_L) [112].

$$L = \frac{v_{ab}\,\Delta I_{factor}}{f_{sw}\,\Delta I_L} \tag{A2.2}$$

where v_{ab} and f_{SW} imply the PCC voltage and inverter switching frequency respectively.

Appendix A3: IEEE 13 Nodes Radial Network Data [97, 104]

a) Line Segment Data

Node A	Node B	Length (feet)	Configuration
632	645	500	603
632	633	500	602
633	634	0	XFM-1
645	646	300	603
650	632	2000	601
684	652	800	607
632	671	2000	601
671	684	300	604
671	680	1000	601
671	692	0	Switch
684	611	300	605
692	675	500	606

b) Overhead Line Configurations

Configuration	Phasing	Phase	Neutral	Spacing
		ACSR	ACSR	ID
601	B A C N	556,500 26/7	4/0 6/1	500
602	C A B N	4/0 6/1	4/0 6/1	500
603	C B N	1/0	1/0	505
604	A C N	1/0	1/0	505
605	C N	1/0	1/0	510

c) Underground Cable Configurations

Configuration	Phasing	Cable	Neutral	Space ID
606	A B C N	250,000 AA, CN	None	515
607	A N	1/0 AA, TS	1/0 Cu	520

d) Spot Load Data

Node	Load	Ph-1	Ph-1	Ph-2	Ph-2	Ph-3	Ph-3
	Model	(kW)	(KVAR)	(kW)	(kVAR)	(kW)	(kVAR)
634	Y-PQ	160	110	120	90	120	90
645	Y-PQ	0	0	170	125	0	0
646	D-Z	0	0	230	132	0	0
652	Y-Z	128	86	0	0	0	0
671	D-PQ	385	220	385	220	385	220
675	Y-PQ	485	190	68	60	290	212
692	D-I	0	0	0	0	170	151
611	Y-I	0	0	0	0	170	80
	Total	1158	606	973	627	1135	753

e) Distributed Load Data

Node A	Node B	Load	Ph-1	Ph-1	Ph-2	Ph-2	Ph-3	Ph-3
		Model	(kW)	(kVAR)	(kW)	(kVAR)	(kW)	(kVAR)
632	671	Y-PQ	17	10	66	38	117	68

f) Shunt Capacitors

Node	Ph-A	Ph-B	Ph-C
	(kVAR)	(kVAR)	(kVAR)
675	200	200	200
611			100
Total	200	200	300

g) Transformer Data

	kVA	kV-high	kV-low	R - %	X - %
Substation:	5,000	115 - D	4.16 Gr. Y	1	8
XFM -1	500	4.16 - Gr.W	0.48 - Gr.W	1.1	2

h) Overhead Line Spacing (500, 505 and 510)

Spacing ID	500	505	510
Type	Three-Phase, 4 Wire	Two-Phase, 3 Wire	Single-Phase, 2 Wire
Figure	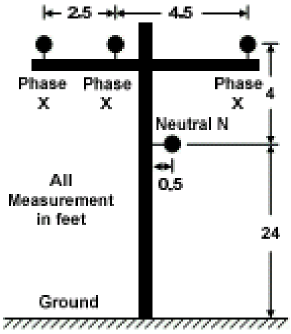	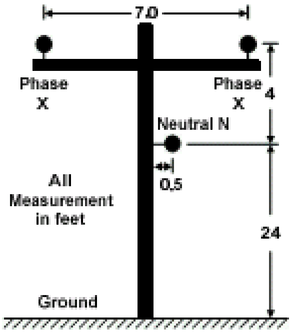	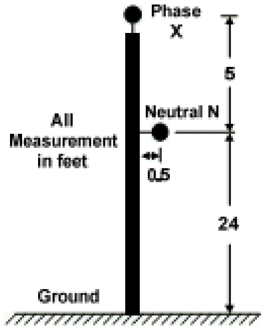

h) Underground Cable Spacing (515 and 520)

Spacing ID	515	520
Type	Three-Phase, 4 Wire	Single-Phase, 2 Wire
Figure	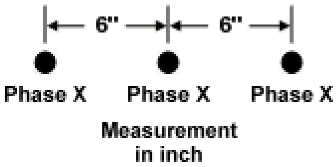	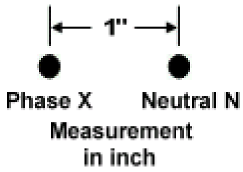

Appendix A4: Links of Publications Included in This Thesis

1) **S R Deeba**, R. Sharma, T. K. Saha, D. Chakraborty and A. Thomas, "Evaluation of Technical and Financial Benefits of Battery-Based Energy Storage Systems in Distribution Networks", *IET Renewable Power Generation*, vol. 10, no. 8, pp. 1149-1160, September 2016.
Link: http://ieeexplore.ieee.org/document/7564619/

2) **S. R. Deeba**, "A Battery Management Approach to Improve Steady State Voltage Performance of an LV Distribution Feeder", *Australasian Universities Power Engineering Conference*, 25-28 September, 2016, Brisbane, Australia.
Link: http://ieeexplore.ieee.org/document/7749352/

3) **S. R. Deeba**, R. Sharma, T. K. Saha and A. Thomas, "Investigation of Voltage Performance of an LV Distribution Network for Improving Rooftop Photovoltaic Uptake in Australia", *IEEE Power and Energy Society General Meeting*, 17-21 July, 2016, Boston, MA, USA.
Link: http://ieeexplore.ieee.org/document/7742037/

4) **S. R. Deeba**, R. Sharma, T. K. Saha and D. Chakraborty, "A Tool to Estimate Maximum Arbitrage from Battery Energy Storage by Maintaining Voltage Limits in an LV Network", *IEEE PES Asia-Pacific Power and Energy Engineering Conference*, 15-18 November, 2015, Brisbane, Australia.
Link: http://ieeexplore.ieee.org/abstract/document/7380894/

5) **S. R. Deeba**, R. Sharma and T. K. Saha, "Coordinated Control of Multi-Functional Battery Energy Storage System in an Unbalanced Network", *Australasian Universities Power Engineering Conference*, 28 September-1 October, 2014, Perth, Australia.
Link: http://ieeexplore.ieee.org/abstract/document/6966642/